Cenozoic High Latitude Paleoceanography: New Perspectives from the Arctic and Subantarctic Pacific

by

Lindsey M. Waddell

A dissertation submitted in partial fulfillment
of the requirements for the degree of
Doctor of Philosophy
(Oceanography: Marine Geology and Geochemistry)
in The University of Michigan
2009

Doctoral Committee:

Assistant Professor Ingrid L. Hendy, Chair
Professor Mary Anne Carroll
Professor Lynn M. Walter
Associate Professor Christopher J. Poulsen

Table of Contents

List of Figures iii

List of Tables v

List of Appendices vi

Abstract vii

Chapter
1. Introduction 1

2. Ventilation of the Abyssal Southern Ocean During the Late Neogene: A New Perspective from the Subantarctic Pacific 21

3. Global Overturning Circulation During the Late Neogene: New Insights from Hiatuses in the Subantarctic Pacific 55

4. Salinity of the Eocene Arctic Ocean from Oxygen Isotope Analysis of Fish Bone Carbonate 73

5. The Isotopic Integrity of Biogenic Apatite Carbonate in Deep Sea Settings 109

6. Conclusions and Future Research 130

Appendices 134

List of Figures

Figure 2.1. Bathymetric map of the study region, depicting the core locations of MV0502-4JC (50°20'S, 148°08'W, 4286 m) and pre-existing Eltanin core ELT 25-11 (50°02'S, 127°31'W, 3969 m), for which new results are presented in this study. **43**

Figure 2.2. Map showing the location of existing benthic stable isotope records that are compared to MV0502-4JC in this study. **43**

Figure 2.3. Compilation of the results from MV0502-4JC. **44**

Figure 2.4. Compilation of the results from ELT 25-11. ..... **45**

Figure 2.5. Comparison of the benthic $\delta^{13}C$ record of the late Miocene carbon shift from MV0502-4JC to that of ODP Site 704 in the South Atlantic. **46**

Figure 2.6. Comparison of the MV0502-4JC (red) benthic $\delta^{13}C$ (top) and $\delta^{18}O$ (bottom) records of the late Pliocene climate transition to records from ODP Sites 849 (black, Pacific Ocean), 607 (green, North Atlantic), and 704/1090 (blue, South Atlantic). **47**

Figure 3.1. Bathymetric map of the study region, depicting the core locations of MV0502 4JC (50°20'S, 148°08'W, 4286 m) and Eltanin cores, ELT 25-11 (50°02'S, 127°31'W, 3969 m) and ELT 20-2 (49°00'S, 144°50'W, 4517 m). **67**

Figure 3.2. Temperature of water at 4 km water depth relative to the core locations discussed in this chapter. **67**

Figure 3.3. Benthic stable isotope (*Cibicidoides* spp.) and weight percent $CaCO_3$ results from MV0502-4JC. **68**

Figure 4.1. Paleoreconstruction of the Arctic Region at 50 Ma showing the location of the Arctic Coring Expedition (ACEX) 302 Sites examined in this study. **98**

Figure 4.2. Secondary electron images of fish bone taken from Sample 11X 2W 46-48 ..... **99**

Figure 4.3. Results of a linear regression performed on the zero-salinity Intercepts and slopes of the $\delta^{18}O_w$-salinity equations listed in Table 4.2 for the North Atlantic and Arctic. **100**

Figure 4.4 (**a**, **b**) Oxygen and carbon isotopic composition of fish debris from IODP Expedition 302, Holes M0002A and M0004A. **(c)** Temperatures used in calculating Arctic salinity. (**d**) Calculated salinity range based on $\delta^{18}O$ data in (a) and temperatures shown in (c). **101**

Figure 5.1. Comparison of the $\delta^{18}O$ (**left**) and $\delta^{13}C$ (**right**) values of benthic foramininifera, planktonic foraminifera, and fish debris obtained in this study with the results of Dutton et al. (2005) from ODP Site 1209 on the Shatsky Rise. **123**

Figure 5.2. Comparison of the $\delta^{18}O$ (**top**) and $\delta^{13}C$ (**bottom**) values of fish debris and benthic foraminifera from the late Miocene portion of subantarctic Pacific core MV0502-4JC.....**124**

Figure 5.3. Plot showing the stable isotope values of fish apatite carbonate from all of the locations listed in Table 1. .....**125**

List of Tables

Table 2.1. Location and Water Depth of Late Neogene Stable Isotope Records Discussed in This Study. **41**

Table 2.2. Important Age Datums Identified in MV0502-4JC. **41**

Table 2.3. Important Age Datums Identified in ELT 25-11 ..... **42**

Table 4.1. Chemical Treatment Test Performed on Sample M0002A-55X-CC **95**

Table 4.2. $\delta 18O_w$-Salinity Relation for Sites in the Arctic and North Atlantic Obtained from Surface Water Measurements Across Diverse Modern Salinity Gradients **95**

Table 4.3. Stable Isotope Data Generated from the Analysis of Fish Bones in ACEX Holes 302 M0002A and M0004A and the Calculated Salinity Range for Each Sample. **96**

Table 4.4. Estimates of Arctic Salinity Based on Different Assumptions of $\Delta\delta^{18}O_w/\Delta S$, $\delta^{18}O$ of Precipitation ($\delta^{18}Op$), and Temperature for the PETM, the *Azolla* Event, 47.6 Ma (A Possible Low Salinity Event), 46.3 Ma (A Possible High Salinity Event), Average Eocene Conditions, and Miocene Sample 44X-CC. **97**

Table 4.5. Comparison Between Stable Isotope Values Obtained from Early Eocene Untreated Fish Bone and Teeth from ODP Hole 913B in the Norwegian-Greenland Sea and Full-Marine DSDP Hole 550 in the Northeastern Atlantic by Andreasson et al. [1997] versus This Study **97**

Table 5.1. Location of core sites discussed in this study. **120**

Table 5.2. Oxygen and carbon isotopic composition of Eocene fish apatite and foraminifera from ODP Leg 198, Sites 1209 and 1212, Shatsky Rise. **120**

Table 5.3. Oxygen and carbon isotopic composition of Miocene fish apatite and foraminifera from MV0502-4JC, Subantarctic Pacific. **121**

Table 5.4. Oxygen and carbon isotopic composition of fish apatite and foraminifera from the Røsnæs Clay Formation (from Andreasson et al., 1996; Schmitz et al., 1996). **121**

Table 5.5. Oxygen and carbon isotopic composition of fish apatite and foraminifera from DSDP Hole 550 (from Andreasson et al., 1996; Charisi and Schmitz, 1996). **122**

List of Appendices

Appendix A. Stable Isotope and Compositional Data from MV0502-4JC.....**134**

Appendix B: Radiolarian biostratigraphy for MV0502-4JC **141**

Appendix C: Weight Percent $CaCO_3$ from MV0502-4JC.....**142**

Appendix D. Stable Isotope and Compositional Data from ELT 25-11.....**143**

Appendix E: Radiolarian biostratigraphy for ELT 25-11.....**145**

Appendix F: Weight Percent $CaCO_3$ from ELT 25-11 and ELT 20-2 .....**146**

Appendix G. Stable Isotope Data from ELT 25-11 .....**147**

Appendix H. Radiolarian biostratigraphy from ELT 20-2 .....**148**

Appendix I. Laboratory Procedure for the Preparation of Fish Debris for Oxygen and Carbon Stable Isotope Analysis.....**149**

Appendix J. Uncertainties in the Stable Isotope Measurements **150**

Abstract

The polar oceans are closely linked to climate through their role in the formation and ventilation of the world's deep water masses, but the feedbacks between climate and deep convection during the Cenozoic remain poorly understood. In this thesis, stable carbon and oxygen isotopes are used to investigate circulation changes in the polar oceans during two intervals of significant climatic interest. First, this thesis examines the paleoceanography of the abyssal subantarctic Pacific during the cooling and ice sheet expansion of the late Neogene, and second, a novel stable isotope technique is used to reconstruct the hydrography of the Arctic Ocean during the exceptionally warm, ice-free conditions of the early Eocene.

This thesis presents a new stable isotope record from the subantarctic Pacific (50˚20'S, 148˚08'W, 4286m). This record was found to contain three major hiatuses spanning the early Pliocene-early Late Pliocene, ~1.57-0.68 Ma, and ~0.53-0.19 Ma. The timing of these hiatuses suggests enhanced vigor of the Antarctic Circumpolar Current (ACC) during three periods: the middle Pliocene and the Mid-Pleistocene and Mid-Brunhes climatic transitions. Correlation with other globally-distributed deep-sea records supports the hypothesis that these periods were associated with intensified global deep water circulation. In contrast, benthic $\delta^{18}O$ and $\delta^{13}C$ suggest the development of a large pool of cold, CO_2-rich deep water in the abyssal Southern Ocean during the late Pliocene expansion of the Northern Hemisphere ice sheets.

Stable isotopic data was obtained from the structural carbonate component of fish apatite found in the carbonate-poor Eocene Arctic sediments recovered during IODP Expedition 302. Although stable isotope analysis of deep-sea apatite carbonate has rarely been undertaken, an assessment of the isotopic integrity of bioapatite shows its potential to record large-scale paleoceanographic trends in carbonate-poor samples. The $\delta^{18}O$ values

obtained from Eocene Arctic fish debris averaged -4.89‰ compared to 2.77‰ for a Miocene sample from the same site. Thus the Arctic Ocean had an average salinity of 21-25‰ during the Eocene, with the lowest salinities occurring during the Paleocene Eocene Thermal Maximum and two freshwater events at ~48.7 Ma (the *Azolla* event) and ~47.6 Ma

Chapter 1
Introduction

1. Deepwater Circulation: Examining the Past to Understand the Future

Deepwater circulation is closely linked to climate through its role in the redistribution of heat and salt in the global ocean and its influence over atmospheric pCO_2. Because deep waters are formed through the sinking of cold, salty waters in the polar regions, changes in high latitude climate can also have a significant effect on the formation of these waters. In the modern ocean, deep waters form in the North Atlantic and Southern Ocean. Warm, salty surface waters that have been subjected to evaporation in the subtropical Atlantic are carried northward by the Gulf Stream to the Greenland-Norwegian Sea, where the waters cool and sink as North Atlantic Deepwater (NADW), filling the Atlantic Ocean between the depths of 2 and 4 km. In conjunction with the effect of the westerly winds, the intense heat loss to the atmosphere associated with NADW formation is thought to be an important in the maintenance of the mild climatic conditions of northwestern Europe. After sinking, NADW flows south to the Southern Ocean, where the Antarctic Circumpolar Current (ACC) mixes it with the densest water in the world ocean, Antarctic Bottom Water (AABW), which forms through the sinking of extremely cold shelf waters along the Antarctic continental margin. The mixture of NADW and AABW creates a new water mass known as Circumpolar Deep Water (CDW), which is driven to upwell at the Antarctic Divergence on the southern side of the ACC. A portion of the upwelled CDW flows south and returns to the deep ocean almost immediately as AABW while the other portion flows north to become subantarctic water. As CDW enters the deep Pacific, it becomes Pacific Deepwater (PDW), gradually becoming warmer, fresher, oxygen-poorer, and nutrient-richer along its northward journey, and ultimately upwelling in the North Pacific and returning south at mid-depth.

Although the North Atlantic dominates the overturning and deepwater circulation of the modern ocean, the strength of North Atlantic overturning appears to have varied

widely over the Cenozoic. The current consensus among climate scientists, as expressed in the 2007 IPCC assessment report, is that meridional overturning circulation (MOC) in the North Atlantic is likely to decrease during the 21st century under continued anthropogenic CO_2 emissions (Meehl et al., 2007). In contrast to early studies (e.g. Dixon et al., 1999), which suggested that an increase in the amount of freshwater supplied to the high latitudes under a warmer atmosphere would be the primary cause of reduced North Atlantic MOC, Gregory et al. (2005) found in an intercomparison of eleven climate models that the predicted decrease in MOC in the North Atlantic would actually be driven more by changes in surface heat flux than by increased freshwater input. As for the effects of increased atmospheric CO_2 concentrations on overturning circulation in the Southern Ocean, the IPCC report acknowledges that "few simulations have also addressed the changes in overturning circulation in the South Atlantic and Southern Ocean. In addition to water mass modifications, this also has an effect on the transport by the Antarctic Circumpolar Current, but results are not yet conclusive. (Meehl et al., 2007)" In a recently published modeling study, de Boer et al. (2008) demonstrate that the dominance of global overturning circulation tends to shift from the North Atlantic to the Southern Ocean and North Pacific regions when 1) there is an increase in mean ocean temperatures and/or wind strength, either in the Southern Ocean or globally or 2) the hydrological cycle is weak, as the Southern Ocean and North Pacific are more susceptible to salinity changes than the North Atlantic. Because a stronger hydrological cycle would accompany warmer mean ocean temperatures, de Boer et al. (2008) suggest, based on paleobservations of more widely distributed sinking during the warm early Pliocene, that increases in mean paleotemperature and wind strength may outweigh the affects of a more vigorous hydrological cycle on overturning circulation as global temperatures increase. Clearly, however, this is a preliminary conclusion, and more research is needed into past circulation patterns in order to better understand how global-scale overturning circulation is likely to respond to forcing in the future.

Part of the reason behind our incomplete knowledge of past deepwater circulation patterns has been the lack of data available from high latitude regions. Stable isotopic analysis ($\delta^{18}O$ and $\delta^{13}C$) of carbonate from marine sediments can provide a wealth of information about past variations in climate and circulation. However, the polar regions

have been notoriously difficult to access and carbonate preservation in the sediments is often poor. This dissertation focuses on the construction and interpretation of new stable isotope records from two of the most poorly understood regions of the polar oceans: the Arctic Ocean and the subantarctic southeast Pacific. The first of these, the Arctic, can now be studied in detail thanks to an international effort by the 2004 Integrated Ocean Drilling Program (IODP) Expedition 302 (the Arctic Coring Expedition, or ACEX), which led the first successful deep sea drilling project to the Arctic Ocean, recovering ~340 m of sediments spanning ~55 million years. The second region, the southeast subantarctic Pacific, was visited by a recent site survey cruise, the 2005 South Pacific Latitudinal Transect (SPLAT), which recovered several sediment cores, most notably a carbonate-rich core, MV0502-4JC, from abyssal depths (50˚20'S, 148˚08'W, 4286 m). The stable isotope record obtained from MV0502-4JC has interesting implications for the circulation of the abyssal Southern Ocean during the Late Neogene, and thus is the focus of **Chapters 2 and 3** of this dissertation, of which Chapter 2 is currently undergoing review for *Paleoceanography*. In contrast to MV0502-4JC, the cores recovered from the Arctic Ocean by ACEX contain very little carbonate, making conventional stable isotope analysis of foraminifera impossible. The Eocene portion of the ACEX cores, however, is unusually rich in fish bone, and bone contains a small structural CO_3^- component (4% by weight according to Koch (1997)) that can be subjected to stable isotope analysis in lieu of foraminifera. **Chapter 4**, which has already been published in the journal *Paleoceanography*, discusses this stable isotope record and its implications for the salinity of the Arctic Ocean during the warm greenhouse climate of ~55 to 45 Ma. Because stable isotope analysis of the structural carbonate component of bone is a technique that has rarely been applied in the reconstruction of deep sea environments, **Chapter 5** is dedicated to assessing the integrity of this technique by comparing the $\delta^{18}O$ values of foraminifera and fish bone carbonate obtained in carbonate-rich cores.

To establish a context for my dissertation work, this chapter is intended to provide an overview of our current state of knowledge of the evolution of climate and oceanic circulation over the Cenozoic. While the opening and closing of oceanic gateways has affected deepwater circulation patterns on a large scale over the Cenozoic, of particular interest here is the nature of overturning circulation during warm climatic regimes of the

past, the overall evolution of circulation during the progression of climate from a greenhouse to an icehouse state, and more recently, circulation differences between the "warmer" and "colder" climate states of the late Neogene. First, however, I review the principles behind the use of stable isotopes in the reconstruction of past oceanic conditions.

2. The Use of Stable Isotopes in Paleoceanographic Applications

The stable isotopic compositions of oxygen and carbon are expressed as the ratio R of the isotopic abundance of the heavy isotope divided by that of the light isotope:

$$R = {}^{18}O/{}^{16}O \text{ or } R={}^{13}C/{}^{12}C$$

For carbonates, this ratio is measured from the CO_2 generated by reaction with phosphoric acid at a controlled temperature. To reduce systematic errors in measurements made on different mass spectrometers, stable isotope results are expressed in δ notation relative to a standard, Vienna Pee Dee Belemnite (VPDB) for carbonates or standard mean ocean water (SMOW) for all other oxygen bearing compounds.

$$\delta(‰) = ((R_{sample}-R_{standard})/R_{standard})*10^3$$

2.1 Oxygen Isotopes

Because the fractionation of oxygen isotopes between two phases is temperature dependent, the $\delta^{18}O$ of marine carbonate can be used to calculate the temperature of the seawater in which the solid phase was formed. In general, an increase in the temperature of seawater of ~4°C will be recorded as a 1‰ decrease in $\delta^{18}O$ of calcium carbonate. However, the $\delta^{18}O$ of marine carbonate is also dependent upon the oxygen isotope composition of the seawater itself ($\delta^{18}O_w$), which can vary based on global ice volume and local salinity changes. Vital effects, or the deviation of the stable isotope values of an organism from equilibrium due to biological processes, must also be known and must be used to correct the $\delta^{18}O$ values obtained from different calcareous species.

Variations in the $\delta^{18}O_w$ of seawater are the result of Rayleigh distillation of precipitation. Water that is evaporated from the ocean is depleted in ^{18}O relative to mean ocean water and becomes increasingly depleted on its journey to higher latitudes/elevations due to the combined effect of decreasing temperature and an increasing number of rain-out events. Surface water $\delta^{18}O$ values decrease by as much as 1.5‰ between low and high latitude open ocean waters due to Rayleigh distillation (Broecker, 1989). Also, the formation of polar ice sheets from precipitation that is highly enriched in ^{16}O results in a corresponding increase in the ^{18}O content (and $\delta^{18}O_w$ value) of the mean ocean. Today, the oceans have a mean $\delta^{18}O$ value of 0‰, but the $\delta^{18}O$ value of mean ocean water has been estimated at ~-1‰ during the ice-free Early Paleogene and ~1‰ during the glacial maxima of the late Pleistocene.

Estimates of past $\delta^{18}O_w$ have been made based upon $\delta^{18}O$ values of benthic foraminifera, by either assuming negligible changes in bottom water temperatures or by placing constraints on the minimum temperature of deep ocean during particular time periods (Zachos et al., 1994). Researchers have also utilized a variety of independent marine paleothermometers in order to better separate signals of temperature and $\delta^{18}O_w$ in marine carbonates, including the Mg/Ca ratio of foraminiferal calcite and the organic proxy known as TEX-86 that is based upon the number of cyclopentane rings in Crenarchaeota membrane lipids. Each of these techniques has its own set of weaknesses, and as a result, the estimation of $\delta^{18}O_w$, and thus past ice volume, remains an active area of research.

An additional consideration, particularly in coastal areas, is the effect of salinity on $\delta^{18}O_w$. Salinity and $\delta^{18}O_w$ are linearly related, with a slope $\Delta\delta^{18}O_w/\Delta S$ that varies regionally due to Rayleigh distillation and a zero-salinity intercept that reflects the $\delta^{18}O$ value of the local precipitation and runoff. As a result, oceanic regions receiving large freshwater inputs display lower $\delta^{18}O_w$ values relative to the coeval open ocean.

2.2 Carbon Isotopes

The $\delta^{13}C$ of marine carbonate is influenced by a number of processes including surface water productivity, deep water ventilation, and changes in global carbon mass balance. Primary producers preferentially absorb ^{12}C, and organic carbon is therefore

depleted in ^{13}C relative to the VPDB standard, although the magnitude of the depletion depends upon the organism's metabolic pathway (C3, C4, etc.). Thus, in the ocean, ^{12}C is removed from the surface waters by photosynthetic organisms and is exported to the deep ocean, where it is released through respiration, creating a vertical carbon isotope gradient between the surface and deep waters. As a result, the shells of planktonic foraminifera show an enrichment in ^{13}C relative to benthic foraminifera, and changes in the $\Delta\delta^{13}C$ gradient between planktonic and benthic foraminifera can be used to reconstruct past variations in primary productivity.

Due in large part to the role of biologic productivity in the distribution of carbon isotopes in the ocean, deep water masses can obtain distinct $\delta^{13}C$ values that can be used to discern their source region and/or age. Prior to sinking, deepwaters obtain a preformed $\delta^{13}C$ value that is reflective of productivity and air-sea exchange processes in the source region. Deepwater sourced from surface water in which productivity and/or air-sea exchange processes are strong would have a much higher $\delta^{13}C$ value than deepwater sourced from a region in which these processes were inhibited by the presence of sea ice. As a deep water mass circulates throughout the ocean, its $\delta^{13}C$ value changes as it mixes with other water masses and "ages." The longer that a water mass circulates within the deep ocean, the more enriched in ^{12}C it becomes due to the respiration of organic carbon at depth in the ocean. Thus, an interbasinal $\delta^{13}C$ gradient develops in which the oldest water mass in the ocean, currently Pacific Deepwater, exhibits the lowest $\delta^{13}C$ value.

Lastly, changes in global carbon cycling can result in the large-scale redistribution of carbon isotopes amongst the Earth's carbon reservoirs. For example, increased burial of organic carbon in marine sediments would likely raise the $\delta^{13}C$ value of the whole ocean-atmosphere system. In contrast, a decline in continental biomass during the late Pleistocene glaciations has been estimated to have caused a decrease of 0.32‰ in the $\delta^{13}C$ value of the oceanic carbon reservoir (Duplessy et al., 1988).

3. The Early Paleogene Greenhouse

The early Paleogene (~65-40 Ma) is known for its extreme climatic warmth and thus presents a unique opportunity to explore oceanic circulation under unusually high atmospheric CO_2 concentrations. The partial pressure of atmospheric CO_2 (pCO_2) during

the greenhouse world of the early Paleogene has been estimated at 1000-2000+ ppm (Lowenstein and Demicco, 2006; Pagani et al., 2005; Zachos et al., 2008), compared to a modern value of 380 ppm. The highest pCO_2 values of the early Paleogene occurred during brief intervals (less than a few tens of thousands of years) of extreme warmth known as hyperthermals, the largest and best-studied of which is the Paleocene-Eocene Thermal Maximum, or PETM, at ~55 Ma, but several smaller events have also been identified, including the Eocene Thermal Maximum 2 at ~53 Ma (Cramer et al., 2003; Lourens et al., 2005; Zachos et al., 2008). The early Cenozoic hyperthermals were the result of rapid, short-lived injections of isotopically-depleted carbon into the ocean/atmosphere system, as evidenced by negative carbon isotope excursions in both marine and terrestrial records and deep-sea carbonate dissolution horizons.

The PETM was first identified in the Weddell Sea, where benthic and planktonic foraminifera were found to record a short-term negative $\delta^{13}C$ excursion of 2.5-4‰, accompanied by decreases in $\delta^{18}O$ of 1-2‰, near the Paleocene-Eocene boundary (Kennett and Stott, 1991). The negative carbon isotope excursion was rapid, occurring with ~20kyr, and was followed by a more gradual recovery period of ~170 kyr (Röhl et al., 2000). Peak surface water temperatures during the PETM in the shallow Weddell Sea were estimated at ~21°C (Kennett and Stott, 1991), and use of the new organic paleothermometer TEX_{86}'on PETM sediments recently recovered by ACEX indicate that the temperature of Arctic surface waters increased from 18°C to 23°C during the PETM (Sluijs et al., 2006). Considering the large magnitude and rapid onset of the negative carbon isotope excursion, the most attractive explanation for the PETM, and for the smaller hyperthermals that followed, is the sudden dissociation of oceanic methane hydrate deposits, which would have been triggered by an increase in bottom water temperatures preceeding the early Eocene Climatic Optimum (~52-50 Ma) (Dickens et al., 1995). The early Eocene Climatic Optimum, and thus release of methane hydrate during the PETM, could have been driven by increased subaerial volcanism in the mid-Paleocene and early Eocene, particularly in the North Atlantic region (Eldholm and Thomas, 1993; Thomas and Bralower, 2005). Alternatively, Lourens et al. (2005) suggest that the dissociation of methane hydrates during both the PETM and the ETM2 could have been orbitally-forced, as both events appear to correspond to maxima in the

~405 kyr and ~100 kyr eccentricity cycles. In the latter case, the lower amplitude of the carbon isotope excursions displayed during ETM2 and the other lesser hyperthermal events that followed can be attributed to the failure of the oceanic methane hydrate reservoir to fully recover following the PETM and to increased sensitivity of the reservoir to shorter eccentricity cycles during the early Eocene Climatic Optimum (Lourens et al., 2005).

Oceanic circulation patterns during the warm climates of the early Paleogene remain poorly understood. With the high latitude regions too warm to support permanent ice, some have actually argued for a reversal of deep oceanic circulation during the Paleogene in which the sinking of warm, salty waters in low latitude regions (similar to deep waters formed in the Mediterranean and Red Sea today) not only took on increased importance but the upwelling of those waters in the high latitude regions also helped to maintain a warm, equitable polar climate. Originally proposed by Chamberlain (1906), the "Warm Saline Deep Water" hypothesis was invoked by Kennett and Stott (1991) to explain the abrupt warming of global bottom water temperatures at the PETM. Later studies, however, have suggested that before the PETM deepwater production either switched from the high southern latitudes to the high northern latitudes (Bice and Marotzke, 2002; Nunes and Norris, 2006) or went relatively unchanged (Thomas et al., 2003). Based on their study of deep circulation during the warm climates of the late Maastrichtian (~67 Ma), D'Hondt and Arthur (2002) stimate that no more than 11% of late Maastrichtian deep waters could have been produced directly from sea surface evaporation in the low latitudes; instead, evaporation in the low and mid-latitudes likely played a greater role in "preconditioning" the waters delivered to the high latitudes for sinking during the winter months.

From isotopic analysis of Shatsky Rise sediments, Frank et al. (2005) and Thomas (2004) conclude that, although the Southern Ocean was the stronger intermediate water source to the Pacific sector during relatively cool intervals, North Pacific downwelling was greater during intervals of relative warmth. The neodymium and stable isotope data specifically indicate that intermediate water production gradually shifted from the North Pacific to the Southern Ocean during the global cooling of the early Maastrichtian (Frank et al., 2005) and later returned to the North Pacific during the warm climates of the early

Paleogene (65-40 Ma) (Thomas, 2004). Thus, these results suggest that meridional overturning circulation patterns were a consequence and not a cause of climatic change, and that under the tectonic and climatic conditions of the early Paleogene, the North Pacific was less vulnerable to fresh water runoff than it is today (Thomas, 2004). An open Central American Seaway, through which saline, subtropical Atlantic surface waters would have reached the North Pacific basin, likely encouraged overturning in the North Pacific during the early Paleogene (Bice and Marotzke, 2002), although tectonic separation of the North Pacific from the Arctic Ocean during that period may have also played a role (Johnson et al., 1994).

The greatest source of deepwater to the Atlantic sector during the early Paleogene appears to have been the Southern Ocean (Nunes and Norris, 2006; Thomas et al., 2003). Nunes and Norris (2006) report a distinct benthic $\delta^{13}C$ shift in the Atlantic, however, that suggests a brief interval (~40 kyr) of strong North Atlantic overturning concurrent with the onset of the PETM. This shift in overturning circulation has not been detected in the neodymium isotope records available from the Atlantic sector (Thomas et al., 2003). However, a switch to deep North Atlantic overturning at the PETM is in agreement with the results of my study of Eocene Arctic Ocean salinity (**Chapter 4**), which show that the salinity of the Arctic was unusually low during the PETM, perhaps due in part to brief a separation of the Arctic from the North Atlantic Ocean during that period. Mammal migrations are thought to have occurred across the Greenland-Faroe Ridge between Europe and Greenland at the PETM (Knox, 1998), and Bice and Marotzke (2002) find that inclusion of such land bridge in their model simulation of early Paleogene circulation does indeed trigger an abrupt shift to Northern Hemisphere sinking at the PETM.

4. The Icehouse Descent

The incredible warmth of the early Eocene Climatic Optimum was followed by a long-term climatic cooling that culminated in the formation of the first continental-scale ice sheet on Antarctica in the earliest Oligocene (the Oi-1 glaication at ~34 Ma). While sea level and benthic $\delta^{18}O$ records suggest the existence of small, ephemeral ice sheets in the Late Cretaceous and Eocene (Miller et al., 2005b), the Oi-1 glaciation is thought to represent the first major glaciation of Antarctica during which ice extended to the

Antarctic coast. Originally, the onset of Antarctic glaciation was attributed to the thermal isolation of the Southern Ocean by the ACC (Kennett, 1977), but studies now suggest that the full development of the ACC was probably delayed until the opening of the Drake Passage in the latest Oligocene or earliest Miocene (Barker and Thomas, 2004; Lyle et al., 2007; Pfuhl and McCave, 2005). Furthermore, DeConto and Pollard (2003) demonstrate in model simulations that the formation of the ACC alone could not have been responsible for the Oi-1 glaciation, and that declining CO_2 levels and orbital modulation likely played a primary role in the climatic transition instead. These results have been supported by the recent finding of ice-rafted debris dating to ~45 Ma in Arctic and ~38 Ma in the Norwegian Greenland Sea (Eldrett et al., 2007; Moran et al., 2006). Discoveries of this nature are in disagreement with the benthic Mg/Ca results of Lear et al. (2000), which suggested that the ~1-1.5‰ increase in benthic $\delta^{18}O$ recorded at the Oi-1 event was largely the result of an ice-volume increase on Antarctica rather than declining bottom water temperatures, but the integrity of the benthic Mg/Ca paleothermometer during intervals of changing carbonate ion concentration, such as the Eocene/Oligocene boundary, has since been questioned (Lear et al., 2008). Thus, the Oi-1 glaciation is now widely interpreted as the manifestation of a global climatic cooling driven by declining CO_2 levels (Lear et al., 2000; Schouten et al., 2008; Thomas, 2008), but the relative importance of Northern Hemisphere ice during that period remains almost completely unexplored.

From the Oligocene to the middle Miocene, the Antarctic ice sheet was in a transitional state, undergoing many cycles of growth and decay prior to a significant buildup of the East Antarctic Ice Sheet in the middle Miocene (~14 Ma). Estimates of pCO_2 from alkenones suggest a rapid decline in atmospheric CO_2 levels during this interval, with concentrations reaching near modern levels by the latest Oligocene (Pagani et al., 2005). Pälike et al. (2006) have identified that the more extreme Oligocene glaciation events appear to have been paced by the amplitude modulation of the 127 and 96 ka eccentricity cycles, the 1200 ka obliquity cycle, and a 405 ka eccentricity-based forcing of the carbon cycle (Pälike et al., 2006). Interestingly, the 405 ka eccentricity forcing remains coherent with changes in global ice volume and carbon reservoirs into the Miocene, where the cycle is prominently displayed in the carbon isotope maxima of

the well-known Monterey carbon excursion (16.9-13.5 Ma) (Holbourn et al., 2007), but following the dramatic expansion of the cryosphere in the middle Miocene, that 400 kyr cyclity "stretches" into 500 kyr in the $\delta^{13}C$ record and wanes in the $\delta^{18}O$ record (Wang et al., 2004). While the rhythm of Oligocene glaciation and deglaciation is becoming clear, the magnitude of the events is still relatively unresolved. For example, a signficiant deglaciation of East Antarctica in the late Oligocene has been inferred from a decline in benthic $\delta^{18}O$ in composite stable isotope records (Zachos et al., 2001), but Pekar et al. (2006) argue that the $\delta^{18}O$ decrease is actually the artifact of a change in the location of the source data from the Southern Ocean before 25 Ma to Atlantic ODP Site 929 after 25 Ma. Thus, Pekar et al. (2006) argue that, although ice volume likely fluctuated on orbital timescales, Antarctica could have remained mostly glaciated (equivalent to at least 50% of present-day EAIS) throughout the late Oligocene.

Over the course of the Oligocene and Miocene, oceanic circulation patterns assumed a greater resemblance to those of the modern day. Two tectonic events, the subsidence of the Greenland-Scotland Ridge and the shoaling of the Central American Seaway, likely played important roles in the evolution of deep-sea circulation during this time period. Subsidence of the Greenland-Faroe Ridge would have allowed Norwegian Overflow Water, an important component of modern NADW, to enter the North Atlantic Ocean for the first time, thus marking an important step in the evolution of the modern mode of Atlantic circulation. From their analysis of $\delta^{13}C$ data and the subsidence history of the Greenland-Faroe Ridge, Wright and Miller (1996) place the introduction of Norwegian Overflow Water to the world ocean at ~20 Ma, synchronous with a switch in siliceous sedimentation from the North Atlantic to the marginal North Pacific and eastern equatorial Pacific in the early middle Miocene (Keller and Barron, 1983). However, Via and Thomas (2006) argue based on evidence of drift sedimentation in the North Atlantic and Nd data from the southeastern Atlantic that the timing of the first overflow from the Norwegian-Greenland Sea was actually closer to 33 Ma, the time of the Oi-1 glaciation. Thus, the depth history of the Greenland-Faroe ridge may be more complicated than previously thought.

As for the second gateway, the Central American Seaway (CAS), biostratigraphic work by Duque-Caro (1990) indicates a major uplift of the Panama sill to

a depth of ~1000 m between 13 and 12 Ma, which model simulations show would likely have impeded the flow of NADW into the Pacific Ocean (Nisancioglu et al., 2003). The results of Lyle et al. (1995), which show a dramatic shoaling of the calcium carbonate compensation depth in the Pacific Ocean at ~10 Ma (known as the "late Miocene carbonate crash"), are consistent with this scenario, indicating an end to the presence of NADW in the Pacific in the late middle Miocene. The results of a modeling study by von der Heydt and Dijkstra (2006) demonstrate that the flow of NADW through the CAS may actually have been impeded much earlier than the late middle Miocene due to the widening of the Southern Ocean passages and closure of the Tethys seaway, and a reversal of CAS flow in the early Miocene, which they obtain in their study, is consistent with a demise of warm water corals in the Caribbean during that period. In their simulation, von der Heydt and Dijkstra (2006) find that, while shallow overturning circulation could have occurred in both the North Atlantic and North Pacific during the Oligocene, following the reversal of flow through the CAS in the Miocene, the presence of AABW would have taken on increased importance in the deep Pacific Ocean.

The build-up of the East Antarctic Ice Sheet in the middle Miocene is recorded by an increase in benthic $\delta^{18}O$ values of 1-1.3‰ between ~16 and 12.5 Ma (Miller and Katz, 1987; Shackleton and Kennett, 1975), as well as significant changes in benthic and planktonic foraminifera species, most notably a near disappearance of Oligocene to lower Miocene benthic assemblages during that period (Keller and Barron, 1983; Woodruff and Douglas, 1981). The timing of the establishment of the West Antarctic Ice Sheet (WAIS) within the Miocene has unfortunately not been as easy to constrain. Formation of the WAIS has generally been assigned to the late Miocene, as hypothesized by Ciesielski et al. (1982) and Kennett and Barker (1990) based on late Miocene depositional changes in the Southern Ocean such as the appearance of terrigenous turbidites on the Weddell abyssal plain and the arrival of hemipelagic muds, IRD, and increased quantities of chlorite and illite at ODP Site 696. The amplitude of benthic $\delta^{18}O$ variations is remarkably small during the late Miocene (Westerhold et al., 2005), but due to its low elevation and small, marine-based nature build-up of the WAIS could have had very little impact on oceanic $\delta^{18}O$ values (Ciesielski et al., 1982). While an increase in benthic $\delta^{18}O$ has been noted in some locales, particularly ODP Site 1088 in the subantarctic Atlantic,

in the latest Miocene (~7.4-6.9 Ma), it is by no means ubiquitously present and may thus be better explained by a cooling of deepwaters sinking in the Southern Ocean rather than an increase in ice volume (Billups, 2002). Alternatively, evidence has recently been presented for several grounding events of the WAIS on the Ross Sea outer continental shelf during the Middle Miocene, which would suggest that the WAIS may have developed more or less in synchrony with the EAIS (Chow and Bart, 2003). However, this hypothesis is not widely favored because the conditions necessary for grounding the ice sheet below sea level are not thought to have been met until well after the full establishment of the EAIS (Ciesielski et al., 1982).

The late Miocene, with fully established Antarctic ice sheets and a tectonic configuration similar to that of the present day, presents an interesting opportunity to examine oceanic circulation patterns independent of the influence of the ice sheets that would later develop in the Northern Hemisphere. **Chapter 2** examines a new stable isotope record from the abyssal subantarctic southeast Pacific that not only provides a new perspective on how oceanic circulation has evolved since the late Miocene, but also suggests that the Southern Ocean may have had an active role in amplification of Northern Hemisphere Glaciation. At the focus of Chapter 2 are two large negative $\delta^{13}C$ excursions, each of which may have been associated with significant changes in the ventilation of the deep ocean since the Late Miocene. The first is a permanent negative $\delta^{13}C$ shift known as the Late Miocene Carbon Shift (LMCS) that occurred between 7.7 and 6.6 Ma and has been recognized in stable isotope records from all of the major ocean basins (Tedford and Kelley, 2004). While the carbon shift does have a component that can be attributed to a change global carbon mass balance associated with the expansion of C4 plants in the late Miocene (Diester-Haass et al., 2006) of interest here is the possibility that the LMCS also involved a change in interbasinal $\delta^{13}C$ gradients and thus may have marked an important step in the evolution of modern oceanic circulation (Hodell and Venz-Curtis, 2006).

The second negative $\delta^{13}C$ excursion discussed in Chapter 2 has previously been observed only in carbon isotope records from the deep subantarctic Atlantic (Hodell et al., 2002; Hodell and Venz, 1992; Hodell and Venz-Curtis, 2006), and thus recognition of this feature in the abyssal subantarctic Pacific region is of great interest. The $\delta^{13}C$

excursion spans a period known as the late Pliocene climatic transition (LPCT), which consists of a series of $\delta^{18}O$ enrichment events that record the onset and amplification of Northern Hemisphere Glaciation between ~3.1 and 2.4 Ma. Thus, the excursion indicates changes in the circulation and ventilation of the Southern Ocean during a critical period of cryospheric development. Chapter 2 discusses the nature of these changes and whether the deep Southern Ocean could hold the key to the increased growth of the Northern Hemisphere ice sheets in the Late Pliocene.

The development of glacial climate over the Plio-Pleistocene was punctuated by multiple steps or "transitions." The best known of these transitions is the Mid-Pleistocene Transition at ~0.9 Ma (MIS 22), which marked a change in the dominant period of the glacial-interglacial cycles from 41 ka ("obliquity-based") to 100 ka ("eccentricity-based"). A second, known as the Mid-Brunhes Event occurred at the termination of MIS 12 (~0.42 Ma) and brought with it interglacial intervals characterized by warmer temperatures and/or less ice volume (Hodell et al., 2003b). Lesser known is a transition at ~1.5 Ma (MIS 52) that marked a significant reduction in the ventilation of deep Southern Ocean relative to that of the Pacific during glacial intervals (Venz and Hodell, 2002). Wang et al. (2004) observe that $\delta^{13}C$ maxima, which are recorded during MIS 13, MIS 27-29 and MIS 53-57, preceded each of these climatic transitions, thus suggesting that long-term changes in carbon reservoirs, which operate at their own ~500 kyr cyclicty, can modify the response of the climate system to orbital forcing. These $\delta^{13}C$ maxima have been associated with changes in productivity, the oceanic "rain ratio," and increased carbonate dissolution in the Indo-Pacific (Wang et al., 2004). In **Chapter 3**, based upon my study of hiatuses in the subantarctic Pacific cores, I suggest that these intervals, as well as a period of climatic amelioration known as the early Pliocene warm period, are also associated with an increase the strength of oceanic circulation. Considering that the Earth system is currently passing through a new carbon maximum event, which began at MIS 3 (~50-60 ka), improved understanding of the long-term carbon cycle is of particular importance, and as Wang et al. (2004) stress, without that understanding, the prediction future natural changes in global climate system is compromised.

REFERENCES

Barker, P.F., and Thomas, E., 2004, Origin, signature and palaeoclimatic influence of the Antarctic Circumpolar Current: Earth Science Reviews, v. 66, p. 143-162.

Bice, K.L., and Marotzke, J., 2002, Could changing ocean circulation have destabilized methane hydrate at the Paleocene/Eocene boundary?: Paleoceanography, v. 17, p. 1018, doi:10.1029/2001PA000678.

Billups, K., 2002, Late Miocene through early Pliocene deep water circulation and climate change viewed from the sub-Antarctic South Atlantic: Palaeogeography, Palaeoclimatology, Palaeoecology, v. 185, p. 287-307.

Broecker, W.S., 1989, The salinity contrast between the Atlantic and Pacific oceans during glacial time: Paleoceanography, v. 4, p. 207-212.

Chamberlain, T.C., 1906, On a possible reversal of deep-sea circulation and its influence on geologic climates: Journal of Geology, v. 14, p. 363-373.

Chow, J.M., and Bart, P.J., 2003, West Antarctic ice sheet grounding events on the Ross Sea outer continental shelf during the middle Miocene: Palaeogeography, Palaeoclimatology, Palaeoecology, v. 198, p. 169-186.

Ciesielski, P.F., Ledbetter, M.T., and Ellwood, B.B., 1982, The development of Antarctic glaciation and the Neogene paleoenvironment of the Maurice Ewing Bank: Marine Geology, v. 46, p. 1-51.

Cramer, B.S., Wright, J.D., Kent, D.V., and Aubry, M.-P., 2003, Orbital climate forcing of $\delta^{13}C$ excursions in the late Paleocene-early Eocene (chrons C24n-C25n): Paleoceanography, v. 18, p. 1097, doi:10.1029/2003PA000909.

de Boer, A.M., Toggweiler, J.R., and Sigman, D.M., 2008, Atlantic dominance of the meridional overturning circulation: Journal of Physical Oceanography, v. 38, p. 435-449.

DeConto, R.M., and Pollard, D., 2003, Rapid Cenozoic glaciation of Antarctica induced by declining atmospheric CO_2: Nature, v. 421, p. 245-249.

D'Hondt, S., and Arthur, M.A., 2002, Deep water in the late Maastrichtian ocean: Paleoceanography, v. 17, p. 1008, 10.1029/1999PA000486.

Dickens, G.R., O'Neil, J.R., Rea, D.K., and Owen, R.M., 1995, Dissociation of oceanic methane hydrate as a cause of the carbon isotope excursion at the end of the Paleocene: Paleoceanography, v. 10, p. 965-971.

Diester-Haass, Billups, K., and Emeis, K.C., 2006, The late Miocene carbon isotope shift and marine biological productivity: was there a (dusty) link?: Paleoceanography, v. 21, p. PA4216, doi:10.1029/2006PA001267.

Duplessy, J.-C., Shackleton, N.J., Fairbanks, R.G., Labeyrie, L., Oppo, D.W., and Kallel, N., 1988, Deepwater source variations during the last climatic cycle and their impact on the global deepwater circulation: Paleoceanography, v. 3, p. 343-360.

Duque-Caro, H., 1990, Neogene stratigraphy, paleoceanography and paleobiology in northwest South America and the evolution of the Panama Seaway: Palaeogeography, Palaeoclimatology, Palaeoecology, v. 77, p. 203-234.

Eldholm, O., and Thomas, E., 1993, Environmental impact of volcanic margin formation: Earth and Planetary Science Letters, v. 117, p. 319-329.

Eldrett, J.S., Harding, I.C., Wilson, P.A., Butler, E., and Roberts, A.P., 2007, Continental ice in Greenland during the Eocene and Oligocene: Nature, v. 446, p. 176-179, doi:10.1038/nature05591.

Frank, T.D., Thomas, D.J., Leckie, R.M., Arthur, M.A., Brown, P.R., Jones, K., and Lees, J.A., 2005, The Maastrichtian record from Shatsky Rise (northwest Pacific): A tropical perspective on global ecological and oceanographic changes: Paleoceanography, v. 20, p. PA1008, doi:10.1029/2004PA001052.

Gregory, J.M., Dixon, K.W., Stouffer, R.J., Weaver, A.J., Driesschaert, E., Eby, M., Fichefet, T., Hasumi, H., Hu, A., Jungclaus, J.H., Kamenkovich, I.V., Levermann, A., Montoya, M., Murakami, S., Nawrath, S., Oka, A., Sokolov, A.P., and Thorpe, R.B., 2005, A model intercomparison of changes in the Atlantic thermohaline circulation response to increasing atmospheric CO_2 concentration: Geophysical Research Letters, v. 32, p. L12703, doi:10.1029/2005GL023209.

Hodell, D.A., Gersonde, R., and Blum, P., 2002, Leg 177 Synthesis: Insights into Southern Ocean paleoceanography on tectonic to millennial timescales, *in* Gersonde, R., Hodell, D.A., and Blum, P., eds., Proceedings of the Ocean Drilling Program, Scientific Results, Volume 177: College Station, TX, Ocean Drilling Program.

Hodell, D.A., and Venz, K., 1992, Toward a high-resolution stable isotope record of the Southern Ocean during the Pliocene-Pleistocene (4.8 to 0.8 Ma), *in* Kennett, J.P., and Warnke, D.A., eds., The Antarctic Paleoenvironment: A perspective on global change, Antarct. Res. Ser., Volume 56: Antarctic Research Series: Washington D.C., AGU, p. 265-310.

Hodell, D.A., and Venz-Curtis, K.A., 2006, Late Neogene history of deepwater ventilation in the Southern Ocean: Geochemistry, Geophysics, Geosystems, v. 7, p. Q09001, doi:10.1029/2005GC001211.

Holbourn, A., Kuhnt, W., Schulz, M., Flores, J.-A., and Andersen, N., 2007, Orbitally-paced climate evolution during the middle Miocene "Monterey" carbon-isotope excursion: Earth and Planetary Science Letters, v. 261, p. 534-550.

Johnson, G.L., Pogrebitsky, J., and Macnab, R., 1994, Arctic Structural Evolution: Relationship to Paleoceanography, *in* Johannessen, O.M., Muench, R.D., and Overland, J.E., eds., The Polar Oceans and Their Role in Shaping the Global Environment: The Nansen Centennial Volume: Geophysical Monograph Series 85: Washington D.C., American Geophysical Union, p. 285-294.

Keller, G., and Barron, J.A., 1983, Paleoceanographic implications of Miocene deep-sea hiatuses: Geological Society of America Bulletin, v. 94, p. 590-613.

Kennett, J.P., 1977, Cenozoic evolution of Antarctic glaciation, the circum-Antarctic oceans and their impact on global paleoceanography: Journal of Geophysical Research, v. 82, p. 3843-3859.

Kennett, J.P., and Barker, P.F., 1990, Latest Cretaceous to Cenozoic climate and oceanographic developments in the Weddell Sea, Antarctica: An ocean-drilling perspective: Proceedings of Ocean Drilling Program, Scientific Results, v. 113, p. 937-960.

Kennett, J.P., and Stott, L.D., 1991, Abrupt deep-sea warming, palaeoceanographic changes and benthic extinctions at the end of the Palaeocene: Nature, v. 353, p. 225-229.

Knox, R.W.O.B., 1998, The tectonic and volcanic history of the North Atlantic region during the Paleocene-Eocene transition: Implications for NW European and global biotic events, *in* Aubry, M.P., Lucas, S.G., and Berggren, W.A., eds., Late Paleocene-Early Eocene climatic and biotic events in the marine and terrestrial records: New York, Columbia University Press, p. 91-102.

Koch, P.L., Tuross, N., and Fogel, M.L., 1997, The effects of sample treatment and diagenesis on the isotopic integrity of carbonate in biogenic hydroxylapatite.: Journal of Archaeological Science, v. 24, p. 417-429.

Lear, C.H., Bailey, T.R., Pearson, P.N., Coxall, H.K., and Rosenthal, Y., 2008, Cooling and ice growth across the Eocene-Oligocene transition: Geolgy, v. 36, p. 251-254.

Lear, C.H., Elderfield, H., and Wilson, P.A., 2000, Cenozoic deep-sea temperatures and global ice volumes from Mg/Ca in benthic foraminifral calcite: Science (Washington, D. C., 1883-), v. 287, p. 269-272.

Lourens, L.J., Sluijs, A., Kroon, D., Zachos, J.C., Thomas, E., Röhl, U., Bowles, J., and Raffi, I., 2005, Astronomical pacing of late Palaeocene to early Eocene global warming events: Nature, v. 435, p. 1083-1087, doi:10.1038/nature03814.

Lowenstein, T.K., and Demicco, R.V., 2006, Elevated Eocene atmospheric CO_2 and its subsequent decline: Science, v. 313, p. 1928.

Lyle, M., Dadey, K.A., and Farrell, J.W., 1995, The Late Miocene (11-8 Ma) eastern Pacific carbonate crash: Evidence for reorganization of deep-water circulation by the closure of the Panama gateway., *in* Pisias, N.G., Mayer, L.A., Janecek, T.R., Palmer-Julson, A., and van Andel, T.H., eds., Proceedings of the Ocean Drilling Program, Scientific Results, 138: College Station, Texas, Ocean Drilling Program, p. 821-838.

Lyle, M., Gibbs, S., Moore, T.C., and Rea, D.K., 2007, Late Oligocene initiation of the Antarctic Circumpolar Current: Evidence from the South Pacific: Geology, v. 35, p. 691-694.

Meehl, G.A., Stocker, T.F., Collins, W.D., Friedlingstein, P., Gaye, A.T., Gregory, J.M., Kitoh, A., Knutti, R., Murphy, J.M., Noda, A., Raper, S.C.B., Watterson, I.G., Weaver, A.J., and Zhao, Z.-C., 2007, Global Climate Projections, *in* Solomon, S., Quin, D., Manning, M., Chen, Z., Marquis, M., Averyt, K.B., Tignor, M., and Miller, H.L., eds., Climate Change 2007: The Physical Science Basis. Contribution of Working Group 1 to the Fourth Assessment Report of the Intergovernmental Panel on Climate Change: Cambridge, U.K. and New York, N.Y., Cambridge University Press.

Miller, K.G., and Katz, M.E., 1987, Oligocene to Miocene benthic foraminiferal and abyssal circulation changes in the North Atlantic: Micropaleontology, v. 33, p. 97-149.

Miller, K.G., Wright, J.D., and Browning, J.V., 2005, Visions of ice sheets in a greenhouse world: Marine Geology, v. 217, p. 215-231.

Moran, K., Backman, J., Brinkhuis, H., Clemens, S.C., Cronin, T.M., Dickens, G.R., Eynaud, F., Gattacceca, J., Jakobsson, M., Jordan, R.W., Kaminski, M., King, J., Koc, N., Krylov, A., Martinez, N., Matthiessen, J., McInroy, D., MOore, T.C., Onodera, J., O'Regan, M., Palike, H., Rea, B., Rio, D., Sakamoto, T., Smith, D.C., Stein, R., St John, K., Suto, I., Suzuki, N., Takahashi, K., Watanabe, M., Yamamoto, M., Farrell, J., Frank, M., Kubik, P., Jokat, W., and Kristoffersen, Y., 2006, The Cenozoic palaeoenvironment of the Arctic Ocean: Nature, v. 441, p. 601-605.

Nisancioglu, K.H., Raymo, M.E., and Stone, P.H., 2003, Reorganization of Miocene deep water circulation in response to the shoaling of the Central American Seaway: Paleoceanography, v. 18, p. 1006, doi:10.1029/2002PA000767.

Nunes, F., and Norris, R.D., 2006, Abrupt reversal in ocean overturning during the Palaeocene/Eocene warm period: Nature, v. 439, p. 60-63.

Pagani, M., Zachos, J.C., Freeman, K.H., Tipple, B., and Bohaty, S., 2005, Marked Decline in atmospheric carbon dioxide concentrations during the Paleogene: Science, v. 309, p. 600-603.

Pälike, H., Norris, R.D., Herrle, J.O., Wilson, P.A., Coxall, H.K., Lear, C.H., Shackleton, N.J., Tripati, A.K., and Wade, B.S., 2006, The heartbeat of the Oligocene climate system: Science, v. 314, p. 1894-1898.

Pekar, S.F., DeConto, R.M., and Harwood, D.M., 2006, Resolving a late Oligocene conundrum: Deep-sea warming and Antarctic glaciation: Palaeogeography, Palaeoclimatology, Palaeoecology, v. 231, p. 29-40.

Pfuhl, H.A., and McCave, I.N., 2005, Evidence for late Oligocene establishment of the Antarctic Circumpolar Current: Earth and Planetary Science Letters, v. 235, p. 715-728.

Röhl, U., Bralower, T.J., Norris, R.D., and Wefer, G., 2000, New chronology for the late Paleocene thermal maximum and its environmental implications: Geology, v. 28, p. 927-930.

Schouten, S., Eldrett, J.S., Greenwood, D.R., Harding, I.C., Baas, M., and Sinninghe Damsté, J.S., 2008, Onset of long-term cooling of Greenland near the Eocene-Oligocene boundary as revealed by branched tetraether lipids: Geolgy, v. 36, p. 147-150.

Shackleton, N.J., and Kennett, J.P., 1975, Paleotemperature history of the Cenozoic and initiation of Antarctic glaciation: oxygen and carbon isotopic analyses in DSDP Sites 277, 279, and 281, *in* Kennett, J.P., and Houtz, J.P., eds., Init. Rep. DSDP, Volume 29, p. 743-755.

Sluijs, A., Schouten, S., Pagani, M., Woltering, M., Brinkhuis, H., Damste, J.S.S., Dickens, G.R., Huber, M., Reichart, G.-J., Stein, R., Matthiessen, J., Lourens, L.J., Pedentchouk, N., Backman, J., Moran, K., and Scientists, E., 2006, Subtropical Arctic Ocean temperatures during the Paleocene/Eocene thermal maximum: Nature, v. 441, p. 610-613.

Tedford, R.A., and Kelley, D.C., 2004, A deep-sea record of the Late Miocene carbon shift from the Southern Tasman Sea, *in* Exon, N., Kennett, J.P., and Malone, M., eds., The Cenozoic Southern Ocean: Tectonics, Sedimentation and Climate Change between Australia and Antarctica, Geophysical Union Monograph Series 151: Geophysial Monograph: Washington D.C., American Geophysical Union, p. 273-290.

Thomas, D.J., 2004, Evidence for production of North Pacific deep waters during the early Cenozoic warm interval: Nature, v. 430, p. 65-68.

Thomas, D.J., and Bralower, T.J., 2005, Sedimentary trace element constraints on the role of North Atlantic Igneous Province volcanism in late Paleocene-early Eocene environmental change: Marine Geology, v. 217, p. 233-254.

Thomas, D.J., Bralower, T.J., and Jones, C.E., 2003, Neodymium isotopic reconstruction of late Paleocene-early Eocene thermohaline circulation: Earth and Planetary Science Letters, v. 209, p. 309-322.

Thomas, E., 2008, Descent into the icehouse: Geology, v. 36, p. 191-192.

Via, R.K., and Thomas, D.J., 2006, Evolution of Atlantic thermohaline circulation: Early Oligocene onset of deep-water production in the North Atlantic: Geology, v. 34, p. 441-444.

von der Heydt, A., and Dijkstra, H.A., 2006, Effect of ocean gateways on the global ocean circulation in the late Oligocene and early Miocene: Paleoceanography, v. 21, p. PA1011, doi:10.1029/2005PA001149.

Wang, P., Tian, J., Cheng, X., Liu, C., and Xu, J., 2004, Major Pleistocene stages in a carbon perspective: The South China Sea record and its global comparison: Paleoceanography, v. 19, p. PA4005, doi:10.1029/2003PA00091.

Westerhold, T., Bickert, T., and Röhl, U., 2005, Middle to late Miocene oxygen isotope stratigraphy of ODP Site 1085 (SE Atlantic): new constrains on Miocene climate variability and sea-level fluctuations: Palaeogeography, Palaeoclimatology, Palaeoecology, v. 217, p. 205-222.

Woodruff, F., and Douglas, R.G., 1981, Response of deep-sea benthic foraminifera to Miocene paleoclimatic events, DSDP Site 289: Marine Micropaleontology, v. 6, p. 617-632.

Wright, J.D., and Miller, K.G., 1996, Control of North Atlantic Deep Water circulation by the Greenland-Scotland Ridge: Paleoceanography, v. 11, p. 157-170.

Zachos, J., Pagani, M., Sloan, L., Thomas, E., and Billups, K., 2001, Trends, rhythms, and aberrations in global climate 65 Ma to present: Science, v. 292, p. 686-693.

Zachos, J., Stott, L.D., and Lohmann, K.C., 1994, Evolution of early Cenozoic marine temperatures: Paleoceanography, v. 9, p. 353-387.

Zachos, J.C., Dickens, G.R., and Zeebe, R.E., 2008, An early Cenozoic perspective on greenhouse warming and carbon-cycle dynamics: Nature, v. 451, p. 279-283, doi:10.1038/nature06588.

Chapter 2

Ventilation of the Abyssal Southern Ocean During the Late Neogene: A New Perspective from the Subantarctic Pacific

Abstract

New stable isotope records from the abyssal subantarctic Pacific reveal the development of cold, poorly ventilated bottom waters in the Southern Ocean during the late Pliocene climate transition (LPCT) at ~2.75 Ma. Carbon isotope data indicate that poorly ventilated conditions likely persisted following the LPCT until ~1.7 Ma, when both benthic and planktonic $\delta^{13}C$ values finally show a return to pre-LPCT values, suggesting that the deep Southern Ocean may have played a role in the amplification of Northern Hemisphere Glaciation during the late Pliocene through the sequestration of CO_2. These results are in sharp contrast to those obtained for the late Miocene carbon shift (LMCS), during which $\delta^{13}C$ values in the abyssal subantarctic Pacific remain nearly identical to those previously reported from ODP Site 704 in the South Atlantic, indicating a well-mixed late Miocene Southern Ocean free of vertical or interbasinal $\delta^{13}C$ gradients.

1. Introduction

Carbon isotopic records from the South Atlantic reveal stepped declines in the $\delta^{13}C$ of deepwater in the Southern Ocean as climatic conditions deteriorated over the late Neogene. The first of these declines, the late Miocene carbon shift (LMCS) at ~7 Ma, has been identified in carbon isotope records from all major ocean basins, while the second shift during the late Pliocene climatic transition (LPCT) at ~2.7 Ma has been identified only in benthic $\delta^{13}C$ records from >2500 m depth in the Atlantic sector of the Southern Ocean (Hodell et al., 2002; Hodell and Venz, 1992; Hodell and Venz-Curtis, 2006). Both the LMCS and the LPCT were associated with shifts in interbasinal $\delta^{13}C$ gradients in which carbon isotope values in the South Atlantic became increasingly "Pacific-like," and thus it has been posited that these carbon events may mark step

toward increased CO_2 sequestration in the deep Southern Ocean over the late Neogene (Hodell and Venz-Curtis, 2006).

The ocean holds 50 times more inorganic carbon than the atmosphere, and abundant evidence now exists for significant changes in Southern Ocean circulation during the late Quaternary glaciations. While changes in ocean biology have often been invoked to explain low glacial atmospheric CO_2 levels, less than half of the observed glacial-interglacial variation in atmospheric CO_2 can be explained by changes to the marine biological pump (Kohfeld et al., 2005), requiring that CO_2 also be sequestered within the deep ocean by physical mechanisms. In the modern ocean, the upwelling of Circumpolar Deepwater at the Antarctic Divergence is the primary mechanism by which waters deeper than 2500 m are exposed to the atmosphere, and with this exposure, CO_2 respired at depth can be released. However, during glacial periods, ventilation of these deep waters may be inhibited by physical changes such as increased surface water stratification (Brunnelle et al., 2007; de Boer et al., 2007; Francois et al., 1997; Jaccard et al., 2005; Sigman et al., 1999; Sigman et al., 2007; Sigman et al., 2004), increased sea ice cover (Adkins et al., 2002; Stephens and Keeling, 2000), and decreased upwelling (Toggweiler et al., 2006; Watson and Naveira Garabato, 2006).

Evidence now suggests that many of the physical mechanisms that likely hindered the release of respired CO_2 from the deep Southern Ocean during the glaciations of the late Quaternary were also active during the late Pliocene. While the Northern Hemisphere ice sheets were still in their infancy during the late Pliocene, evidence suggests that Antarctica was reaching an advanced state of glaciation and that the circulation of the Southern Ocean was altered as a result. For example, nitrogen isotopes support for the development of a strong halocline in the Antarctic and subarctic Pacific coincident with the onset of Northern Hemisphere Glaciation at 2.73 Ma (Haug et al., 1999; Sigman et al., 2004), and Burckle et al. (1990) and Kennett and Barker (1990) present diatom evidence for the expansion of Antarctic sea ice to the South Orkney microcontinent by 2.5-2.4 Ma. Most importantly, the decline in benthic $\delta^{13}C$ in the deep South Atlantic (>2500 m) at ~2.7 Ma suggests that a consequence of this late Pliocene expansion of the Antarctic cryosphere may have been increased sequestration of CO_2 within the deep Southern Ocean (Hodell and Venz-Curtis, 2006).

Unfortunately, our current knowledge of carbon isotope changes in the Southern Ocean during the late Neogene is based almost entirely on stable isotope records from sediment cores recovered from the South Atlantic region. Thus, while Hodell and Venz-Curtis (2006) have shown that the LMCS and LPCT were associated with shifts in interbasinal $\delta^{13}C$ gradients between the North Atlantic, South Atlantic, and Pacific Oceans, the nature, or in the case of the LPCT, even the existence, of these shifts in the Pacific-sector of the Southern Ocean has remained largely unknown. The Late Pliocene was a critical period for the growth and expansion of the Northern Hemisphere ice sheets, and a decline in atmospheric pCO_2 to preindustrial levels may have been a requirement for the initiation of ice sheets in the Northern Hemisphere (Lunt et al., 2008). Thus a greater understanding of the magnitude and extent of the carbon isotope shift associated with the LPCT is needed in order to better elucidate the carbon budget of the deep Southern Ocean during the late Pliocene.

Herein I offer new stable isotope records from piston cores obtained from the poorly understood subantarctic Pacific region. Not only do these new records provide a circum-Antarctic perspective for the carbon isotope shifts associated with the LMCS and LPCT, but these piston cores were also obtained from depths of up to 4300 m and are therefore among the deepest stable isotope records yet available from the late Neogene Southern Ocean.

2. Background

2.1 $\delta^{13}C$ as a Tracer for Changes in Deepwater Circulation

2.1.1 Controls on the $\delta^{13}C$ of Deepwater

$\delta^{13}C$ is a valuable water mass tracer that can be used to reconstruct deepwater circulation patterns. Due in large part to the role of biologic productivity in the distribution of carbon isotopes in the ocean, deep water masses can obtain distinct $\delta^{13}C$ values that can be used to discern their source region and/or age. Prior to sinking, deepwaters obtain a preformed $\delta^{13}C$ value that is reflective of productivity and air-sea exchange processes in the source region. Deepwater sourced from surface water in which productivity and/or nutrient utilization is high will have a high $\delta^{13}C$ value and a low nutrient concentration compared to deepwater sourced in regions of low

productivity/nutrient utilization. For example, in the modern ocean, North Atlantic Deepwater (NADW) has $\delta^{13}C$ values between 1.0 and 1.5‰ due to high nutrient utilization in its source waters, which originate in the subtropics above a strong thermocline, whereas Antarctic Bottom Water (AABW) has an average $\delta^{13}C$ value of 0.3‰ due to nutrient underutilization near Antarctica (Kroopnick, 1985). During the LGM, stratification of Antarctic surface waters, as suggested by Francois et al. (1997), would have reduced exchange between nutrient-rich deepwaters and the surface, resulting in lower productivity and a lower preformed $\delta^{13}C$ value for AABW.

The effect of air-sea exchange on the preformed $\delta^{13}C$ value in the source region is dependent upon temperature, wind speed, and residence time in the source area. Thus, while the isotopic equilibration of the dissolved inorganic carbon (DIC) in the surface water with atmospheric CO_2 raises the $\delta^{13}C$ value of the water under cold temperatures and lowers it under warm temperatures, the residence time of the water at the air-sea interface is usually shorter than the time required to reach isotopic equilibrium. Thus, the influence of air-sea exchange is usually higher in areas where wind speeds are high, such as the modern subantarctic, where planktonic foraminifera record a $\delta^{13}C$ enrichment of up to 1‰ (Broecker and Maier-Reimer, 1992; Charles and Fairbanks, 1990; Lynch-Stieglitz et al., 1995; Ninnemann and Charles, 1997). In comparison, the air-sea exchange signature of the modern North Atlantic is low (-0.4‰) due to less equilibration with the atmosphere at low temperatures, and Southern Ocean surface waters bear an intermediate signature (+0.2‰) (Lynch-Stieglitz and Fairbanks, 1994). The development of sea ice in the source regions acts to further decrease the preformed $\delta^{13}C$ value of deepwater, as not only is gas exchange reduced, but productivity as well

As a deepwater mass circulates within the ocean, its $\delta^{13}C$ value will evolve as it mixes with other water masses and "ages," accumulating ^{12}C as sinking organic carbon is oxidized and incorporated into the bottom water mass. The most nutrient-rich water ($\delta^{13}C \approx 0$) in the ocean today is found at mid-depth in the North Pacific (~2000 m), where nutrients become "trapped" as PDW upwells to return south at mid-depth, mixing with CDW and increasing its $\delta^{13}C$ value along its path (Matsumoto et al., 2002).

2.1.2 $\delta^{13}C$ Distribution in the Glacial Ocean

The carbon isotope distribution in the glacial ocean appears to have been fundamentally different from that of the present day. First of all, a decline in continental biomass during glaciations has been estimated to have caused a decrease of 0.32‰ in the $\delta^{13}C$ value of the ocean (Duplessy et al., 1988), a change that should be recorded equally in all $\delta^{13}C$ records. However, additional changes to the $\delta^{13}C$ values of foraminifera indicate significant modifications to oceanic circulation. One of the best resolved changes is a reduction in the formation of NADW during the Last Glacial Maximum (LGM) that resulted in a shoaling and northward migration of the mixing front between AABW and NADW (Curry and Oppo, 2005; Duplessy et al., 1988; Oppo and Fairbanks, 1987). Thus, the deep North Atlantic was filled with nutrient-rich AABW, and nutrient-depleted Glacial North Atlantic Intermediate Water (GNAIW) became important above a depth of 2000 meters.

Circulation changes in the Pacific Ocean are not as well understood as those in the Atlantic, but $\delta^{13}C$ data suggest that during the LGM, the nutrient-rich, low $\delta^{13}C$ water mass at mid-depth in the North Pacific shifted downward to depth of 2500-3000 m and that a distinct upper water mass with a high $\delta^{13}C$ value was present above 2000 m (Keigwin, 1998; Matsumoto et al., 2002) . Although the possibility exists that the high $\delta^{13}C$ water mass was sourced from GNAIW or subantarctic water (Lynch-Stieglitz et al., 1996), a more likely scenario is that the water was newly-ventilated within the North Pacific and was perhaps a stronger and more deeply penetrating version of today's North Pacific Intermediate Water (NPIW) (Keigwin, 1998; Matsumoto et al., 2002). Modern NPIW is defined by a salinity minimum between 300-800 m depth and is thought to be sourced from brine rejection in the Sea of Okhotsk. During the LGM, sea ice formation, and thus brine rejection, may have increased NPIW production in the Sea of Okhotsk (Hendy and Kennett, 2003) and/or along the Bering Shelf (Ohkushi et al., 2003).

In the Atlantic sector of the Southern Ocean, Ninnemann and Charles (2002) find $\delta^{13}C$ evidence for the existence of a sharp chemocline at 2.7 km during the LGM that separated well-ventilated intermediate waters with $\delta^{13}C$ values similar to modern values from poorly ventilated deep waters with a $\delta^{13}C$ signature ~1‰ lower than modern. During glacials after 1.55 Ma, $\delta^{13}C$ values in the deep South Atlantic actually became lower than those of deep Pacific (Hodell et al., 2002; Hodell and Venz-Curtis, 2006), a

perplexing phenomenon because such variations cannot entirely be explained by declines in NADW. Nicknamed the "Southern Ocean low $\delta^{13}C$" problem, the altered $\delta^{13}C$ gradient implies a fundamental change in Southern Ocean circulation during glacial events since 1.55 Ma (Ninnemann and Charles, 2002). Hodell and Venz Curtis (2006) propose that the change in $\delta^{13}C$ likely reflects reduced ventilation of the deep Southern Ocean resulting from changes in the Antarctic source region such as increased sea ice cover, enhanced surface water stratification, decreased Ekman-induced upwelling, and reduced vertical mixing across the thermocline. In a model simulation, Toggweiler et al. (2006) find that in the absence of a source of well-ventilated deepwater in the Southern Ocean, the North and subantarctic Pacific become weak secondary sources of intermediate water, and the deep South Atlantic essentially becomes the most isolated water mass in the world ocean.

2.2 Setting and Oceanography

Two carbonate-rich cores from the subantarctic Pacific region were examined in this study: MV0502-4JC (50˚20'S, 148˚08'W, 4286 m) and ELT 25-11 (50˚02'S, 127˚31'W, 3969m) (**Figure 2.1**). These cores were recovered from the southern edge of the Southwest Pacific Basin near the Eltanin Fracture Zone system, a 1000 km offset between the Pacific Antarctic Ridge and the Southern East Pacific Rise (Lonsdale, 1994). The Subantarctic Zone, which extends north from the Subantarctic Front to the Subtropical Front, is distinguished by the presence of Subantarctic Surface Water and biocalcareous sedimentation. An unusually deep carbonate compensation depth in the region of approximately 4750 meters allows for the preservation of carbonate-rich sediments at abyssal depths (Lyle et al., 2007). To the south of the sites, the Subantarctic Front and the Polar Front are strongly guided by topography to flow though the Eltanin and Udintsev Fracture Zones (Gille et al., 2004), making past migrations of the fronts over the sites unlikely.

The deepwater mass bathing the core sites examined in this study is lower Circumpolar Deepwater (CDW). CDW, the deepwater mass of the ACC, is divided into three components, upper CDW (1400-2800 m), largely returning Pacific Deepwater (PDW) characterized by low oxygen and high nutrient concentrations, middle CDW

(2800-3400 m), a high salinity layer within the maximum influence of the NADW, and lower CDW (>3800 m), a cold, low salinity water mass primarily composed of AABW (Hall et al., 2003). After AABW forms through the sinking of extremely cold shelf waters in regions such as the Weddell Sea, the Ross Sea, and the Adélie Coast, its flow is impeded by sills such as the Drake Passage, and due to its high density, AABW is largely confined to the Southern Ocean basins until entrained upward into the ACC. While AABW manages to enter the Atlantic Ocean through a deep gap in the South Scotia Ridge, AABW is thought to be ponded within the Australian-Antarctic and Southeast Pacific Basins by the ridge systems to the north (Orsi et al., 1999). Therefore, the bottom water that ultimately fills the Southwest Pacific Basin, as well as the entire deep North Pacific, PDW, is water that has been sourced from the lower part of CDW and has been transported northward along the New Zealand platform by the Deep Western Boundary Current (DWBC), ultimately becoming warmer, fresher, oxygen-poorer, and nutrient-richer along its journey to the North Pacific (Whitworth et al., 1999).

3. Methods

3.1 Processing and Analysis of the Sediment

Sediment samples were washed with distilled water over a 63 μm sieve and oven dried. In order to calculate the weight percent sediment >63μm, dry sediment samples were weighed both before and after and sieving. Ice rafted debris and manganese micronodules were counted from the >150μm size range. For stable isotope analyses, foraminifera were picked from the >125μm size fraction, cleaned in methanol, and roasted under vacuum at 200˚C for one hour. Analyses were conducted in the University of Michigan Stable Isotope Laboratory, where samples were reacted at 75˚C with phosphoric acid in a Kiel automatic carbonate preparation device linked to a Finnigan MAT 251 mass spectrometer. Stable isotope data are reported in standard δ-notation relative to the Vienna Peedee belemnite (VPDB) standard. Analytical precision, which was monitored through the regular analysis of the standard reference carbonate NBS-19, was ±0.03‰ for $\delta^{13}C$ and ±0.08‰ for $\delta^{18}O$ (1σ, N=153). Planktonic samples generally consisted of six specimens of *Globigerina bulloides*, and benthic samples consisted of three specimens of either *Cibicidoides mundulus* (*Cibicidoides kullenbergi*), *Planulina*

wuellerstorfi (*Cibicidoides wuellerstorfi*), or *Cibicidoides robertsonianus*. A correction factor of +0.64‰ was applied to the benthic oxygen isotope values to correct for the known departures from isotopic equilibrium of *C. mundulus* and *P. wuellerstorfi* (Shackleton and Hall, 1997). The same correction factor of +0.64‰ was also used for *C. robertsonianus* because comparison of the oxygen isotope values of *C. robertsonianus* and *P. wuellerstorfi* in samples containing both species demonstrated no significant offset.

3.2 Comparison to Existing Stable Isotope Records

The benthic stable isotope record obtained in this study from MV0502-4JC is compared to existing benthic stable isotope records from ODP Site 607 in the North Atlantic, ODP Sites 704 and 1090 in the South Atlantic, and ODP Site 849 in the Pacific, as compiled by Hodell and Venz Curtis (2006). Site 607, which is located on the western flank of the Mid Atlantic Ridge, monitors for changes in NADW (Raymo et al., 1990), and Site 849, located on the western flank of the East Pacific Rise, records the characteristics of average Pacific Deepwater (Mix et al., 1995). The stable isotope records from Site 704 on the Meteor Rise and Site 1090/TN057-6 on the Agulhas Ridge (Hodell and Venz, 1992; Müller et al., 1991; Venz and Hodell, 2002) were combined by Hodell and Venz-Curtis (2006) to create a single continuous record of CDW in the South Atlantic. Additionally, ODP Site 1088, also located on the Agulhaus Ridge, provides an important record of South Atlantic intermediate water (<2500 m) variation (Billups, 2002; Hodell et al., 2003; Hodell and Venz-Curtis, 2006). The locations of these sites are depicted in **Figure 2.2**, and the location and depth information of the stable isotope records discussed in this study can be found in **Table 2.1**.

4. Results

4.1 Chronology

4.1.1. MV0502-4JC

A compilation of the results from MV0502-4JC (**Figure 2.1**; 50˚20'S, 148˚08'W, 4286 m) can be seen in **Figure 2.3**. For raw data, see **Appendices 1, 2, and 3**. The chronology for MV0502-4JC was developed based primarily upon radiolarian and stable isotope stratigraphy (**Table 2.2)**. To ensure that the core top was intact, ^{14}C analysis of

G. bulloides was conducted at the University of Arizona AMS laboratory, yielding dates of 9,849±51 kyr for 4-6 cmbsf and 16,799±96 kyr for 16-18 cmbsf. Oxygen isotope stages were identified based on the dates provided by the radiolarians and comparison of the stable isotope record to the Plio-Pleistocene oxygen isotope stack of Lisiecki and Raymo (2005). Overall, MV0502-4JC was found to extend from the Holocene to the Late Miocene with three major hiatuses: an early Pliocene-early late Pliocene hiatus (Hiatus A, between ~10.7 and 10.2 MBSF), and two Pleistocene hiatuses from ~1.57-0.7 Ma (Hiatus B, ~4 MBSF) and ~0.45-0.25 Ma (Hiatus C, ~2.4 MBSF). Hiatus A was not fully constrained due to severe dissolution and reworking within the interval 10.7 to 10.2 MBSF.

An approximate age-depth relationship was developed for the late Pliocene-early Pleistocene interval of the core between Hiatuses A and B (~10.2-4 MBSF). The most distinctive feature of this portion of the core is the late Pliocene climate transition (LPCT) (Hodell and Ciesielski, 1990; Hodell and Venz, 1992). Because the sedimentation rate appears to increase within this interval, I use two separate linear age-depth models with a break at 7.32 MBSF, the depth at which I identify the MIS 71/72 boundary. Below 7.32 MBSF, I correlate the onset of the $\delta^{13}C$ shift associated with the LPCT in Core MV0502-4JC with the onset of the shift at Site 704/1090, in accordance with the age model for Site 704/1090 as compiled by Hodell and Venz-Curtis (2006). Above 7.32 MBSF, I calculated the linear age-depth relation based on the ages of the marine isotope stages 71, 67, 63, 61, 59, and 55 in the oxygen isotope stack of Lisiecki and Raymo (2005).

In the Pleistocene portion of the core above Hiatus B, I was able to identify a few marine isotope stages, including 16, 15, 6, 5, and 2. However, the vast majority of the section is missing due to Hiatuses B and C, and the few glacial-interglacial cycles that are represented appear to have been significantly averaged due to the low sedimentation rate. For example, at 1.32 MBSF, where individual specimens of *G. bulloides* were measured, the standard deviation for $\delta^{13}C$ and $\delta^{18}O$ was found to be ±0.44‰ and ±0.26‰ (N=6), respectively.

In the late Miocene portion of the core below Hiatus C, an age model could not be constructed because I only have one age datum, the late Miocene carbon shift, a global event that has been dated to 7.7 and 6.6 Ma by Tedford and Kelley (2004) and is clearly

distinguished in MV0502-4JC by the permanent nature of the negative $\delta^{13}C$ shift, a concurrent increase in carbonate dissolution, and the absence of an accompanying change in $\delta^{18}O$. Radiolarians appear to be reworked within the late Miocene interval, yielding an age estimate of 10-13 Ma that is incongruous with the LMCS, and thus were not used to provide additional age constraints.

4.1.2. ELT 25-11

In **Figure 2.4**, I present results from an Eltanin piston core ELT 25-11 (Figure 1; 50˚02'S, 127˚31'W, 3969m), which was recovered approximately 1000 km to the east of MV0502-4JC on the flank of the East Pacific Rise. For raw data, see **Appendices 4, 5, and 6**. The new radiolarian and stable isotope data acquired from ELT 25-11 have allowed for the improvement of an existing nannofossil chronology developed by Geitzenauer and Huddlestun (1972) and modified by King (1988) (**Table 2.3**). Overall, the ELT 25-11 record extends into the late Pliocene, and the stable isotope record, while coarse, displays the distinctive late Pliocene features of the MV0502-4JC record, including the positive benthic $\delta^{18}O$ and negative benthic $\delta^{13}C$ excursions of the late Pliocene climate transition and large positive planktonic and benthic $\delta^{13}C$ shifts of ~+1‰ near the late Pliocene/Pleistocene boundary. In the earlier chronology, a hiatus was placed at ~3.74 MBSF and assigned a maximum age range of ~1.95-0.30 Ma, but I suggest that the hiatus actually spans from 1.55-0.3 Ma and is located closer to 1.94 MBSF, synchronous with a significant $CaCO_3$ dissolution event. The original placement of the hiatus was based on the disappearance of *P. laconosa* above 3.89 MBSF. However, our radiolarian stratigraphy indicates that the core is early Pleistocene in age at 2.65 MBSF, and the large positive planktonic and benthic $\delta^{13}C$ shifts of ~1‰ that I identify in ELT 25-11 between ~3.24 and 2.54 MBSF clearly correlate to similar shifts that I date to the early Pleistocene in MV0502-4JC.

4.2. Description of the Results

4.2.1. The Late Miocene

The late Miocene portion of Core MV0502-4JC spans from ~17.2 to 10.7 MBSF (**Figure 2.3**). Benthic $\delta^{18}O$ values obtained between 17.17 to 12.11 MBSF are the lowest and least variable of the $\delta^{18}O$ measurements acquired from MV0502-4JC, averaging 3.59±0.11‰, with a maximum of 3.85‰ and a minimum of 3.32‰, consistent with the

finding of Westerhold et al. (2005) for remarkably small $\delta^{18}O$ variation during the early portion of the late Miocene. Before the prominent negative $\delta^{13}C$ shift of ~1‰ in the benthic record at ~15.3 MBSF, identified as the LMCS, $\delta^{13}C$ values average 1.13±0.18‰, and following the shift, $\delta^{13}C$ values average 0.28±0.16‰. Benthic $\delta^{13}C$ values in MV0502-4JC are very similar to those recorded at Site 704 both before and after the LMCS (**Figure 2.5**), and the benthic $\delta^{18}O$ values at the two sites are also quite comparable.

Sedimentation rates in Core MV0502-4JC are very low throughout the late Miocene (≤0.25 cm/kyr), and carbonate dissolution appears to have been particularly severe following the LMCS. Before the LMCS, carbonate contents average ~70-80% and a few well-preserved planktonic foraminifera are present, although coccolithophorids account for most of the carbonate content of the core, whereas after the LCMS, weight percent carbonate falls to ~13-29% and whole planktonic foraminifera become exceedingly rare. Throughout the late Miocene, an abundance of manganese micronodules provides an additional indication of low sedimentation rates, and ice rafted debris is present in only trace amounts.

4.2.2 The Late Pliocene

The late Pliocene portion of Core MV0502-4JC spans from ~10.2 to 6 MBSF and follows Hiatus A **(Figure 2.3**). Between 10.2 and 9.6 MBSF (~3.0-2.75 Ma), benthic $\delta^{18}O$ values are briefly comparable to those of the late Miocene (3.63±0.09‰ on average), and are very similar to those recorded at Site 704, while $\delta^{13}C$ values are more "Pacific-like" than those at Site 704 (0.31±0.17‰ on average) (**Figure 2.6**). The late Pliocene portion of MV0502-4JC displays dramatic changes associated with the late Pliocene climate transition (LPCT), most notably shifts in mean benthic $\delta^{18}O$ and $\delta^{13}C$ of ~+1.1‰ and ~-1.05‰, respectively, between 9.6 and 7.3 MBSF (~2.75-1.9 Ma). Following these shifts, $\delta^{18}O$ values recorded by MV0502-4JC are significantly higher than those recorded at Sites 704 and 1090 during the late Pliocene. Overall, a comparison between the $\delta^{18}O$ values recorded by MV0502-4JC to those of the deep Pacific (Site 849), Atlantic (Site 607), and subantarctic Atlantic (Sites 704/1090) suggests that mean $\delta^{18}O$ values were 0.75 to 1‰ higher at the site of MV0502-4JC (at >4000 m water depth) than at the other sites toward the end of the late Pliocene (<2.4 Ma). The

$\delta^{13}C$ values recorded by MV0502-4JC following the shift are similar to those of deep Pacific Site 849, as are the $\delta^{13}C$ values of subantarctic Atlantic Sites 704/1090, but become lower than the deep Pacific in the latest Pliocene.

Also following the benthic $\delta^{18}O$ and $\delta^{13}C$ shifts, ice rafted debris becomes significant for the first time in MV0502-4JC at ~8.9 MBSF and manganese micronodules decrease to trace amounts by ~8.4 MBSF (**Figure 2.3**). Initially, the benthic $\delta^{18}O$ and $\delta^{13}C$ shifts are associated with carbonate dissolution between ~8.6-8.3 MBSF but are followed by a dramatic increase in the preservation of planktonic foraminifera as well as a corresponding increase in the sedimentation rate to ~1.1 cm/kyr by ~7.3 MBSF. Ash is present in samples throughout this interval and the reworking of radiolarians of Miocene-Oligocene age was noted at 8.07 MBSF.

Core ELT 25-11 also shows significant shifts in benthic $\delta^{18}O$ and $\delta^{13}C$ during the late Pliocene (**Figure 2.4**). Benthic $\delta^{18}O$ shifts by ~+1.1 from 3.59‰ at 6.3 MBSF to 4.7‰ near 3.7 MBSF, and benthic $\delta^{13}C$ shifts by ~-1.6‰ over the same interval from 1.09‰ at 6.3 MBSF to -0.5‰ at 3.7 MBSF. While the benthic $\delta^{18}O$ shift in Core ELT 25-11 is very similar to that of MV0502-4JC during the late Pliocene, the benthic $\delta^{13}C$ shift in Core ELT 25-11 is significantly larger. Although $\delta^{13}C$ values are similar in the two cores after the shift, $\delta^{13}C$ values are significantly higher in Core ELT 25-11 prior to the shift and are actually quite "Atlantic-like," exhibiting values similar to those of Site 607.

4.4. The Pleistocene

The Pleistocene portion of Core MV0502-4JC spans from ~6 to 0 MBSF and contains Hiatuses B and C (**Figure 2.3**). Hiatus B occurs at ~4.0 MBSF and appears to be associated with a significant decline in $CaCO_3$. Below this hiatus, which spans from ~1.57-0.68 Ma, I tentatively identify the early Pleistocene isotope stages 64 to 54 (~1.8-1.57 Ma) between ~6 and 4.1 MBSF. A distinctive feature of the early Pleistocene record is an ~1‰ increase in the benthic and planktonic $\delta^{13}C$ values between 5.62 and 4.77 MBSF. This ~1‰ increase in benthic and planktonic $\delta^{13}C$ is also recorded in ELT 25-11 between ~3.24 and 2.54 MBSF and marks the return of benthic $\delta^{13}C$ to values comparable to those recorded prior to the late Pliocene climate transition.

Above Hiatus B, carbonate contents recover and a strong, distinctive glacial event, which I identify as MIS 16, occurs at ~3.77 MBSF, during which both benthic and planktonic foraminifera exhibit the highest $\delta^{18}O$ values of the entire record, reaching maximum values of 5.19‰ and 3.95‰, respectively. Following MIS 15 and 14, Hiatus C occurs at ~2.57 MBSF, coinciding with a decline in $CaCO_3$ at 2.70 MBSF, which is followed by a second $CaCO_3$ decline at 2.30 MBSF. Above the hiatus I identify isotope stages 1-6. In this uppermost section of the core, abundances of planktonic foraminifera reach a maximum, and sedimentation rates are ~1.2 cm/kyr.

5. Discussion

5.1. The Late Miocene Carbon Shift (LMCS)

The LMCS remains poorly understood but seems to consist of two distinct components. First and foremost, the event involved a change in global carbon mass balance that is recorded as a negative $\delta^{13}C$ shift in both benthic and planktonic oceanic records. The negative $\delta^{13}C$ shift at many sites could be largely explained by enhanced erosion and the addition of $\delta^{13}C$-depleted organic soil material to the ocean under the expansion of C4 plants (Diester-Haass et al., 2006). Increased carbonate dissolution and a biogenic bloom event that accompany the LMCS at many sites are also consistent with this hypothesis. Second, the LMCS is marked by a significant reorganization of interbasinal $\delta^{13}C$ gradients. Hodell and Venz-Curtis (2006) emphasize the development of a modern interbasinal gradient between North Atlantic Site 982 (57°31'N, 15°53'W, 1145 m) and South Atlantic Site 704 during the LMCS. While benthic $\delta^{13}C$ values at Sites 704 and 982 were similar prior to the LMCS, the magnitude of the carbon shift was greater in the South Atlantic than the North Atlantic, thereby marking the inception of the modern interbasinal gradient in which South Atlantic $\delta^{13}C$ values fall midway between those of the North Atlantic and Pacific. Interestingly, in this study I find that benthic $\delta^{13}C$ values at the site of MV0502-4JC were similar to those of Site 704 both before and after the LMCS. Thus, while an interbasinal $\delta^{13}C$ gradient developed between the North and South Atlantic during the LMCS, a gradient did not form between the Atlantic and Pacific sectors of the Southern Ocean at that time, suggesting that the ACC was quite strong.

Because the LMCS has been linked to the expansion of C4 plants, and because C4 photosynthesis is favored over C3 photosynthesis under low CO_2 conditions, Cerling et al (1997) suggest that the LMCS may have been associated with a decline in atmospheric CO_2. The Southern Ocean, which exhibited a particularly large $\delta^{13}C$ shift during the LMCS compared to the North Atlantic, would have been a likely player in a potential CO_2 drawdown during the LMCS. After all, growth of the West Antarctic Ice Sheet has been widely assigned to the late Miocene (Ciesielski et al., 1982; Kennett and Barker, 1990). However, benthic $\delta^{13}C$ values indicate that the Southern Ocean was exceptionally well-mixed during the late Miocene, with $\delta^{13}C$ values at Sites 704 and 1088 showing no sign of the chemocline that would later come to separate the deep and intermediate waters of the Southern Ocean during the LGM (Hodell and Venz-Curtis, 2006; Ninnemann and Charles, 2002). Likewise, $\delta^{13}C$ values recorded in MV0502-4JC are also remarkably close to those recorded at the much shallower Site 704.

Thus, with an exceptionally well-mixed Southern Ocean during the late Miocene, significant changes in Southern Ocean ventilation or circulation are not easily implicated as key players in the LMCS. The establishment of bottom water formation processes similar to the modern day (i.e. under ice shelves) could have lowered the $\delta^{13}C$ value of AABW (Hodell and Venz-Curtis, 2006). However, the most prevalent explanation for the development of the interbasinal gradient between the North and South Atlantic during the LMCS is an increase in the production of NADW. The late Miocene brought ocean-wide changes in carbonate preservation, including a deepening of the CCD in the South Atlantic (Moore et al., 1984), which suggests an increased presence of NADW in the Atlantic basin. Billups (2002) argues based on the carbon isotope record from Site 1088 that prior to 6.6 Ma, NADW did not extend into the Atlantic sector of the Southern Ocean and that after 6.6 Ma, tectonic changes, including the closure of the Central American Seaway or the subsidence of the Greenland-Scotland Ridge, led to an increased presence of NADW in the Atlantic basin.

The appeal of finding that the Southern Ocean had a participatory, rather than a passive, role in the interbasinal gradient changes of the LMCS is that the Southern Ocean is capable of providing a link between the otherwise disparate changes in oceanic circulation and carbon mass balance associated with the event. Otherwise, one simply

has to accept that tectonic changes conducive to greater NADW production fortuitously coincided with the carbon mass balance changes of the LMCS. Factors such as uplift of the Himalaya-Tibetan Plateau and American mountain belts or the late Miocene-early Pliocene biogenic bloom, a dramatic increase in marine biological productivity between 9.0 and 3.5 Ma (with a maximum at 6.0 to 5.0 Ma) that was likely fueled by increased terrestrial erosion (Hermoyian and Owen, 2001), could have provided the CO_2 drawdown necessary to account for the expansion of C4 plants during the LMCS. However, even if the Southern Ocean did not play an active role in the LMCS, Antarctica would likely have responded to a decline in atmospheric CO_2 associated with the event.

A long-standing debate has centered around whether the LMCS may have involved a glacioeustatic sea level drop related to the growth of the West Antarctic Ice Sheet (e.g. (Loutit, 1981)). An unusual aspect of the LMCS, however, is that most benthic $\delta^{18}O$ values are remarkably stable during that period, and MV0502-4JC is no exception, although there is no particular reason to believe that the build-up of the small, marine-based West Antarctic Ice Sheet would have had a noticeable impact on oceanic $\delta^{18}O$ values. While the timing of the formation of the West Antarctic Ice Sheet remains unresolved, a few observations support cryospheric expansion during the LMCS, including a $\delta^{18}O$ increase at Site 1088, which likely records a cooling of intermediate waters and the appearance of ice rafted debris at Southern Ocean ODP Sites 699 and 701 immediately following the LMCS (Billups, 2002; Warnke et al., 1992). Overall, the possibility that the interbasinal gradient changes originated in the Southern Ocean, perhaps as a response to the LMCS, should not be ruled out.

5.2. The Late Pliocene Climate Transition (LPCT)

Unlike the LMCS, which brought subtle changes to the Southern Ocean, the LPCT marked the onset of more dramatic changes in the Southern Ocean, particularly at the site of MV0502-4JC. In general, the LPCT is known for a series of $\delta^{18}O$-enrichment events of increasing magnitude at 3.1, 2.7, 2.6, and 2.4 Ma that signal the onset and gradual amplification of Northern Hemisphere Glaciation (Keigwin, 1986). The magnitude of these late Pliocene glacial-interglacial $\delta^{18}O$ variations is not particularly impressive when compared to the climatic oscillations of the late Pleistocene. At Site

607, for example, $\delta^{18}O$ values oscillate 0.5‰ between 3.1 and 2.95 Ma and 0.9‰ between 2.7 and 2.4 Ma, compared to 1.75‰ during the last glaciation, and it was not until after 2.95 Ma that "glacial" $\delta^{18}O$ values at Site 607 became more positive than those of the present interglacial (Raymo et al., 1992). Thus, based on the relatively small amplitude of late Pliocene glacial-interglacial $\delta^{18}O$ variations alone, the LPCT has not generally been regarded as a period drastic oceanic change. However, following the first ODP cruise to the subantarctic Atlantic, Hodell and Ciesielski (1990) discovered that Site 704 recorded an interesting feature during the LPCT that deep sea cores from other regions did not: a 0.5‰ decrease in mean benthic $\delta^{13}C$.

Prior to the LPCT, $\delta^{13}C$ values at Site 704 had increased to once again become very similar to those of the North Atlantic, and thus the interbasinal gradient that had developed between the North and South Atlantic during to the LMCS had lessened significantly (Hodell and Venz-Curtis, 2006). However, after ~2.75 Ma, $\delta^{13}C$ values at Site 704 underwent a sharp decline (Hodell et al., 2002; Hodell and Venz, 1992). Hodell and Venz (1992) explained the decrease in $\delta^{13}C$ in the South Atlantic as a decline in NADW formation after 2.7 Ma. In support of this interpretation, data from equatorial Atlantic ODP Sites 925 and 929 reveal that the NADW/AABW boundary in the Atlantic was at reduced depth during the late Pliocene (~2.6-2.1 Ma), suggesting a greater influence of southern source water during that period. However, Hodell and Venz-Curtis (2006) also noticed that while mean benthic $\delta^{13}C$ values at Site 704 declined during the LPCT, $\delta^{13}C$ values at Site 1088 remained the same, marking the development of a chemical divide in the South Atlantic basin at ~2500 m depth. Thus, the $\delta^{13}C$ shift recorded at Site 704 appears to be the artifact of not only a decline in NADW during the LPCT, but also a significant reduction in the ventilation of the deep Southern Ocean, as first proposed by Hodell and Ciesielski (1990).

Hodell and Venz-Curtis (2006) suggest that increased sea ice and enhanced surface water stratification impeded air-sea gas exchange and contributed to lower preformed $\delta^{13}C$ values in AABW during glacial periods after 2.75 Ma. The LPCT definitely brought significant changes to the Antarctic cryosphere, including the first significant ice-rafting to MV0502-4JC and Sites 704 and 1092 (Murphy et al., 2002; Warnke et al., 1992), the development of a strong halocline at 2.73 Ma (Haug et al.,

1999; Sigman et al., 2004), and significant sea ice expansion by ~2.5-2.4 Ma (Burckle et al., 1990; Kennett and Barker, 1990). Moreover, because these changes coincide with the onset of Northern Hemisphere Glaciation, the Southern Ocean has been suggested as a possible player in the growth of the Northern Hemisphere ice sheets (Hodell and Ciesielski, 1990; Hodell and Venz-Curtis, 2006; Sigman et al., 2004). As discussed below, the new stable isotope records from MV0502-4JC and ELT 25-11 lend additional weight to this idea.

Like Site 704, the benthic stable isotope records from MV0502-4JC and ELT 25-11 also record a significant decline in $\delta^{13}C$ around the LPCT. However, while the LPCT at Site 704 appears to record the onset of a glacial-interglacial pattern of deep water ventilation in the Southern Ocean, with consistently poorer ventilation during glacials than interglacials, combined with a significant episode of $\delta^{18}O$ enrichment, the transition in MV0502-4JC and ELT 25-11 appears to signal a far more dramatic shift in conditions in the abyssal Southern Ocean. First, the benthic $\delta^{13}C$ shift was more extensive and prolonged in these deep subantarctic Pacific records than in the pre-existing records from the South Atlantic, and second, the $\delta^{13}C$ decrease was matched by an equally dramatic increase in benthic $\delta^{18}O$ that stands out amongst other deep sea records from that period. Particularly unusual is the length of time that the low $\delta^{13}C$ values, and hence poorly ventilated conditions, persisted in MV0502-4JC and ELT 25-11 (>1 myr), as well as the dramatic return of the $\delta^{13}C$ values to pre-LPCT values after ~1.7 Ma, which is recorded as a 1‰ increase in both the benthic and planktonic records.

We interpret these benthic $\delta^{13}C$ and $\delta^{18}O$ shifts, which in MV0502-4JC amount to -1.05‰ and +1.1‰, respectively, over the period 2.7 to 1.9 Ma (9.6-7.3 MBSF), as an indication that the abyssal Southern Ocean was filled with very cold, poorly ventilated waters following the LPCT. Whereas I have found that benthic $\delta^{18}O$ values >4.5‰ were attained in the abyssal (>4000 m water depth) subantarctic Pacific during the latest Pliocene, $\delta^{18}O$ values that high were not recorded at Sites 607, 849, and 704 until the glaciations of the late Pleistocene, at which time the temperature of the deep Atlantic, Pacific, and Southern Oceans is thought to have been within error of freezing point of seawater (Adkins et al., 2002). Thus, I can easily infer that the waters of the abyssal subantarctic Pacific were 1) near the freezing point during the latest Pliocene, especially

considering that ice volume was significantly lower during the late Pliocene than during the LGM, and 2) formed largely through brine rejection, similar to the bottom waters of the LGM (Adkins et al., 2002). Further support for a dramatic cooling of Antarctic bottom waters during the LPCT comes from the results of Hayward et al. (2007), who found that a succession of pulsed declines and extinctions of benthic foraminifera with unusual aperture types originated in southern sourced deep waters (AABW and CDW) during the late Pliocene, later extending into NADW and Antarctic Intermediate Water (AAIW) during the mid-Pleistocene climate transition (MPT, 1.2-0.55 Ma). Thus, by 2.4 Ma, as the Northern Hemisphere was beginning to grow ice sheets and the magnitude of the benthic $\delta^{18}O$ oscillations was just more than half that of the last glacial-interglacial cycle, it appears that the Antarctic cryosphere had reached a point at which conditions in the deepest parts of the Southern Ocean were not significantly unlike those of the LGM.

These new stable isotope records from the abyssal subantarctic Pacific call for a reassessment of the role of the Southern Ocean in the LPCT. The progressive nature of the $\delta^{18}O$ and $\delta^{13}C$ shifts between 2.7 and 1.9 Ma suggests that an ever-larger percentage of cold, poorly-ventilated AABW accumulated in the abyssal Southern Ocean over this period as a result of increasingly pervasive sea ice cover, which may have been accompanied by a reduction in the upwelling of the deepest waters of the Southern Ocean. Because the core sites of MV0502-4JC and ELT 25-11 are located just outside of the Southern Ocean basin, and thus record the signature of lower CDW rather than AABW itself, I infer that, at a minimum, the pool of cold, poorly-ventilated water was sizeable enough to fill the Pacific sector of the Southern Ocean below a depth of 4000 m. The existence of such a large, isolated water mass in the abyssal Southern Ocean during the late Pliocene is not only a surprising finding but also has significant implications for the amplification of Northern Hemisphere Glaciation during that period.

This pool of poorly ventilated water appears to persist until 1.7 Ma, at which time the $\delta^{13}C$ values in MV0502-4JC and ELT 25-11 show a return to pre-LPCT values and the initiation of more "typical" pattern of glacial-interglacial variation. The fact that planktonic, as well as benthic, $\delta^{13}C$ values were unusually low during the latest Pliocene and earliest Pleistocene, provides further support for the existence of pervasive sea ice between 2.7 and 1.7 Ma, as sea ice cover would have led to nutrient underutilization

south of the Polar Front and we could therefore expect the northward migration of low $\delta^{13}C$ surface water into the subantarctic region. After 1.7 Ma, both the planktonic and benthic $\delta^{13}C$ records show an increase of 1‰, which likely signals a retreat of the sea ice because, as the sea ice cover diminishes, we would expect 1) the deepwater sinking in the Southern Ocean to acquire a higher preformed $\delta^{13}C$ value and 2) the surface waters arriving in the subantarctic Pacific to display a higher $\delta^{13}C$ value due to increased nutrient utilization to the south. An increase in upwelling would also have aided in the progressive release of CO_2 from the abyssal Southern Ocean and would have contributed to a higher air-sea exchange signature in the surface waters moving northward into the subantarctic region.

Thus, overall, cooling associated with the LPCT appears to have induced Antarctica into the final stages of cryospheric development, including a significant sea ice expansion, as originally suggested by Kennett and Barker (1990). This study specifically suggests that the sea ice persisted in the Southern Ocean between 2.7 and 1.7 Ma, despite relatively warm temperatures. Further investigations of sea ice conditions, particularly in the Pacific sector of the Southern Ocean, are needed to verify the extent and permanence of this sea ice. However, the existence of an extensive Southern Ocean sea ice cover is less difficult to reconcile with warm late Pliocene temperatures when we consider that moisture delivery to the region would probably have been accentuated under such conditions.

6. Conclusion

Although Hodell and Venz (2006) identify the late Miocene carbon shift (LMCS) as an important step in the evolution of the modern interbasinal $\delta^{13}C$ gradient, our comparison of new stable isotope results from the abyssal subantartic Pacific with existing records from the South Atlantic reveal that the LMCS did not mark the development of a $\delta^{13}C$ gradient within the Southern Ocean. Benthic $\delta^{13}C$ and $\delta^{18}O$ values as recorded in MV0502-4JC were nearly identical to those of South Atlantic Site 704 both before and after the LMCS. Consequently, there was not an interbasinal $\delta^{13}C$ gradient within the Southern Ocean during the late Miocene, and vertical $\delta^{13}C$ and $\delta^{18}O$ gradients were also absent. Thus, during the late Miocene, despite potential cryospheric

changes involved in the LMCS, communication between the Atlantic and Pacific sectors of the Southern Ocean remained strong, and the water column appears to have been well-mixed, well-ventilated, and of uniform temperature.

The late Pliocene climate transition (LPCT), in sharp contrast to the LMCS, did mark the development of significant vertical $\delta^{13}C$ and $\delta^{18}O$ gradients in the deep Southern Ocean. From the results of Hodell and Ciesielski (1990) and Hodell and Venz-Curtis (2006), we know that $\delta^{13}C$ values at Site 704 declined by 0.5‰ at 2.7 Ma while $\delta^{13}C$ values at intermediate Site 1088 remained unchanged, marking the development of a chemical divide in the South Atlantic basin at ~2500 m depth. However, the results of our study of the abyssal subantarctic Pacific cores MV0502-4JC and ELT 25-11 reveals that the abyssal Southern Ocean experienced changes during the LPCT that were far greater than those at Site 704. MV0502-4JC records benthic $\delta^{13}C$ and $\delta^{18}O$ shifts of -1.05‰ and +1.1‰, respectively, over the period 2.7 to 1.9 Ma (9.6-7.3 MBSF), which I interpret as an indication that the abyssal Southern Ocean was filled with very cold, poorly ventilated waters originating from brine rejection following the LPCT. The sea ice and the cold, poorly ventilated bottom waters appear to have persisted in the Southern Ocean until ~1.7 Ma, a period of a million years, at which time the re-ventilation of the Southern Ocean is recorded in both the benthic and planktonic $\delta^{13}C$ records as an increase of ~+1‰. Thus, while this study cannot identify the cause of the LPCT itself, I have discovered that the LPCT led to the development of an isolated, poorly-ventilated water mass in the abyssal Southern Ocean that could have been important in the amplification of Northern Hemisphere Glaciation.

ACKNOWLEDGEMENTS

I would like to acknowledge my coauthors on this chapter, Ingrid Hendy, Ted Moore, and Mitch Lyle. I was supported through the Sweetland Dissertation Writing Institute while preparing this manuscript. The South Pacific Latitudinal Transect (SPLAT) cruise was supported by the National Science Foundation grants OCE-0240924 to the University of Michigan and OCE-0240906 to Boise State University. I want to thank Lora Wingate of the University of Michigan Stable Isotope Laboratory for the carbonate analyses.

Table 2.1. Location and Water Depth of Late Neogene Stable Isotope Records Discussed in This Study.

Site/Core	Location	Water Depth	Reference
ODP 704	46°52'S, 7°5'E	2532 m	(Hodell and Venz, 1992) (Müller et al., 1991)
ODP 1090	42°55', 8°54'E	3702 m	(Venz and Hodell, 2002)
ODP 1088	41°08'S, 13°34'E	2082 m	(Billups, 2002) (Hodell et al., 2003) (Hodell and Venz-Curtis, 2006)
ODP 607	41°00'N, 33°37'W	3427 m	(Raymo et al., 1990)
ODP 849	0°11'N, 110°31'W	3850 m	(Mix et al., 1995)
MV0502-4JC	50°20'S, 148°08'W	4286m	this study
ELT 25-11	50˚02'S, 127˚31'W	3969m	this study

Table 2.2. Important Age Datums Identified in MV0502-4JC.

Depth	Age or Age Range	Basis for Age Assignment
Radiocarbon dates		
4-6 cm	9,849±51 kyr	
16-18 cm	16,799±96 kyr	
Radiolarian biostratigraphy		
166-168 cm	<0.425 Ma	LO *Stylatractus universus*
256-258 cm	0.425 Ma	LO *Stylatractus universus*
	–1.08 Ma	FO *Lamprocyrtis nigrinii*
391-393 cm	1.08 Ma	FO *Lamprocyrtis nigrinii*
	–1.63 Ma	FO Th*eocorythium trachelium*
511-513 cm	1.63 Ma	FO *Theocorythium trachelium*
	–1.79 Ma	LO *Lamprocyrtis heteroporus*
806-808 cm	1.85 Ma	FO *Triceraspyris antarctica*
	–2.38 Ma	FO *Antarctissa denticulata*
1021-1023 cm	2.5 Ma	FO *Cycladophora davisiana*
	–3.29 Ma	FO *Lamprocyrtis heteroporus*
Stable isotope stratigraphy		
1530 cm	7.7-6.6 Ma	Late Miocene $\delta^{13}C$ Shift (Tedford and Kelley, 2004)
962 cm	~2.75 Ma	Late Pliocene $\delta^{13}C$ shift (Hodell and Venz-Curtis, 2006)

Table 2.3. Important Age Datums Identified in ELT 25-11.

Depth	Age or Age Range	Basis for Age Assignment
Nannofossil biostratigraphy (King, 1988)		
74 cm	0.26 Ma	CN14b/CN15 boundary
404 cm	1.95 Ma	CN12d/CN13a boundary
Radiolarian biostratigraphy		
153-154 cm	<0.425 Ma	LO *Stylatractus universus*
264-266 cm	1.85 Ma	FO *Triceraspyris antarctica*
	–2.38 Ma	FO *Antarctissa denticulata*
334-336 cm	1.85 Ma	FO *Triceraspyris antarctica*
	–2.38 Ma	FO *Antarctissa denticulata*
Stable isotope stratigraphy		
647 cm	~2.75 Ma	Late Pliocene $\delta^{13}C$ shift (Hodell and Venz-Curtis, 2006)

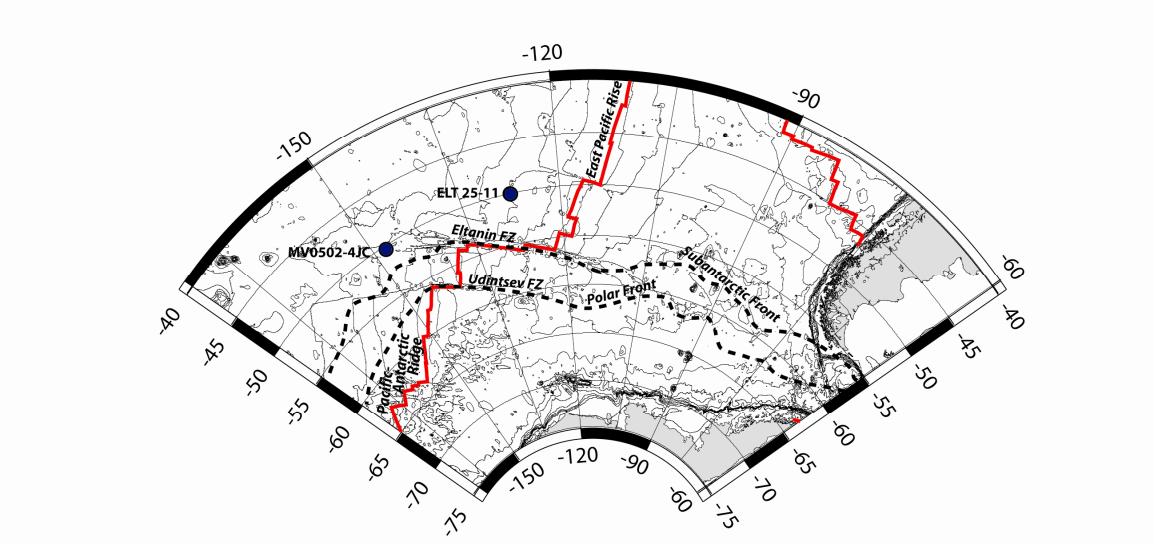

Figure 2.1. Bathymetric map of the study region, depicting the core locations of MV0502-4JC (50°20'S, 148°08'W, 4286 m) and ELT 25-11 (50°02'S, 127°31'W, 3969 m), for which new results are presented in this study. Red solid line represents the mid-ocean ridge, black dotted lines represent oceanic fronts. (Online Map Creation at www.aquarius.ifm-geomar.de)

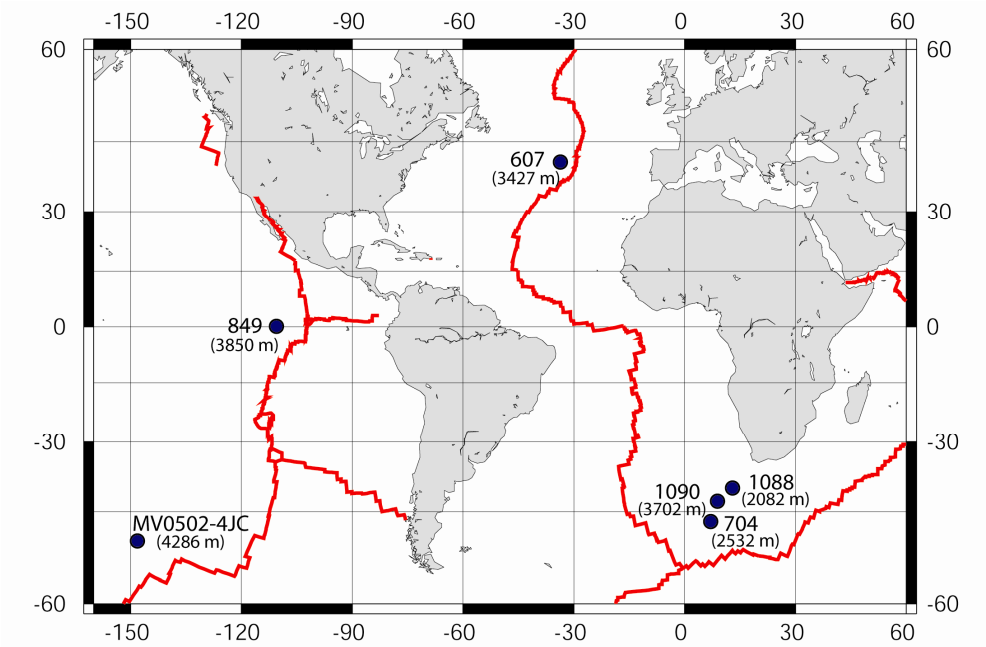

Figure 2.2. Map showing the location of existing benthic stable isotope records that are compared to MV0502-4JC in this study. Red solid line represents the mid-ocean ridge. (Online Map Creation at www.aquarius.ifm-geomar.de)

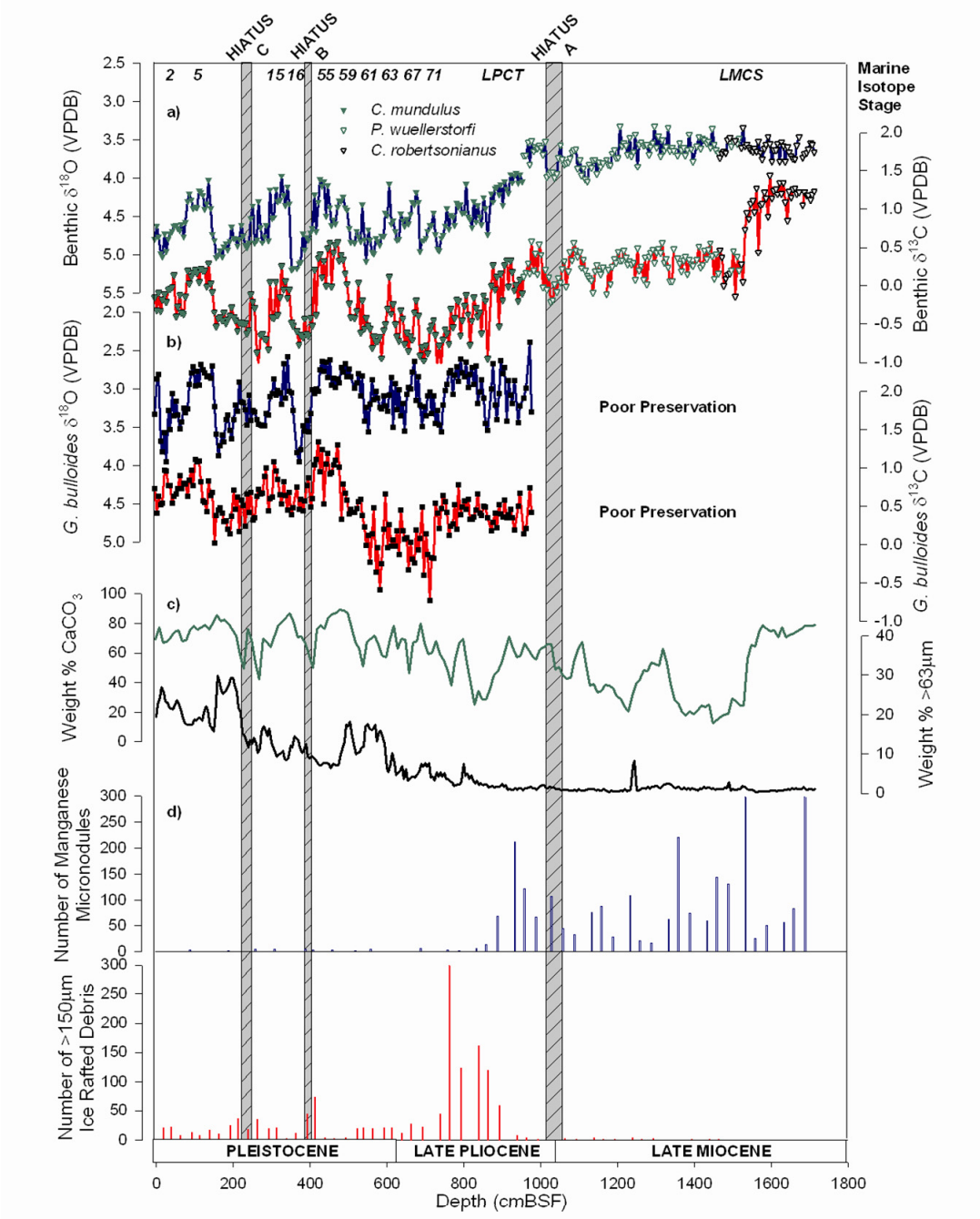

Figure 2.3. Compilation of the results from MV0502-4JC. (a) Benthic $\delta^{18}O$ represented by blue line with triangles (top) and benthic $\delta^{13}C$ represented by red line with triangles (bottom). Closed green, open green, and open black triangles depict data points obtained from the benthic species *C. mundulus*, *P. wuellerstorfi*, and *C. robertsonianus*, respectively. (b) *G. bulloides* $\delta^{18}O$ represented by blue line with black squares (top) and *G. bulloides* $\delta^{13}C$ represented by red line with black squares (bottom). (c) Weight percent $CaCO_3$ (top) and weight percent of the sediment >63 µm (bottom) (d) Counts of manganese micronodules (top) and ice rafted debris (bottom). Age constraints are from radiolarian and stable isotope stratigraphy. The ages assigned to the hiatuses are as follows: Hiatus A= early Pliocene-early late Pliocene, Hiatus B= ~1.57-0.68 Ma, and Hiatus C=~0.53-0.19 Ma.

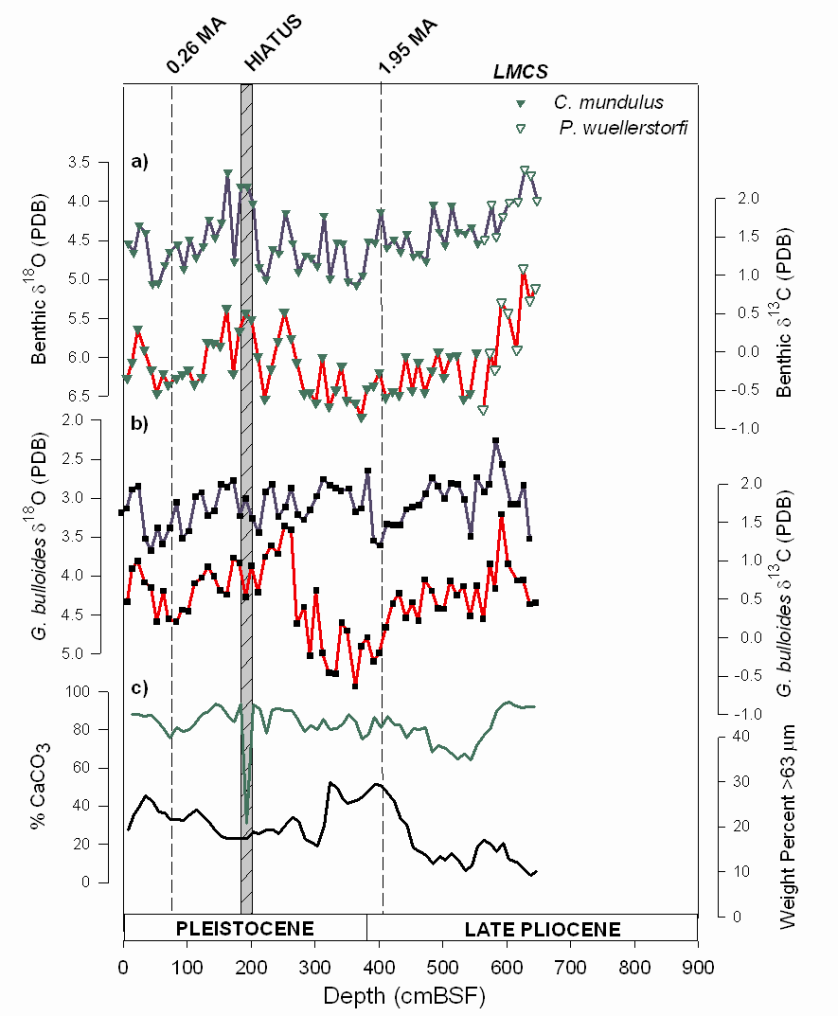

Figure 2.4. Compilation of the results from ELT 25-11. (a) Benthic $\delta^{18}O$ represented by blue line with triangles (top) and benthic $\delta^{13}C$ represented by red line with triangles (bottom). Closed green and open green, triangles depict data points obtained from the benthic species *C. mundulus* and *P. wuellerstorfi*, respectively. (b) *G. bulloides* $\delta^{18}O$ represented by blue line with black squares (top) and *G. bulloides* $\delta^{13}C$ represented by red line with black squares (bottom). (c) Weight percent $CaCO_3$ (top) and weight percent of the sediment >63 µm (bottom) The age constraints shown (dashed lines) are from nannofossil biostratigraphy by King (1988). The hiatus was assigned an age of ~1.55-0.3 Ma in this study.

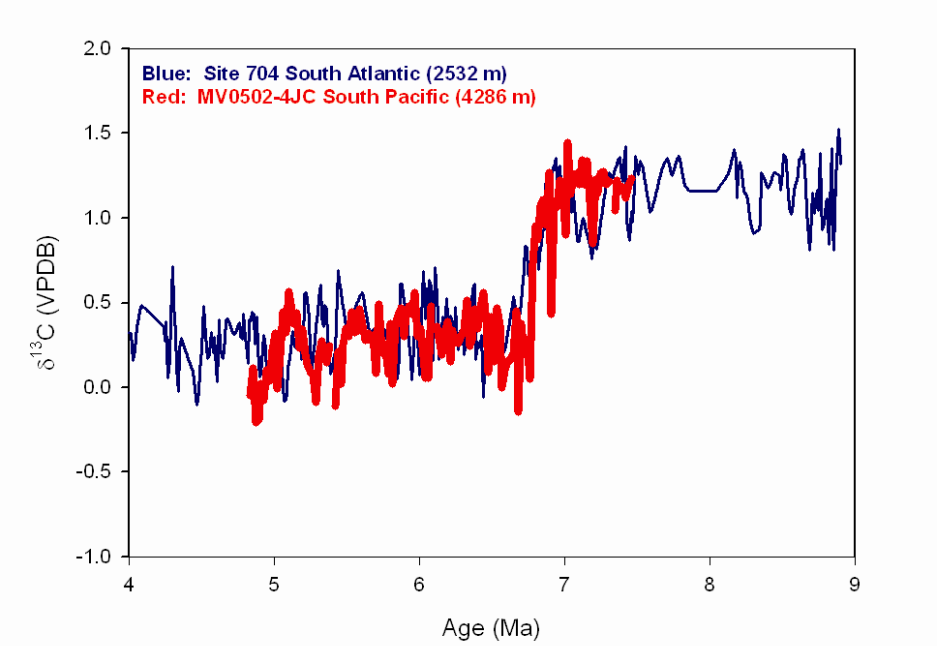

Figure 2.5. Comparison of the benthic $\delta^{13}C$ record of the late Miocene carbon shift from MV0502-4JC to that of ODP Site 704 in the South Atlantic.

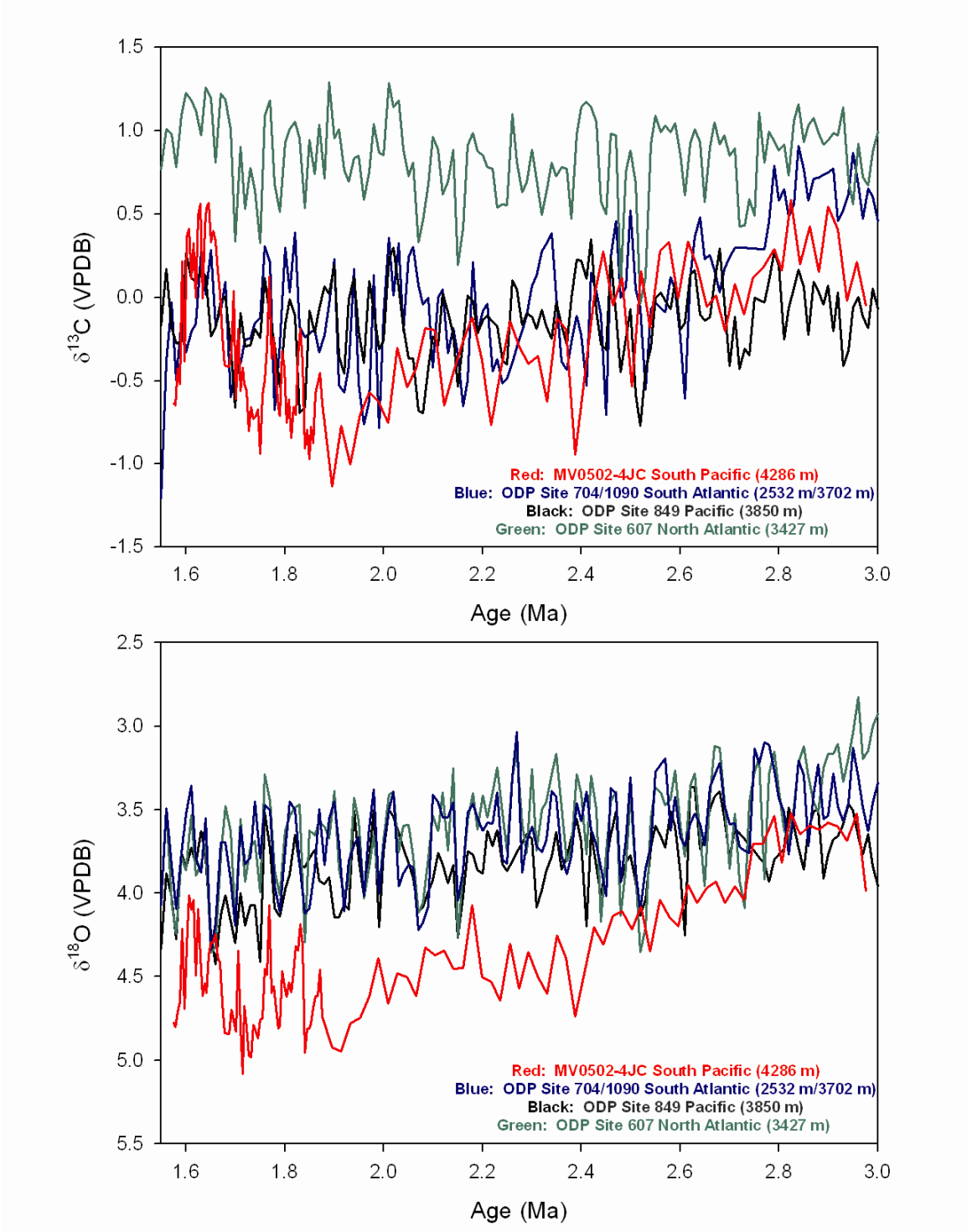

Figure 2.6. Comparison of the MV0502-4JC (red) benthic $\delta^{13}C$ (top) and $\delta^{18}O$ (bottom) records of the late Pliocene climate transition to records from ODP Sites 849 (black, Pacific Ocean), 607 (green, North Atlantic), and 704/1090 (blue, South Atlantic).

REFERENCES

Adkins, J.F., McIntyre, K., and Schrag, D.P., 2002, The salinity, temperature, and $\delta^{18}O$ of the glacial deep ocean: Science, v. 298, p. 1769-1773.

Billups, K., 2002, Late Miocene through early Pliocene deep water circulation and climate change viewed from the sub-Antarctic South Atlantic: Palaeogeography, Palaeoclimatology, Palaeoecology, v. 185, p. 287-307.

Broecker, W., and Maier-Reimer, E., 1992, The influence of air and sea exchange on the carbon isotope distribution in the sea: Global Biogeochemical Cycles, v. 6, p. 315-320.

Brunnelle, B.G., Sigman, D.M., Cook, M.S., Keigwin, L.D., Haug, G.H., Plessen, B., Schettler, G., and Jaccard, S.L., 2007, Evidence from diatom-bound nitrogen isotopes for subarctic Pacific stratification during the last ice age and a link to North Pacific denitrification changes: Paleoceanography, v. 22, p. PA1215, doi:10.1029/2005PA001205.

Burckle, L.H., Gersonde, R., and Abrams, N., 1990, Late Pliocene-Pleistocene paleoclimate in the Jane Basin Region: ODP Site 697: Proceedings of Ocean Drilling Program Scientific Results, v. 113, p. 803-809.

Charles, C.D., and Fairbanks, R.G., 1990, Glacial and interglacial changes in the isotopic gradients of Southern Ocean surface water, *in* Bleil, U., and Theide, J., eds., Geological history of the polar oceans: Arctic versus Antarctic: Norwell, Mass., Kluwer Academic, p. 519-538.

Ciesielski, P.F., Ledbetter, M.T., and Ellwood, B.B., 1982, The development of Antarctic glaciation and the Neogene paleoenvironment of the Maurice Ewing Bank: Marine Geology, v. 46, p. 1-51.

Curry, W.B., and Oppo, D.W., 2005, Glacial water mass geometry and the distribution of $\delta 13C$ and ΣCO_2 in the Western Atlantic Ocean.: Paleoceanography, p. doi:10.1029/2004PA001021.

de Boer, A.M., Sigman, D.M., Toggweiler, J.R., and Russell, J.L., 2007, Effect of global ocean temperature change on deep ocean ventilation: Paleoceanography, v. 22, p. PA2210, doi:10.1029/2005PA001242.

Diester-Haass, Billups, K., and Emeis, K.C., 2006, The late Miocene carbon isotope shift and marine biological productivity: was there a (dusty) link?: Paleoceanography, v. 21, p. PA4216, doi:10.1029/2006PA001267.

Duplessy, J.-C., Shackleton, N.J., Fairbanks, R.G., Labeyrie, L., Oppo, D.W., and Kallel, N., 1988, Deepwater source variations during the last climatic cycle and their impact on the global deepwater circulation: Paleoceanography, v. 3, p. 343-360.

Francois, R., Altabet, M.A., Yu, E.-F., Sigman, D.M., Bacon, M.P., Frank, M., Bohrmann, G., Bareille, G., and Labeyrie, L.D., 1997, Contribution of Southern Ocean surface-water stratification to low atmospheric CO_2 concentrations during the last glacial period: Nature, v. 389, p. 929-935.

Geitzenauer, K.R., and Huddlestun, P., 1972, An upper Pliocene-Pleistocene calcareous nannofossil flora from a subantarctic Pacific deep-sea core: Micropaleontology, v. 18, p. 405-409.

Gille, S.T., Metzger, E.J., and Tokmakian, R., 2004, Seafloor Topography and Ocean Circulation: Oceanography, v. 17, p. 2004.

Hall, I.R., McCave, I.N., Zahn, R., Carter, L., Knutz, P.C., and Weedon, G.P., 2003, Paleocurrent reconstruction of the deep Pacific inflow during the middle Miocene: Reflections of East Antarctic Ice Sheet Growth: Paleoceanography, v. 18, p. 1040, doi:10.1029/2002PA000817.

Haug, G.H., Sigman, D.M., Tiedemann, R., Pederson, T.F., and Sarnthein, M., 1999, Onset of permanent stratification in the subarctic Pacific Ocean: Nature, v. 401, p. 779-782.

Hayward, B.W., Kawagata, S., Grenfell, H.R., Sabaa, A.T., and O'Neill, T., 2007, Last global extinction in the deep sea during the mid-Pleistocene climate transition: Paleoceanography, v. 22, p. PA3103, doi:10.1029/2007PA001424.

Hendy, I.L., and Kennett, J.P., 2003, Tropical forcing of North Pacific intermediate water distribution during Late Quaternary rapid climate change?: Quaternary Science Reviews, v. 22, p. 673-689.

Hermoyian, C.S., and Owen, R.M., 2001, Late Miocene-early Pliocene biogenic bloom: Evidence from low-productivity regions of the Indian and Atlantic Oceans: Paleoceanography, v. 16, p. 95-100.

Hodell, D.A., and Ciesielski, P.F., 1990, Southern Ocean response to the intensification of Northern Hemisphere Glaciation at 2.4 Ma., *in* Bleil, U., and Theide, J., eds., Geological History of the Polar Oceans: Arctic vs. Antarctic: Dordrecht, Kluwer Academic Publishers, p. 707-728.

Hodell, D.A., Gersonde, R., and Blum, P., 2002, Leg 177 Synthesis: Insights into Southern Ocean paleoceanography on tectonic to millennial timescales, *in* Gersonde, R., Hodell, D.A., and Blum, P., eds., Proceedings of the Ocean Drilling

Program, Scientific Results, Volume 177: College Station, TX, Ocean Drilling Program.

Hodell, D.A., and Venz, K., 1992, Toward a high-resolution stable isotope record of the Southern Ocean during the Pliocene-Pleistocene (4.8 to 0.8 Ma), *in* Kennett, J.P., and Warnke, D.A., eds., The Antarctic Paleoenvironment: A perspective on global change, Antarct. Res. Ser., Volume 56: Antarctic Research Series: Washington D.C., AGU, p. 265-310.

Hodell, D.A., Venz, K.A., Charles, C.D., and Ninnemann, U.S., 2003, Pleistocene vertical carbon isotope and carbonate gradients in the South Atlantic sector of the Southern Ocean: Geochemistry, Geophysics, Geosystems, v. 4, p. 1004, doi:10.1029/2002GC000367.

Hodell, D.A., and Venz-Curtis, K.A., 2006, Late Neogene history of deepwater ventilation in the Southern Ocean: Geochemistry, Geophysics, Geosystems, v. 7, p. Q09001, doi:10.1029/2005GC001211.

Jaccard, S.L., Haug, G.H., Sigman, D.M., Pederson, T.F., Thierstein, H.R., and Röhl, U., 2005, Glacial/Interglacial Changes in Subarctic North Pacific Stratification: Nature, v. 308, p. 1003-1006.

Keigwin, L.D., 1986, Pliocene stable-isotope record of Deep Sea Drilling Project Site 606: Sequential events of ^{18}O enrichment beginning at 3.1 Ma: Initial Reports of the Deep Sea Drilling Program, v. 94, p. 911-920.

—, 1998, Glacial-age hydrography of the far northwest Pacific Ocean: Paleoceanography, v. 13, p. 323-339.

Kennett, J.P., and Barker, P.F., 1990, Latest Cretaceous to Cenozoic climate and oceanographic developments in the Weddell Sea, Antarctica: An ocean-drilling perspective: Proceedings of Ocean Drilling Program, Scientific Results, v. 113, p. 937-960.

King, R.E., Jr., 1988, Sediment distribution, accumulation rates, and climatic change in the southeast Pacific [Master's thesis]: Hattiesburg, University of Southern Mississippi.

Kohfeld, K.E., Le Quéré, C., Harrison, S.P., and Anderson, R.F., 2005, Role of marine biology in glacial-interglacial CO_2 cycles: Science, v. 308, p. 74-78.

Kroopnick, P.M., 1985, The distribution of ^{13}C of ΣCO_2 in the world oceans: Deep-Sea Research Part A, v. 32, p. 57-84.

Lisiecki, L.E., and Raymo, M.E., 2005, A Plio-Pleistocene stack of 57 globally distributed benthic $\delta^{18}O$ records: Paleoceanography, v. 20, p. PA1003, doi:10.1029/2004PA001071.

Lonsdale, P., 1994, Structural geomorphology of the Eltanin fault system and adjacent transform faults of the Pacific-Antarctic plate boundary: Marine Geophysical Researches, v. 16, p. 105-143.

Loutit, T.S., 1981, Late Miocene paleoclimatology: Subantarctic water mass, southwest Pacific: Marine Micropaleontology, v. 6, p. 1-27.

Lunt, D.J., Foster, G.L., Haywood, A.M., and Stone, E.J., 2008, Late Pliocene Greenland glaciation controlled by a decline in atmospheric CO_2 levels: Nature, v. 454, p. 1102-1106.

Lyle, M., Gibbs, S., Moore, T.C., and Rea, D.K., 2007, Late Oligocene initiation of the Antarctic Circumpolar Current: Evidence from the South Pacific: Geology, v. 35, p. 691-694.

Lynch-Stieglitz, J., and Fairbanks, R.G., 1994, A conservative tracer for glacial ocean circulation from carbon isotope and palaeo-nutrient measurements in benthic foraminifera: Nature, v. 369, p. 308-310.

Lynch-Stieglitz, J., Stocker, T.F., Broecker, W., and Fairbanks, R.G., 1995, The influence of air-sea exchange on the isotopic composition of oceanic carbon: Observations and modeling: Global Biogeochemical Cycles, v. 9, p. 653-665.

Lynch-Stieglitz, J., van Geen, A., and Fairbanks, R.G., 1996, Interocean exchange of Glacial North Atlantic Intermediate Water: Evidence from Subantarctic Cd/Ca and carbon isotope measurements: Paleoceanography, v. 11, p. 191-201.

Matsumoto, K., Oba, T., Lynch-Stieglitz, J., and Yamamoto, H., 2002, Interior hydrography and circulation of the glacial Pacific Ocean: Quaternary Science Reviews, v. 21, p. 1693-1704.

Mix, A.C., Pisias, N.G., Rugh, W., Wilson, J., Morey, A., and Hagelberg, T.K., 1995, Benthic foraminifer stable isotope record from Site 849 (0-5 Ma): Local and global climate changes, *in* Pisias, N.G., Mayer, L.A., Janecek, T.R., Palmer-Julson, A., and van Andel, T.H., eds., Proceedings of the Ocean Drilling Program, Scientific Results, Volume 138: College Station, TX, Ocean Drilling Program.

Moore, T.C., Jr., Rabinowitz, P.D., Borella, P.D., Shackleton, N.J., and Boersma, A., 1984, History of the Walvis Ridge, *in* Moore, T.C., Jr., and Rabinowitz, P.D., et al., eds., Initial Reports of DSDP, Volume 74: Washington D.C., US Government Printing Office, p. 873-894.

Müller, D.W., Hodell, D.A., and Ciesielski, P.F., 1991, Late Miocene to earliest Pliocene (9.8-4.5 Ma) paleoceanography of the subantarctic southeast Atlantic: Stable isotopic, sedimentologic, and microfossil evidence: Proceedings of Ocean Drilling Program Scientific Results, v. 114, p. 459-474.

Murphy, L., Warnke, D.A., Andersson, C., Channell, J., and Stoner, J., 2002, History of ice rafting at South Atlantic ODP Site 177-1092 during the Guass and the late Gilbert Chron: Palaeogeography, Palaeoclimatology, Palaeoecology, v. 182, p. 183-196.

Ninneman, U.S., and Charles, C.D., 2002, Changes in the mode of Southern Ocean circulation over the last glacial cycle revealed by foraminiferal stable isotopic variability: Earth and Planetary Science Letters, v. 201, p. 383-396.

Ninnemann, U.S., and Charles, C.D., 1997, Regional differences in Quaternary Subantarctic nutrient cycling: Link to intermediate and deep water ventilation: Paleoceanography, v. 12, p. 560-567.

—, 2002, Changes in the mode of Southern Ocean circulation over the last glacial cycle revealed by foraminiferal stable isotopic variability: Earth and Planetary Science Letters, v. 201, p. 383-396.

Ohkushi, K.i., Itaki, T., and Nemoto, N., 2003, Last Glacial-Holocene change in intermediate-water ventilation in the Northwestern Pacific: Quaternary Science Reviews, v. 22, p. 1477-1484.

Oppo, D.W., and Fairbanks, R.G., 1987, Variability in the deep and intermediate water circulation of the Atlantic during the past 25,000 years: Northern Hemisphere modulation of the Southern Ocean: Earth and Planetary Science Letters, v. 86, p. 1-15.

Orsi, A.H., Johnson, G.C., and Bullister, J.L., 1999, Circulation, mixing, and production of Antarctic Bottom Water: Progress in Oceanography, v. 43, p. 55-109.

Powell, D.C., Markus, T., and Stössell, A., 2005, Effects of snow depth forcing on Southern Ocean sea ice simulations: Journal of Geophysical Research, v. 110, p. C06001, doi:10.1029/2003JC002212.

Raymo, M.E., Hodell, D.A., and Jansen, E., 1992, Response of deep ocean circulation to initiation of Northern Hemisphere Glaciation (3-2 Ma): Paleoceanography, v. 7, p. 645-672.

Raymo, M.E., Ruddiman, W.F., Shackleton, N.J., and Oppo, D.W., 1990, Evolution of Atlantic-Pacific $\delta^{13}C$ gradients over the last 2.5 m.y.: Earth and Planetary Science Letters, v. 97, p. 353-368.

Sigman, D.M., Altabet, M.A., McCorkle, D.C., and Gaillard, J.-F., 1999, The isotopic composition of diatom-bound nitrogen in Southern Ocean sediments: Paleoceanography, v. 14, p. 118-134.

Sigman, D.M., de Boer, A.M., and Haug, G.H., 2007, Antarctic stratification, atmospheric water vapor, and Heinrich events: A hypothesis for late Pleistocene deglaciations, in Past and Future Changes of the Oceanic Meridional Overturning Circulation: Mechanisms and Impacts, *in* Schmittner, A., Chiang, J.H.C., and Hemming, S.R., eds., AGU Geophysical Monograph 173, p. 335-350.

Sigman, D.M., Jaccard, S.L., and Haug, G.H., 2004, Polar ocean stratification in a cold climate: Nature, v. 428, p. 59-63.

Stephens, B.B., and Keeling, R.F., 2000, The influence of Antarctic sea ice on glacial-interglacial CO_2 variations: Nature, v. 404, p. 171-174.

Tedford, R.A., and Kelley, D.C., 2004, A deep-sea record of the Late Miocene carbon shift from the Southern Tasman Sea, *in* Exon, N., Kennett, J.P., and Malone, M., eds., The Cenozoic Southern Ocean: Tectonics, Sedimentation and Climate Change between Australia and Antarctica, Geophysical Union Monograph Series 151: Geophysial Monograph: Washington D.C., American Geophysical Union, p. 273-290.

Toggweiler, J.R., Russell, J.L., and Carson, S.R., 2006, Midlatitude westerlies, atmospheric CO_2, and climate change during the ice ages: Paleoceanography, v. 21, p. PA2005, doi:10.1029/2005PA001154.

Venz, K.A., and Hodell, D.A., 2002, New evidence for changes in Plio-Pleistocene deep water circulation from Southern Ocean ODP Leg 177 Site 1090: Palaeogeography, Palaeoclimatology, Palaeoecology, v. 182, p. 197-220.

Warnke, D.A., Allen, C.P., Müller, D.W., Hodell, D.A., and Brunner, C.A., 1992, Miocene-Pliocene Antarctic glacial evolution as reflected in the sedimentary record: A synthesis of IRD, stable isotope, and planktonic foraminiferal indicators, *in* Kennett, J.P., and Warnke, D.A., eds., The Antarctic Paleoenvironment: A perspective on global change, Antarct. Res. Ser., Volume 56: Antarctic Research Series: Washington D.C., AGU, p. 311-325.

Watson, A.J., and Naveira Garabato, A., 2006, The role of Southern Ocean mixing and upwelling in glacial-interglacial atmospheric CO_2 change: Tellus, v. 58B, p. 73-87.

Westerhold, T., Bickert, T., and Röhl, U., 2005, Middle to late Miocene oxygen isotope stratigraphy of ODP Site 1085 (SE Atlantic): new constrains on Miocene climate variability and sea-level fluctuations: Palaeogeography, Palaeoclimatology, Palaeoecology, v. 217, p. 205-222.

Whitworth, T., III, Warren, B.A., Nowlin, W.D., Jr., Rutz, S.B., Pillsbury, R.D., and Moore, M.I., 1999, On the deep western-boundary current in the Southwest Pacific Basin: Progress in Oceanography, v. 1999, p. 1-54.

Chapter 3
Global Overturning Circulation During the Late Neogene: New Insights from Hiatuses in the Subantarctic Pacific

Abstract

The response of oceanic circulation to a warming climate is a topic that is often approached from a "North Atlantic" perspective, and thus while many predictions have been made for the fate of North Atlantic overturning circulation in the coming centuries, relatively few studies have examined how global overturning circulation as a whole is likely to respond. In this study, I identify hiatuses in the abyssal subantarctic Pacific region that suggest three intervals of increased Antarctic Circumpolar Current (ACC) strength during the late Neogene: 1) the early Pliocene-early Late Pliocene, 2) ~1.57-0.68 Ma, and 3) ~0.53-0.19 Ma. Because these hiatuses correlate well with intervals of erosion or reduced deposition at sites of focused bottom water flow throughout the global ocean, I argue that these hiatuses represent periods not only of increased ACC strength but also of enhanced global overturning circulation. Additionally, these hiatuses appear to correspond to the Early Pliocene Warm Period and the climatic transitions of the Mid-Pleistocene Revolution and Mid-Brunhes, which marked the initiation of longer and/or more extreme interglacial events, and thus may suggest a link between warmer climates and stronger global circulation during the late Neogene.

1. Introduction

Current climate models suggest that North Atlantic overturning circulation will decrease as atmospheric CO_2 concentrations rise over the next century (Gregory et al., 2005). These models predict that this decrease in meridional overturning will result primarily from changes in surface heat flux (Gregory et al., 2005), rather than from increased flux of freshwater to the North Atlantic region under a warmer atmosphere, as predicted by earlier models (e.g. Dixon et al., 1999). Climate models have improve dramatically over the past few decades in their representation of the complexities of the

ocean-atmosphere system, but the key test is how well these models can reproduce the circulation changes that took place during past climatic transitions. A great deal of effort has been invested, for example, in understanding the nature of oceanic circulation during the Last Glacial Maximum (LGM), and paleoceanographic data support a weaker North Atlantic overturning circulation during the LGM relative to the present day (Lynch-Stieglitz et al., 2007). Thus, the available data suggest that ocean circulation strengthened as climate warmed 18000 years ago, a finding in sharp contrast to the weakening of North Atlantic overturning circulation that is predicted over the next century in response to anthropogenic warming.

In a recent modeling study, de Boer et al. (2008) examined overturning circulation as a global energy-driven system rather than as an Atlantic-dominated phenomenon and found a tendency towards a more vigorous, globally-distributed overturning during warm climatic intervals as opposed to a weaker, Atlantic-dominated state during cold intervals. These results are consistent with paleoceanographic data, which suggest more vigorous overturning circulation during the climatic warmth of the early Pliocene, a period often invoked as an analog for future climate under continued anthropogenic warming. Ravelo and Andreasen (2000) and Hodell and Venz-Curtis (2006) show that $\delta^{13}C$ gradients were significantly reduced throughout the global ocean during this interval of climatic warmth, a strong indication that overturning was stronger and less Atlantic-dominated during the early Pliocene relative to today.

In order to achieve more a vigorous overturning circulation under a warmer climate, stronger winds would be needed (de Boer et al., 2008; Toggweiler and Russell, 2008). A longstanding notion in the literature has been that glacial climates are characterized by stronger winds, and thus stronger oceanic circulation, due to a larger pole-to-equator temperature gradient. Recently, however, it has been observed that as modern atmospheric CO_2 levels have increased over the past few decades, surface wind patterns have been changing as a result of greater thermal gradients in the middle atmosphere rather than at the Earth's surface (Fyfe and Saenko, 2005). Specifically, the Southern Annular Mode (SAM) has been trending over the past 40 years toward a high-index state characterized by increasing meridional pressure gradients between the sub-Antarctic and mid-latitudes. A current manifestation of this trend has been a

strengthening and poleward shift of the westerly winds over the Southern Ocean (Thompson and Solomon, 2002; Trenberth et al., 2007), as well as an increase in the strength of the Antarctic Circumpolar Current (ACC) (Aoki et al., 2005).

More observational data related to the relative strength of oceanic circulation during past climatic regimes are clearly needed as we seek to improve climatic models, and thus to refine our predictions for the future of overturning circulation. One way in which to identify periods in which circulation was at its strongest is to study hiatuses, or intervals of erosion or non-deposition, in ocean sediments. Periods of vigorous oceanic circulation should be indicated by erosion in regions of concentrated bottom currents. Bottom water flow is generally quite slow, usually not exceeding velocities of 1-2 cm/s, but in areas where bottom currents become focused against the western margins of the oceans by the Coriolis force, velocities of 10-20 cm/s are not uncommon, and bottom current velocities exceeding 200 cm/s have been reported in narrow passages such as fracture zones (Stow et al., 2002). The deep-sea hiatus record can be difficult to interpret, as 1) not all areas of the seafloor are subject to concentrated bottom water flow and 2) material that is eroded from one location is deposited downstream in a sediment drift. However, a more coherent picture of the relative vigor of oceanic circulation can be obtained by considering only hiatuses at sites at which bottom current velocity is generally high (such as oceanic passageways) and at which it has exceeded ~15 m/s (the velocity at which erosion outweighs deposition) only in a few exceptional circumstances.

In this study, in order to identify periods in the past during which vigorous, globally-distributed overturning circulation may have existed, I constrain the hiatuses in a new (MV0502-4JC) and two existing (ELT 25-11 and ELT 20-2) piston cores from the southeast subantarctic Pacific region (**Figure 3.1**) and compare these hiatuses to those known from other high flow velocity regions (**Figure 3.2**). The three cores examined in this study, MV0502-4JC (50˚20'S, 148˚08'W, 4286 m), ELT 25-11 (50˚02'S, 127˚31'W, 3969m**)**, and ELT 20-2 (49˚00'S, 144˚50'W, 4517 m**),** were recovered along the Subantarctic Front (SAF) of the ACC, and are thus ideally situated to provide insights into past changes in the strength of oceanic circulation. The ACC is largely wind-driven, yet its flow extends to the seafloor in many areas (Barker and Thomas, 2004), and thus there is the potential for the ACC to create hiatuses and drift deposits through sediment

redistribution. This is particularly true for sediment in the path of the SAF, which accounts for the bulk of ACC transport (Rintoul and Sokolov, 2001). Specific advantages of this new core are that 1) the position of the SAF appears to be tied to the Eltanin Fracture Zone near the core site, making local migrations of the SAF unlikely, and 2) the site is located to the north of the Pacific-Antarctic Ridge and thus should not be affected by the circulation of Antarctic Bottom Water.

2. Age Constraints for Hiatuses in the Southeast Subantarctic Pacific Region

The hiatuses in MV0502-4JC, as well as two USNS *Eltanin* cores from the subantarctic Pacific region, ELT 25-11 and ELT 20-2, were identified and constrained using a combination of radiolarian biostratigraphy, stable isotope stratigraphy, and weight percent carbonate. For MV0502-4JC, a radiocarbon date from *G. bulloides* was also obtained from the University of Arizona AMS laboratory in order to ensure an intact core top. A detailed description of the age assignments for the hiatuses in MV0502-4JC, ELT 25-11, and ELT 20-2 is provided below. For raw data, see **Appendices 1-8**.

2.1 MV0502-4JC (50˚20'S, 148˚08'W, 4286 m)

The ages of the hiatuses in MV0502-4JC were determined using a combination of radiolarian and stable isotope stratigraphy (**Figure 3.3**). In the Miocene portion of the core (>~10.7 MBSF), it is assumed that the radiolarians, which yielded ages of 10-13 Ma, have been reworked, because the presence of the Late Miocene Carbon Shift (LMCS) , a distinctive permanent global shift in $\delta^{13}C$ between 7.7 and 6.6 Ma (Tedford and Kelley, 2004) at ~15.3 MBSF serves as a more reliable chronologic indicator. **Hiatus A** (10.7 and 10.2 MBSF) was identified based on the appearance of *Lamprocyrtis heteroporus* (FO 3.29 Ma) at ~10.2 MBSF. The base of Hiatus A is poorly constrained, but is likely early Pliocene in age. The top of the hiatus is late Pliocene in age, likely between ~3.2 and 2.8 Ma, because the site records the positive benthic $\delta^{18}O$ and negative benthic $\delta^{13}C$ excursions of the Late Pliocene Climatic Transition, which have been dated to ~2.75 Ma at South Atlantic Site 704 (Hodell and Venz, 1992).

Hiatus B (~4.0 MBSF) is indicated by a change in radiolarian age from 1.63-1.79 Ma at 5.1 MBSF to 0.425-1.08 Ma at 2.6 MBSF. The stable isotope record shows far too

few marine isotope stages during this interval for it to be considered complete, and a carbonate dissolution event and a change in the nature of the record occurs at ~4 MBSF, above which the glacial-interglacial cycles appear to be more characteristic of the 100 kyr world of the late Pleistocene than the 41 kyr world of the early Pleistocene. Based on the radiolarian ages and distinctive features of the stable isotope record, I place the hiatus directly above MIS 54 and directly below MIS 16, giving the hiatus an age span of 0.68-1.57 Ma according to the oxygen isotope stack of Lisiecki and Raymo (2005).

Hiatus C (~2.4 MBSF) is indicated by several missing glacial-interglacial cycles between the top of the core, which radiocarbon dating has indicated is Holocene in age, and 2.6 MBSF, where *Stylatractus universus* (LO 0.425 Ma) was noted. Like Hiatus B, Hiatus C is also characterized by a decline in $CaCO_3$, in this case in two discrete events. Thus, below Hiatus C but above Hiatus B, MIS 14-16 are preserved, and above Hiatus C, MIS 1-6 are preserved, giving the hiatus an age span of 0.19-0.53 Ma according to the oxygen isotope stack of Lisiecki and Raymo (2005).

2.2 ELT 25-11 (50˚02'S, 127˚31'W, 3969m)

ELT 25-11 contains a single large hiatus that appears to be equivalent to **Hiatuses B and C** in MV0502-4JC. Previous nannofossil work on the core had identified a hiatus with a maximum age span of 0.30-1.95 Ma at ~3.74 MBSF (Geitzenauer and Huddlestun, 1972; King, 1988). However, after developing a radiolarian stratigraphy and stable isotope record for Core ELT 25-11, I suggest that the hiatus is actually located at a prominent carbonate dissolution event at 1.94 MBSF and has a slightly shorter age span of ~0.3-1.55 Ma. The original placement of the hiatus by Geitzenauer and Huddlestun (1972) and King (1988) was primarily based on the disappearance of *P. laconosa* above 3.89 MBSF rather than on the presence of any key indicator species. Our radiolarian stratigraphy and stable isotope record for ELT 25-11 both suggest that the hiatus is located nearer to the top of the core, at least above 2.54 MBSF. The stable isotope record from ELT 25-11 (**Fig 2.4**), while coarse, displays the distinctive Late Pliocene features of the MV0502-4JC record, including the positive benthic $\delta^{18}O$ and negative benthic $\delta^{13}C$ excursions of the Late Pliocene Climatic Transition and large positive planktonic and benthic $\delta^{13}C$ shifts of ~1‰ near the Late Pliocene/Pleistocene boundary. The large

positive planktonic and benthic $\delta^{13}C$ shifts end just before the hiatus, providing a lower boundary for the hiatus of ~1.55 Ma according to our MV0502-4JC stratigraphy. The upper boundary of the hiatus is more difficult to constrain based upon stable isotopes because the record is not as distinctive. Thus, I assign an age of ~0.3 Ma to the top of the hiatus based upon the placement of the CN14b/CN15 boundary (0.26 Ma) at 0.74 MBSF in the aforementioned nannofossil studies.

2.3 ELT 20-2 (49˚00'S, 144˚50'W, 4517 m)

The age of the carbonate-rich upper half of ELT 20-2 was constrained using radiolarian and stable isotopes stratigraphy. A hiatus is indicated by missing glacial-interglacial cycles between the top of the core and 1.03 MBSF, where *Stylatractus universus* (LO 0.425 Ma) was noted. Thus, I place the hiatus at ~0.9 MBSF where the core records a large decline in $CaCO_3$. Assuming that the top of the core was recovered, then only MIS 1-6 are recorded above the hiatus, giving the upper boundary of the hiatus an age of ~0.19 Ma. The lower boundary is not well constrained, but has a maximum age of 0.425 Ma based on the presence of *Stylatractus universus* and a minimum age of 1.63 Ma based on the presence of *Theocorythium trachelium* (FO= 1.63 Ma).

3. The Subantarctic Pacific Hiatuses as an Indication of Past Increases in the ACC

Our results indicate that current activity created three significant hiatuses in MV0502-4JC: an early Pliocene-early Late Pliocene hiatus with an upper boundary at ~3.0 Ma (Hiatus A) and two Pleistocene hiatuses spanning ~1.57-0.68 Ma (Hiatus B) and ~0.53-0.19 Ma (Hiatus C), respectively (**Figure 3.3**). Hiatuses B and C appear to have been combined into the single large hiatus in ELT 25-11, which spans from ~0.3 to 1.55 Ma, and only Hiatus C is recorded in ELT 20-2, the shortest of the three cores.

As all three of these cores were recovered near the SAF, their shared hiatuses likely record increases in the strength of the ACC. In fact, comparison of the hiatuses identified in MV0502-4JC to those on the Maurice Ewing Bank (MEB) in the southwestern Atlantic (Ciesielski et al., 1982), also in the path of the ACC (**Figure 3.2**), reveals some striking similarities. Fluctuations in the intensity of the ACC resulted in deposition on the bank from ~4.5 to 3.9 Ma but widespread erosion and/or non-deposition between ~4.0 and 3.2 Ma. Deposition resumed after 2.8 Ma, but an increase

in circumpolar circulation between 1.2 and 1.0 Ma resulted in a regional disconformity on the MEB spanning from 2.0 to 1.0 Ma. Thus, the findings of Ciesielski et al. (1982) also support an intensification of the ACC in the Pliocene between ~4.0 and 3.2 Ma and in the Pleistocene from 1.2-1.0 Ma, similar to Hiatuses A and B in MV0502-4JC. While Hiatus C, which is of short duration, was not specifically identified on the MEB, sedimentation was intermittent during the Brunhes Chron (0.72 Ma-Present) prior to the deposition of a carbonate ooze on the bank over the past 0.2 Myr (Ciesielski et al., 1982).

4. A Correlation with Hiatuses in Other Regions of Significant Current Activity

Studies of sediments in regions of significant bottom water flow outside of the influence of the ACC have also reported intervals of increased current intensity similar to those recorded in the subantarctic cores examined in this study. Increased late Pliocene bottom water intensity in the Vema Channel (**Figure 3.2)**, a narrow gap in the Rio Grande Rise in the Southwest Atlantic through which AABW flows northward from the Argentine to the Brazil Basin, prior to 2.94-2.90 Ma is consistent with Hiatus A (Ledbetter et al., 1978). In the region where the Indian Ocean deep western boundary current enters the South Australia Basin (**Figure 3.2)**, a coarsening of mean particle size from ~4.3-3.8 Ma and a cessation of intense Pliocene flow at ~2.6 Ma, coincides with Hiatus A (Ledbetter, 1981). Furthermore, an unconformity from ~1.35 to 0.72 Ma is consistent with Hiatus B (Ledbetter, 1981). DSDP Sites 141, 366, 397, and 544B (2800-4000 m depth; **Figure 3.2**) along the continental margin of Northwest Africa, which largely record NADW flow, also exhibit hiatuses or significantly reduced sedimentation rates near the Early-Late Pliocene boundary (with an upper limit at 2.5 Ma) and between 1.6 and 0.78 Ma (Stein et al., 1986), similar to Hiatuses A and B in MV0502-4JC. Hiatus C is not as frequently resolved as Hiatuses A and B, perhaps due to its short duration, but is present at DSDP Site 544B in the form of significantly reduced terrigenous and calcium-carbonate flux rates, which Stein and Sarnthein (1984) attribute to an increase in winnowing and carbonate dissolution after 0.73 Ma.

In addition to erosion, dissolution likely also played a role in the creation of these hiatuses. Marine carbon isotope records show a series of $\delta^{13}C$ maxima at 0.47-0.53 Ma, 0.97-1.04 Ma, and 1.55-1.65 Ma that are accompanied by major changes in glacial cyclicity (Wang et al., 2004). These $\delta^{13}C$ maxima, which have been associated with

changes in productivity, the oceanic "rain ratio," and increased carbonate dissolution in the Indo-Pacific, are a reflection of long-term, high-amplitude oscillations in the global carbon cycle, which has operated at a cyclicity of ~500 kyr during the Pleistocene (Wang et al., 2004). Several mid-Pliocene dissolution events, which are likely the result of transient changes in the carbonate system, such as variations in sea level, circulation, and/or productivity, have also been identified between 3.9 and 3.0 Ma in the equatorial Pacific (Farrell and Prell, 1991). Thus, while carbonate dissolution was likely a factor in the formation of all three of the hiatuses described in this study, certain aspects of the hiatuses, such as reworking associated with Hiatus A, the long duration of Hiatuses A and B, and the excellent preservation of foraminifera prior to, and following Hiatuses B and C, suggest that increased erosion also had a role. Grain size analysis of sediments from the South Australia Basin and DSDP Site 544B also support an increase in current velocity during these hiatus intervals (Ledbetter, 1981; Stein and Sarnthein, 1984).

5. Periods of Increased Global Overturning Circulation during the Late Neogene--Is there a Link to Climate?

With a good correlation found between the hiatuses identified in the subantarctic Pacific and those known from cores recovered in other regions of vigorous flow, I propose that the shared hiatuses may be indicative of periods of increased global overturning circulation. Because modeling studies suggest a link between increases in global circulation and warm climatic conditions (de Boer et al., 2008; Toggweiler et al., 2006), I examine the hiatuses in the relation to the "exceptional warm periods" of the late Neogene: 1) the Early-Mid Pliocene Warm Period, 2) MIS 31 and 21 during the Mid-Pleistocene Revolution, and 3) MIS 11 and MIS 9 (~0.4-0.3 Ma) during the Mid-Brunhes.

ANDRILL results support an extended period of ice-free conditions in the Ross Sea, indicative of a reduced West Antarctic Ice Sheet (WAIS), during both the early Pliocene and MIS 31 (Naish, 2007). The resumption of deposition in MV0502-4JC after ~3.0 Ma is marked by dramatic shifts in benthic $\delta^{18}O$ and $\delta^{13}C$ that record, respectively, and a decrease in the temperature and ventilation of the abyssal Southern Ocean during the Late Pliocene climatic transition (LPCT; **Figure 3.3**). The LPCT, which corresponds to the onset of Northern Hemisphere Glaciation, was associated with the re-expansion of

the Ross Ice Shelf and significant sea ice growth in the Southern Ocean (Kennett and Barker, 1990). Specifically, ANDRILL results also suggest that the Ross Sea alternated between subglacial/ice-proximal and open water conditions between ~2.6 and 2.2 Ma (Naish, 2007). A widespread disconformity and shoaling of the calcium carbonate compensation depth in the Ross Sea marks the regrowth of the ice shelf during the Late Pliocene (Fillon, 1975). Thus, I propose that Hiatus A in MV0502-4JC, with its upper boundary at ~3.0 Ma, may be linked to the exceptional warmth that forced the retreat of the WAIS in the early and middle Pliocene. As for Hiatus B (~1.57-0.68 Ma), which encompasses the extreme interglaciations of MIS 31 and 21 and ends at the initiation of MIS 16, the first significant glaciation of the late Neogene, this hiatus may be linked to the initiation of longer interglacial intervals as glacial-interglacial cycles transitioned from 41 ka to 100 ka during the Mid-Pleistocene Revolution (~1 Ma).

A second transitional period, the "Mid Brunhes transition," occurred at MIS 11 (~420 kyr), at which time interglacial intervals began to exhibit warmer temperatures and/or less ice volume than preceding interglacials (Hodell et al., 2003b). MIS 11 and MIS 9, in particular, are known for prolonged warmth, an extraordinary poleward penetration of warm surface waters (Scherer, 2003), and sea levels higher than those of MIS 5 and the Holocene (Droxler et al., 2003). Much evidence has been presented in support of a significant reduction in sea ice and a southward migration of the polar and subantarctic fronts in the Southern Ocean during MIS 11 (Hodell et al., 2003b; Kunz-Pirrung et al., 2002; Morley, 1989), and much still remains to be learned about MIS 7. Thus, Hiatus C (~0.53-0.19 Ma) could be linked to increased circulation during the stronger interglacial events of the Mid Brunhes (MIS 11, 9, and 7).

6. Enhanced Global Circulation During Warm Climates?

The hiatuses identified in this study suggest that global overturning circulation may have been enhanced during the Early Pliocene Warm Period and the climatic transitions of the Mid-Pleistocene Revolution and the Mid-Brunhes. Because these climatic transitions are both associated with the initiation of longer and/or more extreme interglacials, the hiatus record appears to support a link between warmer climates and stronger global circulation over the late Neogene. These results are consistent with the reduced benthic $\delta^{13}C$ gradients of the early Pliocene (Hodell and Venz-Curtis, 2006;

Ravelo and Andreasen, 2000), and with the modeling results of de Boer et al. (2008), which support a more globally-distributed and less "Atlantic-dominated" overturning during warmer climates.

De Boer et al. (2008) specifically show that under warmer climatic conditions a strengthening of either Southern Ocean or global winds would increase not only the global rate of overturning by forcing greater vertical transport but would also allow overturning to be more globally-distributed through a weakening of salinity gradients. The idea that deep circulation is "pulled" by mechanical mixing (wind-driven upwelling, turbulence and/or tidal interaction with the seafloor) rather than "pushed" by sinking of dense polar waters is now widely accepted (de Boer et al., 2008). Additionally, because ~70% of all wind energy applied to ocean currents globally goes directly into the ACC (Munk and Wunsch, 1998), a strengthening or southward migration of the westerly winds over the Southern Ocean may be all that would have been needed to force an increase in global overturning during intervals of climatic warmth (Toggweiler et al., 2006). Presently the westerly winds (mean position between 45 and 50°S) are not actually aligned with the ACC, whose mean position between 50-56°S is determined by the position of South America. Thus overturning circulation may be expected to increase in the future if the westerly winds over the Southern Ocean continue to strengthen and migrate poleward in response to increased thermal gradients in the middle atmosphere (Fyfe and Saenko, 2005).

Some evidence has been presented for increased Antarctic Bottom Water formation in the Southern Ocean during glacial as opposed to interglacial intervals. Pore fluid measurements, for example, show that the waters of the abyssal Southern Ocean were considerably saltier than today during the LGM (Adkins et al., 2002), which suggests that the sinking of cold, dense brines could potentially have "pushed" a stronger overturning circulation in the Southern Ocean during glacial intervals. Further support for increased AABW formation during cold climates comes from a greater mean sortable silt size at ODP Site 1123 on the North Chatham drift during glacial, relative to interglacial, intervals of the past 1.2 million years (Hall et al., 2001). Despite its positioning along the Deep Western Boundary Current (DWBC), however, Site 1123 is not ideally located for recording increases in DWBC flow independent of northward

migrations of the ACC during glacial intervals. Additionally, $\delta^{13}C$ studies indicate that the deep Southern Ocean (>2500 m) was very poorly ventilated during glacial intervals (Hodell et al., 2003a; Ninneman and Charles, 2002), a finding which is irreconcilable with a strong overturning circulation. Thus, while the sinking of cold, dense waters in the Southern Ocean could have been a relatively important mechanism of bottom water formation during glaciations, this sinking alone does not appear to have been linked to an increase in overturning circulation, and, quite to the contrary appears, consistent with the model of Munk and Wunsch (1998), to have led to the creation of a stagnant pool of dense water at the bottom of the ocean.

7. Conclusions

Hiatuses in MV0502-4JC and two Eltanin piston cores recovered from the subantarctic Pacific region suggest increases in ACC intensity and carbonate dissolution during the Early Pliocene Warm Period as well as the Mid-Pleistocene and Mid-Brunhes climatic transitions. The hiatuses in these cores correlate well with intervals of erosion/ reduced deposition on the Maurice Ewing Bank (Ciesielski et al., 1982), also in the path of the ACC, as well as with intervals of reduced sedimentation reported from diverse regions of bottom water flow including the Vema Channel (Ledbetter et al., 1978), the South Australia Basin (Ledbetter, 1981), and the continental margin of Northwest Africa (Stein et al., 1986). Thus, by examining hiatuses I identify three intervals in the late Neogene sediment record during which the oceans appear to have displayed a stronger and more globally-distributed overturning circulation relative to the present day, and I suggest that the shared link between these three periods may have been exceptional climatic warmth.

The early and middle Pliocene are known for climatic warmth, and the mid-Pleistocene and mid-Brunhes were transitional periods during which interglacial intervals became longer and/or more extreme. Well-known examples of extreme interglacials during these transitions are MIS 31, 21, 11, and 9. Much still remains to be learned about the severity of each of the interglaciations associated with these transitions, however, and further research on cores exhibiting uninterrupted sedimentation will be needed in order to investigate variations in deepwater flow within the mid-Pleistocene and mid-Brunhes intervals. Overall, however, the findings of this study support the modeling results of

deBoer et al. (2008), which demonstrate that, when considered in a global context, overturning circulation has a tendency to become stronger and less "Atlantic-dominated" during warmer climates. Moreover, ~70% of all wind energy applied to ocean currents globally goes directly into the ACC (Munk and Wunsch, 1998), and thus a plausible mechanism for increasing oceanic circulation during warm climatic intervals would be a strengthening and/or poleward shift in the Southern Hemisphere Westerlies (Toggweiler et al., 2006), a trend that has been manifesting in the modern Southern Ocean over the past 40 years (Thompson and Solomon, 2002; Trenberth et al., 2007).

ACKNOWLEDGEMENTS

I would like to thank my coauthors on this chapter Ingrid Hendy, Ted Moore, and Mitch Lyle. I was supported through the Sweetland Dissertation Writing Institute and a Rackham One Term Dissertaion Fellowship during the writing of this manuscript. The South Pacific Latitudinal Transect (SPLAT) cruise was supported by the National Science Foundation grants OCE-0240924 to the University of Michigan and OCE-0240906 to Boise State University. I want to thank Lora Wingate of the University of Michigan Stable Isotope Laboratory for the carbonate analyses.

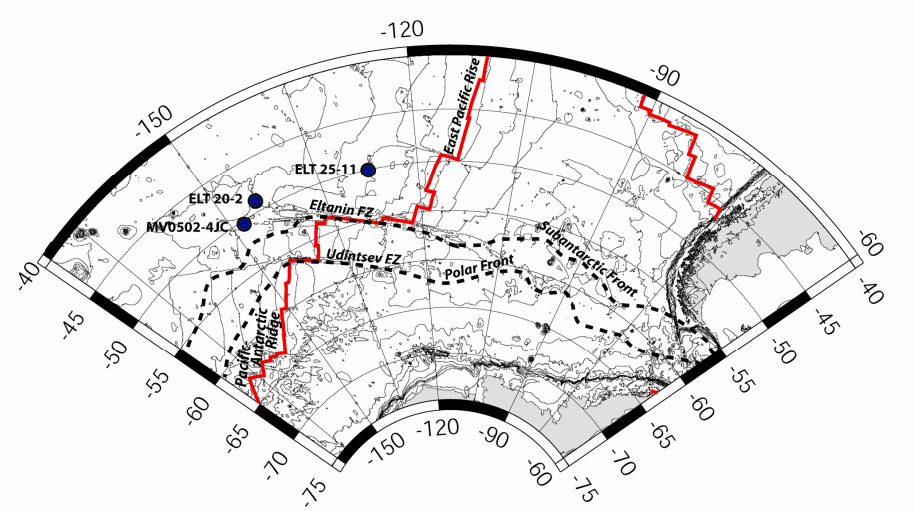

Figure 3.1. Bathymetric map of the study region, depicting the core locations of MV0502 4JC (50°20'S, 148°08'W, 4286 m) and Eltanin cores, ELT 25-11 (50°02'S, 127°31'W, 3969 m) and ELT 20-2 (49°00'S, 144°50'W, 4517 m). Solid lines depict the mid-oceanic ridge system, while dotted lines represent frontal systems.

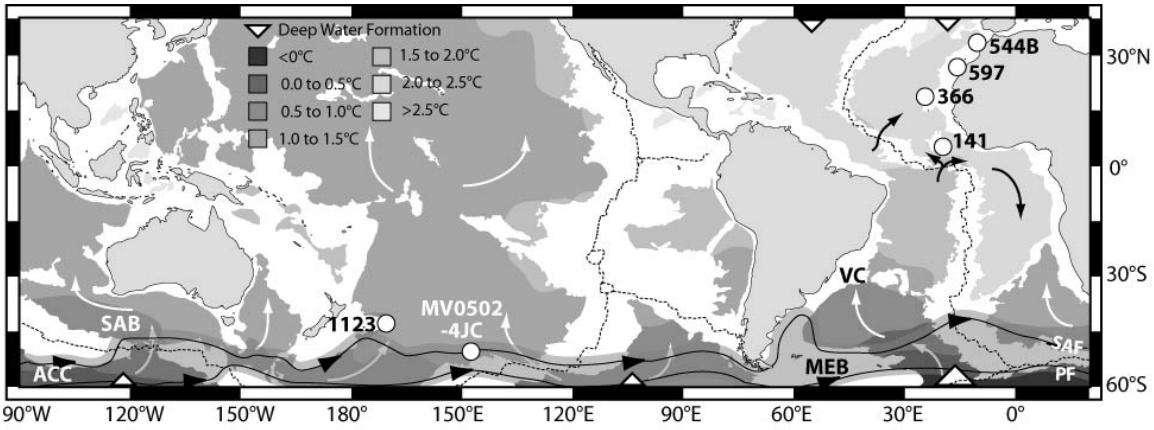

Figure 3.2. Temperature of water at 4 km water depth relative to the core locations discussed in this chapter. MEB=Maurice Ewing Bank, VC=Vema Channel, and SAB=South Australia Basin, SAF=Subantarctic Front, PF=Polar Front. Dotted lines depict the mid-oceanic ridge system, whereas solid lines represent frontal systems and the ACC. Arrows indicate flow direction.

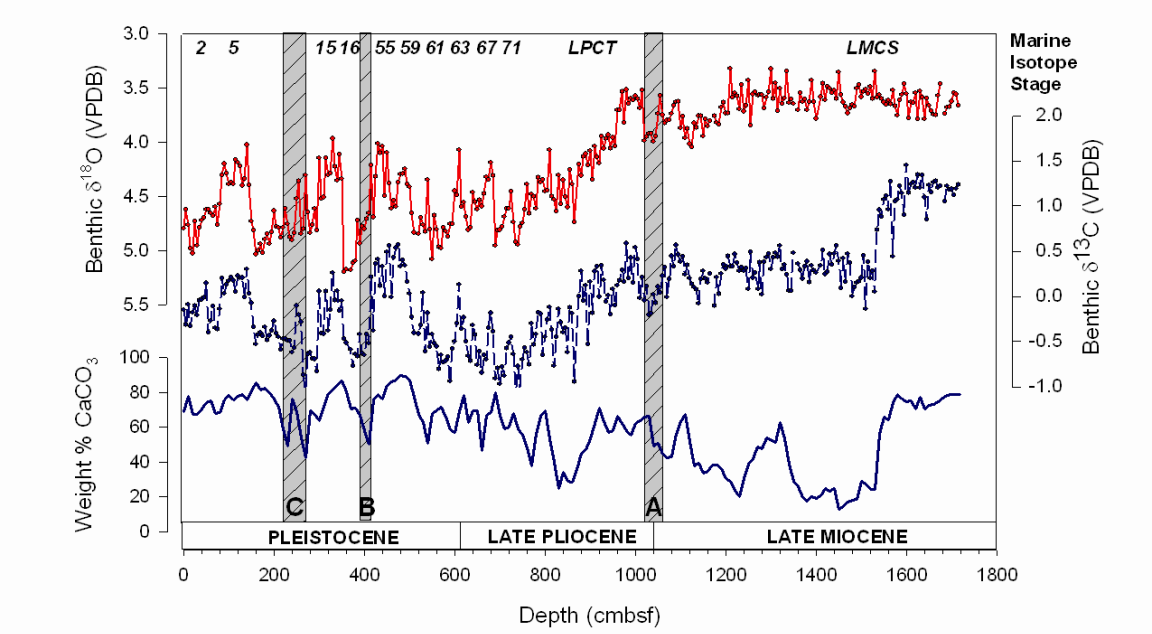

Figure 3.3: Benthic stable isotope (*Cibicidoides* spp.) and weight percent $CaCO_3$ results from MV0502-4JC. Grey patterned areas mark the hiatuses. Ages of the hiatuses are as follows: Hiatus A= early Pliocene-early Late Pliocene, Hiatus B= ~1.57-0.68 Ma, and Hiatus C=~0.53-0.19 Ma. LMCS=Late Miocene Carbon Shift and LPCT=Late Pliocene Climate Transition.

REFERENCES

Adkins, J.F., McIntyre, K., and Schrag, D.P., 2002, The salinity, temperature, and $\delta^{18}O$ of the glacial deep ocean: Science, v. 298, p. 1769-1773.

Aoki, S., Bindoff, N.L., and Church, J.A., 2005, Interdecadal water mass changes in the Southern Ocean between 30°E and 160°E: Geophysical Research Letters, v. 32, p. L07607, doi:10.1029/2004GL022220.

Barker, P.F., and Thomas, E., 2004, Origin, signature and palaeoclimatic influence of the Antarctic Circumpolar Current: Earth Science Reviews, v. 66, p. 143-162.

Ciesielski, P.F., Ledbetter, M.T., and Ellwood, B.B., 1982, The development of Antarctic glaciation and the Neogene paleoenvironment of the Maurice Ewing Bank: Marine Geology, v. 46, p. 1-51.

de Boer, A.M., Toggweiler, J.R., and Sigman, D.M., 2008, Atlantic dominance of the meridional overturning circulation: Journal of Physical Oceanography, v. 38, p. 435-449.

Dixon, K.W., Delworth, T.L., Spelman, M.J., and Stouffer, R.J., 1999, The influence of transient surface fluxes on North Atlantic overturning in a coupled GCM climate change experiment: Geophysical Research Letters, v. 26, p. 2749-2752.

Droxler, A.W., Alley, R.B., Howard, W.R., Poore, R.Z., and Burckle, L.H., 2003, Unique and exceptionally long interglacial Marine Isotope Stage 11: Window into Earth warm future climate, *in* Droxler, A.W., Poore, R.Z., and Burckle, L.H., eds., Earth's Climate and Orbital Eccentricity: The Marine Isotope Stage 11 Question: Washington D.C., American Geophysical Union, p. 1-14.

Farrell, J.W., and Prell, W.L., 1991, Pacific $CaCO_3$ preservation and $\delta^{18}O$ since 4 Ma: Paleoceanic and paleoclimatic implications: Paleoceanography, v. 6, p. 485-498.

Fillon, R.H., 1975, Late Cenozoic paleo-oceanography of the Ross Sea, Antarctica: Geological Society of America Bulletin, v. 86, p. 839-845.

Fyfe, J.C., and Saenko, O.A., 2005, Human-induced change in the Antarctic Circumpolar Current: Journal of Climate, v. 18, p. 3068-3073.

Geitzenauer, K.R., and Huddlestun, P., 1972, An upper Pliocene-Pleistocene calcareous nannofossil flora from a subantarctic Pacific deep-sea core: Micropaleontology, v. 18, p. 405-409.

Gregory, J.M., Dixon, K.W., Stouffer, R.J., Weaver, A.J., Driesschaert, E., Eby, M., Fichefet, T., Hasumi, H., Hu, A., Jungclaus, J.H., Kamenkovich, I.V., Levermann, A., Montoya, M., Murakami, S., Nawrath, S., Oka, A., Sokolov, A.P., and

Thorpe, R.B., 2005, A model intercomparison of changes in the Atlantic thermohaline circulation response to increasing atmospheric CO_2 concentration: Geophysical Research Letters, v. 32, p. L12703, doi:10.1029/2005GL023209.

Hall, I.R., McCave, I.N., Shackleton, N.J., Weedon, G.P., and Harris, S.E., 2001, Intensified deep Pacific inflow and ventilation in Pleistocene glacial times: Nature, v. 412, p. 809-812.

Hodell, D.A., and Venz, K., 1992, Toward a high-resolution stable isotope record of the Southern Ocean during the Pliocene-Pleistocene (4.8 to 0.8 Ma), *in* Kennett, J.P., and Warnke, D.A., eds., The Antarctic Paleoenvironment: A perspective on global change, Antarct. Res. Ser., Volume 56: Antarctic Research Series: Washington D.C., AGU, p. 265-310.

Hodell, D.A., Venz, K.A., Charles, C.D., and Ninnemann, U.S., 2003a, Pleistocene vertical carbon isotope and carbonate gradients in the South Atlantic sector of the Southern Ocean: Geochemistry, Geophysics, Geosystems, v. 4, p. 1004, doi:10.1029/2002GC000367.

Hodell, D.A., Venz, K.A., Charles, C.D., and Sierro, F.J., 2003b, The mid-Brunhes transition in ODP sites 1089 and 1090, *in* Droxler, A.W., Poore, R.Z., and Burckle, L.H., eds., Earth's Climate and Orbital Eccentricity: The Marine Isotope Stage 11 Question, Volume 137: Geophysical Monograph: Washington D.C., American Geophysical Union, p. 113-129.

Hodell, D.A., and Venz-Curtis, K.A., 2006, Late Neogene history of deepwater ventilation in the Southern Ocean: Geochemistry, Geophysics, Geosystems, v. 7, p. Q09001, doi:10.1029/2005GC001211.

Kennett, J.P., and Barker, P.F., 1990, Latest Cretaceous to Cenozoic climate and oceanographic developments in the Weddell Sea, Antarctica: An ocean-drilling perspective: Proceedings of Ocean Drilling Program, Scientific Results, v. 113, p. 937-960.

King, R.E., Jr., 1988, Sediment distribution, accumulation rates, and climatic change in the southeast Pacific [Master's thesis]: Hattiesburg, University of Southern Mississippi.

Kunz-Pirrung, M., Gersonde, R., and Hodell, D.A., 2002, Mid-Brunhes century-scale diatom sea surface temperature and sea ice records from the Atlantic sector of the Southern Ocean (ODP Leg 177, sites 1093, 1094, and core PS2089-2: Palaeogeography, Palaeoclimatology, Palaeoecology, v. 182, p. 305-328.

Ledbetter, M.T., 1981, Paleoceanographic significance of bottom-current fluctuations in the Southern Ocean: Nature, v. 294, p. 554-556.

Ledbetter, M.T., Williams, D.F., and Ellwood, B.B., 1978, Late Pliocene climate and south-west Atlantic abyssal circulation: Nature, v. 272, p. 237-239.

Lisiecki, L.E., and Raymo, M.E., 2005, A Plio-Pleistocene stack of 57 globally distributed benthic $\delta^{18}O$ records: Paleoceanography, v. 20, p. PA1003, doi:10.1029/2004PA001071.

Lynch-Stieglitz, J., Adkins, J.F., Curry, W.B., Dokken, T., Hall, I.R., Herguera, J.C., Hirschi, J.J.-M., Ivanova, E.V., Kissel, C., Marchal, O., Marchitto, T.M., McCave, I.N., McManus, J.F., Mulitza, S., Ninneman, U.S., Peeters, F., Yu, E.-F., and Zahn, R., 2007, Atlantic Meridional Overturning Circulation during the Last Glacial Maximum: Sceince, v. 316, p. 66-69.

Morley, J.J., 1989, Variations in high-latitude oceanographic fronts in the southern Indian Ocean: An estimation based on faunal changes: Paleoceanography, v. 4, p. 547-554.

Munk, W., and Wunsch, C., 1998, Abyssal recipes II: energetics of tidal and wind mixing: Deep Sea Research Part I: Oceanographic Research Papers, v. 45, p. 1977-2010.

Naish, T.R., 2007, Neogene climate history of Antarctica: Initial results from ANDRILL McMurdo Ice Shelf Project: Eos Trans. AGU, v. 88, p. Fall Meet. Suppl., Abstract U21F-03.

Ninneman, U.S., and Charles, C.D., 2002, Changes in the mode of Southern Ocean circulation over the last glacial cycle revealed by foraminiferal stable isotopic variability: Earth and Planetary Science Letters, v. 201, p. 383-396.

Ravelo, A.C., and Andreasen, D.H., 2000, Enhanced circulation during a warm period: Geophysical Research Letters, v. 27, p. 1001-1004.

Rintoul, S.R., and Sokolov, S., 2001, Baroclinic transport variability of the Antarctic Circumpolar Current south of Australia (WOCE repeat section SR3): Journal of Geophysical Research, v. 106, p. 2815-2832.

Scherer, R.P., 2003, Quaternary interglacials and the West Antarctic Ice Sheet, *in* Droxler, A.W., Poore, R.Z., and Burckle, L.H., eds., Earth's Climate and Orbital Eccentricity: The Marine Isotope Stage 11 Question: Washington D.C., American Geophyscial Union, p. 103-112.

Stein, R., and Sarnthein, M., 1984, Late Neogene oxygen-isotope stratigraphy and flux rates of terrigenous sediments at Hole 544B off Morocco, *in* Hinz, K., and Winterer, E.L., et al., eds., Init. Repts. DSDP, Volume 79: Washington (U.S. Govt. Printing Office), p. 385-394.

Stein, R., Sarnthein, M., and Suendermann, J., 1986, Late Neogene submarine erosion events along the north-east Atlantic continental margin, *in* Summerhayes, C.P., and Shackleton, N.J., eds., North Atlantic Paleoceanography: Geological Society Special Publication No. 21, p. 103-118.

Stow, D.A.V., Faugères, J.-C., Howe, J.A., Pudsey, C.J., and Viana, A.R., 2002, Bottom currents, contourites and deep-sea sediment drifts: current state-of-the-art, *in* Stow, D.A.V., Pudsey, C.J., Howe, J.A., Faugères, J-C. and Viana, A.R., ed., Deep-water contourite systems: modern drifts and ancient series, seismic and sedimentary characteristics, Volume 22: Geological Society Memoir: London, UK, Geological Society of London, p. 7-20.

Tedford, R.A., and Kelley, D.C., 2004, A deep-sea record of the Late Miocene carbon shift from the Southern Tasman Sea, *in* Exon, N., Kennett, J.P., and Malone, M., eds., The Cenozoic Southern Ocean: Tectonics, Sedimentation and Climate Change between Australia and Antarctica, Geophysical Union Monograph Series 151: Geophysial Monograph: Washington D.C., American Geophysical Union, p. 273-290.

Thompson, D.W.J., and Solomon, S., 2002, Interpretation of recent Southern Hemisphere climate change: Science, v. 296, p. 895-899.

Toggweiler, J.R., and Russell, J.L., 2008, Ocean circulation in a warming climate: Nature, v. 45.

Toggweiler, J.R., Russell, J.L., and Carson, S.R., 2006, Midlatitude westerlies, atmospheric CO_2, and climate change during the ice ages: Paleoceanography, v. 21, p. PA2005, doi:10.1029/2005PA001154.

Trenberth, K.E., Jones, P.D., Ambenje, P., Bojariu, R., Easterling, D., Klein Tank, A., Parker, D., Rahimzadeh, F., Renwick, J.A., Rusticucci, M., Soden, B., and Zhai, P., 2007, Observations: Surface and atmospheric climate change, *in* Solomon, S., Quin, D., Manning, M., Chen, Z., Marquis, M., Averyt, K.B., Tignor, M., and Miller, H.L., eds., Climate Change 2007: The physical science basis. Contribution to the Working Group I to the Fourth Assessment Report of the Intergovernmental Panel on Climate Change.: Cambridge and New York, Cambridge University Press.

Wang, P., Tian, J., Cheng, X., Liu, C., and Xu, J., 2004, Major Pleistocene stages in a carbon perspective: The South China Sea record and its global comparison: Paleoceanography, v. 19, p. PA4005, doi:10.1029/2003PA00091.

Chapter 4

Salinity of the Eocene Arctic Ocean from Oxygen Isotope Analysis of Fish Bone Carbonate

Abstract

Stable isotope analysis was performed on the structural carbonate of fish bone apatite from early and early middle Eocene samples (~55 to ~45 Ma) recently recovered from the Lomonosov Ridge by IODP Expedition 302 (the Arctic Coring Expedition). The $\delta^{18}O$ values of the Eocene samples ranged from –6.84‰ and –2.96‰ VPDB, with a mean value of -4.89‰, as compared to 2.77‰ for a Miocene sample in the overlying section. An average salinity of 21 to 25‰ was calculated for the Eocene Arctic, as compared to 35‰ for the Miocene, with lower salinities during the Paleocene Eocene Thermal Maximum (PETM), the *Azolla* event at ~48.7 Ma, and a third previously unidentified event at ~47.6 Ma. At the *Azolla* event, where the organic carbon content of the sediment reaches a maximum, a positive $\delta^{13}C$ excursion was observed, indicating unusually high productivity in the surface waters.

1. Introduction

The Arctic is relatively isolated from the world ocean and receives a net surplus of freshwater through the hydrologic cycle, mostly as runoff. The freshwater surplus creates a low salinity layer (32.5‰) in the upper 50 m of the Arctic water column, known as the Polar Mixed Layer, which limits vertical mixing and promotes sea ice formation. As a result, the Arctic exhibits a strong salinity stratification and an estuarine-like circulation pattern, with the lighter, fresher waters of the Polar Mixed Layer overriding Atlantic waters entering through the Fram Strait. Low salinity surface water is exported to the Norwegian-Greenland Sea via the East Greenland Current, where it mixes with relatively warm, saline water from the Atlantic and sets up the deep convection that produces the Denmark Strait Overflow Water (DSOW) and the Iceland Sea Overflow

Water (ISOW), the densest components of North Atlantic Deep Water (NADW), which enter the Atlantic basin through overflow of the Greenland-Faroe Ridge. The Arctic plays a vital role in global climate through its influence on the production of NADW. However, deepwater formation in the Norwegian-Greenland Sea is delicately balance and an increase in the export of fresh water from the Arctic, whether through a reduction in surface salinity or an increase in sea ice discharge, has the potential to cap convective regions and reduce thermohaline circulation (Aagaard and Carmack, 1989). An example of such an event is the "Great Salinity Anomaly" of the late 1960's. During this time a freshening of the surface waters north of Iceland may have resulted from a 25% greater than average outflow of fresh water from the Arctic Ocean over a two year period (Aagaard and Carmack, 1989). The anomaly corresponded with a significant freshening and cooling of North Atlantic Deepwater (Brewer et al., 1983), and its occurrence raises concerns about the threat the Arctic could pose to NADW formation under future anthropogenic warming.

During the greenhouse climate of the early and mid Eocene, plate tectonic reconstructions suggest that the Arctic may have had even less of a deepwater connection to the world ocean than it does today (**Figure 4.1**). Without major continental ice sheets at this time, sea level was substantially (30-100m) higher than in modern times (Miller et al., 2005a); however the Fram Strait, the only deep connection between the Arctic and the world ocean, may not have allowed for bi-directional exchange with the Norwegian-Greenland Sea until 17.5 Ma (Jakobsson et al., 2007) and may not have opened fully until the late Miocene (Lawver et al., 1990). Thus with an intensified hydrologic cycle under a warm Eocene climate and fewer connections to the world ocean, it might be expected that the near surface water of the Eocene Arctic was even fresher than it is today and that the outflow of low salinity water from the basin may have acted to prevent the formation of deepwater in the high latitude northern seas.

Recent evidence suggests significant shifts in deep- and intermediate- water production between the high southern and high northern latitudes in response to changes in global temperature during the late Cretaceous and Paleogene. As the highest latitude ocean basin, the exact role of the Arctic in deep water production during this period is still uncertain. Modeling studies and $\delta^{13}C$ data suggest that a significant intensification

of the hydrologic cycle in response to extreme global warmth may have initiated a switch in deepwater formation from the high southern to the high northern latitudes (Bice and Marotzke, 2002; Nunes and Norris, 2006). During peak warmth, the salinity of Southern Ocean surface waters would have been significantly reduced by an increase in high latitude precipitation, thereby inhibiting convection, but deepwater formation in the North Pacific may have been enhanced by the import of higher salinity subtropical surface waters from the North Atlantic through the Central American Seaway. In the modeling studies of Bice and Marotzke (2002), deep convection occurs in the high northern latitudes at the PETM despite an intensified hydrologic cycle because Arctic outflow is diverted directly into the Northwestern Tethys by the Greenland-Faroe Ridge. Uplift of the North Atlantic region may have severed the Rockall Trough connection between the Atlantic and Arctic and allowed mammal migration between North America and Europe across the Greenland-Faroe Ridge over an approximately 2 million year period in the late Paleocene and early Eocene (Knox, 1998). However, once a surface water connection was reestablished between the Arctic and the North Atlantic, we must be concerned with the possible role of Arctic outflow on oceanic circulation.

To better evaluate oceanographic conditions within the Arctic basin, and thus the possible impact of Arctic outflow on global circulation, this study estimates the salinity of the Eocene Arctic Ocean using $\delta^{18}Oco_3^{2-}$ of fish apatite from cores recently recovered from the Lomonosov Ridge by IODP Expedition 302, the Arctic Coring Expedition (ACEX). The results of this study will also allow an assessment of the degree of isolation of the Arctic Ocean during the Eocene.

2. Tectonic Setting

The modern Arctic Ocean contains two deep basins separated by the Lomonosov Ridge: the Amerasia and Eurasia Basins. The Amerasia Basin, in turn, is divided into two sub-basins, the Canada and Makarov, by the Alpha-Mendeleev Ridge, and the Eurasia Basin is divided into the Nansen and Amundsen sub-basins by the Gakkel Ridge, the Arctic crustal spreading center. Although the tectonic evolution of the Eurasia Basin is much better understood than that of the Amerasia Basin, it is commonly accepted that the Canada sub-basin of the Amerasia Basin opened in the early Cretaceous through

seafloor spreading along a now extinct ridge. The spreading resulted in the counter-clockwise rotation of the Arctic Alaska and Chukotka terranes away from the Arctic Islands and toward their respective present day locations in northern Alaska and Siberia (Lawver et al., 2002). By the mid Cretaceous, circulation between the Arctic and Pacific had been obstructed by the rotated blocks (Johnson et al., 1994), and by the late Cretaceous, the Arctic connection to the Pacific Ocean was probably closed as mammals were able to migrate between Asia and western North America via the Beringia land bridge (Averianov and Archibald, 2003). The complicated arrangement of microplates in easternmost Siberia, however, leaves some doubt about the exact nature of inter-basin passages between the Arctic and the Pacific during the early Cenozoic.

Spreading in the Eurasia basin along the Gakkel Ridge commenced between Anomaly 24 and 25 (~57 Ma), close to the Paleocene/Eocene boundary and approximately contemporaneous with the onset of spreading in the southern Norwegian-Greenland Sea (Thiede and Myhre, 1996). It is widely accepted that the Lomonosov Ridge is of continental origin and was rifted as a series of tilted fault blocks from the Barents/Kara Shelf during the opening of the Eurasia Basin (Johnson et al., 1994). Since rifting, the ridge has subsided to modern depths of approximately 1000-1600 m and has posed a great barrier to deep circulation within the Arctic since its creation (Johnson et al., 1994).

Reconstructions show no clear evidence of a deepwater connection between the Arctic and the world ocean during the Eocene. The opening of the Norwegian-Greenland Sea between Greenland and Svalbard was delayed until Anomaly 13, so the Fram Strait, the only deepwater connection between the Arctic and Norwegian Greenland Sea in existence today, may have allowed only shallow water exchange prior to the early Miocene (17.5 Ma) (Jakobsson et al., 2007), with a full opening and deepwater exchange existing at least since the late Miocene (7.5 to 5 Ma) (Lawver et al., 1990). Also, according to simple thermal subsidence models, the Greenland-Faroe Ridge, an area of anomalously thick crust extending across Iceland from Greenland to the Faroes, likely prevented significant deep water overflow from the Norwegian-Greenland Sea to the North Atlantic until at least the early Miocene (~17 Ma) (Wright, 1998).

There is evidence to support the existence of shallow water connections between the Arctic and the world ocean during the Eocene, but some of these connections may have been intermittent. Sea level was much higher in the Eocene than today due to the absence of large continental ice sheets, but studies of sequence stratigraphy along continental margins have suggested that sea level fluctuations of approximately 20-30 m were superimposed on the high sea levels of the late Cretaceous-Eocene (Miller et al., 2005b). Specifically, hiatuses/sequence boundaries on the New Jersey platform indicate significant sea level lowerings during the early middle Eocene at ~49 Ma, ~48 Ma, and ~46.2 Ma, and at ~42.6 and ~40.2 Ma in the late middle Eocene (Miller et al., 2005b). Miller et al. (2005b) have used benthic foraminiferal $\delta^{18}O$ to link these Cretaceous-Eocene sea level fluctuations to the existence of ephemeral ice sheets on Antarctica. Although oxygen isotope analyses of exceptionally well-preserved foraminifera from the Demerara Rise have challenged the existence of ice sheets during the Cretaceous (Moriya et al., 2007), the existence of small ice sheets on Antarctica during the middle Eocene remains a possibility.

Shallow water connections between the Arctic and the world ocean during the Eocene included the Turgay Strait and a seaway extending into the North Sea Basin (Marincovich et al., 1990). According to Iakovleva et al. (2001), the Turgay Strait probably did not provide a complete connection between the Arctic and Tethys during the Paleocene because dinocyst species of clear Tethyan affinity are not present in the flood deposits of the Sokolovsky Quarry of Kazakhstan. Radionova and Khokhlova (2000), however, have correlated thick Ypressian diatomite units extending from the Kara Sea to the North Turgay region to siliceous sediments in the North Atlantic Ocean, providing evidence for a connection between the North Atlantic and Tethys through the Arctic and Turgay Strait during the early Eocene. By the earliest middle Eocene, however, the connection between the Arctic and the West Siberian basin had apparently ceased to exist (Radionova and Khokhlova, 2000). Shallow water exchange between the Atlantic and Arctic Oceans through the Labrador Sea and Baffin Bay may have developed as early as the Campanian-Maastrichtian (Gradstein and Srivastava, 1980), but the connection was always small. The convergence of Ellesmere Island and northwestern Greenland in the

early Cenozoic further lessened the possibility of significant exchange through this passageway through the narrowing of the Nares Strait (Srivastava, 1985).

3. Results from Previous Work

Vertebrate fauna recovered from Ellesmere Island in the 1970's provided some of the first evidence that temperatures in the early Eocene Arctic were substantially warmer than today. The discovery of early Eocene remains of the varanid lizard, the tortoise *Geochelone*, and the alligator *Allognathosuchus* suggested an Arctic climate similar to that of the southeastern United States today, with winter temperatures that rarely dipped below freezing (Estes and Hutchinson, 1980). Isotopic analysis of cellulose from *Metasequoia* wood recovered at 80˚N on Axel Heiberg Island indicates that the Arctic climate was not only warm (mean annual temperature (MAT) of 13.2±2.0˚C), but also quite humid during the middle Eocene, with an atmospheric water content approximately twice that of today (Jahren and Sternberg, 2003).

Global compilations of $\delta^{18}O$ measurements on deep-sea benthic foraminifera have resolved the middle part of the early Eocene (52 to 50 Ma) as the warmest period of the Cenozoic; the exceptional warmth was the culmination of a pronounced warming trend spanning the mid-Paleocene to the early Eocene and was followed by a 17 my trend toward cooler conditions (Zachos et al., 2001). Embedded within the warming trend was the probable the release of 2,000-4,000 gigatons of carbon from methane hydrates over a period of a thousand years at the PETM (55 Ma) (Dickens, 1999). Increased atmospheric CO_2 levels in the early Eocene would have intensified the hydrologic cycle, resulting in increased subtropical evaporation and increased high latitude precipitation (Manabe, 1997). Because climatic conditions were humid (Jahren and Sternberg, 2003), continental freshwater drainage into the Arctic remained substantial, and the Greenland-Faroe Ridge prevented exchange with the North Atlantic, there is reason to believe that the waters of the Arctic and the Norwegian Greenland Sea may have been brackish during the early Eocene. Prior to the recent drilling expedition to the Lomonosov Ridge, the only existing Arctic deep-sea core of Paleogene age was the mid-Eocene USGS Core Fl-422 from the Alpha Ridge, which measured only 364 cm in length and did not provide a clear indication of Arctic paleosalinity. Clark and Kitchell (1979) believed that the

assemblage of diatom and silicoflagellates in Fl-422 was typical of normal marine conditions during the Paleocene, but Bukry (1984) asserted that the silicoflagellates were representative of an unusual assemblage of Eocene, rather than Paleocene, age. A follow- up study by Magavern et al. (1996) using $^{87}Sr/^{86}Sr$ ratios of fish bones and teeth from Fl-422 yielded $^{87}Sr/^{86}Sr$ values significantly higher than those of the world ocean at the time (Burke et al., 1982), but considerable variability in values obtained from the same sample interval led Magavern et al. (1996) to attribute the high $^{87}Sr/^{86}Sr$ values to diagenetic alteration rather than to low-salinity conditions in an isolated, runoff-dominated basin.

In a study of $\delta^{18}Oco_3^{2-}$ of fish apatite from ODP Leg 151 Hole 913B in the Norwegian-Greenland Sea, Andreasson et al. (1996) found indications that the Greenland Basin was brackish (estimated 22 to 28‰) during the early Eocene. With a humid climate and a weak connection between the Greenland Basin and the North Atlantic, there is a strong possibility that brackish conditions may also have existed throughout the Norwegian-Greenland Sea and the Arctic.

4. Summary of ACEX findings

Thorough investigation of the paleosalinity of the Arctic has been awaiting the acquisition of the first long, continuous, deep-sea sediment cores from the region. In the summer of 2004, the Integrated Ocean Drilling Program (IODP) Expedition 302, Arctic Coring Expedition (ACEX), successfully recovered ~340 m of sediments from the Lomonosov Ridge over a total depth of 428 mbsf (Expedition 302 Scientists, 2005). The recovered material ranges in age from Late Cretaceous to Holocene, with the Late Paleocene sediments resting unconformably on Late Cretaceous sandstone and mudstone bedrock. Although a hiatus exists between the organic-rich (2-3%), biosiliceous oozes of the middle Eocene and the sparsely fossiliferous silty clays of the Miocene, the Paleogene record recovered by ACEX is extensive, spanning from approximately 410 to 200 mbsf in depth and 56 Ma to 44 Ma in age.

Evidence for brackish conditions in the Eocene Arctic Ocean exists in sediments recently recovered by ACEX. The biosiliceous assemblages of diatoms, silicoflagellates, and ebridians (as well as the organic-walled dinocysts) contained in these Eocene

sediments all suggest a productive, brackish water environment (Expedition 302 Scientists, 2006). Fish scales preserved with the bones sampled in the Eocene section indicate a type of smelt (G. Smith, University of Michigan Museum, personal communication, 2005), a small herbivore having a habitat consistent with the productive, brackish water environment indicated by the planktonic microfossils. Within the middle Eocene section, very rare shells of radiolarians were found in two cores. These were the only truly open marine planktonic microfossils observed in the Eocene sections. In one brief interval at the lower/middle Eocene boundary (~306 mbsf, Cores 302-M0004A-11X and 12X), abundant megaspores of the hydopterid fern *Azolla*, which is characteristic of freshwater or very low salinity environments, are present in the sediment (Brinkhuis et al., 2006; Expedition 302 Scientists, 2006). The *Azolla* megaspores (~50-48 Ma) are accompanied by a low Branched and Isoprenoid Tetraether (BIT) index, indicating a minor input of organic matter by rivers—and therefore suggesting an autochthonous origin for the megaspores (Brinkhuis et al., 2006). Also notable are the low-diversity dinocyst assemblages present during the *Azolla* interval, which exhibit low numbers of marine species relative to freshwater and brackish species (Brinkhuis et al., 2006).

5. Considerations in the use of fish bone for paleoenvironmental reconstruction

Reconstruction of the paleosalinity of the Norwegian-Greenland Sea, and the Arctic, is hindered by the absence of calcareous tests in the sediments, so fish bone and teeth must be utilized instead. The scarcity of fish debris in the Norwegian-Greenland Sea and the Arctic further limits $\delta^{18}O$ analysis to structurally bound carbonate within the apatite lattice, rather than the phosphate phase of the apatite itself, because the required sample size is <1 mg for analysis of structural carbonate but several milligrams for analysis of the oxygen in the phosphate phase. $\delta^{18}O$ analysis of phosphate was once preferred to analysis of structurally-bound carbonate because the oxygen in the phosphate site was considered less susceptible to alteration, but the discovery of exchange between phosphate and water under microbially-mediated conditions has further restricted $\delta^{18}O$ analysis of apatite for paleoecological and physiological reconstructions to the use of fossil enamel, which is usually much better preserved than bone (Kolodny et al., 1996; Zazzo et al., 2004). As Kolodny and Luz (1991) emphasize, "in effect, every fossil fish

is a pseudomorph after a fish bone" and during replacement, neither the isotopic composition of oxygen in the carbonate nor the phosphate phase of the apatite is exempt from re-equilibration. Thus, although bone is rarely considered to be a reliable recorder of the life conditions of an organism, fossil bone can be useful for reconstructing paleoenvironmental conditions in the burial environment in which recrystallization occurs. The bones analyzed in this study were buried in the upper porewaters of Lomonosov Ridge, which had a water-depth no greater than a few hundred meters in the Eocene (Moore and Expedition 302 Scientists, 2006), and should thereby provide a reasonable approximation of Arctic near-surface water salinity. Andreasson et al. (1996), for example, found that the carbonate of early Eocene fish apatite from the semi-marine Røsnæs Clay formation and the fully marine DSDP Hole 550 gave $\delta^{18}O$ values similar to those of well-preserved foraminifera from the same samples. An added benefit of performing stable isotope analysis on the structurally bound carbonate of bone rather than phosphate is the acquisition of $\delta^{13}C$ values. In many studies $\delta^{13}C$ data are not discussed. However, Andreasson et al. (1996) found that the organic carbon content of the sediment seemed to have a significant influence on the ^{13}C content of apatite, with bones found in dark organic-rich sediment tending to be more enriched in ^{12}C than those found in pale oxidized sediment.

The use of fossil bone in this study involves a few considerations. First, it is possible for bones to preserve some remnant biogenic apatite, with new authigenic apatite essentially filling the intercrystalline spaces originally occupied by collagen (Hubert et al., 1996; Trueman and Tuross, 2002). I do not believe this to be of significance in our study, however, because the small size, thin cortical walls, and high vascular porosity of the bones makes authigenic apatite growth likely to be pervasive. Examination of the bones using scanning electron microscopy with x-ray microanalysis reveals that the bones are completely overgrown by flourapatite (francolite), which is not biogenic in origin (**Figure 4.2**). If minor amounts of remnant biogenic apatite crystals do remain within the bone, I would expect the difference between the isotopic composition of the biogenic and authigenic apatite components to be relatively small due to the similarities between the life and burial environments. While some fish may have entered river mouths during their lives, the fact remains that their bones are buried on the Lomonosov

Ridge in the middle of the Arctic Ocean, so it is unlikely that all of the bones analyzed belonged to fish that lived the majority of their lives in riverine environments.

Second, I assume that the bones were recrystallized rapidly, ideally while near the sediment-water interface. Changes in the carbon and oxygen isotope compositions of apatite begin within days of death (Zazzo et al., 2004), but bones may remain open to postmortem exchange until the pore spaces originally occupied by collagen are filled with authigenic apatite, which has been found to take up to 50 kyr under some circumstances (Kohn and Law, 2006; Toyoda and Tokonami, 1990; Trueman et al., 2006; Trueman and Tuross, 2002). Recrystallization rates of the bones used in this study are likely to have been fast due to their small size. Additionally, we are largely concerned with variations in Arctic salinity on tectonic and long orbital timescales, so a maximum recrystallization period of 50 kyr is not of great concern, and low sedimentation rates in the Arctic (~1 cm/kyr), ensure that recrystallization of the bones occurred, if not at the sediment-water interface, then at least within the shallow pore waters.

6. Methods

6.1 Chemical Methods

Samples were washed with distilled water over a 150 μm sieve. The coarse fraction was freeze-dried, and fish bone fragments were identified and picked from the coarse fraction under a reflecting-light microscope. Approximately 1-3 mg of bone fragments were collected from each sample, transferred to a microcentrifuge tube, and cleaned in de-ionized water in an ultrasonic bath for approximately 10 seconds, long enough to remove adhering clay without destroying the sample. Bone fragments were separated from contaminants under a microscope, ground into a powder with a mortar and pestle, returned to a pre-weighed microcentrifuge tube, and dried in the oven at 40˚C.

Fish bone samples were then chemically treated using the method recommended by Koch et al. (1997). Bone powders were soaked in 2% NaOCl for 24 hours to oxidize organic matter, rinsed five times with deionized water, and centrifuged between each rinse. The treatment was repeated using 1 M acetic acid-calcium acetate buffer to remove diagenetic carbonates. Samples were then roasted under vacuum at 200˚C for one hour.

The carbon and oxygen isotope composition of the fish bone carbonate was analyzed in the University of Michigan Stable Isotope Laboratory. Samples were reacted at 75˚C with phosphoric acid in a Kiel automatic carbonate preparation device linked to a Finnigan MAT 251 mass spectrometer. Stable isotope data are reported in standard δ-notation relative to the Vienna Peedee belemnite (VPDB) standard. Because the structural carbonate content of bone is ~4% (Koch et al., 1997), only samples weighing more than 0.8 mg following chemical treatment consistently generated enough CO_2 for analysis. Analytical precision, which was monitored through the regular analysis of the standard reference carbonate NBS-19, was better than ±0.1‰ (1σ) for both $\delta^{18}O$ and $\delta^{13}C$. The isotopic variability of a single powder following treatment was found to be ±0.4‰ for $\delta^{18}O$ and ±0.2‰ for $\delta^{13}C$ (1σ, N=11).

In subjecting bone samples to a chemical treatment procedure, uniformity in the concentration, amount of solutions used, and the duration of each treatment step is crucial to achieving results with a consistent isotopic offset (Koch et al., 1997). Koch et al. (1997) found that treated bone samples from land mammals consistently show more positive $\delta^{18}O$ values and more negative $\delta^{13}C$ values than untreated samples. For example, chemical treatment of ACEX sample 2A-55X-CC with 2% NaOCl and 1M acetic acid-calcium acetate buffer produced a mean shift of approximately +0.5‰ for $\delta^{18}O$ and –0.2‰ for $\delta^{13}C$ as compared with untreated samples (**Table 4.1**). The magnitude of the offset, however, can increase when more concentrated acids or longer treatment times are used, possibly the result of progressive dissolution of weakly bonded carbonate within the structural lattice (Koch et al., 1997). Thus, to minimize errors associated with chemical treatment, samples used in this study were treated simultaneously in order to ensure identical chemical conditions, with the exception of the samples older than 50.4 Ma and the Miocene sample 44X-CC, which were treated at a later date.

6.2 Estimation of Salinity

When reasonable independent temperature estimates exist, salinity can be estimated by first calculating the $\delta^{18}O$ value of the water mass ($\delta^{18}O_w$) using the paleotemperature equation of Friedman and O'Neil (1977),

$10^3 \ln\alpha_{CaCO3\text{-}water} = 2.78 \times 10^6/T^2 - 2.89$, where $\alpha_{CaCO3\text{-}water} = (\delta^{18}O_{CaCO3}+10^3)/(\delta^{18}O_w+10^3)$

and then by applying the $\delta^{18}O_w$-salinity relation.

Salinity and $\delta^{18}O_w$ are linearly related, with a slope $\Delta\delta^{18}O_w/\Delta S$ that varies regionally due to Rayleigh distillation of precipitation and a zero-salinity intercept that reflects the $\delta^{18}O$ value of the local precipitation and runoff. In modern open ocean surface waters, $\Delta\delta^{18}O_w/\Delta S$ ranges between 0.1 in the tropics and 0.6 in the high latitudes (Craig and Gordon, 1965), although variations have been noted in marginal seas. In regions with sea ice, a high slope and a "fictitious" zero-salinity intercept with a $\delta^{18}O$ value much lower than the $\delta^{18}O$ of precipitation ($\delta^{18}O_p$) is possible due to the rejection of salt without any significant fractionation of $\delta^{18}O$ (Zahn and Mix, 1991). Several equations relating $\delta^{18}O_w$ and salinity in the North Atlantic and Arctic are shown in **Table 4.2**. The slope $\Delta\delta^{18}O_w/\Delta S$ and the zero-salinity intercept of the $\delta^{18}O_w$-salinity relation are ideally linearly related, and a linear regression performed on these parameters from Table 2 gives the equation y = -36.16* ($\Delta\delta^{18}O_w/\Delta S$) +1.03, where y is the $\delta^{18}O$ value of the freshwater diluent (**Figure 4.3**). Thus, if reasonable estimates exist for the $\delta^{18}O$ value of the regional runoff, then it is possible to calculate a corresponding value for the slope $\Delta\delta^{18}O_w/\Delta S$. Because terrestrial paleoprecipitation proxies have provided estimates for the value of $\delta^{18}O_p$ in the Eocene Arctic (Bice et al., 1996; Jahren and Sternberg, 2002; Tripati et al., 2001), I assume in this study that $\delta^{18}O_p$ provides a reasonable approximation of the $\delta^{18}O$ value of the regional runoff in the Arctic.

7. Results and Discussion

7.1. Oxygen Isotopes

Stable isotope results were acquired from approximately 30 samples from Holes M0002A and M0004A with ages of ~55 to ~45 Ma (**Figures 4a and 4b**, **Table 4.3**). A single sample of middle Miocene age (~18 Ma) was also analyzed. The $\delta^{18}Oco_3^{2-}$ values of the Eocene samples range from –6.84‰ to –3.03‰, with a mean value of –4.89‰. The lowest $\delta^{18}O$ value occurs at ~48.7 Ma ($\delta^{18}O$= -6.84‰ for sample M0004A-11X-3W 46-48), and exceptionally low values were also obtained at ~55 Ma ($\delta^{18}O$ = -6.45‰ and -

6.20‰ for samples M0004A-31X-CC and 30X-CC, respectively) and ~47.6 Ma ($\delta^{18}O$= -6.83‰ and -6.08‰ for samples M0004A-6X-1W 82-84 and 6X-2W 82-84, respectively). Overall, the middle Miocene sample (M0002A-44X-CC) gave the highest $\delta^{18}O$ value ($\delta^{18}O$= 2.77‰), but of the Eocene samples, the highest value occurs at ~46.3 Ma in sample M0002A-56X-CC ($\delta^{18}O$= -3.03).

The low $\delta^{18}O$ values recorded at ~55 Ma in samples M0004A-31X-CC and 30X-CC likely reflect a warming and freshening of the Arctic during the PETM. Samples 31X-CC and 30X-CC are characterized by the presence of the diagnostic dinocyst species *Apectodinium augustum*, which is typical of tropical to subtropical environments but which expanded its distribution during the warm climates of the PETM (Moran et al., 2006).

In the middle Eocene, the negative $\delta^{18}O$ excursion at ~48.7 Ma in sample M0004A-11X-3W 46-48 corresponds with the *Azolla* event. The excursion therefore reflects a freshening of the surface waters contemporaneous with the brief expansion of the freshwater fern into the Arctic Ocean. The negative excursion at ~47.6 Ma in sample M0004A-6X-1W 82-84 probably indicates a third freshwater event. Stickley et al. (2008) observe the first abundant occurrence of *Anulus arcticus*, a diatom thought to be tolerant of low salinities, at ~47.6 Ma, adding support for a significant change in surface water conditions during this period.

The positive $\delta^{18}O$ excursion at ~46.3 Ma found in samples M0002A-56X-CC and 55X-CC may represent a brief increase in Arctic salinity. Stickley et al. (2008) interpret a peak in diatom abundance during this interval as possible evidence that conditions were less brackish. Isolated dropstones were found in Hole M0002A as deep as Section 55X-4 (Expedition 302 Scientists, 2006), so it is also possible that the positive $\delta^{18}O$ excursion may represent an interval of significant cooling near the time of the first appearance of icebergs in the Arctic (Moran et al., 2006; St. John and Willard, 2006). The positive excursion at ~46.3 Ma could therefore reflect a combination of cooler conditions and diminished runoff, and may have been a manifestation of the larger cooling trend from the early middle Eocene through the early Oligocene (Zachos et al., 2001).

By ~18 Ma, a significant shift toward normal marine salinities and cooler temperatures had taken place in the Arctic, as indicated by the very high $\delta^{18}O$ value of

2.77‰ obtained from Miocene sample M0002A-44X-CC. This result is in sharp contrast to the mean $\delta^{18}O$ value of –4.89‰ obtained from the Eocene bone samples. Sample 44X-CC occurs slightly above the ~30 Ma hiatus that separates the middle Eocene and Miocene sediments in Hole M0002A. Part of the shift toward a higher $\delta^{18}O$ value could be explained by the subsidence of the ridge to a depth of ~1000 m by the mid-Miocene, as proposed by Moore et al. (2006), and could therefore reflect the burial and alteration of the fish remains under higher salinity conditions at depth in the water column. Overall, however, the higher $\delta^{18}O$ value of the Miocene sample supports an erosional cause for the hiatus associated with the introduction of North Atlantic waters to the Arctic Ocean (Jakobsson et al., 2007).

7.2 Carbon Isotopes

The $\delta^{13}C_{CO3}$ values of the Eocene Arctic samples range between –16.98‰ and –8.90‰, with a mean value of –12.18‰, and the middle Miocene sample M0002A-44X gave a $\delta^{13}C$ value of -5.25‰. The lowest Eocene $\delta^{13}C$ values of –16.98‰ and –16.96‰ were recorded in the PETM samples M0004A-31X-CC and 30X-CC, respectively, and the highest value of –8.90‰ was from sample 11X-3W 46-48 cm, which corresponds to the *Azolla* event. With high TOC contents (1.5 to >3 wt%) in the Eocene Arctic sediments as compared to the Miocene and younger sediments (<0.4 wt%) (Expedition 302 Scientists, 2005), it appears that bones buried in sediment with a higher TOC content tend to exhibit lower $\delta^{13}C$ values than those buried in a more oxidizing environment (Andreasson et al., 1996).

In the case of the PETM samples, the addition of 2,000-4,000 gigatons of light carbon to the atmosphere at the PETM resulted in an ~-6‰ shift in the $\delta^{13}C$ value of the terrestrial organic matter and TOC buried in the ACEX sediments (Pagani et al., 2006), so the exposure of the fish bones to the ^{12}C-rich organic sediment during diagenesis can therefore explain the light carbon isotopic composition recorded in samples 31X-CC and 30X-CC. During the *Azolla* event at ~49 Ma, however, the TOC content of the sediment reaches a maximum of 4.2 wt% (Expedition 302 Scientists, 2005), while the carbon isotope composition of the bones is the highest of all of the Eocene samples. *Azolla* represents a symbiotic relationship in which cyanobacteria perform nitrogen fixation for a

fern. Thus, during the *Azolla* event, abundant nitrogen provided by the cyanobacteria and a plentiful supply of phosphorus from increased river runoff would have resulted in an increase in primary production in the Arctic. In studying mid-Pleistocene sapropels from the Mediterranean, Meyers and Bernasconi (2005) found that during periods of wet climate conditions and high cyanobacterial primary production, the organic $\delta^{13}C$ values in the sediments increased by ~3-5‰ above background levels due to the depletion of ^{12}C in the surface waters. The positive $\delta^{13}C$ excursion observed in sample M0004A-11X-3W 46-48 cm during the *Azolla* event may therefore be attributable to the burial of the fish bones with ^{13}C-enriched organic matter during a period of extreme primary productivity.

7.3 Salinity Reconstruction for the Arctic Ocean

In order to calculate the salinity of the Arctic Ocean during the early and middle Eocene, reasonable constraints are needed for temperature and the $\delta^{18}O$ value of local precipitation and runoff. TEX_{86} estimates have been made from ACEX Hole M0004A at the PETM, the *Azolla* event, and ~50 Ma (sample 4A-19X-CC), and thus provide good constraints for early Eocene conditions. Using $TEX_{86'}$, Sluijs et al. (2006) found that sea surface temperatures (SSTs) in the Arctic exhibited extreme warmth during the PETM, rising from 18°C in the Late Paleocene to over 23°C during the PETM (top of Core 32X to within Core 29X), and subsequently decreasing to ~17°C following the event. By ~50 Ma, SSTs had cooled to 12°C (A. Sluijs, personal communication, 2006), and TEX_{86} results show that at the *Azolla* event, temperatures had decreased further to 10°C but recovered to 12-14°C following the event (Brinkhuis et al., 2006).

For the early middle Eocene, where TEX_{86} estimates were not available from the ACEX sites, it was necessary to approximate temperatures from the results of regional reconstructions. In general, SSTs were warmer at the beginning of the ~10 million years spanned by the $\delta^{18}Oco_3^{2-}$ record than at the end. Maximum high latitude Southern Ocean SSTs of 10-12°C were recorded by foraminifera during the late Paleocene and early middle Eocene, as compared to 15°C during the early Eocene and 6°C by the late Eocene (Zachos et al., 1994). Global deepwater temperatures of ~12°C were obtained by Lear et al. (2000) at ~47 Ma from Mg/Ca data, declining to ~ 10°C by 45 Ma. Arctic terrestrial proxies give comparable results. Analysis of secondary calcite in fossil *Metasequoia*

wood from Axel Heiberg Island yielded a terrestrial mean annual temperature of 13.2±2.0°C for the middle Eocene (Jahren and Sternberg, 2003), while a multiple regression model of foliar physiognomy and floristic composition on Axel Heiberg and Ellesmere Islands estimated a mean annual temperature of 8.2-9.3°C during the middle Eocene, with a mean annual temperature range spanning 14°C (Greenwood and Wing, 1995). Thus, taking into consideration these estimates, I choose to use a temperature of 12°C in our salinity reconstruction for the early middle Eocene and decrease the value to 10°C by ~45 Ma, as shown in **Table 4.3** and **Figure 4.4c**.

As for local precipitation and runoff, the $\delta^{18}O$ value of the modern mean freshwater diluent in the North Atlantic is –20.6‰ (Craig and Gordon, 1965), and Arctic runoff has a very similar average value (Bauch et al., 1995). Studies of bivalves by Bice et al. (1996) and Tripati et al. (2001) estimated $\delta^{18}O$ values for the late Paleocene freshwater diluent of ~23.5‰ on the North Slope of Alaska and ~–20 to -22‰ on Ellesmere Island, respectively. Studies of fossil cellulose from Axel Heiberg Island by Jahren and Sternberg (2002) yielded a slightly higher $\delta^{18}O$ value of –15.1‰ for meteoric water during the mid to late Eocene. Overall, however, a reduction in the global temperature gradient and higher condensation temperatures in the Arctic during the Paleogene do not appear to have led to significantly higher $\delta^{18}O$ values in high latitude precipitation. Instead, Rayleigh distillation during meridional vapor transport seems to have had a dominant influence over the $\delta^{18}O$ value of Arctic precipitation during the Paleogene (Jahren and Sternberg, 2002; Tripati et al., 2001). Thus, because the $\delta^{18}O$ value of Eocene precipitation was not dramatically different from that of the present day, in reconstructing the salinity of the Eocene Arctic Ocean I choose to use $\delta^{18}O_p$ values between -15 and -20‰ and thereby calculate corresponding $\Delta\delta^{18}O_w/\Delta S$ slopes of 0.44 to 0.58. Thus, a minimum salinity was calculated for each sample interval by assuming $\delta^{18}O_p$ = -15‰, and a maximum salinity was calculated using $\delta^{18}O_p$ = -20‰, except at the PETM, where higher $\delta^{18}O_p$ values of -10 to -15‰ were used in conjunction with smaller slopes of 0.30 and 0.44, respectively, based on the results of Pagani et al. .

Thus, using a mean temperature of 12°C, a $\delta^{18}O$ value of precipitation and runoff between –15‰ and –20‰, corresponding $\Delta\delta^{18}O_w/\Delta S$ slopes of 0.44 and 0.58, respectively, and a mean $\delta^{18}Oco_3^{2-}$ value of –4.89‰, I calculated an average salinity in

the Arctic of ~21 to 25‰ during the early and middle Eocene. By comparison, for middle Miocene sample M0002A-44X-CC, using the same parameters for the $\delta^{18}O$ of precipitation and runoff as for the Eocene samples but a lower mean temperature of 6°C estimated from Lear et al. (2000), I calculated a salinity of the Arctic Ocean of ~35‰, which is slightly high for a modern Arctic surface water salinity but essentially denotes full marine conditions in the Arctic by the early Miocene. A reconstruction demonstrating the large scale variation of Arctic salinity is shown in **Figure 4d**, salinity estimates are given in **Table 4.3**, and results for key intervals are compared in **Table 4.4**.

Because many of our salinity estimates depend on assumed temperatures, I demonstrate in **Table 4.4** the sensitivity of our salinity calculations to temperature over a range of ±3°C. As can be seen from this, our salinity estimates are not highly sensitive to temperature. Adding an error of ±3°C to our estimated temperatures expands our salinity estimates ~1.5-2‰ on either side of the calculated range, and thus our average Eocene salinity estimate changes from ~21-25‰ to ~19.4-26‰.

Additionally, the salinity estimates obtained in this study are not expected to reflect the full extent of freshening in the Arctic surface waters. Onodera and Takahashi (2007) suggest that the co-occurrence of fresh and brackish water microfossils in the ACEX sediments can be explained by the existence of a strong halocline that divided the upper water column into a fresh surface layer and a brackish habitat below. Thus, fish bones buried and altered on the Lomonosov Ridge at a depth of a few hundred meters would probably record the salinity of a lower brackish water layer rather than that of the uppermost freshwater lens.

7.4 Paleocene-Eocene Thermal Maximum

Using the $TEX_{86'}$ temperature estimate of 23°C made from ACEX material by Sluijs et al. (2006) for the PETM and the $\delta^{18}Oco_3^{2-}$ values of -6.45‰ and -6.20‰ obtained from samples M0004A-31X-CC and 30X-CC, respectively, I estimate salinity in the Arctic Ocean at ~17-24‰ during the PETM. Because the SST estimates were made using $TEX_{86'}$, the results may be skewed toward the summer season when phytoplankton productivity was at a maximum, and therefore salinities could have actually been slightly lower than these estimates by a few parts per thousand. The results show that salinity at

the PETM might have been significantly lower than the Eocene average, but the very negative $\delta^{18}Oco_3^{2-}$ values obtained from the interval may largely be the result of extreme sea surface temperatures.

Pagani et al report a significant decrease in the extent of Rayleigh distillation of precipitation in the Arctic during the PETM, as indicated by the hydrogen isotope compositions of the high molecular weight *n*-alkane *n*-C_{29}. During the peak warmth of the early phase of the PETM, Pagani et al. estimate that spring precipitation in the Arctic had a δD value of ~-30 to –55‰, which corresponds through the meteoric water line to a $\delta^{18}O$ value in the range of –5 to –8‰. Such high δD and $\delta^{18}O$ values are usually associated with precipitation in the subtropics and may indicate an increase in the delivery of water vapor to the Arctic as a result of decreased rain-out of subtropical water in the mid-latitudes under reduced meridional and vertical temperature gradients (Pagani et al., 2006). However, as the PETM progressed, Pagani et al. obtained lower δD values of ~-70 to -115‰, which correspond to $\delta^{18}O$ values in the range ~–10 to –15‰. Thus, because the samples examined in this study (M0004A-31X-CC and 30X-CC) are from the latter portion of the PETM, the salinity estimates obtained may not reflect the full extent of surface water freshening possible in the region during conditions of peak warmth.

7.5 The *Azolla* Event and Middle Eocene Salinity Variations

We calculated an Arctic salinity of ~16-21‰ during the *Azolla* event at ~48.7 Ma using the temperature estimate of 10.7°C made by Brinkhuis et al. (2006) and a $\delta^{18}Oco_3^{2-}$ value of -6.84‰ from sample M0004A-11X-3W 46-48. The *Azolla* event appears in our salinity reconstruction as one the lowest salinity periods in the Eocene, and unlike the PETM, during which freshening of the surface waters was probably associated with an increase in regional precipitation, the *Azolla* event was likely the result of the increased isolation of the Arctic during a sea level lowstand. The timing of the *Azolla* event is consistent with a sea-level lowering reported by Miller et al. (2005b) at ~49 Ma during Chron C21r, and a slight decline in Arctic SSTs as reported by *Brinkhuis et al.* (2006) suggests decreased communication with the Atlantic during the event. Similarly, a sudden temperature increase of 3-4°C following the event probably signals the renewed

influx of salt and heat to the Arctic after sea level had been restored (Brinkhuis et al., 2006). Radionova and Khokhlova (2000) report that the Arctic connection to the world ocean through the Turgay Strait ceased to exist at ~49 Ma, and considering that a substantial percentage of the surface area of the Arctic Ocean is continental shelf, the migration of river mouths closer to the center of the Arctic Ocean during a lowstand could also have contributed to decreased salinity on the Lomonosov Ridge.

Other significant middle Eocene salinity variations occur in our reconstruction at ~47.6 Ma, where I calculated a salinity low of ~16-21‰ using a temperature of 11°C and a $\delta^{18}Oco_3^{2-}$ value of -6.83‰ from sample M0004A-6X-1W 82-84, and at ~46.3 Ma, where I calculated a salinity high of ~24-27‰ using a temperature of 10°C and a $\delta^{18}Oco_3^{2-}$ value of -3.03‰ from sample M0002A-56X-CC. Because TEX_{86} estimates were not available for these samples, errors in our temperature estimates are potentially significant. Thus, the low salinity event in our reconstruction at ~47.6 Ma could correlate with the early middle Eocene sea level lowstand of Miller et al. (2005b) at ~48 Ma during Chron 21n, and thus closely resemble the *Azolla* event in origin. However, as shown in **Table 4.4**, a temperature increase of ~3°C at 47.6 Ma could partially account for this negative $\delta^{18}O$ excursion, although no evidence for such a warm interval currently exists. Similarly, the high salinity event ~46.3 Ma in our reconstruction could alternatively be explained by a decrease in temperature of ~3°C, as shown in **Table 4.4**, which is supported by the first appearance of isolated dropstones on the Lomonosov Ridge at ~46 Ma (Moran et al., 2006; St. John and Willard, 2006).

7.6 Comparison to the Norwegian-Greenland Sea

Overall, the $\delta^{18}Oco_3^{2-}$ values obtained in this study for the Eocene Arctic Ocean, which range from -6.84‰ to –2.96‰, are higher than those obtained by Andreasson et al. (1996) from ODP Hole 913B for the Eocene Norwegian-Greenland Sea (-6.70‰ to -8.23‰). Analysis of untreated Eocene fish debris from Hole 913B and fully marine northeastern Atlantic ODP Hole 550 in this study yielded stable isotope values very similar to those obtained by Andreasson et al. (1996) (**Table 4.5**). Thus, differences in inter-laboratory methods can be ruled out, and although the Arctic Ocean samples were chemically treated prior to analysis while the Hole 913B samples were not, the increases

in $\delta^{18}O$ expected from chemical treatment are too small to account for the differences in $\delta^{18}O$ observed between the two localities. The mixing of bones and teeth in the Hole 913B samples could have shifted the $\delta^{18}O$ results toward lower values because teeth are less susceptible to alteration than bone and might therefore better preserve the surface water signal, but Andreasson et al. (1996) found no significant difference between samples composed only of teeth and those with a mixture of teeth and bone.

Temperature differences between Hole 913B and the ACEX sites would have been much too small to explain the large difference in $\delta^{18}O$. It is possible that the salinity at Hole 913B, which was located in close proximity to land according to the high C/N ratios at the site (Andreasson et al., 1996) was influenced by a nearby freshwater outflow. The paleodepth of Hole 913B is uncertain due to the unknown nature of the basement, but it is also possible that the site could have been quite shallow during the early Eocene and that the isotopic composition of the fish debris undergoing alteration at the sediment-water interface might more fully record the extent of freshwater episodes than the ACEX Sites, which, at a paleodepth of a few hundred meters, may have been below the mixed layer.

Alternatively, it is possible that salinities of the Greenland Basin were actually lower than those of the Arctic during the early Eocene. Andreasson et al. (1996) argue that in the early Eocene the Greenland Basin was isolated with a very large drainage area to basin area ratio according to paleogeographic reconstructions. Brinkhuis et al. (2006) correlated the ACEX and Hole 913B cores, assigning an age of ~49.3 Ma to the base of Core 50R and placing the termination of the *Azolla* event at the top of Core 47R. Thus, many of the Hole 913B samples examined by Andreasson et al. (1996) actually correspond to a period when low sea level and relative isolation may have driven salinities to extreme lows, although samples taken from Hole 913 B after the *Azolla* event also show very low $\delta^{18}O$ values. Brinkhuis et al. (2006) hypothesize that freshwater outflows from the Arctic were a source of *Azolla* remains to the sediments of the nearby Nordic Seas, but the results from the Hole 913B samples indicate that the waters of the Norwegian Greenland Sea could have actually been as fresh or fresher than the Arctic Ocean during the early Eocene.

8. Conclusions

Salinity reconstructions using fish bone $\delta^{18}Oco_3^{2-}$ reveal that the Arctic Ocean was probably brackish during most of the early and early middle Eocene, with an average salinity of 21 to 25‰, as compared to ~35‰ at ~18 Ma. During much of this period, a shallow water connection probably existed between the Arctic Ocean and the North Atlantic, and therefore the formation of deep and intermediate water in the North Atlantic may have been affected by the outflow of brackish water from the Arctic. Three negative excursions occur in the $\delta^{18}Oco_3^{2-}$ record, marking the PETM, the *Azolla*, and 47.6 Ma events. The salinity range reconstructed for the PETM of ~17-24‰ indicates that salinities may have been below the Eocene average, but extreme warmth may account for most of the negative excursion in $\delta^{18}Oco_3^{2-}$ during this event. It is possible that the Arctic was isolated from the North Atlantic during the PETM, as Knox (1998) report mammal migrations between North America and Europe across the Greenland-Faroe Ridge. However, the Arctic probably maintained a shallow water connection to the world ocean through the Turgay Strait at this time, so it is likely that low salinities would have developed from conditions of increased regional precipitation and runoff associated with extreme high latitude warmth. The extent of freshening in the Arctic at the PETM is probably not fully recorded in our reconstruction because the samples examined in this study are not from the interval in which Pagani et al. record the highest δD values.

The lowest salinities obtained in this study correspond to the other two negative excursions in the $\delta^{18}Oco_3^{2-}$ record: the *Azolla* event reported by Brinkhuis et al. (2006) at ~48.7 Ma and a previously unidentified event at ~47.6 Ma. Both of these events probably correspond to sea level lowerings of 20-30 m reported by Miller et al. (Miller et al., 2005b) and occur after connections through the Turgay Strait had ceased at 49 Ma (Radionova and Khokhlova, 2000). The salinity range of 16 to 21‰ obtained for these events is probably not low enough to support the growth of *Azolla* in open waters. However, it is possible that the bones were altered to reflect conditions at the sediment-water interface at a depth of a few hundred meters, and that, except in brief seasonal floods, the salinities obtained in this study do not reflect the full extent of freshening in surface waters, but rather provide an upper bound on surface water salinity.

ACKNOWLEDGMENTS

I would like to acknowledge my coauthor on this chapter, Ted Moore, for helping me to see this study all the way through to publication in *Paleoceanography*. Samples were provided by the Integrated Ocean Drilling Program (IODP), which is sponsored by the US National Science Foundation (NSF) and other participating countries. Funding for this research was provided by the U.S. Science Support Program of the Joint Oceanographic Institutions. I wish to thank my reviewers Paul Wilson and Clive Trueman for valuable comments on the manuscript, Lora Wingate of the University of Michigan Stable Isotope Laboratory for the carbonate analyses, James Gleason for valuable collaborations, Joanne Reuss, SarahBradbury, Jenny Kucera, and Shih-Yu Lee for laboratory support, Wenjun Yong for assistance with the SEM, Gerry Smith, Appy Sluijs, and Catherine Stickley, and Paul Koch for helpful discussions, and K. C. Lohmann for helpful suggestions on the manuscript.

Table 4.1. Chemical Treatment Test Performed on Sample M0002A-55X-CC.

	Mass (mg)	$\delta^{13}C$	$\delta^{18}O$	Avg. $\delta^{13}C$	Avg. $\delta^{18}O$	$\Delta\ \delta^{13}C$ Treated-Untreated	$\Delta\ \delta^{18}O$ Treated-Untreated
Untreated	1.2	-13.85	-4.19	-13.78	-3.96	-0.2	+0.5
	1.2	-13.71	-3.73				
Treated	1.7	-13.97	-3.55	-14.00	-3.46		
	1.5	-14.02	-3.37				

Table 4.2. $\delta 18O_w$-Salinity Relation for Sites in the Arctic and North Atlantic Obtained from Surface Water Measurements Across Diverse Modern Salinity Gradients.

Study Region	Equation	Source
East Greenland	$\delta^{18}O_w = 1.01S - 35.02$	Fairbanks et al. (1992)
Central Arctic	$\delta^{18}O_w = 0.7S - 24.6$	Vetshteyn et al. (1974)
Slope Water	$\delta^{18}O_w = 0.63S - 21.67$	Fairbanks et al. (1992)
Laptev Sea	$\delta^{18}O_w = 0.50S - 18.86$	Mueller-Lupp et al.(2003)
German Bight, North Sea	$\delta^{18}O_w = 0.34S - 9.36$	Scheurle and Hebbeln (2003)
Western Equatorial Atlantic	$\delta^{18}O_w = 0.19S - 5.97$	Fairbanks et al. (1992)
Sargasso Sea and Gulf Stream	$\delta^{18}O_w = 0.11S - 3.15$	Fairbanks et al. (1992)
Eastern Equatorial Atlantic	$\delta^{18}O_w = 0.08S - 1.86$	Fairbanks et al. (1992)

Table 4.3. Stable Isotope Data Generated from the Analysis of Fish Bones in ACEX Holes 302 M0002A and M0004A and the Calculated Salinity Range for Each Sample.

Stable Isotope Results									Calculated Salinity		
Hole, core, section, interval (cm)	Wt. (mg)	mcd (m)	Age (Ma)	$\delta^{13}C$ (VPDB)	$\delta^{18}O$ (VPDB)	Avg $\delta^{13}C$ (VPDB)	Avg $\delta^{18}O$ (VPDB)	$\delta^{18}O$ (SMOW)	T [c] °C	Salinity Min	Max
2A-44X-CC	1.2	195.91	17.86	-5.25	2.77[a]	-5.25	2.77	0.42	6	35.09	35.40
2A-52X-1 140-150	1.4	226.41	45.57	-12.26	-5.30	-12.26	-5.30	-6.64	10	19.03	23.16
2A-52X-CC	3.4	226.73	45.58	-12.90	-4.32	-12.84	-4.34	-5.68	10	21.21	24.83
	2.2			-12.78	-4.36						
2A-53X-CC	2.1	231.96	45.80	-12.96	-4.56	-12.96	-4.56	-5.89	10	20.72	24.46
2A-54X-CC-bott	1.0	232.5	45.82	-11.75	-4.98	-11.75	-4.98	-6.31	10	19.76	23.72
2A-55X-bott-CC	1.6	241.42	46.19	-13.26	-3.16	-13.38	-3.105	-4.46	10	23.98	26.94
	1.7			-13.49	-3.05						
2A-56X-CC-bott	2.4	244.8	46.33	-10.63	-3.10	-10.76	-3.03	-4.37	10	24.19	27.10
	1.7			-10.88	-2.96						
2A-58X-CC-bott	1.7	256.61	46.81	-11.96	-4.69	-11.90	-4.73	-6.07	10	20.33	24.15
	1.7			-11.83	-4.76						
2A-59X-CC 0-2	1.0	260.81	46.99	-11.31	-4.56	-11.31	-4.56	-5.89	10	20.71	24.45
2A-60X-CC	1.3	265.07	47.16	-11.47	-4.25	-11.47	-4.25	-5.58	10	21.43	24.99
4A-4X-1 top (0-3)	2.9	265.015	47.16	-11.38	-4.47	-11.38	-4.47	-5.56	11	21.47	25.02
2A-61X-CC 4-6	2.8	267.22	47.25	-11.76	-4.00	-11.71	-4.19	-5.28	11	22.12	25.52
	2.5			-11.66	-4.37						
2A-62X-CC 9-11	2.2	273.51	47.51	-11.01	-4.86	-11.01	-4.86	-5.96	11	20.57	24.34
4A-6X-1W 82-84	1.0	274.33	47.54	-10.97	-6.83	-10.97	-6.83	-7.93	11	16.09	20.93
4A-6X-2W 82-84	1.4	275.83	47.61	-11.91	-6.08	-11.91	-6.08	-7.17	11	17.81	22.24
4A 6X-CC bott	1.4	278.78	47.73	-12.06	-3.83	-12.06	-3.83	-4.93	11	22.92	26.13
4A-8X-CC bott	1.8	282.58	47.88	-12.20	-3.97	-12.06	-3.87	-4.96	11	22.83	26.06
	1.3			-11.92	-3.76						
4A-9X-CC bott	0.6	287.66	48.09	-11.64	-5.50	-11.64	-5.50	-6.60	11	19.12	23.23
4A-10X-2 147-150 cm	1.8	294.84	48.39	-11.59	-4.27	-11.59	-4.27	-5.12	12	22.48	25.79
4A-10X-CC bott	2.3	297.19	48.49	-12.46	-4.44	-12.46	-4.44	-5.29	12	22.09	25.50
4A-11X-3W 46-48	1.4	300.78	48.67	-8.90	-6.84	-8.90	-6.84	-8.01	10.7	15.91	20.79
4A-12X-CC bott	1.5	301.37	48.71	-11.64	-5.10	-11.64	-5.10	-5.95	12	20.58	24.35
4A-15X-CC bott	2.7	313.61	49.67	-12.10	-4.87	-12.10	-4.87	-5.72	12	21.11	24.75
4A-18X-CC bott	2.7	318.96	50.09	-12.47	-4.69	-12.47	-4.69	-5.54	12	21.51	25.06
4A-19X-CC top[b]	1.0	323.54	50.45	-12.21	-5.30	-12.21	-5.30	-6.15	12	20.13	24.00
4A-20X-CC top[b]	1.5	328.07	50.81	-11.25	-5.40	-11.25	-5.40	-6.25	12	19.90	23.83
302-M4A-22X-CC bott[b]	0.9	339.98	51.74	-12.76	-4.30	-12.76	-4.30	-5.15	12	22.41	25.74
302-M4A-23X-1 top[b]	1.0	341.6	51.87	-12.12	-4.98	-12.12	-4.98	-5.84	12	20.84	24.55
302-M4A-23X-CC bott[b]	1.8	345.67	52.19	-12.50	-5.33	-12.50	-5.33	-6.18	12	20.07	23.96
302-M4A-30X-CC bott[b]	1.4	384.54	55.15	-16.96	-6.45	-16.96	-6.45	-4.64	22.7	17.74	23.57
302-M4A-31X-CC bott[b]	1.5	385.25	55.19	-16.98	-6.20	-16.98	-6.20	-4.90	22.6	16.86	22.97

[a] $\delta^{18}O$ value corrected by +1.5‰ because replicate samples treated alongside sample 2A-44X-CC in a later batch were found to be consistently more negative than previous analyses by this amount.
[b]Separate treatment batch from other samples.
[c]Temperatures for samples 4A-30X and 31X are from Sluijs et al.(2006) , 4A-11X is from Brinkhuis et al. (2006), and 4A-19X is from A. Sluijs (personal communication, 2006). Temperatures for other samples approximated.

Table 4.4. Estimates of Arctic Salinity Based on Different Assumptions of $\Delta\delta^{18}O_w/\Delta S$, $\delta^{18}O$ of Precipitation ($\delta^{18}Op$), and Temperature for the PETM, the *Azolla* Event, 47.6 Ma (A Possible Low Salinity Event), 46.3 Ma (A Possible High Salinity Event), Average Eocene Conditions, and Miocene Sample 44X-CC.

Sample	Age (Ma)	$\delta^{18}O\ CO_3^{2-}$ (VPDB)	$\delta^{18}Ow$ (SMOW)	T (˚C)	$\delta^{18}Op$ (SMOW)	Assumed $\Delta\delta^{18}O_w/\Delta S$	Salinity (‰)	T sensitivity	
								Salinity (‰) (T-3˚C)	Salinity (‰) (T+3˚C)
4A-30X-CC bott (PETM)	55.15	-6.45	-4.39	22.7[1]	-10[2]	0.30	17.74	15.59	19.83
					-15	0.44	23.57	22.09	25.01
4A-31X-CC bott (PETM)	55.19	-6.20	-4.64	22.6[1]	-10[2]	0.30	16.86	14.70	18.95
					-15	0.44	22.97	21.48	24.40
4A-11X-3W 46-48 (*Azolla* Event)	48.67	-6.84	-8.21	10.7[3]	-15	0.44	15.91	14.24	17.53
					-20	0.58	20.79	19.51	22.02
4A-6X-1W 82-84	47.54	-6.83	-7.93	11	-15	0.44	16.09	14.43	17.71
					-20	0.58	20.93	19.66	22.16
2A-56X-CC-bott	46.33	-3.03	-4.37	10	-15	0.44	24.19	22.50	25.83
					-20	0.58	27.10	25.81	28.34
Eocene Average	55-45	-4.89	-5.54	12	-15	0.44	21.06	19.41	22.66
					-20	0.58	24.71	23.45	25.93
Miocene	17.86	2.77	0.42	6	-15	0.44	35.09	33.31	36.80
					-20	0.58	34.40	34.05	36.71

[1]Sluijs et al. (2006)
[2]Pagani et al.
[3]Brinkhuis et al. (2006)

Table 4.5. Comparison Between Stable Isotope Values Obtained from Early Eocene Untreated Fish Bone and Teeth from ODP Hole 913B in the Norwegian-Greenland Sea and Full-Marine DSDP Hole 550 in the Northeastern Atlantic by Andreasson et al. [1997] versus This Study.

Andreasson et al. (1997)			This Study		
	$\delta^{18}O$	$\delta^{13}C$		$\delta^{18}O$	$\delta^{13}C$
151-913B-			151-913B-		
46R-CC	-6.73	-9.26	Mixture of 48 2W 23.5-25, 46 3 21-22.5, 50 4W 81.5-83, 49 2W 54.5-66.5	-8.44	-8.34
47R-1, 108-110	-7.78	-9.25			
48R-CC	-8.23	-10.11			
49R-3 118-121	-7.28	-8.00			
50R-4 94-97	-6.70	-4.56			
80-550-			80-550-		
24-	-1.35	-0.09	24R-3 52-60	0.17	0.17
24-1 135-138	-0.17	-0.14			

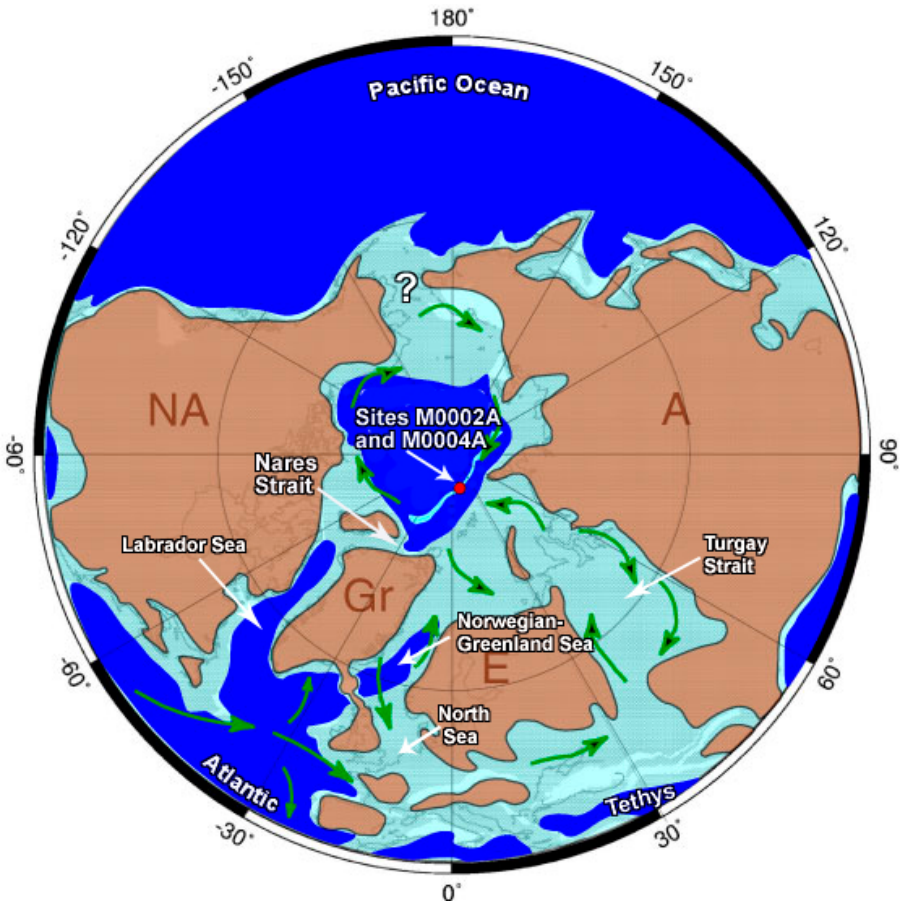

Figure 4.1. Paleoreconstruction of the Arctic Region at 50 Ma showing the location of the Arctic Coring Expedition (ACEX) 302 Sites examined in this study. (Modified from the IODP Expedition 302 Report (Expedition 302 Scientists, 2006).)

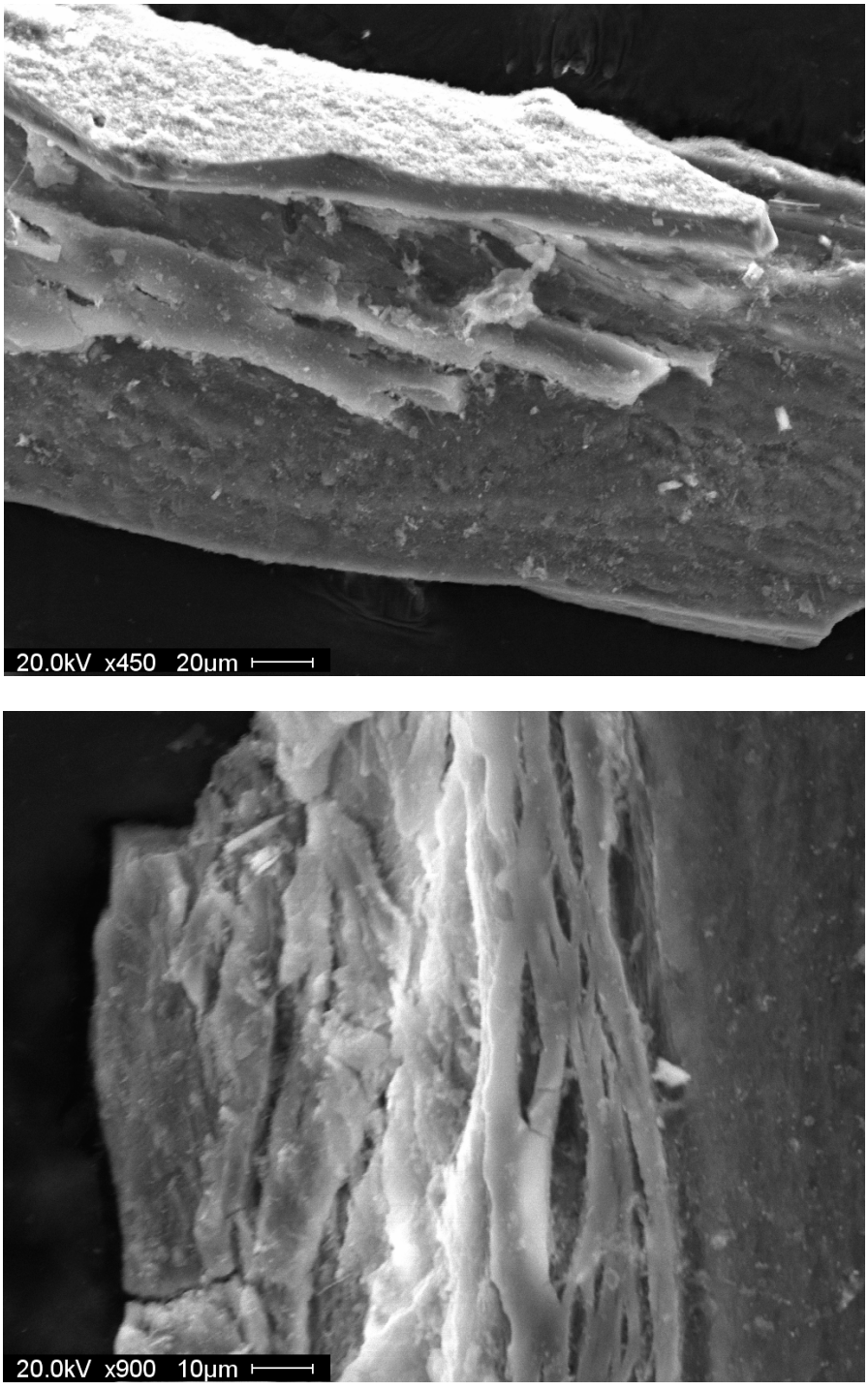

Figure 4.2. Secondary electron images of fish bone taken from Sample 11X 2W 46-48. Authigenic flourapatite dominates the bones.

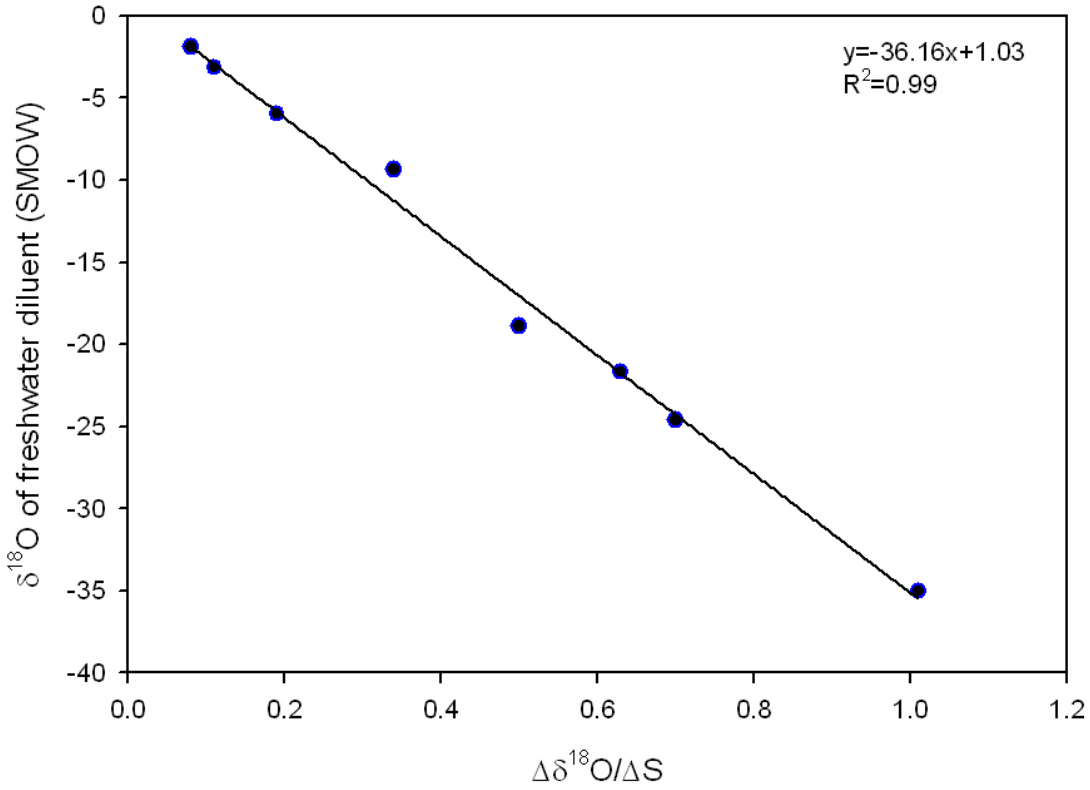

Figure 4.3. Results of a linear regression performed on the zero-salinity intercepts and slopes of the $\delta^{18}O_w$-salinity equations listed in Table 4.2 for the North Atlantic and Arctic.

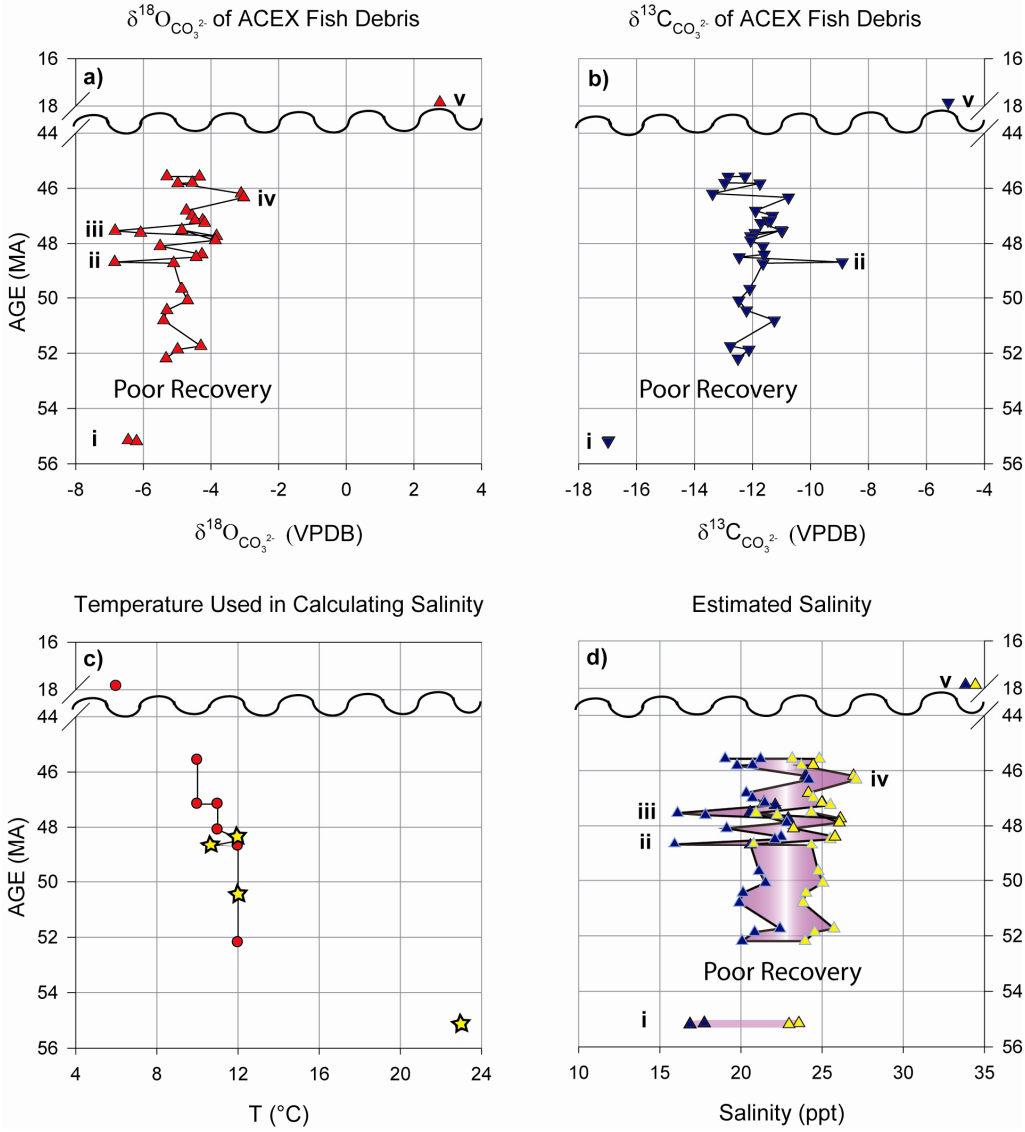

Figure 4.4. (**a**, **b**) Oxygen and carbon isotopic composition of fish debris from IODP Expedition 302, Holes M0002A and M0004A. Ages are based on Backman et al. (2008), and the wavy line indicates a hiatus. Features of interest include negative $\delta^{18}O$ excursions at (i) 55 Ma (The Paleocene-Eocene Thermal Maximum), (ii) 48.7 Ma (The Azolla Event), and (iii) 47.6 Ma, as well as positive $\delta^{18}O$ excursions at (iv) 46.3 Ma and (v) 17.9 Ma. Also of interest are a negative $\delta^{13}C$ excursion at (i) and relatively positive $\delta^{13}C$ values at (ii) and (v).
(c) Temperatures used in calculating Arctic salinity. Stars indicate independent temperature estimates from ACEX material made by Sluijs et al. (2006) and Brinkhuis et al. (2006). For the other intervals, it was necessary to approximate temperatures based on the results of other Eocene paleotemperature studies, as described in the text.
(**d**) Calculated salinity range based on $\delta^{18}O$ data in (a) and temperatures shown in (c). Minimum salinity was calculated by assuming $\delta^{18}O_p$ = -15‰, and maximum salinity was calculated using $\delta^{18}O_p$ = -20‰, except at the PETM where a $\delta^{18}O_p$ range of -10 to -15‰ was used.

REFERENCES

Aagaard, K., and E. C. Carmack (1989), The role of sea ice and other fresh water in the Arctic circulation, *J. Geophys. Res., 94*(C10), 14485-14498.

Andreasson, F. P., B. Schmitz, and D. Spiegler (1996), Stable isotopic composition ($\delta^{18}O_{CO3}^{2-}$ and $\delta^{13}C$) of early Eocene fish-apatite from Hole 913B: An indicator of the early Norwegian-Greenland Sea paleosalinity., in *Proceedings of the Ocean Drilling Program, Scientific Results, 151*, edited by J. Thiede, J. V. Firth, G. L. Johnson and W. F. Ruddiman, pp. 583-591, Ocean Drilling Program, College Station, Texas.

Averianov, A. O., and J. D. Archibald (2003), Mammals from the Upper Cretaceous Aitym Formation, Kyzylkum Desert, Uzbekistan, *Cretaceous Res., 24*, 171-191.

Backman, J., M. Jakobsson, M. Frank, F. Sangiorgi, H. Brinkhuis, C. Stickley, M. O'Regan, H. Løvlie, D. Pälike, J. Spofforth, J. Gattacecca, and K. Moran (2008), Age model and core-seismic integration for the Cenozoic Arctic Coring Expedition sediments from the Lomonosov Ridge., *Paleoceanography*, doi:10.1029/2007PA001476, in press.

Bauch, D., P. Schlosser, and R. G. Fairbanks (1995), Freshwater balance and the sources of deep and bottom waters in the Arctic Ocean inferred from the distribution of $H_2{}^{18}O$, *Prog. Oceanog., 35*, 53-80.

Bice, K. L., M. A. Arthur, and L. Marincovich, Jr. (1996), Late Paleocene Arctic Ocean shallow-marine temperatures from mollusc stable isotopes, *Paleoceanography, 11*(3), 241-249.

Bice, K. L., and J. Marotzke (2002), Could changing ocean circulation have destabilized methane hydrate at the Paleocene/Eocene boundary?, *Paleoceanography, 17*(2), 1018, doi:10.1029/2001PA000678.

Brewer, P. G., W. S. Broecker, W. J. Jenkins, P. B. Rhines, C. G. Rooth, J. H. Swift, T. Takahashi, and R. T. Williams (1983), The climatic freshening of the deep Atlantic north of 50°N over the past 20 years, *Science, 222*, 1237-1239.

Brinkhuis, H., S. Schouten, M. E. Collinson, A. Sluijs, J. S. S. Damste, G. R. Dickens, M. Huber, T. M. Cronin, J. Onodera, K. Takahashi, J. P. Bujak, R. Stein, J. van der Burgh, J. S. Eldrett, I. C. Harding, A. R. Lotter, F. Sangiorgi, H. van Konijnenburg-van Cittert, J. W. de Leeuw, J. Matthiessen, J. Backman, K. Moran, and E. Scientists (2006), Episodic fresh surface water in the Eocene Arctic Ocean, *Nature, 441*, 606-609.

Bukry, D. (1984), Paleogene paleoceanography of the Arctic Ocean is constrained by the middle or late Eocene age of USGS Core Fl-422: Evidence from silicoflagellates., *Geology, 12*, 199-201.

Burke, W. H., R. E. Denison, E. A. Hetherington, H. F. Koepnick, H. F. Nelson, and J. B. Otto (1982), Variation of seawater $^{87}Sr/^{86}Sr$ throughout Phanerozoic time, *Geology, 10*, 516-519.

Clark, D. C., and J. A. Kitchell (1979), Comment on "The terminal Cretacoues event: A geological problem with an oceanographic solution", *Geology, 7*, 228.

Craig, H., and L. I. Gordon (1965), Deuterium and oxygen 18 variations in the ocean and the marine atmosphere, in *Stable Isotopes in Oceanographic Studies and Paleotemperatures*, edited by E. Tongiorgi, pp. 9-130, CNR-Laboratorio di Geologia Nucleare, Pisa.

Dickens, G. R. (1999), The blast in the past, *Nature, 401*, 752-755.

Estes, R., and J. H. Hutchinson (1980), Eocene Lower Vertebrates from Ellesmere Island, Canadian Arctic Archipelago, *Palaeogeogr., Palaeoclimatol., Palaeoecol., 30*, 325-347.

Expedition 302 Scientists (2005), Arctic Coring Expedition (ACEX): Paleoceanographic and tectonic evolution of the central Arctic Ocean., in *IODP Preliminary Report, 302*, doi:10.2204/iodp.pr.302.2005.

Expedition 302 Scientists (2006), Sites M0001-M0004, in *Proceeedings IODP, 302*, edited by J. Backman, K. Moran, D. B. McInroy, L. Mayer and Expedition 302 Scientists, Integrated Ocean Drilling Program Management International, Inc., Edinburg, doi.10.2204/iodp.proc.302.104.2006.

Fairbanks, R. G., C. D. Charles, and J. D. Wright (1992), Origin of global meltwater pulses, in *Radiocarbon after four decades*, edited by R. E. Taylor, pp. 473-500, Springer, Berlin Heidelberg New York.

Friedman, I., and J. R. O`Neil (1977), Compilation of Stable Isotope Fractionation Factors of Geochemical Interest, in *U.S. Geological Survey Professional Paper 440-KK*, U.S. Geological Survey, Washington D.C.

Gradstein, F. M., and S. P. Srivastava (1980), Aspects of Cenozoic stratigraphy and paleoceanography of the Labrador Sea and Baffin Bay, *Palaeogeogr., Palaeoclimatol., Palaeoecol., 30*, 261-295.

Greenwood, D. R., and S. L. Wing (1995), Eocene continental climates and latitudinal temperature gradients, *Geology, 23*, 1044-1048.

Hubert, J. F., P. T. Panish, D. J. Chure, and K. S. Prostak (1996), Chemistry, microstructure, petrology, and diagenetic model of Jurassic dinosaur bones, Dinosaur National Monument, Utah, *J. Sed. Res., 66*(3), 531-547.

Iakovleva, A. I., H. Brinkhuis, and C. Cavagnetto (2001), Late Paleocene-Early Eocene dinoflagellate cysts from the Turgay Strait, Kazakhstan; correlations across ancient seaways, *Palaeogeogr., Palaeoclimatol., Palaeoecol., 172*, 243-268.

Jahren, A. H., and L. S. L. Sternberg (2002), Eocene meridional weather patterns reflected in the oxygen isotopes of Arctic fossil wood, *GSA Today, 12*(1), 4-9.

Jahren, A. H., and L. S. L. Sternberg (2003), Humidity estimate for the middle Eocene Arctic rain forest, *Geology, 31*(5), 463-466.

Jakobsson, M., J. Backman, B. Rudels, J. Nycander, M. Frank, L. Mayer, W. Jokat, F. Sangiorgi, M. O'Regan, H. Brinkhuis, J. King, and K. Moran (2007), The early Miocene onset of a ventilated circulation regime in the Arctic Ocean, *Nature, 447*, 986-990.

Johnson, G. L., J. Pogrebitsky, and R. Macnab (1994), Arctic Structural Evolution: Relationship to Paleoceanography, in *The Polar Oceans and Their Role in Shaping the Global Environment: The Nansen Centennial Volume*, edited by O. M. Johannessen, R. D. Muench and J. E. Overland, pp. 285-294, American Geophysical Union, Washington D.C.

Knox, R. W. O. B. (1998), The tectonic and volcanic history of the North Atlantic region during the Paleocene-Eocene transition: Implications for NW European and global biotic events, in *Late Paleocene-Early Eocene climatic and biotic events in the marine and terrestrial records*, edited by M. P. Aubry, S. G. Lucas and W. A. Berggren, pp. 91-102, Columbia University Press, New York.

Koch, P. L., N. Tuross, and M. L. Fogel (1997), The effects of sample treatment and diagenesis on the isotopic integrity of carbonate in biogenic hydroxylapatite., *J. Archaeol. Sci., 24*, 417-429.

Kohn, M. J., and J. M. Law (2006), Stable isotope chemistry of fossil bone as a new paleclimate indicator, *Geochim. Cosmochim. Acta, 70*, 931-946.

Kolodny, Y., and B. Luz, Jr. (1991), Oxygen isotopes in phosphates of fossil fish--Devonian to Recent, in *Stable Isotope Geochemistry: A Tribute to Samuel Epstein*, edited by H. P. Taylor, J. R. O`Neil and I. R. Kaplan, pp. 105-119, The Geochemical Society, San Antonio, Texas.

Kolodny, Y., B. Luz, M. Sander, and W. A. Clemens (1996), Dinosaur bones: fossils or psuedomorphs? The pitfalls of physiology reconstruction from apatitic fossils, *Palaeogeogr., Palaeoclimatol., Palaeoecol., 126*, 161-171.

Lawver, L. A., A. Grantz, and L. M. Gahagan (2002), Plate kinematic evolution of the present Arctic region since the Ordovician, in *Tectonic Evolution of the Bering Shelf--Chuckchi Sea--Arctic Margin and Adjacent Landmasses*, edited by E. L. Miller, A. Grantz and S. L. Klemperer, pp. 333-358, The Geological Society of America, Boulder, Colorado.

Lawver, L. A., R. D. Mülller, S. P. Srivastava, and W. Roest (1990), The opening of the Arctic Ocean, in *Geological History of the Polar Oceans: Arctic versus Antarctic*, edited by U. Bleil and J. Thiede, pp. 29-62, Kluwer Academic Publishers, Dordrecht.

Lear, C. H., H. Elderfield, and P. A. Wilson (2000), Cenozoic deep-sea temperatures and global ice volumes from Mg/Ca in benthic foraminifral calcite, *Science (Washington, D. C., 1883-), 287*, 269-272.

Magavern, S., D. L. Clark, and S. L. Clark (1996), $^{87/86}$Sr, phytoplankton, and the nature of the Late Cretaceous and Early Cenozoic Arctic Ocean, *Mar. Geol., 133*, 183-192.

Manabe, S. (1997), Early development in the study of greenhouse warming: The emergence of climate models, *Ambio, 26*(1), 47-51.

Marincovich, L., Jr., E. M. Brouwers, D. Hopkins, M., and M. M. McKenna (1990), Late Mesozoic and Cenozoic paleogeographic and paleoclimatic history of the Arctic Ocean Basin, based on shallow-water marine faunas and terrestrial vertebrates, in *The Arctic Ocean Region*, edited by A. Grantz, L. Johnson and J. F. Sweeney, Geological Society of America, Boulder, Colorado.

Meyers, P. A., and S. M. Bernasconi (2005), Carbon and nitrogen isotope excursions in mid-Pleistocene sapropels from the Tyrrhenian Basin: Evidence for climate-induced inrease in microbial primary production, *Mar. Geol., 220*, 41-58.

Miller, K. G., M. A. Kominz, J. V. Browning, J. D. Wright, G. S. Mountain, M. E. Katz, P. J. Sugarman, B. S. Cramer, N. Christie-Blick, and S. F. Pekar (2005a), The Phanerozoic record of global sea-level change, *Science, 310*, 1293-1298.

Miller, K. G., J. D. Wright, and J. V. Browning (2005b), Visions of ice sheets in a greenhouse world, *Mar. Geol., 217*, 215-231.

Moore, T. C., and Expedition 302 Scientists (2006), Sedimentation and subsidence history of the Lomonosov Ridge, in *Proceedings IODP, 302*, edited by J. Backman, K. Moran, D. B. McInroy, L. Mayer and Expedition 302 Scientists, Integrated Ocean Drilling Program Management International, Inc., Edinburg, doi:10.2204/iodp.proc.302.105.2006.

Moran, K., J. Backman, H. Brinkhuis, S. C. Clemens, T. M. Cronin, G. R. Dickens, F. Eynaud, J. Gattacceca, M. Jakobsson, R. W. Jordan, M. Kaminski, J. King, N. Koc, A. Krylov, N. Martinez, J. Matthiessen, D. McInroy, T. C. MOore, J. Onodera, M. O'Regan, H. Palike, B. Rea, D. Rio, T. Sakamoto, D. C. Smith, R. Stein, K. St John, I. Suto, N. Suzuki, K. Takahashi, M. Watanabe, M. Yamamoto, J. Farrell, M. Frank, P. Kubik, W. Jokat, and Y. Kristoffersen (2006), The Cenozoic palaeoenvironment of the Arctic Ocean, *Nature, 441*, 601-605.

Moriya, K., P. A. Wilson, O. Friedrich, J. Erbacher, and H. Kawahata (2007), Testing for ice sheets during the mid-Cretaceous greenhouse using glassy foraminiferal calcite from the mid-Cenomanian tropics on the Demerara Rise, *Geology, 35*(7), 615-618.

Mueller-Lupp, T., H. Erlenkueser, and H. A. Bauch (2003), Seasonal and interannual variability of Siberian river discharge in the Laptev Sea inferred from stable isotopes in modern bivalves, *Boreas, 32*, 292-303.

Nunes, F., and R. D. Norris (2006), Abrupt reversal in ocean overturning during the Palaeocene/Eocene warm period, *Nature, 439*, 60-63.

Onodera, J., and K. Takahashi (2007), The Eocene silicoflagellate and ebridian paleoceanography in the central Arctic Ocean, *Paleoceanography, PA1S15, doi:10.1029/2007PA001474*.

Pagani, M., N. Pedentchouk, M. Huber, A. Sluijs, S. Schouten, H. Brinkhuis, J. S. S. Damste, G. R. Dickens, and E. Scientists (2006), Arctic hydrology during global warming at the Paleocene/Eocene thermal maximum, *Nature, 442*, 671-675.

Radionova, E. P., and I. E. Khokhlova (2000), Was the North Atlantic connected with the Tethys via the Arctic in the early Eocene? Evidence from siliceous plankton., *GFF, 122*, 133-134.

Scheurle, C., and D. Hebbeln (2003), Stable oxygen isotopes as recordersof salinity and reiver discharge in the German Bight, North Sea, *Geo-Marine Letters, 23*, 130-136.

Sluijs, A., S. Schouten, M. Pagani, M. Woltering, H. Brinkhuis, J. S. S. Damste, G. R. Dickens, M. Huber, G.-J. Reichart, R. Stein, J. Matthiessen, L. J. Lourens, N. Pedentchouk, J. Backman, K. Moran, and E. Scientists (2006), Subtropical Arctic Ocean temperatures during the Paleocene/Eocene thermal maximum, *Nature, 441*, 610-613.

Srivastava, S. P. (1985), Evolution of the Eurasian basin and its implications to the motion of Greenland along Nares Strait, *Tectonophysics, 114*, 29-53.

St. John, K., and D. Willard (2006), Cenozoic (0-46 Ma) ice-rafting history of the Central Arctic: Terrigenous sands on the Lomonosov Ridge, *Eos Trans. AGU, 87*(52), Fall Meet. Suppl., Abstract U24A-07.

Stickley, C., N. Koc, H.-J. Brumsack, R. W. Jordan, and I. Suto (2008), A siliceous microfossil view of Middle Eocene Arctic paleoenvironments: A window of biosilica production and preservation, *Paleoceanography*, doi:10.1029/2007PA001485.

Thiede, J., and A. M. Myhre (1996), Introduction to the North Atlantic-Arctic gateways: Plate tectonic-paleoceanographic history and significance, in *Proceedings of the Ocean Drilling Program, Scientific Results, 151*, edited by J. Thiede, A. M. Myhre, J. V. Firth, G. L. Johnson and W. F. Ruddiman, pp. 3-23, Ocean Drilling Program, College Station, Texas.

Toyoda, K., and M. Tokonami (1990), Diffusion of rare-earth elements in fish teeth from deep-sea sediments, *Nature, 345*, 607-609.

Tripati, A., J. Zachos, L. Marincovich, Jr., and K. L. Bice (2001), Late Paleocene Arctic coastal climate inferred from molluscan stable and radiogenic isotope ratios, *Palaeogeogr., Palaeoclimatol., Palaeoecol., 170*, 101-113.

Trueman, C. N., A. K. Behrensmeyer, R. Potts, and N. Tuross (2006), High-resolution records of location and stratigraphic provenance from the rare earth element composition of fossil bones, *Geochim. Cosmochim. Acta, 70*, 4343-4355.

Trueman, C. N., and N. Tuross (2002), Trace elements in recent and fossil bone apatite, in *Reviews in Mineralogy & Geochemistry*, vol. 48, edited by M. J. Kohn, J. Rakovan and J. M. Hughes, pp. 489-521.

Vetshteyn, V. Y., G. A. Malyuk, and V. P. Rusanov (1974), Oxygen-18 distribution in the Central Arctic Basin, *Oceanology, 14*(4), 514-519.

Wright, J. D. (1998), Role of the Greenland-Scotland Ridge in Neogene climate changes, in *Tectonic boundary conditions for climate reconstructions*, edited by T. J. Crowley and K. C. Burke, pp. 192-211, Oxford University Press, Oxford, U.K.

Zachos, J., M. Pagani, L. Sloan, E. Thomas, and K. Billups (2001), Trends, rhythms, and aberrations in global climate 65 Ma to present, *Science, 292*, 686-693.

Zachos, J., L. D. Stott, and K. C. Lohmann (1994), Evolution of early Cenozoic marine temperatures, *Paleoceanography, 9*(2), 353-387.

Zahn, R., and A. C. Mix (1991), Benthic foraminiferal $\delta^{18}O$ in the ocean's temperature-salinity-density field: Constraints on ice age thermohaline circulation, *Paleoceanography, 6*(1), 1-20.

Zazzo, A., C. Lécuyer, and A. Mariotti (2004), Experimentally-controlled carbon and oxygen isotope exchange between bioapatites and water under inorganic and microbially-mediated condtions, *Geochim. Cosmochim. Acta, 68*, 1-12.

Chapter 5

The Isotopic Integrity of Biogenic Apatite Carbonate in Deep Sea Settings

Abstract

Stable isotope analysis of bone has been used for decades to obtain paleodietary and paleoenvironmental information from continental settings. However, the potential for obtaining useful stable isotopic information from fish bone in carbonate-poor deep-sea settings has been virtually unexplored. In order to assess the isotopic integrity of the structural carbonate component of marine apatite, fish debris from two deep-sea core sites with existing foraminiferal stable isotope records was subjected to stable isotope analysis. The $\delta^{13}C$ values obtained from the apatite carbonate in these cores show a close resemblance overall to the values obtained from benthic foraminifera, while the $\delta^{18}O$ values display a positive offset relative to the benthic values. Thus, the stable isotopic composition of the fish debris is generally consistent with recrystallization in a benthic environment, but the positive $\delta^{18}O$ offsets displayed in this study indicate that further study will be required before stable isotope analysis of apatite carbonate would prove worthwhile for most deep sea applications.

1. Introduction

Stable isotope analysis of biogenic carbonate has served as an indispensable paleoceanographic tool since the pioneering studies of Emiliani (1954; 1955; 1966). Unfortunately, however, while stable isotope records of increasingly high resolution have become available from the shallower portions of the world ocean, carbonate undersaturation in the deep sea has prevented the attainment of even low resolution stable isotope records from some important oceanic sectors, particularly the deep Pacific and polar oceans. Sediments recovered from these deep regions, while lacking in carbonate microfossils, sometimes contain appreciable amounts of fish bone and teeth, which

harbor carbonate within the apatite structure and thus have the potential to yield an alternative source of stable isotopic data from carbonate-poor sediments.

In continental settings, stable isotope geochemistry has been used for decades to obtain paleodietary and paleoenvironmental information from mammal bones and teeth. Longinelli (1984) and Luz et al.(1984) established that, due to the constant 37°C body temperature maintained by mammals, the oxygen isotope composition of mammalian bone phosphate could be used to determine the $\delta^{18}O$ value of the local meteoric water ingested by the animal, which, in turn, is a function of the mean annual temperature (Dansgaard, 1964). While the oxygen isotope systematics of the carbonate component of mammalian apatite remained poorly understood for many years, Bryant et al. (1996) found that the oxygen isotope composition of structural carbonate is also related to the $\delta^{18}O$ of body water, and that the $\delta^{18}O$ values of the structural carbonate and phosphate phases are strongly correlated.

The finding that the structural carbonate component, which is effectively an ionic impurity within the phosphate position (and to a lesser extent the hydroxyl position) of the hydroxyapatite structure $Ca_{10}(P0_4)_6(OH)_2$, could carry a climate signal was significant for a number of reasons. First, stable isotope analysis of the carbonate component also yields a $\delta^{13}C$ value, which can provide dietary information, such as an herbivore's relative intake of C3 to C4 plants (Lee-Thorp and van der Merwe, 1987; Macfadden and Cerling, 1996; Quade et al., 1992). Second, the procedures involved in analysis of carbonate oxygen are considerably less complicated, less expensive, and can be conducted on much smaller quantities of bone than those for phosphate oxygen, and lastly, if significant quantities of sample exist, analysis of both oxygen phases can provide a check for diagenetic alteration (Iacumin et al., 1996).

An important consideration analyzing the carbonate component of biogenic apatite, however, is its high susceptibility to diagenetic alteration, and thus to isotopic exchange, within the depositional environment (Koch et al., 1997; Kolodny and Luz, 1991). From the beginning, paleoenvironmental studies, including early reconstructions of marine paleotemperatures from fish debris (Kolodny et al., 1983; Kolodny and Raab, 1988), have concentrated on the $\delta^{18}O$ of the phosphate oxygen of bioapatite due to its known resistance to isotopic exchange under inorganic conditions. Some later studies

have asserted, however, that under microbially-mediated conditions the phosphate oxygen in bone and dentine can also undergo isotopic exchange (Ayliffe et al., 1992; Quade et al., 1992; Zazzo et al., 2004), and thus, to obtain a primary $\delta^{18}O$ signal, analysis of phosphate oxygen is now primarily limited to the enamel.

With its small crystal size, high porosity, and high organic carbon content, bone is much more susceptible to postmortem recrystallization and isotopic exchange than enamel, which is denser and has larger crystallites. Stable isotope analysis of enamel phosphate, which requires several milligrams of material, is achievable in studies using the teeth of large herbivorous mammals, but it is usually not realistic in studies involving very small teeth. Estimates of marine paleotemperature have been made from the $\delta^{18}O$ of enamel phosphate in fish teeth from shallow platform deposits (Pucéat et al., 2007; Pucéat et al., 2003), where larger teeth tend to be abundant. However, the large sample size required for stable isotope analysis has prevented similar studies on small fish teeth from deep sea settings, although new techniques using laser-assisted heating techniques are being developed that may someday permit the reliable extraction of primary $\delta^{18}O$ values from smaller teeth (Jones et al., 1999; Lindars et al., 2001; Passey and Cerling, 2006).

Alternatively, to obtain information about the burial environment, some stable isotopic studies have specifically taken advantage of the high potential for bone to undergo rapid and extensive post-mortem recrystallization. For example, in their study of terrestrial sequences, Kohn and Law (2006) found that the stable isotopic composition of the carbonate component of fossil bone appears to record trends in soil water composition and temperature analogous to that of pedogenic carbonates in the next higher paleosol level. As bone fossilizes, its mineralogy becomes dominated by authigenic francolite (carbonate fluor-apatite), its density and crystallinity increases, its organic content decreases, and the concentration of REE's and U within its structure increases by several orders of magnitude (Trueman and Tuross, 2002). These changes can begin within days of death (Zazzo et al., 2004) and are believed to reach completion within a few kyr to tens of kyr (Kohn and Law, 2006; Trueman and Tuross, 2002). Recrystallization is necessary for the preservation of bone in most pore water environments, but once a bone has been recrystallized and its pores filled, it is unlikely that the bone would continue to

exchange with its surrounding environment, which, in essence, makes bone a natural "timed sampling device" (Trueman et al., 2006; Trueman and Tuross, 2002).

Because the fish bones recovered from deep sea sequences are particularly small and thin, it may be reasonable to assume that rapid and extensive recrystallization of the bone occurred on the sediment surface or within the uppermost pore waters. In this case, fish bone could provide a $\delta^{18}O$ record reflective of the deepwater mass in which it was recrystallized, and thus could potentially serve as an alternative source of stable isotopic data from sequences lacking benthic foraminifera. The $\delta^{18}O$ results obtained from fish bone carbonate in Eocene Arctic sediments (**Chapter 4**) appear promising. However, very few studies have analyzed the isotopic composition of fish bone obtained from deep sea environments, and even fewer have examined the stable isotope values of fish bone and benthic foraminifera recovered from the same sequence.

To investigate the possibility of using the structural carbonate of fish bone as a substitute for benthic foraminifera in carbonate-poor marine sequences, I have obtained new stable isotope data from two deep sea sediment sequences known to contain both fish debris and foraminifera: Eocene sediments from ODP Sites 1209B and 1212A on the Shatsky Rise in the North Pacific and late Miocene sediments recovered in piston core MV0502-4JC from the subantarctic Pacific. I also examine data from Andreasson et al. (1996), which include stable isotope analyses on fish bone from Eocene Norwegian-Greenland Sea ODP Hole 913B sediments, as well foraminifera and fish bone from the Eocene intervals of the Røsnæs Clay Formation in Denmark and DSDP Hole 550 in the northeastern Atlantic. I then revisit the Eocene Arctic Ocean data from **Chapter 4** to examine the likely isotopic integrity of those fish bone samples in light of the new results presented in this chapter.

2. Methods

Foraminifera and bones and teeth on the order of ~1 mm in size were picked from the coarse fraction (>125 μm) of sediment samples from ODP Sites 1209B (16H-CCW 0-5) and 1212A (8H-CCW 0-5, 9H-CCW 0-5) and from piston core MV0502-4JC (1156-1168 cmbsf, 1216-1228 cmbsf, 1261-1275 cmbsf, 1611-1623 cmbsf). The locations of these and other cores sites mentioned in this chapter are given in **Table 5.1**. The samples

from the Shatsky Rise (Sites 1209 and 1212) range from lowermost Eocene (~55 Ma for 1212A-9H-CC) to middle Eocene (~45 Ma for 1209B-16H-CC) in age, whereas the subantarctic Pacific samples from MV0502-4JC are late Miocene in age, with most samples younger than ~6.5 Ma (except for the sample from 1611-1623 cmbsf, which predates the late Miocene carbon shift and is therefore older than ~8 Ma).

Because carbonate only accounts for ~6% of bone by weight (Lee-Thorp, 2002), at least 1 mg of teeth and bone fragments was required per bioapatite sample. These samples were gently ground, transferred to a microcentrifuge tube and treated chemically with 1 M acetic acid buffered with calcium acetate in order remove exogenous carbonate while minimizing possible effects to the structural carbonate (Koch et al., 1997). After 24 hours in the acetic acid-calcium acetate buffer solution, each sample was rinsed five times with deionized water, centrifuged between each rinse, and dried in an oven at 40˚C.

Because slight variations in the chemical concentrations, amount of solutions used, and the duration of the treatment can lead to inconsistencies in the isotopic offsets obtained for bioapatite (Koch et al., 1997), a control consisting of fish bone from the Pliocene Snake River Plain was treated alongside each batch of samples. Often, bioapatite is also treated with 2% NaOCl in order to oxidize organic matter, but this step was omitted for the samples from MV0502-4JC and ODP Sites 1209 because organic concentrations in the sediment are very low and the use of this treatment step on test samples produced no isotopic offset.

The carbon and oxygen isotope composition of the foraminifera and fish bone carbonate were analyzed in the University of Michigan Stable Isotope Laboratory. Samples were roasted under vacuum at 200˚C for one hour preceding analysis and were then reacted at 75˚C with phosphoric acid in a Kiel automatic carbonate preparation device linked to a Finnigan MAT 251 mass spectrometer. Stable isotope data are reported in standard δ-notation relative to the Vienna Peedee belemnite (VPDB) standard. Analytical precision, which was monitored through the regular analysis of the standard reference carbonate NBS-19, was ±0.03‰ for $\delta^{13}C$ and ±0.08‰ for $\delta^{18}O$ (1σ), and the Snake River Plain bioapatite that was used as a control displayed an isotopic variability of ±0.2‰ for $\delta^{18}O$ and ±0.3‰ for $\delta^{13}C$ (1σ).

A total of six planktonic foraminifera and three benthic foraminfera were analyzed per sample. A correction factor of +0.64‰ was applied to the benthic $\delta^{18}O$ values obtained from the late Miocene portion of MV0502-4JC to correct for the known departure of *Planulina wuellerstofi* from isotopic equilibrium (Shackleton and Hall, 1997). (The same correction factor was also used for *Cibicidoides robertsonianus* based upon the similar stable isotope values obtained for *Planulina wuellerstofi* and *Cibicidoides robertsonianus* at depths where the two species co-occurred.) Stable isotope values obtained from the Eocene benthic foraminifera analyzed from ODP Sites 1209 and 1212 were corrected for vital effects determined by Katz et al. (2003), and these corrections were also applied to the stable isotope values of Eocene benthic foraminifera given in Andreasson et al. (1996) for the Røsnæs Clay Formation in Denmark (Schmitz et al., 1996) and DSDP Hole 550 (Charisi and Schmitz, 1996) in the northeastern Atlantic.

3. Results

3.1 Eocene Fish Debris from the Shatsky Rise

As shown in **Table 2**, the $\delta^{18}Oco_3^{2-}$ values obtained from the Shatsky Rise fish debris are more similar to the $\delta^{18}O$ values of the benthic, rather than planktonic, foraminifera. However, the $\delta^{18}O$ values of the fish debris are offset from the benthic foraminifera by ~+1‰ (+0.90‰ for 1209B 16H-CC, +0.77‰ for 1212A 8H-CC, and +1.15‰ for 1212A 9H-CCW 0-3). **Figure 5.1** displays these results with the benthic and planktonic stable isotope data obtained by Dutton et al. (2005) from the Shatsky Rise. Their results show a decrease in benthic $\delta^{18}O$ from ~0.5 to -0.4‰ in the lowermost Eocene, a stabilization of benthic $\delta^{18}O$ values between -0.4 and 0.0‰ for the duration of the lower Eocene and lower middle Eocene, and a rapid increase in benthic $\delta^{18}O$ from ~-0.4 to 0.9‰ in the middle Eocene. These trends are reflected in the $\delta^{18}O$ values of the benthic foraminifera and fish debris obtained in this study. The benthic foraminifera from lowermost Eocene sample 1212A-9H-CC yield a $\delta^{18}O$ value of 0.51‰, which is followed by a decrease to -0.13‰ in lower Eocene sample 1212A 8H-CC and an increase to 1.33‰ in middle Eocene sample 1209B-16H-CC. The fish debris from these samples also record this trend toward lower $\delta^{18}O$ values in the lower Eocene and higher values in the middle Eocene but are offset by ~+1‰ from the benthic values.

The benthic and planktonic $\delta^{13}C$ values obtained from the Shatsky Rise samples also show good agreement with the results of Dutton et al. (2005). Planktonic $\delta^{13}C$ values are ~2‰ higher than the values obtained from the fish debris, but the $\delta^{13}C$ values of the fish debris and benthic foraminifera are quite similar, showing only small differences.

3.2 Late Miocene fish debris from the Subantarctic Pacific

The stable isotope results obtained from subantarctic Pacific core MV0502-4JC are shown in **Table 5.3**. The late Miocene portion of the core is characterized by relatively invariable benthic $\delta^{18}O$ values, typical of late Miocene marine records (**Figure 5.2**). Unfortunately, planktonic foraminifera are not present due to dissolution. However, comparison between the $\delta^{18}O$ values of benthic foraminifera and fish debris reveals that, similar to the results from the Shatsky Rise, the $\delta^{18}Oco_3^{2-}$ values of the fish debris at this location also display a positive offset relative to the benthic foraminifera. In this case, however, the offset displayed by most of the samples is almost 2‰ (+1.42‰ for 1156-1168 cmbsf, +1.80‰ for 1216-1228 cmbsf, +1.90‰ for 1261-1275 cmbsf, and +1.82‰ for 1281-1298 cmbsf), with the exception of the sample from 1611-1623 cmbsf, which shows an offset of only +0.54‰.

The $\delta^{13}C$ values of the fish debris from MV0502-4JC do not show the late Miocene carbon shift, a large permanent excursion of ~-1‰ displayed by the benthic $\delta^{13}C$ values at 1530 cmbsf (**Figure 5.2**). The $\delta^{13}C$ value of the fish debris instead remains fairly constant during the late Miocene. Thus, while the carbon isotope values of the fish debris and benthic foraminifera are quite similar overall, the fish debris sample from 1611-1623 cmbsf, which pre-dates the late Miocene carbon shift, is significantly depleted in ^{13}C relative to the benthic foraminifera (**Figure 5.2**).

4. Discussion

4.1 The positive $\delta^{18}O$ offsets in the Shatsky Rise and subantarctic Pacific samples

The positive $\delta^{18}O$ values of fish debris relative to benthic foraminifera in both the Shatsky Rise and subantarctic Pacific cores could be a consequence of the nannofossil ooze sediment type shared by the two sites. Nannofossils, or coccoliths, make up the majority of the bulk carbonate in deep sea sediments, and the $\delta^{18}O$ value of bulk

carbonate is on average 2‰ higher than for surface-dwelling planktonic foraminifera, most likely due to vital effects in the coccoliths (Schrag et al., 1995). At high latitude sites, such as the subantarctic Pacific, the temperature gradient between the surface and deep ocean is small. Thus, the $\delta^{18}O$ value of bulk carbonate would be expected to undergo only small changes upon exposure to cold pore fluids during early diagenesis on the seafloor (Schrag et al., 1995). Likewise, the difference between the $\delta^{18}O$ values of planktonic and benthic foraminifera should also be small, especially during the late Miocene when the Southern Ocean appears to have been exceptionally well-mixed. (**Chapter 2**). Thus, the recrystallization of the structural carbonate of fish apatite while in the presence of bulk carbonate possessing a $\delta^{18}O$ value ~2‰ higher than that of the foraminifera in the same sediment could account for the offset of nearly +2‰ exhibited by the subantarctic fish debris.

While the fish debris from the Shatsky Rise would also be expected to show a positive offset relative to benthic foraminifera, the offset would be expected to be of a smaller magnitude. The greater vertical temperature gradient in the mid- and low latitude oceans would lead to a lower $\delta^{18}O$ composition in the carbonate produced in the surface waters. Thus, while the $\delta^{18}O$ values of the bulk carbonate would still be offset from planktonic foraminifera by +2‰, the $\delta^{18}O$ values of bulk carbonate at this mid-latitude site would not be as high relative to bulk carbonate at a high-latitude site, whereas the benthic $\delta^{18}O$ values at the two sites would be nearly identical. Thus, fish debris recrystallized on the seafloor at a carbonate-rich mid-latitude site like the Shatsky Rise should show a smaller positive $\delta^{18}O$ offset relative to benthic foraminifera than fish debris recrystallized in a high latitude region like the subantarctic Pacific, which can explain the smaller $\delta^{18}O$ enrichment of +1‰ in the Shatsky Rise fish debris.

The small offset of +0.54‰ between fish debris and benthic foraminifera from 1611-1623 cmbsf in MV0502-4JC can be explained by a similar mechanism—warmer surface water temperatures in the subantarctic Pacific preceding the late Miocene carbon excursion, or alternatively, a change in the nannofossil assemblage (and thus the vital effect) following the late Miocene carbon shift. A cooling of subantarctic Pacific surface waters at that time is a distinct possibility because the late Miocene carbon excursion may

have been accompanied by glacioeustatic sea level drop related to build-up of the West Antarctic Ice Sheet (Loutit, 1981).

However, the possibility that the relatively positive $\delta^{18}O$ values obtained from the fish debris samples from the Shatsky Rise and subantarctic Pacific are the result of offsets induced by the chemical pre-treatment procedure is also a possibility. Although the control that was treated alongside the fish debris samples did not demonstrate any statistically significant offset after treatment with buffered 1 M acetic acid, this could be the result of a more resistant mineralogy/preservation in the fish bone from the Snake River Plain. Koch et al. (1997) found that treatment with acetic acid systematically increased the $\delta^{18}O$, and decreased the $\delta^{13}C$, values of apatite carbonate relative to untreated samples, with $\delta^{18}O$ displaying the largest offsets. Thus, the possibility exists that apatite carbonate could acquire and retain a stable isotope composition similar to that of coeval benthic foraminifera. Moreover, the $\delta^{13}C$ values obtained from the fish debris are very similar to those of the benthic foraminifera, at least to first order, and are in no way representative of a surface water signal. The exception is the subantarctic Pacific sample obtained below the late Miocene carbon shift, which gave an anomalously low $\delta^{13}C$ value. This could be the result of diagenetic overprinting in the lower part of the core, as $\delta^{13}C$ values obtained from the few planktonic foraminifera present in that interval of the core were also found to be anomalously low.

4.2 Comparison to stable isotope results from other studies

Comparison of the subantarctic Pacific and Shatsky Rise results to the only other stable isotope data known to exist from coeval fish debris and foraminifera (**Tables 5.4 and 5.5**) provides an expanded view of the type of results that can be obtained from the analysis of marine apatite carbonate, in this case from untreated samples. In the Eocene Røsnæs Clay Formation, which was formed at middle bathyal depths (600-1000m) in a semi-marine environment but is now exposed along the coast of Denmark, the $\delta^{18}O$ values of the fish debris are more closely aligned with those of planktonic, rather than benthic, foraminifera, but the $\delta^{13}C$ values are generally anomalously low, raising the question of whether the debris could have been altered or affected by meteoric water. As for the Eocene interval of DSDP Hole 550, which is a fully marine nannofossil chalk, the data are sparse, but again the fish debris $\delta^{18}O$ and $\delta^{13}C$ values are much lower than those

obtained from benthic foraminifera. The large negative $\delta^{18}O$ and $\delta^{13}C$ offsets of the fish debris from benthic foraminifera at these sites contrast with the results obtained from the subantarctic Pacific and Shatsky Rise and highlight the need for more data in order to more fully assess the isotopic integrity of apatite carbonate in deep sea settings.

Figure 5.4 shows all of the apatite carbonate stable isotope data discussed in this chapter, as well as additional data from the Eocene Norwegian Greenland Sea (Andreasson et al., 1996) and Arctic Ocean that were discussed in **Chapter 4**. This plot shows that, on a large scale, carbonate apatite accurately records the paleoenvironmental differences between each of these sites. The fish debris from the Pliocene Snake River Plain is from a freshwater environment and thus displays the lowest $\delta^{18}O$ value. The fish debris from the warm, brackish Eocene Norwegian Greenland Sea and Arctic Ocean display the next lowest $\delta^{18}O$ values, followed by the semi-marine Røsnæs Clay Formation. The $\delta^{18}O$ values of the fish debris from the fully marine sites then increase in order of decreasing temperature, with the warm, Eocene northeast Atlantic and Shatsky Rise sites displaying lower values and the colder Miocene Arctic Ocean and subantarctic Pacific sites showing the highest values. Low $\delta^{13}C$ values also distinguish the relatively reducing conditions of the Eocene Norwegian Greenland Sea and Arctic Ocean from the more oxidizing environments of the other sites.

4.3 Implications for the fish debris from the Eocene Arctic Ocean

In **Chapter 4**, it was shown that fish debris can record stable isotope shifts within the marine environment. In particular, Arctic fish debris was found to record the shifts in $\delta^{13}C$ and $\delta^{18}O$ associated with the Paleocene Eocene Thermal Maximum and the *Azolla* event, but due to the carbonate-poor nature of the sediments, it was not possible to check these results against values from benthic foraminifera. If the diagenetic explanation suggested for the positive $\delta^{18}O$ offset in the Shatsky Rise and subantarctic samples is correct, then the Arctic fish debris would likely not record this offset due to the fact that it was not recrystallized within a carbonate-rich environment. Moreover, analyses of samples from 302-2A-55X both before and after treatment do not support the acquisition of a large positive $\delta^{18}O$ offset as a result of the chemical treatment procedure (**Table 4.1**). Thus, unlike the fish bones preserved in the nannofossil oozes of the Shatsky Rise and subantarctic Pacific, the Arctic fish bones may have been able to recrystallize in isotopic

equilibrium with seawater due to the carbonate-poor nature of the host sediments. This scenario is supported by the $\delta^{18}O$ value of the Miocene Arctic fish bone sample analyzed in **Chapter 4**, but needs further support from the analysis of bulk carbonates from the Shatsky Rise and subantartic Pacific cores.

5. Conclusions

While the stable isotopic composition of carbonate apatite clearly reflects large scale trends in the marine environment, the potential for carbonate apatite to serve as a substitute for benthic foraminifera in paleoceanographic studies remains equivocal. The stable isotope results from the Shatsky Rise and subantarctic Pacific appear promising, showing a relatively good correlation between the stable isotope values of fish debris and benthic foraminifera. However, stable isotope data from coeval fish debris and foraminifera in the Røsnæs Clay Formation and DSDP Hole 550 is less encouraging, as the $\delta^{18}O$ and $\delta^{13}C$ values of the fish debris at these sites reflect either planktonic values or post-diagenetic alteration.

The positive offsets of ~+1‰ and ~+2‰ between the $\delta^{18}O$ of fish debris and benthic foraminifera from the Shatsky Rise and subantarctic Pacific sites, respectively, could indicate that the fish debris either acquired a $\delta^{18}O$ signal similar to that of bulk carbonate during early diagenesis or underwent significant alteration during the chemical pretreatment procedure. Future work should involve the measurement of the $\delta^{18}O$ values of bulk carbonate at each of these sites and an assessment of the effects of pretreatment on the small bones characteristic of deep sea sediments. An examination of the mineral chemistry of fish bone from diverse marine environments should also be undertaken to determine whether differences in mineralogy/preservation may account for the better isotopic integrity of some fish debris samples.

Table 5.1. Location of core sites discussed in this study.

Site/Core	Location	Latitude/Longitude	Water Depth
ODP Site 1209	Shatsky Rise, North Pacific	32°39'N, 158°30'E	2387 m
ODP Site 1212	Shatsky Rise, North Pacific	32°27'N, 157°43'E	2683 m
MV0502-4JC	Subantarctic southeast Pacific	50°20'S, 148°08'W	4286 m
DSDP Hole 550	Goban Spur, northeastern Atlantic	48°31'S, 13°26'W	4432 m
Røsnæs Clay Formation	Albæk Hoved, Denmark	--	--
Snake River Plain	Idaho	--	--
ODP Hole 913B	Greenland-Norwegian Sea	75°29'S, 6°57'W	3318 m
IODP Hole M0002A	Lomonosov Ridge, Arctic Ocean	87°55'N, 139°22'E	1209 m
IODP Hole M0004A	Lomonosov Ridge, Arctic Ocean	87°52'N, 136°11'E	1288 m

Table 5.2. Oxygen and carbon isotopic composition of Eocene fish apatite and foraminifera from ODP Leg 198, Sites 1209 and 1212, Shatsky Rise.

Core Sample	Fish Apatite Carbonate		Benthic Foraminifera			Planktonic Foraminifera		
	$\delta^{18}O$	$\delta^{13}C$	$\delta^{18}O$	$\delta^{13}C$	Species	$\delta^{18}O$	$\delta^{13}C$	Species
1209B 16H-CCW 0-5	2.10	1.06	1.33	0.35	*Cibicidoides* spp.	-0.23	2.80	*Acarina bulbrooki*
1212A 8H-CCW 0-5	0.77	0.74	-0.13	0.83	*Oridorsalis* spp.	-0.90	2.35	*Morozovella aragonensis*
						-1.06	2.06	*Acarina bulbrooki*
						-0.71	2.28	*Morozovella subbotinae*
1212A 9H-CCW 0-3	1.66	0.98	0.51	1.19	*Nuttalides* spp.	-1.14	3.23	*Morozovella subbotinae*

Table 5.3. Oxygen and carbon isotopic composition of Miocene fish apatite and foraminifera from MV0502-4JC, Subantarctic Pacific.

Depth (cmbsf)	Fish Apatite Carbonate		Benthic Foraminifera		
	$\delta^{18}O$	$\delta^{13}C$	$\delta^{18}O$	$\delta^{13}C$	Species
1156-1168	5.23	0.51			
1156-1158			3.79	0.19	*Planulina wuellerstorfi*
1161-1163			3.85	0.15	*Planulina wuellerstorfi*
1166-1168			3.80	0.25	*Planulina wuellerstorfi*
1216-1228	5.37	0.57			
1216-1218			3.59	0.33	*Planulina wuellerstorfi*
1221-1223			3.54	0.47	*Planulina wuellerstorfi*
1226-1228			3.58	0.37	*Planulina wuellerstorfi*
1261-1275	5.43	0.39			
1261-1263			3.56	0.21	*Planulina wuellerstorfi*
1266-1268			3.54	0.26	*Planulina wuellerstorfi*
1273-1275			3.57	0.08	*Planulina wuellerstorfi*
1281-1298	5.42	0.35			
1281-1283			3.56	0.02	*Planulina wuellerstorfi*
1286-1288			3.69	0.38	*Planulina wuellerstorfi*
1291-1293			3.59	0.43	*Planulina wuellerstorfi*
1296-1298			3.54	0.47	*Planulina wuellerstorfi*
1611-1623	4.15	0.37			
1611-1613			3.63	1.24	*Cibicidoides robertsonianus*
1616-1618			3.64	1.26	*Cibicidoides robertsonianus*
1621-1623			3.55	1.20	*Cibicidoides robertsonianus*

Table 5.4. Oxygen and carbon isotopic composition of fish apatite and foraminifera from the Røsnæs Clay Formation (from Andreasson et al., 1996; Schmitz et al., 1996).

Meters above base	Fish Apatite Carbonate		*Subbotina patagoncia* (planktonic)		*Cibicidoides ungerianus* (benthic)	
	$\delta^{18}O$	$\delta^{13}C$	$\delta^{18}O$	$\delta^{13}C$	$\delta^{18}O$	$\delta^{13}C$
14.55	-2.10	-3.79	-2.50	1.20	-1.49	0.08
14.45	-2.71	-3.49	-2.96	1.21	-1.95	0.39
14.35	-2.82	-4.17	-3.05	1.33	-1.94	0.40
14.05	-3.02	-4.64	-3.09	0.99	-2.01	0.27
13.45[1]	-3.26	-4.09	-2.81	0.07	-2.6	-1.27
13.35[1]	-2.54	-3.58	-2.97	-0.27	-2.49	-1.29
11.20	-4.84	-0.65	-2.53	0.12	-1.2	-0.37
11.00	-2.94	-3.81	-2.61	-0.36	-1.97	-0.17
10.90	-2.64	-0.67	-2.59	-0.29	-1.91	-0.14

[1]Carbonate apatite treated with tri-ammonium citrate

Table 5.5. Oxygen and carbon isotopic composition of fish apatite and foraminifera from DSDP Hole 550 (from Andreasson et al., 1996 and Charisi and Schmitz, 1996).

Section, interval (cm)	Fish apatite carbonate		*Subbotina patagoncia* (planktonic)		*Oridorsalis umbonatus* (benthic)		*Nuttalides truempyi* (benthic)	
	$\delta^{18}O$	$\delta^{13}C$	$\Delta^{18}O$	$\delta^{13}C$	$\delta^{18}O$	$\delta^{13}C$	$\delta^{18}O$	$\delta^{13}C$
24-	-1.35	-0.09			0.23	0.98	0.08	1.03
24-1, 135-138	-0.17	-0.14						
25-	-1.65	0.58			-0.34	1.27	-0.38	1.03
28/29-	-2.38	-1.75	-0.85	0.57	-0.30	0.11	-0.37	0.18

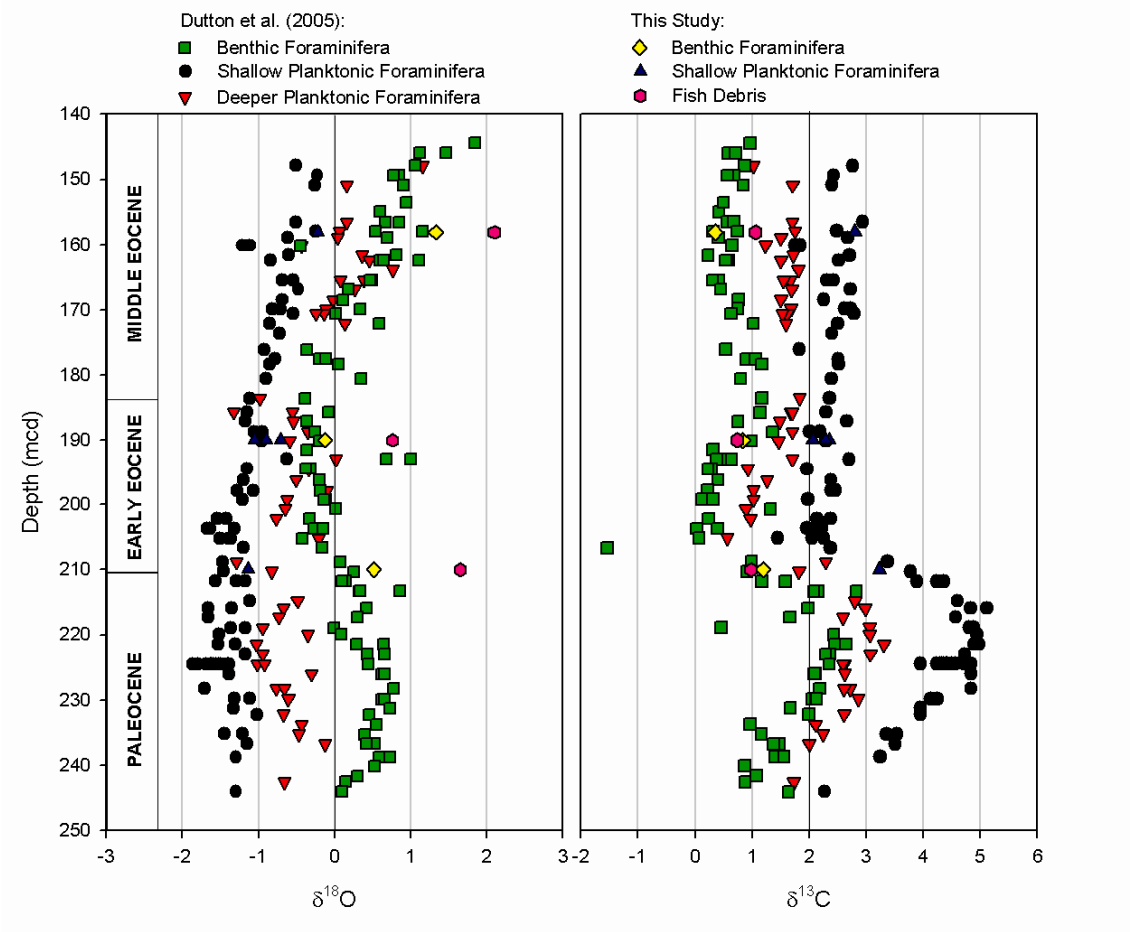

Figure 5.1. Comparison of the $\delta^{18}O$ (**left**) and $\delta^{13}C$ (**right**) values of benthic foraminifera, planktonic foraminifera, and fish debris obtained in this study with the results of Dutton et al. (2005) from ODP Site 1209 on the Shatsky Rise.

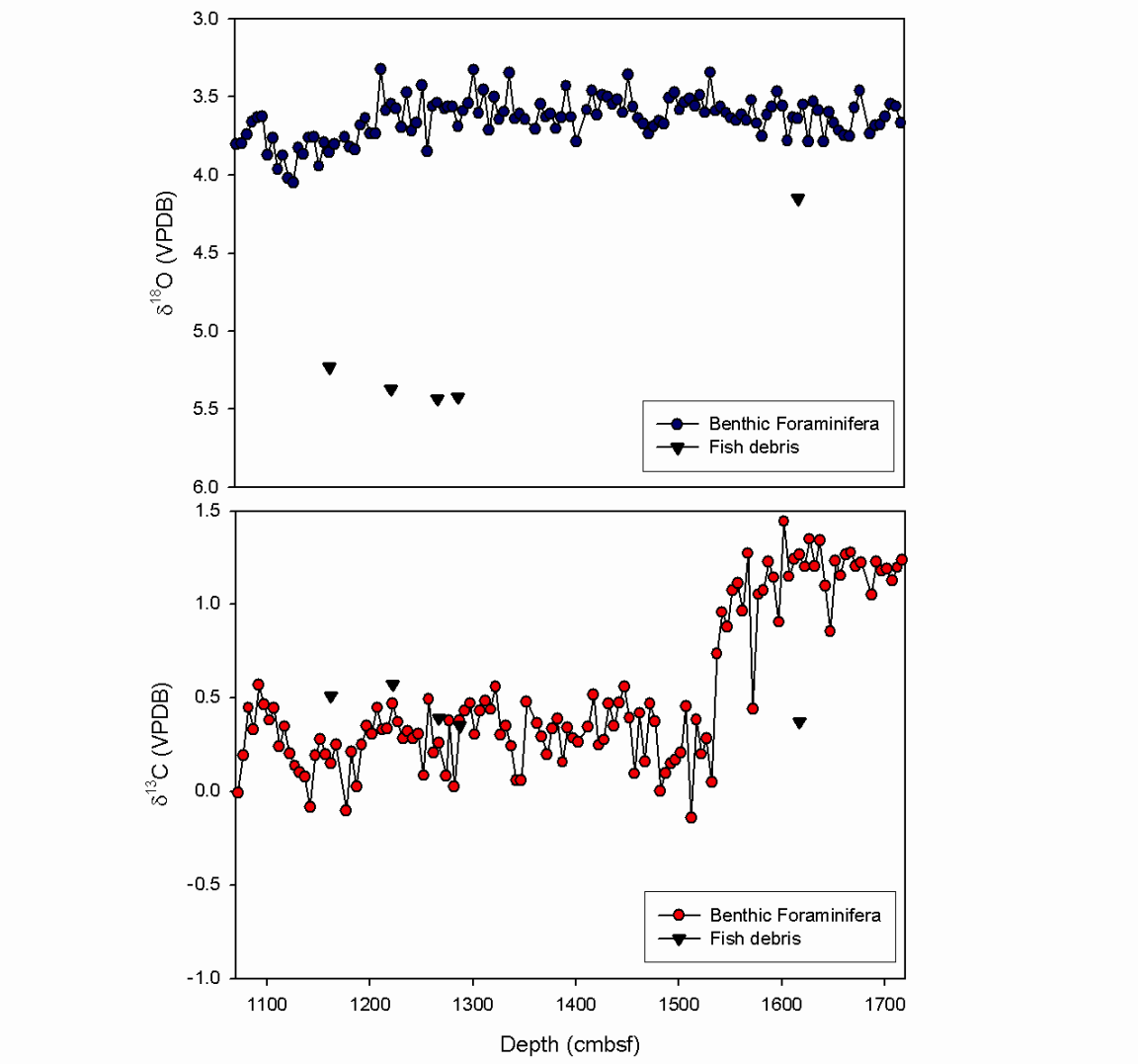

Figure 5.2. Comparison of the $\delta^{18}O$ (**top**) and $\delta^{13}C$ (**bottom**) values of fish debris and benthic foraminifera from the late Miocene portion of subantarctic Pacific core MV0502-4JC.

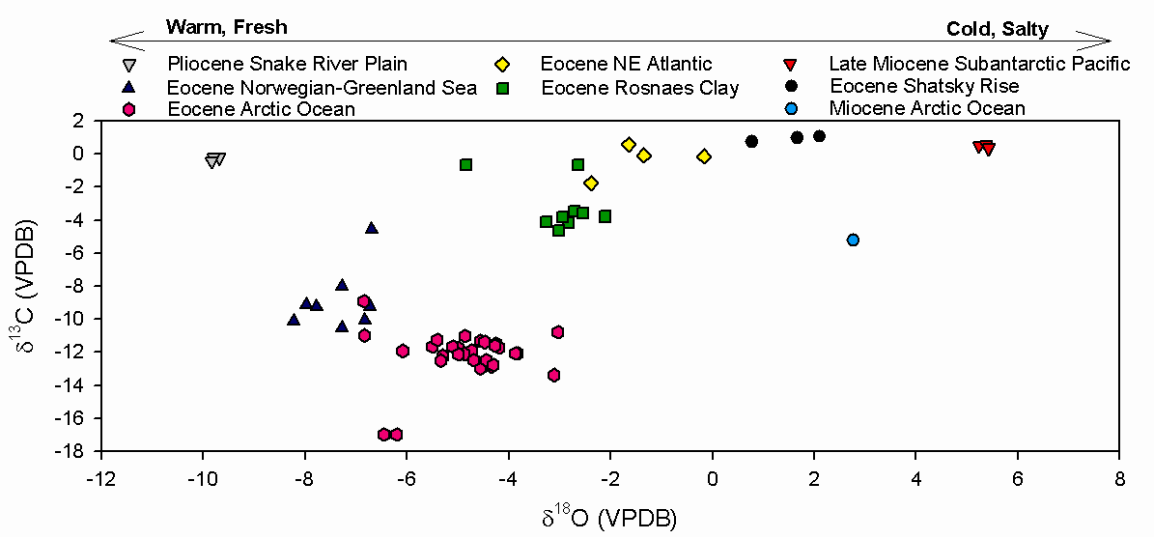

Figure 5.3: Plot showing the stable isotope values of fish apatite carbonate from all of the locations listed in Table 1.

REFERENCES

Andreasson, F.P., Schmitz, B., and Spiegler, D., 1996, Stable isotopic composition ($\delta^{18}O_{CO3}^{2-}$ and $\delta^{13}C$) of early Eocene fish-apatite from Hole 913B: An indicator of the early Norwegian-Greenland Sea paleosalinity., *in* Thiede, J., Firth, J.V., Johnson, G.L., and Ruddiman, W.F., eds., Proceedings of the Ocean Drilling Program, Scientific Results, 151: College Station, Texas, Ocean Drilling Program, p. 583-591.

Ayliffe, L.K., Lister, A.M., and Chivas, A.R., 1992, The preservation of glacial-interglacial climatic signatures in the oxygen isotopes of elephant skeletal phosphate: Palaeogeography, Palaeoclimatology, and Palaeoecology, v. 99, p. 179-191.

Bryant, J.D., 1996, Oxygen isotope partitioning between phosphate and carbonate in mammalian apatite: Geochimica et Cosmochimica Acta, v. 60, p. 5145-5148.

Charisi, S.D., and Schmitz, B., 1996, Early Eocene paleoceangraphy and paleoclimatology of the eastern North Atlantic: stable iostope results for DSDP Hole 550, *in* Knox, R.W.O.B., Corfield, R.M., and Dunay, R.E., eds., Correlation of the Early Paleogene in Northwest Europe, Volume 101: Special Publications: London, Geological Society, p. 457-472.

Dansgaard, W., 1964, Stable isotopes in precipitation: Tellus, v. XVI, p. 436-438.

Dutton, A., Lohmann, K.C., and Leckie, R.M., 2005, Insights from the Paleogene tropical Pacific: Foraminiferal stable isotope and elemental results from Site 1209, Shatsky Rise: Paleoceanography, v. 20, p. PA3004, doi:10.1029/2004PA001098.

Emiliani, C., 1954, Depth habitats of some species of pelagic foraminifera as indicated by oxygen isotope ratios: American Journal of Science, v. 252, p. 149-158.

—, 1955, Pleistocene temperatures: Journal of Geology, v. 63, p. 538-578.

—, 1966, Paleotemperature analysis of Caribbean cores P6304-8 and P6304-9 and a generalized temperature curve for the past 425,000 years: Journal of Geology, v. 74, p. 109-126.

Iacumin, P., Bocherens, H., Mariotti, A., and Longinelli, A., 1996, Oxygen isotope analyses of co-exisiting carbonate and phosphate in biogenic apatite: a way to monitor diagenetic alteration of bone phosphate?: Earth and Planetary Science Letters, v. 142, p. 1-6.

Jones, A.M., Iacumin, P., and Young, E.D., 1999, High-resolution $\delta^{18}O$ analysis of tooth enamel phosphate by isotope ratio monitoring gas chromatography mass

spectrometry and ultraviolet laser fluorination: Chemical Geology, v. 153, p. 241-248.

Katz, M.E., Katz, D.R., Wright, J.D., Miller, K.G., Pak, D.K., Shackleton, N.J., and Thomas, E., 2003, Early Cenozoic benthic foraminiferal isotopes: Species reliability and interspecies correction factors: Paleoceanography, v. 18, p. 1024, doi:10.1029/2002PA000798.

Koch, P.L., Tuross, N., and Fogel, M.L., 1997, The effects of sample treatment and diagenesis on the isotopic integrity of carbonate in biogenic hydroxylapatite.: Journal of Archaeological Science, v. 24, p. 417-429.

Kohn, M.J., and Law, J.M., 2006, Stable isotope chemistry of fossil bone as a new paleclimate indicator: Geochimica et Cosmochimica Acta, v. 70, p. 931-946.

Kolodny, Y., and Luz, B., Jr., 1991, Oxygen isotopes in phosphates of fossil fish--Devonian to Recent, *in* Taylor, H.P., O`Neil, J.R., and Kaplan, I.R., eds., Stable Isotope Geochemistry: A Tribute to Samuel Epstein: Special Publication No. 3: San Antonio, Texas, The Geochemical Society, p. 105-119.

Kolodny, Y., Luz, B., and Navon, O., 1983, Oxygen isotope variations in phosphate of biogenic apatites, I. Fish bone apatite--rechecking the rules of the game: Earth and Planetary Science Letters, v. 64, p. 398-404.

Kolodny, Y., and Raab, M., 1988, Oxygen isotopes in phosphatic fish remains from Israel: Paleothermometry of tropical Cretaceous and Tertiary shelf waters: Palaeogeography, Palaeoclimatology, and Palaeoecology, v. 64, p. 59-67.

Lee-Thorp, J., 2002, Two decades of progress towards understanding fossilization processes and isotopic signals in calcified tissue minerals: Archaeometry, v. 44, p. 435-446.

Lee-Thorp, J.A., and van der Merwe, N.J., 1987, Carbon isotope analysis of fossil bone apatite: South African Journal of Science: South African Journal of Science, v. 83, p. 712-714.

Lindars, E.S., Grimes, S.T., Mattey, D.P., Collinson, M.E., Hooker, J.J., and Jones, T.P., 2001, Phosphate $\delta^{18}O$ determination of modern rodent teeth by direct laser fluorination: An appraisal of methodology and potential application to palaeoclimate reconstruction: Geochimica et Cosmochimica Acta, v. 65, p. 2535-2548.

Longinelli, A., 1984, Oxygen isotopes in mammal bone phosphate: A new tool for paleohydrological and paleoclimatological research?: Geochimica et Cosmochimica Acta, v. 48, p. 385-390.

Loutit, T.S., 1981, Late Miocene paleoclimatology: Subantarctic water mass, southwest Pacific: Marine Micropaleontology, v. 6, p. 1-27.

Luz, B., Kolodny, Y., and Horowitz, M., 1984, Fractionation of oxygen isotopes between mammalian bone-phosphate and environmental drinking water: Geochimica et Cosmochimica Acta, v. 48, p. 1689-1693.

Macfadden, B.J., and Cerling, T.E., 1996, Mammalian herbivore communities, ancient feeding ecology, and carbon isotopes: A million-year sequence from the Neogene of Florida: Journal of Vertebrate Paleontology, v. 16, p. 103-115.

Passey, B.H., and Cerling, T.E., 2006, In situ stable isotope analysis ($\delta^{13}C$, $\delta^{18}O$) of very small teeth using laser ablation GC/IRMS: Chemical Geology, v. 235, p. 238-249.

Pucéat, E., Lécuyer, C., Donnadieu, Y., Naveau, P., Cappetta, H., Ramstein, G., Huber, B.T., and Kriwet, J., 2007, Fish tooth $\delta^{18}O$ revising Late Cretaceous meridional upper ocean water temperature gradients: Geology, v. 35, p. 107-110.

Pucéat, E., Lécuyer, C., Sheppard, S.M.F., Dromart, G., Reboulet, S., and Grandjean, P., 2003, Thermal evolution of Cretaceous Tethyan marine waters inferred from oxygen isotope composition of fish tooth enamels: Paleoceanography, v. 18, p. 1029, doi:10.1029/2002PA000823.

Quade, J., Cerling, T.E., Barry, J.C., Morgan, M.E., Pilbeam, D.R., Chivas, A.R., Lee-Thorp, J.A., and van der Merwe, N.J., 1992, A 16-Ma record of paleodiet using carbon and oxygen isotopes in fossil teeth from Pakistan: Chemical Geology, v. 94, p. 183-192.

Schmitz, B., Heilmann-Clausen, C., King, C., Steurbaut, E., Andreasson, F.P., Corfield, R.M., and Cartlidge, J.E., 1996, Stable isotope and biotic evolution in the North Sea during the early Eocene: the Albæk Hoved Section, Denmark, *in* Knox, R.W.O.B., Corfield, R.M., and Dunay, R.E., eds., Correlation of the Early Paleogene in Northwest Europe, Volume 101: Special Publication: London, Geological Society, p. 275-306.

Schrag, D.P., DePaolo, D.J., and Richter, F.M., 1995, Reconstructing past sea surface temperatures: Correcting for diagenesis of bulk marine carbonate: Geochimica et Cosmochimica Acta, v. 59, p. 2265-2278.

Shackleton, N.J., and Hall, M.A., 1997, The late Miocene stable isotope record, Site 926: Proceeding of the Ocean Drilling Program, Scientific Results, v. 154, p. 367-373.

Trueman, C.N., Behrensmeyer, A.K., Potts, R., and Tuross, N., 2006, High-resolution records of location and stratigraphic provenance from the rare earth element composition of fossil bones: Geochimica et Cosmochimica Acta, v. 70, p. 4343-4355.

Trueman, C.N., and Tuross, N., 2002, Trace elements in recent and fossil bone apatite, *in* Kohn, M.J., Rakovan, J., and Hughes, J.M., eds., Reviews in Mineralogy & Geochemistry, Volume 48, p. 489-521.

Zazzo, A., Lécuyer, C., and Mariotti, A., 2004, Experimentally-controlled carbon and oxygen isotope exchange between bioapatites and water under inorganic and microbially-mediated condtions: Geochimica et Cosmochimica Acta, v. 68, p. 1-12.

Chapter 6
Conclusions and Future Research

This dissertation has explored paleoceanographic change in two distinct high latitude regions—an isolated polar sea surrounded by land and a polar ocean that mixes water from and provides a linkage between the major oceans—during two very different climatic intervals—from an ice-free world through the establishment of permanent polar ice. **Chapters 2 and 3** focused on changes in the abyssal subantarctic Pacific during the climatic cooling and cryosphere development of the Late Neogene, and **Chapter 4** provided a unique view of the response of Arctic Ocean hydrography to the extreme warmth of the ice-free early Eocene world. **Chapter 2** demonstrated that with the global cooling trend of the Late Neogene came dramatic changes in the circulation of the abyssal Southern Ocean that may have amplified global cooling and helped to establish Northern Hemisphere ice sheets. The Antarctic Divergence, the southern boundary of the Antarctic Circumpolar Current (ACC), provides the main pathway through which waters deeper than 2500 m are exposed to the atmosphere. Thus, once the Antarctic cryosphere reached a stage in the late Pliocene whereby sea ice expansion and water mass stratification began to inhibit Southern Ocean ventilation, CO_2 sequestration within the abyssal Southern Ocean was able to drive continued global climatic cooling through a positive feedback cycle. Until the Antarctic cryosphere reached this advanced stage in late Pliocene, however, the build-up of ice on Antarctica did not have an effect on the vertical or interbasinal $\delta^{13}C$ or $\delta^{18}O$ gradients in the Southern Ocean. Despite the growth of the West Antarctic Ice Sheet in the late Miocene, the water column in both the Atlantic and Pacific sectors of the Southern Ocean remained well-mixed, well-ventilated, and of uniform temperature until the expansion of sea ice in the late Pliocene.

In addition to providing the first Late Neogene stable isotope record of water mass changes in the abyssal Southern Ocean, the subantaractic Pacific sediment core examined in **Chapter 2** was also found to record intervals of increased ACC strength.

Three major hiatuses were identified in the core, and in **Chapter 3**, a mechanism was proposed to explain the timing of these intervals of increased current intensity. The sediments in the subantarctic region are vulnerable to the erosive potential of the ACC, which is driven by strong westerly winds that produce northward Ekman transport, and subsequently a northward pressure gradient, yet extends to the seafloor in many locations. The timing of the younger hiatuses corresponds to significant changes in glacial cyclicity during the Mid-Pleistocene Revolution (~0.9 Ma; MIS 22) and the Mid-Brunhes climatic transition (~0.42 Ma; MIS 12) that were followed by interglacial intervals (MIS 21, MIS 11, and 9) of exceptional warmth and/or length, and the older hiatus corresponds to an unusual period of climatic amelioration known as the Mid-Pliocene warm period. Thus, these hiatuses suggest intensified ACC flow over the study region during periods of exceptional warmth. During warm intervals, the only viable mechanism for increasing ACC strength involves a strengthening and/or poleward shift of the westerly winds over the Southern Ocean, which would have been accompanied by an increase in the upwelling of deep water along the Antarctic Divergence, and consequently, an overall increase in global overturning circulation and bottom water flow, which is supported by the timing of hiatuses in globally-distributed deep-sea records. Future studies could involve the acquisition of grain size records from deep sea sites unbiased by shifts in the position of the ACC in order to better constrain the timing and magnitude of these increases.

In sharp contrast to the Southern Ocean, which has served as an important mixing zone for the world's water masses since the full establishment of the ACC in the Oligocene or earliest Miocene, the Arctic Ocean has always been relatively isolated from the rest of the ocean. **Chapter 4** found that this isolation had significant consequences for the salinity of the Arctic Ocean during the greenhouse climate of the Early Paleogene. Extreme high latitude warmth during the early Eocene led to an increase in the volume of precipitation and runoff received by the Arctic Ocean, resulting in average intermediate water salinities of 21 to 25‰. An interval of even lower salinity occurred during the Paleocene Eocene Thermal Maximum, which lends support for a separation of the Arctic and North Atlantic Oceans by a land bridge during that period. Two other "freshwater events" were found at ~48.7 Ma (the *Azolla* event) and ~47.6 Ma and may have been the

result of declines in eustatic sea level during which the Arctic-Atlantic connection may have been severed again. Only during these lower salinity events would strong overturning circulation have been possible in the North Atlantic. Much like the Pacific Ocean today, the Eocene Atlantic Ocean would have been dominated by deepwater from a southern source due to the influence of low salinity outflows from the Arctic Ocean. Future study could examine the concentration of redox-sensitive elements (Mo, Re, Cd, and Ag) in Arctic sediments because, unlike the Southern Ocean, the Arctic Ocean is vulnerable to low-oxygen conditions due to low salinity surface waters, which inhibit the ocean's ability to mix from top to bottom. Thus, the oxygenation of the intermediate water mass in the Arctic Ocean is highly sensitive to changes in Atlantic water inflow, sea ice-cover, and productivity. Redox-sensitive trace metal analysis could help elucidate past changes in these parameters, thereby improving our understanding of the evolution of Arctic Ocean circulation over the course of the Cenozoic.

Because calcareous microfossils are not preserved in the Arctic Ocean sediments, the paleosalinity estimates presented in **Chapter 4** were based upon $\delta^{18}O$ analysis of the structural carbonate component ($\delta^{18}Oco_3^{2-}$) of fish apatite. The stable isotopic composition of bioapatite has rarely been used to obtain paleoenvironmental information from deep sea settings, and thus the focus of **Chapter 5** was to examine the isotopic integrity of bioapatite in different marine settings. Analysis of bioapatite in nannofossil oozes from the Eocene Shatsky Rise and the Miocene subantarctic Pacific yielded $\delta^{18}Oco_3^{2-}$and $\delta^{13}C$ values similar to those of benthic foraminifera in most cases, but $\delta^{18}Oco_3^{2-}$values show consistent offsets from benthic values of ~1‰ and ~2‰, respectively. Thus the fish debris examined from these sites was clearly recrystallized on the seafloor and the potential exists to record stable isotope values similar to those of coeval benthic foraminifera. However, the source of these offsets would need to be known before stable isotope results from bioapatite could be applied with confidence in carbonate-poor settings. Future work could involve the acquisition of more stable isotope data from fish debris and foraminifera from a wide variety of deep sea settings. The mineral chemistry of the fish debris at each site, as well as the stable isotope composition of the bulk carbonate, should also be examined to check for any patterns in the isotopic integrity/offsets in the bones based on preservation or diagenetic environment. The

effects of chemical pretreatment on the small bones characteristic of deep sea sediments should also be addressed. This will require the acquisition of several milligrams of fish debris from a single sample interval, necessitating the identification of sediment where fish debris is concentrated.

Appendix A: Stable Isotope and Compositional Data from MV0502-4JC

Avg. Depth	*G. bullloides* $\delta^{18}O$	*G. bulloides* $\delta^{13}C$	*Cibicidoides* $\delta^{18}O$ (corrected)	*Cibicidoides* $\delta^{13}C$	*Cibicidoides* species	Wt% >63µm	Mn Count	IRD Count
2	3.33	0.73	4.79	-0.15	*C. mundulus*	19.37		
7	2.87	0.41	4.62	-0.32	*C. mundulus*	22.56		
12	2.81	0.63	4.76	-0.09	*C. mundulus*	24.46		
17	3.68	0.52	4.98	-0.33	*C. mundulus*	26.88	1	20
22	3.82	0.54	5.03	-0.18	*C. mundulus*	25.67		
27	3.57	0.97	4.73	-0.11	*C. mundulus*	23.25		
32	3.95	0.96	4.95	-0.21	*C. mundulus*	23.01		
37	3.28	0.77	4.79	-0.05	*C. mundulus*	21.69	0	22
42	3.53	0.77	4.72	-0.03	*C. mundulus*	21.57		
47	3.06	0.55	4.70	-0.02	*C. mundulus*	21.39		
52	3.35	0.63	4.62	0.15	*C. mundulus*	22.61		
57	3.16	0.67	4.62	-0.40	*C. mundulus*	23.71		
62	3.34	0.73	4.65	-0.27	*C. mundulus*	22.55	0	7
67	3.52	0.90	4.68	-0.11	*C. mundulus*	21.24		
72	3.43	0.73	4.60	-0.35	*C. mundulus*	19.01		
77	3.25	0.80	4.76	-0.37	*C. mundulus*	17.91		
82	3.31	0.79	4.57	-0.14	*C. mundulus*	17.35		
87	3.26	0.63	4.30	0.20	*C. mundulus*	17.50		
92	2.94	0.84	4.20	0.03	*C. mundulus*	17.42	3	13
97	2.79	0.97	4.29	0.13	*C. mundulus*	17.39		
102	2.71	0.77	4.39	0.17	*C. mundulus*	18.87		
107	2.96	1.11	4.37	0.21	*C. mundulus*	18.43		
112	2.77	1.08	4.39	0.17	*C. mundulus*	19.22	0	7
117	2.95	1.09	4.16	0.05	*C. mundulus*	19.23		
122	2.68	0.82	4.19	0.22	*C. mundulus*	18.42		
127	2.75	0.57	4.22	0.20	*C. mundulus*	20.38		
132	2.79	0.55	4.40	0.20	*C. mundulus*	22.06		
137	2.85	0.43	4.34	-0.01	*C. mundulus*	21.15	0	16
142	2.83	0.83	4.03	0.30	*C. mundulus*	17.18		
147	2.86	0.64	4.40	0.03	*C. mundulus*	16.66		
152	2.70	0.68	4.73	-0.08	*C. mundulus*	15.64		
157	3.23	0.02	4.82	-0.34	*C. mundulus*	20.23		
162	3.59	0.38	5.03	-0.53	*C. mundulus*	29.86	1	10
167	3.87	0.46	5.00	-0.43	*C. mundulus*	28.59		
172	3.75	0.49	4.94	-0.40	*C. mundulus*	25.98		
177	3.60	0.42	5.02	-0.44	*C. mundulus*	25.12		
182	3.69	0.30	4.90	-0.34	*C. mundulus*	25.86		
187	3.40	0.31	4.85	-0.48	*C. mundulus*	26.61		
192	3.34	0.21	4.94	-0.44	*C. mundulus*	27.81	2	24
197	3.54	0.14	4.83	-0.38	*C. mundulus*	29.40		
202	3.65	0.37	4.63	-0.27	*C. mundulus*	29.21		
207	3.40	0.72	4.78	-0.41	*C. mundulus*	27.59		
212	3.21	0.46	4.79	-0.45	*C. mundulus*	25.61	0	36
217	3.29	0.63	4.88	-0.59	*C. mundulus*	21.73		
222	2.91	0.18	4.79	-0.47	*C. mundulus*	20.59		
227	3.17	0.58	4.61	-0.47	*C. mundulus*	15.38		
232	3.18	0.51	4.76	-0.49	*C. mundulus*	14.49		
237	3.28	0.24	4.88	-0.49	*C. mundulus*	13.61	0	18
242	3.47	0.66	4.91	-0.62	*C. mundulus*	11.67		
247	3.08	0.42	4.84	-0.57	*C. mundulus*	13.44		
252	3.41	0.68	4.52	-0.11	*C. mundulus*	12.52		
257	3.28	0.33	4.36	-0.21	*C. mundulus*	14.15		
262	3.30	0.35	4.85	-0.29	*C. mundulus*	12.82	4	35
267	3.40	0.64	4.80	-0.87	*C. mundulus*	10.28		
272	3.46	0.72	4.30	-1.03	*C. mundulus*	11.32		

Avg. Depth	*G. bullloides* $\delta^{18}O$	*G. bulloides* $\delta^{13}C$	*Cibicidoides* $\delta^{18}O$ (corrected)	*Cibicidoides* $\delta^{13}C$	*Cibicidoides* species	Wt% >63µm	Mn Count	IRD Count
277	3.47	0.66	4.65	-0.64	*C. mundulus*	15.69		
282	3.48	0.67	4.84	-0.62	*C. mundulus*	17.03		
287	3.48	0.90	4.76	-0.69	*C. mundulus*	16.01		
292	3.32	1.00	4.61	-0.70	*C. mundulus*	14.56	0	19
297	3.34	0.44	4.81	-0.83	*C. mundulus*	16.36		
302	3.10	0.61	4.15	0.05	*C. mundulus*	12.86		
307	3.06	0.62	4.52	-0.41	*C. mundulus*	11.86		
312	2.87	1.08	4.51	-0.42	*C. mundulus*	10.48	4	20
317	3.08	0.96	4.15	0.05	*C. mundulus*	9.20		
322	3.03	0.85	4.31	-0.38	*C. mundulus*	10.06		
327	3.05	0.65	4.29	-0.15	*C. mundulus*	10.05		
332	3.20	0.53	3.97	0.26	*C. mundulus*	10.78		
337	2.67	0.82	4.23	-0.04	*C. mundulus*	8.61	0	2
342	3.13	0.64	4.35	0.06	*C. mundulus*	8.48		
347	2.58	0.45	4.12	-0.16	*C. mundulus*	9.04		
352	3.03	0.68	4.34	-0.05	*C. mundulus*	12.06		
357	3.06	0.39	5.19	-0.47	*C. mundulus*	11.61		
362	3.28	0.48	5.17	-0.52	*C. mundulus*	14.59	1	11
372	3.83	0.75	5.18	-0.59	*C. mundulus*	13.36		
377	3.95	0.46	5.12	-0.77	*C. mundulus*	11.59		
382	3.79	0.59	5.10	-0.64	*C. mundulus*	10.23		
387	3.48	0.45	4.72	-0.67	*C. mundulus*	10.72		
392	3.55	0.57	4.94	-0.42	*C. mundulus*	12.62	4	44
397	3.41	0.77	4.78	-0.63	*C. mundulus*	9.24		
402	3.56	0.87	4.80	-0.65	*C. mundulus*	8.91		
407	3.32	0.49	4.71	-0.42	*C. mundulus*	9.35		
412	3.01	0.60	4.65	-0.52	*C. mundulus*	9.07	3	73
417	3.06	1.04	4.21	0.21	*C. mundulus*	8.67		
422	3.00	1.11	4.69	-0.38	*C. mundulus*	7.67		
427	3.03	1.34	4.32	0.36	*C. mundulus*	7.05		
432	2.75	0.95	4.01	0.41	*C. mundulus*	7.02		
437	2.64	1.24	4.10	0.11	*C. mundulus*	7.67	0	4
442	2.77	0.53	4.04	0.33	*C. mundulus*	7.74		
447	2.65	1.06	4.50	0.00	*C. mundulus*	7.68		
452	2.85	1.20	4.10	0.49	*C. mundulus*	7.50		
457	2.62	0.92	4.38	0.56	*C. mundulus*	6.28		
462	2.95	0.94	4.62	-0.01	*C. mundulus*	7.53	3	2
467	2.86	1.04	4.54	0.43	*C. mundulus*	7.27		
472	2.98	1.10	4.60	0.54	*C. mundulus*	7.02		
477	2.87	1.30	4.37	0.57	*C. mundulus*	7.16		
482	2.92	1.01	4.30	0.33	*C. mundulus*	9.89		
487	2.72	0.33	4.29	0.40	*C. mundulus*	11.20		
492	2.78	0.79	4.25	0.34	*C. mundulus*	12.95	0	4
497	2.67	0.67	4.39	0.16	*C. mundulus*	17.36		
502	2.84	0.58	4.42	0.03	*C. mundulus*	17.02		
507	2.74	0.40	4.66	-0.23	*C. mundulus*	18.29		
512	2.84	0.46	4.84	-0.41	*C. mundulus*	14.35		
522	3.00	0.42	4.84	-0.42	*C. mundulus*	9.84	2	19
527	2.92	0.47	4.70	-0.32	*C. mundulus*	10.14		
532	2.80	0.56	4.76	0.04	*C. mundulus*	10.34		
537	3.09	0.59	4.83	-0.61	*C. mundulus*	11.51	1	21
542	2.83	0.38	4.35	-0.19	*C. mundulus*	11.72		
547	3.42	0.23	4.81	-0.56	*C. mundulus*	16.76		
552	3.25	-0.01	5.08	-0.42	*C. mundulus*	17.59		
557	3.57	0.12	4.68	-0.52	*C. mundulus*	16.71		

Avg. Depth	*G. bullloides* $\delta^{18}O$	*G. bulloides* $\delta^{13}C$	*Cibicidoides* $\delta^{18}O$ (corrected)	*Cibicidoides* $\delta^{13}C$	*Cibicidoides* species	Wt% >63µm	Mn Count	IRD Count
562	3.20	-0.23	4.80	-0.55	*C. mundulus*	15.99	5	19
567	2.88	0.14	4.97	-0.81	*C. mundulus*	16.19		
572	3.14	0.49	4.98	-0.65	*C. mundulus*	17.42		
577	3.03	-0.35	4.79	-0.73	*C. mundulus*	13.15		
582	3.12	-0.03	4.82	-0.72	*C. mundulus*	15.71		
587	3.24	-0.59	4.87	-0.67	*C. mundulus*	15.79		
592	3.26	-0.25	4.76	-0.94	*C. mundulus*	13.86	0	21
597	3.09	0.20	4.75	-0.58	*C. mundulus*	12.64		
602	3.22	0.66	4.45	-0.50	*C. mundulus*	6.62		
607	3.29	-0.04	4.49	-0.30	*C. mundulus*	5.41		
612	3.08	0.26	4.07	0.13	*C. mundulus*	7.57	0	20
617	2.86	-0.02	4.60	-0.36	*C. mundulus*	10.28		
622	3.50	0.06	4.56	-0.24	*C. mundulus*	7.61		
627	2.93	-0.02	4.69	-0.50	*C. mundulus*	4.56		
632	3.27	0.18	4.81	-0.66	*C. mundulus*	5.20		
637	3.01	-0.13	4.79	-0.72	*C. mundulus*	5.57	0	12
642	3.35	0.45	4.47	-0.32	*C. mundulus*	6.87		
647	3.19	0.19	4.55	-0.43	*C. mundulus*	3.58		
652	3.55	0.07	4.62	-0.76	*C. mundulus*	6.19		
657	3.07	0.09	4.53	-0.61	*C. mundulus*	3.19		
662	2.98	-0.33	4.59	-0.85	*C. mundulus*	3.68	1	27
667	3.00	0.03	4.48	-0.65	*C. mundulus*	4.22		
672	2.78	-0.19	4.32	-0.70	*C. mundulus*	4.23		
677	2.64	-0.24	4.35	-0.35	*C. mundulus*	4.07		
682	3.15	0.19	4.19	-0.19	*C. mundulus*	5.04		
687	2.84	-0.07	4.31	-0.39	*C. mundulus*	5.42		
692	3.22	0.09	4.96	-0.91	*C. mundulus*	7.41	6	22
697	3.49	0.49	4.81	-0.80	*C. mundulus*	6.70		
702	3.23	-0.40	4.81	-0.97	*C. mundulus*	7.79		
707	3.35	0.14	4.78	-0.78	*C. mundulus*	6.68		
712	3.09	-0.13	4.69	-0.88	*C. mundulus*	7.79		
717	3.04	-0.73	4.61	-0.57	*C. mundulus*	3.88		
722	3.32	-0.17	4.61	-0.52	*C. mundulus*	4.20		
727	3.09	-0.18	4.46	-0.45	*C. mundulus*	3.16		
732	3.46	0.54	4.74	-0.64	*C. mundulus*	5.40		
737	3.28	0.41	4.92	-1.14	*C. mundulus*	4.15	1	44
742	3.47	0.21	4.94	-0.78	*C. mundulus*	5.32		
747	3.56	0.47	4.78	-1.01	*C. mundulus*	4.17		
752	3.21	0.64	4.75	-0.70	*C. mundulus*	5.21		
757	3.02	0.57	4.62	-0.57	*C. mundulus*	3.63		
762	2.94	0.42	4.39	-0.62	*C. mundulus*	3.71	3	315
767	2.79	0.12	4.66	-0.76	*C. mundulus*	2.97		
772	2.76	0.24	4.48	-0.30	*C. mundulus*	2.86		
777	3.08	0.27	4.50	-0.54	*C. mundulus*	1.88		
782	2.82	0.52	4.62	-0.42	*C. mundulus*	2.09		
787	2.72	0.20	4.33	-0.18	*C. mundulus*	2.22		
792	2.90	0.78	4.37	-0.20	*C. mundulus*	2.28	2	123
797	2.61	0.40	4.35	-0.65	*C. mundulus*	2.97		
802	2.79	0.49	4.45	-0.45	*C. mundulus*	7.45		
807	2.85	0.57	4.45	-0.26	*C. mundulus*	4.38		
812	2.65	0.46	4.07	-0.12	*C. mundulus*	4.93		
817	2.98	0.59	4.50	-0.37	*C. mundulus*	3.54		
822	2.81	0.33	4.53	-0.77	*C. mundulus*	4.63		
827	2.72	0.33	4.64	-0.45	*C. mundulus*	3.31		
832	2.94	0.36	4.30	-0.14	*C. mundulus*	2.35		

Avg. Depth	*G. bullloides* $\delta^{18}O$	*G. bulloides* $\delta^{13}C$	*Cibicidoides* $\delta^{18}O$ (corrected)	*Cibicidoides* $\delta^{13}C$	*Cibicidoides* species	Wt% >63µm	Mn Count	IRD Count
837	2.70	0.45	4.57	-0.29	*C. mundulus*	3.24	6	161
842	3.19	0.66	4.35	-0.40	*C. mundulus*	2.01		
847	3.04	0.41	4.50	-0.35	*C. mundulus*	2.68		
852	2.88	0.38	4.60	-0.62	*C. mundulus*	2.03		
857	3.12	0.50	4.25	-0.12	*C. mundulus*	2.30		
862	3.45	0.49	4.39	-0.19	*C. mundulus*	2.17	14	119
867	3.55	0.35	4.74	-0.95	*C. mundulus*	1.48		
872						1.32		
877	3.00	0.18	4.20	0.00	*C. mundulus*	1.84		
882	2.67	0.29	4.31	0.28	*C. mundulus*	1.55		
887	3.21	0.41	4.14	-0.05	*C. mundulus*	1.58		
892	3.40	0.22	4.11	0.12	*C. mundulus*	1.68	68	59
897	3.07	0.52	4.22	-0.53	*C. mundulus*	1.56		
902	2.63	0.40	4.08	0.16	*C. mundulus*	2.44		
907	2.80	0.36	4.35	-0.18	*C. mundulus*	1.55		
912	2.72	0.58	4.04	0.27	*C. mundulus*	1.96		
917	3.42	0.35	4.14	0.33	*C. mundulus*	0.88		
922	2.89	0.39	4.20	-0.01	*C. mundulus*	1.04		
927	3.08	0.46	3.95	0.34	*C. mundulus*	0.93		
932	3.19	0.35	4.06	0.18	*C. mundulus*	0.85		
937	2.89	0.19	3.97	-0.06	*C. mundulus*	1.37	212	8
942			3.93	0.01	*C. mundulus*	0.94		
947	3.44	0.50	4.06	-0.20	*C. mundulus*	1.17		
952	3.22	0.67	3.96	0.08	*C. mundulus*	1.33		
957			4.04	-0.10	*C. mundulus*	0.68		
962	3.13	0.15	3.71	0.12	*C. wuellerstorfi*	1.28	121	3
967	2.99	0.21	3.71	0.18	*C. wuellerstorfi*	1.23		
973			3.54	0.29	*C. wuellerstorfi*	1.49		
977	2.39	0.74	3.82	0.16	*C. wuellerstorfi*	1.68		
982	3.31	0.42	3.52	0.58	*C. wuellerstorfi*	1.32		
987			3.65	0.20	*C. wuellerstorfi*	1.21		
992			3.59	0.42	*C. wuellerstorfi*	0.94	67	1
997			3.61	0.15	*C. wuellerstorfi*	1.18		
1002	3.14	0.43	3.58	0.54	*C. wuellerstorfi*	1.86		
1007	2.79	0.58	3.60	0.41	*C. wuellerstorfi*	2.00		
1012	2.68	0.46	3.69	-0.02	*C. wuellerstorfi*	1.99		
1017	2.60	0.67	3.52	0.21	*C. wuellerstorfi*	1.23		
1022	3.36	0.56	3.99	-0.05	*C. wuellerstorfi*	1.22		
1027	3.26	0.41	3.95	0.11	*C. wuellerstorfi*	1.61		
1032	2.49	0.55	3.92	-0.21	*C. wuellerstorfi*	1.45	107	0
1037	2.51	0.68	3.92	-0.19	*C. wuellerstorfi*	1.37		
1042			4.00	0.02	*C. wuellerstorfi*	1.12		
1047	2.39	0.26	3.95	-0.08	*C. wuellerstorfi*	1.02		
1052	3.28	0.32	3.74	0.10	*C. wuellerstorfi*	1.08		
1057	3.32	0.46	3.57	0.04	*C. wuellerstorfi*	0.77		
1062			3.75	0.22	*C. wuellerstorfi*	0.88	45	2
1067			3.83	0.32	*C. wuellerstorfi*	0.93		
1072	3.62	0.26	3.80	-0.01	*C. wuellerstorfi*	0.89		
1077			3.80	0.19	*C. wuellerstorfi*	0.66		
1082			3.74	0.44	*C. wuellerstorfi*	0.70		
1087			3.66	0.33	*C. wuellerstorfi*	0.65		
1092			3.63	0.57	*C. wuellerstorfi*	0.85	33	1
1097			3.63	0.46	*C. wuellerstorfi*	0.58		
1102			3.87	0.38	*C. wuellerstorfi*	1.05		
1107			3.76	0.44	*C. wuellerstorfi*	0.76		

Avg. Depth	*G. bullloides* $\delta^{18}O$	*G. bulloides* $\delta^{13}C$	*Cibicidoides* $\delta^{18}O$ (corrected)	*Cibicidoides* $\delta^{13}C$	*Cibicidoides* species	Wt% >63µm	Mn Count	IRD Count
1117			3.88	0.34	*C. wuellerstorfi*	0.78		
1122			4.02	0.20	*C. wuellerstorfi*	0.90		
1127			4.05	0.14	*C. wuellerstorfi*	1.15		
1132			3.83	0.10	*C. wuellerstorfi*	1.11		
1137	3.00	0.14	3.87	0.07	*C. wuellerstorfi*	1.16	75	4
1142	3.30	0.52	3.76	-0.08	*C. wuellerstorfi*	0.97		
1147	3.28	0.61	3.76	0.19	*C. wuellerstorfi*	0.65		
1152	3.19	0.33	3.94	0.28	*C. wuellerstorfi*	0.79		
1157			3.79	0.19	*C. wuellerstorfi*	0.68		
1162			3.85	0.15	*C. wuellerstorfi*	0.73	88	1
1167	3.53	0.29	3.80	0.25	*C. wuellerstorfi*	1.16		
1172						0.70		
1177			3.76	-0.11	*C. wuellerstorfi*	0.54		
1182			3.82	0.21	*C. wuellerstorfi*	0.35		
1187			3.84	0.02	*C. wuellerstorfi*	0.66		
1192			3.68	0.25	*C. wuellerstorfi*	0.50	29	1
1197			3.63	0.35	*C. wuellerstorfi*	0.39		
1202			3.73	0.30	*C. wuellerstorfi*	0.56		
1207	3.10	0.92	3.74	0.45	*C. wuellerstorfi*	0.40		
1212	3.30	0.42	3.32	0.33	*C. wuellerstorfi*	0.66		
1217			3.59	0.33	*C. wuellerstorfi*	0.56		
1222			3.54	0.47	*C. wuellerstorfi*	1.08		
1227			3.58	0.37	*C. wuellerstorfi*	0.49		
1232			3.70	0.28	*C. wuellerstorfi*	0.78		
1237	3.39	0.45	3.47	0.32	*C. wuellerstorfi*	0.89	108	3
1242	3.56	0.50	3.72	0.28	*C. wuellerstorfi*	6.90		
1247	3.46	0.38	3.67	0.31	*C. wuellerstorfi*	8.26		
1252			3.43	0.08	*C. wuellerstorfi*	0.74		
1257	3.21	0.24	3.85	0.49	*C. wuellerstorfi*	0.71		
1262			3.56	0.21	*C. wuellerstorfi*	0.96	21	1
1267			3.54	0.26	*C. wuellerstorfi*	1.33		
1274			3.57	0.08	*C. wuellerstorfi*	1.33		
1277	3.10	0.69	3.56	0.38	*C. wuellerstorfi*	0.97		
1282			3.56	0.02	*C. wuellerstorfi*	1.66		
1287			3.69	0.38	*C. wuellerstorfi*	1.16		
1292			3.59	0.43	*C. wuellerstorfi*	1.67	16	2
1297			3.54	0.47	*C. wuellerstorfi*	1.59		
1302			3.33	0.30	*C. wuellerstorfi*	1.95		
1307			3.60	0.43	*C. wuellerstorfi*	1.83		
1312			3.46	0.48	*C. wuellerstorfi*	1.33		
1317			3.71	0.44	*C. wuellerstorfi*	1.48		
1322			3.50	0.56	*C. wuellerstorfi*	2.28		
1327			3.64	0.30	*C. wuellerstorfi*	2.24		
1332			3.59	0.35	*C. wuellerstorfi*	2.41		
1337			3.35	0.24	*C. wuellerstorfi*	2.40	62	0
1342			3.64	0.06	*C. wuellerstorfi*	2.14		
1347			3.61	0.06	*C. wuellerstorfi*	1.95		
1352			3.64	0.48	*C. wuellerstorfi*	1.35		
1357						1.40		
1362			3.71	0.36	*C. wuellerstorfi*	1.66	221	0
1367			3.54	0.29	*C. wuellerstorfi*	1.12		
1372			3.63	0.19	*C. wuellerstorfi*	1.06		
1377			3.61	0.33	*C. wuellerstorfi*	1.38		
1382			3.70	0.39	*C. wuellerstorfi*	0.96		
1387			3.63	0.15	*C. wuellerstorfi*	1.17		

Avg. Depth	*G. bullloides* $\delta^{18}O$	*G. bulloides* $\delta^{13}C$	*Cibicidoides* $\delta^{18}O$ (corrected)	*Cibicidoides* $\delta^{13}C$	*Cibicidoides* species	Wt% >63µm	Mn Count	IRD Count
1392			3.43	0.34	*C. wuellerstorfi*	0.80	74	1
1397			3.63	0.28	*C. wuellerstorfi*	1.32		
1402			3.78	0.26	*C. wuellerstorfi*	1.04		
1407						1.14		
1412			3.58	0.34	*C. wuellerstorfi*	0.78		
1417			3.46	0.51	*C. wuellerstorfi*	1.17		
1422			3.62	0.24	*C. wuellerstorfi*	1.05		
1427			3.49	0.27	*C. wuellerstorfi*	1.55		
1432			3.50	0.46	*C. wuellerstorfi*	1.34		
1437			3.55	0.35	*C. wuellerstorfi*	1.43	60	1
1442			3.52	0.47	*C. wuellerstorfi*	1.42		
1447			3.60	0.56	*C. wuellerstorfi*	1.14		
1452			3.36	0.39	*C. wuellerstorfi*	1.21		
1457			3.57	0.09	*C. wuellerstorfi*	0.89		
1462			3.64	0.42	*C. wuellerstorfi*	1.01	144	1
1467			3.67	0.16	*C. wuellerstorfi*	1.00		
1472			3.73	0.47	*C. robertsonianus*	1.06		
1477			3.69	0.37	*C. robertsonianus*	1.12		
1482			3.65	0.00	*C. robertsonianus*	1.48		
1487			3.67	0.10	*C. robertsonianus*	1.21		
1492			3.51	0.15	*C. robertsonianus*	2.75	130	0
1497			3.47	0.16	*C. robertsonianus*	0.78		
1502			3.58	0.21	*C. wuellerstorfi*	1.14		
1507			3.53	0.45	*C. wuellerstorfi*	0.85		
1512			3.51	-0.14	*C. robertsonianus*	0.87		
1517			3.56	0.38	*C. wuellerstorfi*	1.16		
1522			3.49	0.20	*C. wuellerstorfi*	1.14		
1527			3.60	0.28	*C. robertsonianus*	1.87		
1532			3.34	0.05	*C. robertsonianus*	1.65		
1537			3.59	0.73	*C. robertsonianus*	1.42	527	0
1542			3.56	0.95	*C. robertsonianus*	0.93		
1547			3.60	0.88	*C. robertsonianus*	0.88		
1552			3.64	1.07	*C. robertsonianus*	0.85		
1557			3.65	1.11	*C. robertsonianus*	0.76		
1562			3.62	0.96	*C. robertsonianus*	0.37	26	0
1567			3.65	1.27	*C. robertsonianus*	0.24		
1572			3.52	0.44	*C. robertsonianus*	0.41		
1577			3.67	1.05	*C. robertsonianus*	0.39		
1582			3.75	1.07	*C. robertsonianus*	0.48		
1587			3.61	1.22	*C. robertsonianus*	0.52		
1592			3.56	1.14	*C. robertsonianus*	0.39	50	0
1597			3.47	0.90	*C. robertsonianus*	0.53		
1602			3.56	1.45	*C. robertsonianus*	0.62		
1607			3.78	1.14	*C. robertsonianus*	0.58		
1612			3.63	1.24	*C. robertsonianus*	0.61		
1617			3.64	1.26	*C. robertsonianus*	0.47		
1622			3.55	1.20	*C. robertsonianus*	0.77		
1627			3.79	1.34	*C. robertsonianus*	0.66		
1632			3.53	1.20	*C. robertsonianus*	0.59		
1637			3.59	1.34	*C. robertsonianus*	0.82	56	0
1642			3.79	1.10	*C. robertsonianus*	0.88		
1647			3.60	0.85	*C. robertsonianus*	0.99		
1652			3.66	1.23	*C. robertsonianus*	0.82		
1657			3.72	1.15	*C. robertsonianus*	1.21		
1662			3.75	1.26	*C. robertsonianus*	1.04	83	0

Avg. Depth	*G. bullloides* $\delta^{18}O$ (VPDB)	*G. bulloides* $\delta^{13}C$ (VPDB)	*Cibicidoides* $\delta^{18}O$ (corrected) (VPDB)	*Cibicidoides* $\delta^{13}C$ (VPDB)	*Cibicidoides* species	Wt% >63µm	Mn Count	IRD Count
1667			3.75	1.27	*C. robertsonianus*	1.28		
1672	2.65	1.14	3.57	1.20	*C. robertsonianus*	1.03		
1677			3.46	1.22	*C. robertsonianus*	1.14		
1682	2.84	1.11				1.13		
1687			3.74	1.05	*C. robertsonianus*	1.62		
1692			3.68	1.22	*C. robertsonianus*	0.84	690	0
1697			3.68	1.18	*C. robertsonianus*	0.95		
1702	3.36	0.63	3.63	1.18	*C. robertsonianus*	1.08		
1707	3.25	0.69	3.54	1.12	*C. robertsonianus*	1.00		
1712	1.89	2.19	3.56	1.19	*C. robertsonianus*	0.92		
1717	1.63	2.11	3.67	1.23	*C. robertsonianus*	1.15		

Appendix B: Radiolarian biostratigraphy for MV0502-4JC

Sample Depth (cmbsf)			166-168	256-258	391-393	511-513	806-808	951-953	976-978	1021-1023	1071-1073	1141-1143	1526-1528	1701-1703
Species	top age	bott age												
Antarctissa cylindrica	0.61			?		+	-	-						
Antarctissa deflandrei		12.7							+	+	+	-	+	+
Antarctissa denticulata		2.38	+	+	+	+	+	-	-		-	-		
Antarctissa strelkovi			+	+	+	+	?	+	+	+	+	+	+	-
Carpocanopsis cristata	10.1	16.22					-	R	R	+	+	+	+	+
Cycladophora davisiana		2.5	+	+	+	+	+	-	+	-	-	-		
Cycladophora humerus	9.9	14.2									?	-	?	+
Cycladophora pliocenica	1.73				-	-	+	+	+	+	+	+	+	+
Cyrtocapsella tetrapera	11.89						R			-	-	+	+	+
Cyrtocapsella japonica	10.09						-			-	+	+	+	+
Cyrtocapsella longithorax	14.1								-	-	-	-	+	+
Dendrospyris megalocephalis		12.45						+	+	+	+	+	+	
Didymocyrtis laticonus	7.4	16.06							-	-	+	-	+	+
Didymocyrtis prismatica	15.96										?		?	?
Eucyrtidium pseudoinflatum		10								+			?	?
Eucytrtidium calvertense	1.85	12.4	+	+	+	+	+	+	+	+	+	+	+	+
Lamprocyrtis heteroporus	1.79	3.29		?	-	++	-	+	+	+	-	-		-
Lamprocyrtis neoheroporous	1.07	3.25			-	+	-	-	-	-		-		-
Lamprocyrtis nigrinii		1.08	+	+										
Lychnocanium grande	4.6						R	-	-	-	+	-	+	+
Pterocanium trilobum	0.8		+	-	+	+	-	-	-	-	-	-		
Stauroxiphos communis	11.94	18.4										-	+	+
Stichocorys delmontensis	2.8	21.1					?r	R	R	+	+	+	+	+
Stichocorys peregrina	2.7	8.4							?					
Stylatractus universus	0.425		-	+	+	++	+	+	+	+	+	+	+	-
Theocorythium trachelium		1.63	+	+	-	+	-	-	-	-	-	-		
Theocorythium vetulum	1.21	5.16		-	-	+	-	-	-	-	-	-		
Triceraspyris antarctica		1.85	+	+	+	+	-	-	-	-	-	-		
Sample Age (Ma)			<0.425	0.425-1.08	1.08-1.63	1.63-1.79	1.85-2.38	2.38-2.5	2.38-2.5	2.5-3.29	10.1-11.89	11.89-11.94	11.94-12.7	11.94-12.7

R = Rare, + = Common, ++ = Abundant, - = Looked for but not found

Appendix C: Weight Percent $CaCO_3$ from MV0502-4JC

Depth	% $CaCO_3$	Depth	% $CaCO_3$	Depth	% $CaCO_3$	Depth	% $CaCO_3$	Depth	% $CaCO_3$
0	68.86	340	84.29	700	66.33	1050	50.55	1400	19.03
10	77.65	350	86.65	710	59.19	1060	44.63	1410	20.83
20	67.17	360	80.38	720	60.18	1070	42.68	1420	24.67
30	67.39	370	70.50	730	67.94	1080	43.02	1430	23.39
40	70.42	380	70.99	740	59.25	1090	55.75	1440	25.03
50	74.18	390	66.73	750	55.28	1100	62.99	1450	12.78
60	75.42	400	58.29	760	48.17	1110	67.60	1460	14.52
70	67.97	410	50.09	770	38.06	1120	52.08	1470	16.98
80	68.40	420	75.72	780	56.00	1130	37.79	1480	18.05
90	75.45	430	78.97	790	66.36	1140	39.18	1490	18.65
100	78.48	440	76.15	800	69.64	1150	33.56	1500	29.03
110	75.62	450	83.92	810	53.37	1160	34.56	1510	27.56
120	77.66	460	86.17	820	39.73	1170	38.47	1520	24.46
130	78.96	470	87.10	830	25.11	1180	38.25	1530	24.40
140	75.77	480	89.46	840	34.40	1190	36.36	1540	56.10
150	80.68	490	88.90	850	28.86	1200	30.81	1550	65.59
160	85.71	500	87.10	860	28.48	1210	29.22	1560	64.23
170	81.65	520	67.43	870	35.67	1220	24.03	1570	74.38
180	82.45	530	62.96	880	44.96	1230	20.28	1580	78.70
190	79.73	540	50.98	890	47.28	1240	30.63	1590	76.37
200	75.98	550	67.71	900	53.18	1250	38.88	1600	74.63
210	71.64	570	71.69	920	71.27	1260	41.96	1610	75.11
220	59.02	580	65.85	930	63.42	1270	48.54	1620	70.38
230	49.38	590	58.47	940	57.10	1280	47.93	1630	77.31
240	76.40	600	57.13	950	58.07	1290	53.72	1640	70.69
250	68.86	610	68.83	960	66.46	1310	51.48	1650	72.36
260	53.77	620	78.30	970	62.25	1320	62.71	1660	73.23
270	42.30	630	62.73	980	58.22	1330	53.48	1670	74.60
280	69.38	640	69.70	990	55.62	1340	38.84	1680	76.56
290	67.30	650	69.31	1000	62.20	1350	28.87	1690	78.33
300	63.94	660	46.53	1010	63.78	1360	25.98	1700	78.56
310	71.58	670	66.99	1020	65.98	1370	19.75	1710	78.68
320	79.10	680	68.27	1030	66.16	1380	17.70	1717	78.90
330	81.12	690	79.72	1040	49.14	1390	20.28		

Appendix D: Stable Isotope and Compositional Data from ELT 25-11

Avg. Depth	*G. bullloides* $\delta^{18}O$ (VPDB)	*G. bulloides* $\delta^{13}C$ (VPDB)	*Cibicidoides* $\delta^{18}O$ (corrected) (VPDB)	*Cibicidoides* $\delta^{13}C$ (VPDB)	*Cibicidoides* species	Wt% >63µm
8	3.19	0.47	4.53	-0.34	*C. mundulus*	30.68
16	3.13	0.89	4.66	-0.13	*C. mundulus*	26.29
25	2.89	1.00	4.31	0.31	*C. mundulus*	28.19
35	2.85	0.72	4.40	0.03	*C. mundulus*	23.69
46	3.52	0.65	5.06	-0.23	*C. mundulus*	32.59
55	3.68	0.21	5.05	-0.54	*C. mundulus*	32.73
65	3.38	0.61	4.81	-0.28	*C. mundulus*	29.52
73	3.59	0.25	4.64	-0.43	*C. mundulus*	25.74
85	3.38	0.21	4.55	-0.34	*C. mundulus*	24.42
95	3.05	0.36	4.87	-0.29	*C. mundulus*	23.50
104	3.52	0.35	4.49	-0.23	*C. mundulus*	20.91
114	3.42	0.71	4.72	-0.42	*C. mundulus*	20.20
125	2.98	0.78	4.58	-0.33	*C. mundulus*	14.66
134	2.92	0.93	4.23	0.12	*C. mundulus*	12.74
144	3.22	0.80	4.46	0.11	*C. mundulus*	7.92
154	3.16	0.61	4.27	0.08	*C. mundulus*	8.31
164	2.82	0.56	3.63	0.56	*C. mundulus*	6.54
174	2.86	1.04	4.77	-0.28	*C. mundulus*	6.74
184	2.77	0.97	3.81	0.28	*C. mundulus*	5.45
194	3.23	0.53	3.81	0.51	*C. mundulus*	7.13
203	3.01	0.94	4.02	0.42	*C. mundulus*	11.17
213	3.26	0.59	4.84	-0.06	*C. mundulus*	16.90
224	3.44	1.05	4.99	-0.61	*C. mundulus*	12.33
234	2.92	1.20	4.60	-0.22	*C. mundulus*	9.61
244	2.82	1.09	4.67	0.14	*C. mundulus*	9.71
254	3.23	1.46	4.14	0.52	*C. mundulus*	12.50
265	3.11	1.40	4.53	0.18	*C. mundulus*	15.42
274	2.87	0.18	4.91	-0.14	*C. mundulus*	26.60
285	3.21	0.40	4.69	-0.54	*C. mundulus*	23.22
294	3.28	-0.23	4.72	-0.53	*C. mundulus*	
304	3.15	0.62	4.83	-0.66	*C. mundulus*	23.17
314	2.97	-0.20	4.18	-0.07	*C. mundulus*	24.16
324	2.75	-0.46	4.99	-0.71	*C. mundulus*	23.34
335	2.84	-0.47	4.53	-0.50	*C. mundulus*	17.08
344	2.87	0.20	4.53	-0.18	*C. mundulus*	18.31
352	2.91	0.09	5.02	-0.63	*C. mundulus*	20.34
365	2.88	-0.64	5.07	-0.66	*C. mundulus*	22.47
375	3.17	-0.11	4.94	-0.85	*C. mundulus*	19.20
384	3.13	0.01	4.51	-0.48	*C. mundulus*	21.06
394	2.65	-0.31	4.52	-0.44	*C. mundulus*	21.46
403	3.55	-0.20	4.13	-0.27	*C. mundulus*	20.58
413	3.61	0.14	4.59	-0.59	*C. mundulus*	22.77
424	3.33	0.44	4.49	-0.52	*C. mundulus*	25.94
434	3.34	0.57	4.65	-0.57	*C. mundulus*	27.60
444	3.35	0.26	4.41	-0.05	*C. mundulus*	20.17
454	3.14	0.46	4.70	-0.50	*C. wuellerstorfi*	21.96
464	3.11	0.22	4.67	-0.13	*C. mundulus*	26.38
474	3.09	0.76	4.77	-0.53	*C. mundulus*	25.25
485	2.94	0.61	4.04	-0.24	*C. mundulus*	20.76
495	2.74	0.38	4.38	0.01	*C. mundulus*	19.79
504	2.85	0.37	4.56	-0.33	*C. mundulus*	15.75
514	3.01	0.74	4.05	-0.05	*C. mundulus*	14.31
524	2.81	0.55	4.40	-0.04	*C. mundulus*	13.73
535	2.82	0.67	4.41	-0.62	*C. mundulus*	12.28
545	3.02	0.28	4.33	-0.53	*C. mundulus*	12.49

Avg. Depth	*G. bullloides* $\delta^{18}O$ (VPDB)	*G. bulloides* $\delta^{13}C$ (VPDB)	*Cibicidoides* $\delta^{18}O$ (corrected) (VPDB)	*Cibicidoides* $\delta^{13}C$ (VPDB)	*Cibicidoides* species	Wt% >63µm
555	3.49	0.68	4.54	-0.01	*C. mundulus*	11.69
565	2.73	0.25	4.49	-0.75	*C. wuellerstorfi*	7.97
576	2.92	0.96	4.04	-0.01	*C. wuellerstorfi*	5.21
584	2.82	0.64	4.45	-0.23	*C. wuellerstorfi*	3.50
594	2.26	1.61	4.19	0.65	*C. wuellerstorfi*	2.72
604	2.57	0.96	4.01	0.51	*C. wuellerstorfi*	2.06
618	3.07	0.75	4.00	0.03	*C. wuellerstorfi*	2.34
628	3.07	0.75	3.59	1.09	*C. wuellerstorfi*	1.88
638	2.84	0.44	3.66	0.67	*C. wuellerstorfi*	1.00
647	3.52	0.45	3.99	0.83	*C. wuellerstorfi*	1.33

Appendix E: Radiolarian biostratigraphy for ELT 25-11

Sample Depth (cmbsf)			153-154	264-266	334-336
Species	top age	bottom age			
Antarctissa cylindrica	0.61			+	+
Antarctissa deflandrei		12.7	+	+	+
Antarctissa denticulata		2.38	+	+	+
Carpocanopsis cristata	10.1	16.22	+	+	+
Cycladophora davisiana		2.5	+	+	+
Cycladophora pliocenica	1.73			+	+
Cyrtocapsella tetrapera	11.89		rwk	rwk	rwk
Cyrtocapsella japonica	10.09			rwk	rwk
Eucytrtidium calvertense	1.85	12.4		+	+
Lamprocyrtis heteroporus	1.79	3.29		?	
Pterocanium trilobum	0.8			+	?
Stauroxiphos communis	11.94	18.4		rwk	
Stichocorys delmontensis	2.8	21.1	rwk	rwk	rwk
Stylatractus universus	0.425		?	+	+
Theocorythium trachelium		1.63	+		
Triceraspyris antarctica		1.85	+	+	+
Sample Age (Ma)			<0.4	1.73-1.85	1.73-1.85

+ = Present, rwk = Reworked

Appendix F: Weight Percent $CaCO_3$ from ELT 25-11 and ELT 20-2

ELT 25-11

Depth	% $CaCO_3$	Depth	% $CaCO_3$	Depth	% $CaCO_3$	Depth	% $CaCO_3$
13.5	88.0	173.5	83.9	333.5	80.5	493.5	71.6
23.5	87.9	183.5	93.3	343.5	82.9	503.5	70.3
33.5	87.1	193.5	31.0	353.5	88.3	513.5	67.8
43.5	87.4	203.5	92.9	363.5	84.8	523.5	64.8
53.5	84.4	213.5	91.2	373.5	75.2	533.5	67.2
63.5	80.0	223.5	78.1	383.5	77.5	543.5	64.3
73.5	75.4	233.5	90.8	393.5	86.6	553.5	71.5
83.5	81.3	243.5	90.9	403.5	81.2	563.5	76.7
93.5	78.9	253.5	89.8	413.5	87.2	573.5	80.1
103.5	80.3	263.5	89.8	423.5	82.4	583.5	89.7
113.5	83.4	273.5	85.8	433.5	82.6	593.5	93.2
123.5	88.0	283.5	79.1	443.5	75.6	603.5	94.5
133.5	89.7	293.5	81.9	453.5	80.8	613.5	92.6
143.5	93.3	303.5	79.9	463.5	79.9	623.5	91.3
153.5	92.7	313.5	85.6	473.5	80.9	633.5	92.2
163.5	87.4	323.5	79.8	483.5	68.4	643.5	91.9

ELT 20-2

Depth	% $CaCO_3$	Depth	% $CaCO_3$	Depth	% $CaCO_3$	Depth	% $CaCO_3$
5.5	64.6	225.5	31.4	445.5	3.9	665.5	0.5
15.5	68.6	235.5	4.2	455.5	4.0	675.5	0.5
25.5	74.4	245.5	3.1	465.5	2.5	685.5	0.4
35.5	60.9	255.5	1.5	475.5	2.4	695.5	0.4
45.5	65.7	265.5	1.3	485.5	1.6	705.5	0.3
55.5	64.4	275.5	1.7	495.5	1.6	715.5	0.3
65.5	66.9	285.5	1.9	505.5	2.0	725.5	1.8
75.5	76.0	295.5	3.8	515.5	2.2	735.5	3.8
85.5	62.1	305.5	1.6	525.5	1.4	745.5	2.3
95.5	28.4	315.5	2.3	535.5	0.0	755.5	1.7
105.5	55.6	325.5	1.7	545.5	0.9	765.5	0.9
115.5	44.5	335.5	3.8	555.5	0.3	775.5	0.9
125.5	56.2	345.5	2.0	565.5	0.3	785.5	0.6
135.5	52.0	355.5	2.7	575.5	0.4	795.5	0.5
145.5	58.0	365.5	0.8	585.5	0.6	805.5	0.4
155.5	63.8	375.5	0.8	595.5	0.4	815.5	0.4
165.5	82.3	385.5	1.2	605.5	0.5	825.5	0.3
175.5	50.4	395.5	3.4	615.5	0.3	835.5	0.3
185.5	24.0	405.5	3.4	625.5	0.3	845.5	1.0
195.5	38.8	415.5	3.3	635.5	0.2	855.5	1.4
205.5	27.5	425.5	2.4	645.5	0.3	865.5	0.8
215.5	39.6	435.5	4.7	655.5	0.3		

Appendix G: Stable Isotope Data from ELT 20-2

Avg. Depth	*G. bullloides* $\delta^{18}O$ (VPDB)	*G. bulloides* $\delta^{13}C$ (VPDB)	*Cibicidoides* $\delta^{18}O$ (corrected) (VPDB)	*Cibicidoides* $\delta^{13}C$ (VPDB)	*Cibicidoides* species
1	3.46	0.94	4.95	-0.18	*C. mundulus*
13	3.90	1.24	4.97	-0.04	*C. mundulus*
21	3.51	0.93	4.77	-0.01	*C. mundulus*
33	3.27	0.76	4.64	-0.15	*C. mundulus*
43	2.95	0.69	4.63	-0.29	*C. mundulus*
51	2.76	1.05	4.36	0.30	*C. mundulus*
63	3.47	0.61	5.04	-0.23	*C. mundulus*
71			5.00	-0.57	*C. mundulus*
83	4.16	0.01	4.69	-0.54	*C. mundulus*
91	3.10	0.21	4.69	-0.44	*C. mundulus*
103	3.91	0.44	4.85	-0.52	*C. mundulus*
111	3.44	0.46	4.75	-0.54	*C. mundulus*
123	3.66	0.80	4.64	-0.73	*C. mundulus*
131	2.94	0.31	4.30	-0.47	*C. mundulus*
143	3.27	1.09	4.11	-0.16	*C. mundulus*
151	3.72	0.65	4.63	-0.23	*C. mundulus*
163	2.65	0.78	4.23	0.40	*C. mundulus*
171	3.09	0.67	4.59	0.34	*C. mundulus*
183	3.03	0.92	4.87	-0.54	*C. mundulus*
191	2.67	0.82	4.45	-0.57	*C. mundulus*
203	3.37	0.33	4.90	-0.61	*C. mundulus*
211	2.99	0.23	4.68	-0.48	*C. mundulus*
223	3.35	0.46	4.63	-0.69	*C. mundulus*

Appendix H: Radiolarian biostratigraphy for ELT 20-2

Sample Depth (cmbsf)			12-14	50-52	102-104	150-152	202-204
Species	top age	bottom age					
Acrosphera labrata		7	+	+	+	+	
Antarctissa deflandrei		12.7	+	+	+	+	+
Antarctissa denticulata		2.38	+	+	+	+	+
Antarctissa strelkovi			+	+	+	+	+
Cycladophora davisiana		2.5	+	+	+	+	+
Cycladophora pliocenica	1.73				-		-
Dendrospyris megalocephalis		12.45	+	+	+	+	+
Eucytrtidium calvertense	1.85	12.4			-		-
Lamprocyrtis heteroporus	1.79	3.29			r		-
Lamprocyrtis neoheroporous	1.07	3.25			-		-
Lamprocyrtis nigrinii		1.08			-		-
Lychnocanium grande	4.6				-		-
Pterocanium trilobum	0.8				-		+
Stylatractus universus	0.425				+	+	+
Theocorythium trachelium		1.63	+	+	+	+	+
Triceraspyris antarctica		1.85	+	+	+	+	+
Sample Age (Ma)			<0.425	<0.425	0.425-1.63	0.425-1.63	0.425-1.63

R = Rare, + = Common, - = Looked for but not found

Appendix I: Laboratory Procedure for the Preparation of Fish Debris for Oxygen and Carbon Stable Isotope Analysis

1. Freeze-dry sediment samples overnight. (Samples should be frozen for at least 24 hours prior to being placed in the freeze drier.)

2. Wash the sediment samples with distilled water over a 125 μm sieve. Collect the coarse fraction over filter paper and dry it overnight in drying oven.

3. Under a reflecting-light microscope, pick fish debris from each sample.

4. Weigh the fish debris by carefully transferring it to a pre-weighed micro-centrifuge tube with a paint brush and allowing it to dry in the oven. (Sample sizes >1 mg are preferred because some material will be lost during the pre-treatment process and samples <0.8 mg will not generate enough CO_2 for an analysis.)

5. If clay particles can be seen adhering to the surface of the bones, the fish debris can be cleaned in an ultrasonic bath for approximately 10 seconds, long enough to remove adhering clay without destroying the sample. An eyedropper can then be used to transfer the fish debris from the microcentrifuge tube to a watch glass so that the bones can be separated from the contaminants under a microscope.

6. If the sample size is large enough (>1.2 mg), gently grind the bones with a small mortar and pestle, return to a pre-weighed microcentrifuge tube using an eyedropper, and dry the samples in oven. (If the samples are <1.2 mg, the safest route is to individually break up large teeth and bones using a sharp-point.)

7. Chemically treat the samples using the method of Koch et al. (1997). It is recommended that you subject a control to chemical treatment alongside your samples in order to monitor for differences between treatment batches.

   a. Soak the bone powders in 2% NaOCl for 24 hours to remove organic contaminants.
   b. Place the tubes in the centrifuge and spin for 2-3 minutes.
   c. Remove and discard the supernatant with an eyedropper, rinse the sample with distilled water, and spin in the centrifuge again. Repeat 4 times for a total of five rinses.
   d. Soak the bone powders in 1 M acetic acid buffered with 1 M Ca-acetate for 24 hours in order to remove secondary carbonates and rinse five times as above.
   e. Allow the samples to dry in the oven.

8. Weigh the samples again to obtain a post-treatment weight.

9. Load the samples into boats using weighing paper.

10. Roast the samples under vacuum at 200°C for one hour prior to analysis.

Appendix J: Uncertainties in the Stable Isotope Measurements

All of the stable isotope analyses included in this dissertation were conducted in the University of Michigan Stable Isotope Laboratory, where analytical accuracy and precision were monitored through the regular analysis of the standard reference carbonate NBS-19. For the stable isotope results included in **Chapter 4**, analytical precision was found to be better than ±0.1‰ (1σ) for both $\delta^{18}O$ and $\delta^{13}C$ (**Table J.1**), and for the stable isotope results in **Chapters 2, 3, and 5** analytical precision was found to be ±0.03‰ for $\delta^{13}C$ and ±0.08‰ for $\delta^{18}O$ (1σ, N=153) (**Table J.2**).

Table J.1: NBS-19 Measurements Used to Assess Analytical Precision of Stable Isotope Results in Chapter 4

Sample	DATE	TIME	$\delta^{13}C$ (KIS)	±	$\delta^{18}O$ (KIS)	±	$\delta^{13}C$ (VPDB)	$\delta^{18}O$ (VPDB)	Max P
NBS 19	10/4/05	13:13:23	5.74	0.02	2.28	0.02	**1.89**	**-2.29**	389
NBS 19	10/4/05	21:14:19	5.76	0.01	2.33	0.02	**1.91**	**-2.24**	676
NBS 19	10/5/05	5:16:25	5.78	0.01	2.37	0.02	**1.93**	**-2.21**	698
NBS 19	10/5/05	14:10:42	5.77	0.01	2.27	0.02	**1.92**	**-2.30**	667
NBS 19	10/5/05	22:17:30	5.76	0.02	2.34	0.02	**1.91**	**-2.23**	749
NBS 19	10/6/05	6:20:08	5.78	0.04	2.41	0.03	**1.94**	**-2.16**	597
NBS 19	10/6/05	10:29:38	5.77	0.03	2.38	0.02	**1.92**	**-2.19**	597
NBS 19	10/6/05	18:45:54	5.80	0.02	2.38	0.02	**1.95**	**-2.19**	853
NBS 19	10/7/05	2:43:44	5.77	0.01	2.33	0.02	**1.92**	**-2.24**	721
NBS 19	10/7/05	2:43:44	5.77	0.01	2.33	0.02	**1.92**	**-2.24**	721
NBS 19	10/7/05	9:59:17	5.73	0.01	2.37	0.02	**1.89**	**-2.20**	650
NBS 19	10/7/05	18:09:20	5.74	0.02	2.42	0.02	**1.90**	**-2.15**	689
NBS 19	10/12/2006	14:18:13	5.92	0.01	2.51	0.02	**1.98**	**-2.14**	1097
NBS 19	10/12/2006	15:05:58	5.91	0.02	2.47	0.02	**1.98**	**-2.17**	1200
NBS 19	10/13/2006	23:10:42	5.90	0.02	2.48	0.02	**1.97**	**-2.16**	1009
NBS 19	10/13/2006	23:53:44	5.91	0.01	2.51	0.03	**1.98**	**-2.14**	990
NBS 19	10/14/2006	2:45:41	5.87	0.02	2.57	0.02	**1.94**	**-2.07**	885
NBS 19	10/14/2006	3:20:10	5.91	0.02	2.47	0.02	**1.98**	**-2.17**	938
						Mean	**1.94***	**-2.20***	
						Stdev	**0.03**	**0.06**	

***expected values +1.95/-2.20 ± (better than) 0.1‰**

Table J.2: NBS-19 Measurements Used to Assess Analytical Precision of Stable Isotope Results in Chapters 2, 3, and 5

Sample	DATE	TIME	$\delta^{13}C$ (KIS)	±	$\delta^{18}O$ (KIS)	±	$\delta^{13}C$ (VPDB)	$\delta^{18}O$ (VPDB)	Max P
NBS 19	12/23/2005	11:22:27	5.68	0.02	2.25	0.04	**1.87**	**-2.13**	787
NBS 19	12/23/2005	16:21:10	5.72	0.01	2.29	0.02	**1.91**	**-2.09**	838
NBS 19	12/23/2005	16:57:41	5.72	0.02	2.18	0.03	**1.91**	**-2.20**	1021
NBS 19	12/23/2005	01:12:27	5.68	0.02	2.13	0.03	**1.87**	**-2.25**	1041
NBS 19	12/23/2005	15:12:37	5.78	0.01	2.37	0.08	**1.97**	**-2.01**	1141
NBS 19	12/23/2005	10:45:55	5.69	0.04	2.08	0.05	**1.88**	**-2.30**	1173
NBS 19	12/23/2005	01:54:00	5.72	0.02	2.15	0.03	**1.91**	**-2.23**	1219
NBS 19	12/23/2005	14:34:11	5.81	0.02	2.34	0.03	**2.00**	**-2.04**	1251
NBS 19	1/18/2006	19:00:26	5.76	0.02	2.22	0.02	**1.95**	**-2.16**	1205
NBS 19	1/18/2006	19:45:59	5.75	0.02	2.18	0.02	**1.94**	**-2.20**	1214
NBS 19	1/19/2006	21:44:22	5.72	0.02	2.13	0.02	**1.91**	**-2.25**	1192
NBS 19	1/19/2006	22:38:50	5.75	0.01	2.20	0.03	**1.94**	**-2.18**	1175
NBS 19	1/21/2006	13:55:38	5.74	0.01	2.27	0.01	**1.93**	**-2.11**	1053
NBS 19	1/21/2006	14:40:54	5.73	0.02	2.14	0.03	**1.92**	**-2.24**	1205
NBS 19	3/3/2006	13:41:41	5.88	0.02	2.40	0.01	**1.98**	**-2.16**	1129
NBS 19	3/3/2006	14:20:29	5.81	0.01	2.16	0.02	**1.91**	**-2.40**	1163
NBS 19	3/4/2006	12:38:33	5.79	0.02	2.31	0.02	**1.89**	**-2.25**	748
NBS 19	3/4/2006	13:27:00	5.84	0.01	2.19	0.02	**1.94**	**-2.37**	1190
NBS 19	3/6/2006	12:16:37	5.88	0.02	2.28	0.03	**1.98**	**-2.28**	1158
NBS 19	3/6/2006	12:52:37	5.85	0.01	2.36	0.03	**1.95**	**-2.20**	963
NBS 19	3/7/2006	19:05:37	5.88	0.02	2.27	0.02	**1.98**	**-2.29**	1004
NBS 19	3/7/2006	19:45:11	5.89	0.01	2.31	0.02	**1.99**	**-2.25**	1016
NBS 19	3/13/2006	12:47:31	5.83	0.02	2.36	0.03	**1.93**	**-2.20**	973
NBS 19	3/13/2006	13:29:15	5.89	0.01	2.43	0.02	**1.98**	**-2.13**	1119
NBS 19	3/14/2006	01:54:49	5.84	0.02	2.24	0.04	**1.94**	**-2.32**	1153
NBS 19	3/14/2006	02:36:53	5.86	0.01	2.40	0.03	**1.96**	**-2.16**	1063
NBS 19	3/14/2006	17:46:08	5.86	0.01	2.26	0.02	**1.96**	**-2.30**	1078
NBS 19	3/14/2006	18:25:00	5.86	0.01	2.38	0.02	**1.96**	**-2.18**	1051
NBS 19	3/15/2006	09:33:02	5.88	0.01	2.34	0.01	**1.98**	**-2.22**	1190
NBS 19	3/15/2006	10:19:47	5.81	0.01	2.23	0.03	**1.91**	**-2.33**	1090
NBS 19	3/15/2006	14:46:49	5.84	0.03	2.24	0.02	**1.94**	**-2.32**	1031
NBS 19	3/15/2006	15:32:43	5.88	0.02	2.33	0.02	**1.98**	**-2.23**	1161
NBS 19	3/28/2006	15:55:21	5.78	0.01	2.30	0.03	**1.89**	**-2.22**	806
NBS 19	3/28/2006	16:34:08	5.80	0.01	2.24	0.03	**1.91**	**-2.28**	1036
NBS 19	3/29/2006	06:17:15	5.80	0.01	2.29	0.03	**1.90**	**-2.23**	562
NBS 19	3/29/2006	08:54:02	5.84	0.01	2.39	0.01	**1.95**	**-2.13**	775
NBS 19	3/30/2006	00:01:26	5.80	0.02	2.31	0.04	**1.91**	**-2.21**	1007
NBS 19	3/30/2006	00:41:36	5.81	0.02	2.29	0.04	**1.92**	**-2.23**	1012
NBS 19	5/11/2006	17:39:03	5.89	0.01	2.38	0.03	**1.97**	**-2.22**	1029
NBS 19	5/11/2006	18:22:09	5.89	0.02	2.29	0.03	**1.97**	**-2.32**	1253
NBS 19	5/13/2006	15:06:53	5.86	0.02	2.49	0.02	**1.95**	**-2.12**	1085
NBS 19	5/13/2006	15:47:42	5.86	0.01	2.41	0.03	**1.95**	**-2.20**	1063
NBS 19	5/14/2006	04:50:31	5.87	0.01	2.28	0.02	**1.96**	**-2.32**	1239
NBS 19	5/14/2006	14:11:46	5.92	0.02	2.49	0.01	**2.00**	**-2.12**	924

NBS 19	5/14/2006	14:54:57	5.90	0.02	2.31	0.02	**1.99**	**-2.29**	1197
NBS 19	5/14/2006	20:03:53	5.89	0.02	2.33	0.02	**1.97**	**-2.27**	1200
NBS 19	5/16/2006	16:17:01	5.91	0.02	2.41	0.02	**1.99**	**-2.19**	1190
NBS 19	5/17/2006	14:24:49	5.84	0.01	2.32	0.02	**1.93**	**-2.28**	1192
NBS 19	5/17/2006	15:07:44	5.86	0.02	2.36	0.03	**1.94**	**-2.24**	1058
NBS 19	5/11/2006	17:39:03	5.89	0.01	2.38	0.03	**1.97**	**-2.22**	1029
NBS 19	5/11/2006	18:22:09	5.89	0.02	2.29	0.03	**1.97**	**-2.32**	1253
NBS 19	6/4/2006	13:43:56	5.87	0.01	2.29	0.03	**1.95**	**-2.31**	1209
NBS 19	6/4/2006	14:26:40	5.88	0.02	2.38	0.02	**1.96**	**-2.22**	1038
NBS 19	6/5/2006	05:30:42	5.90	0.01	2.38	0.01	**1.99**	**-2.22**	1231
NBS 19	6/6/2006	04:22:15	5.77	0.02	2.40	0.04	**1.85**	**-2.20**	907
NBS 19	6/6/2006	11:14:21	5.88	0.01	2.25	0.02	**1.96**	**-2.36**	1234
NBS 19	6/6/2006	11:53:49	5.88	0.01	2.53	0.02	**1.96**	**-2.08**	814
NBS 19	06/10/2006	18:09:43	5.91	0.02	2.43	0.02	**1.99**	**-2.18**	1139
NBS 19	06/10/2006	18:47:08	5.87	0.01	2.42	0.03	**1.95**	**-2.19**	1156
NBS 19	6/6/2006	15:09:56	5.87	0.02	2.37	0.03	**1.96**	**-2.23**	1058
NBS 19	6/6/2006	15:50:47	5.87	0.01	2.34	0.02	**1.96**	**-2.26**	1095
NBS 19	6/7/2006	17:32:46	5.89	0.01	2.44	0.02	**1.97**	**-2.16**	1095
NBS 19	6/7/2006	18:15:24	5.86	0.01	2.45	0.02	**1.95**	**-2.15**	868
NBS 19	6/12/2006	04:59:52	5.88	0.01	2.41	0.03	**1.97**	**-2.20**	1136
NBS 19	6/12/2006	05:39:49	5.90	0.01	2.44	0.01	**1.98**	**-2.17**	1097
NBS 19	6/11/2006	14:54:46	5.88	0.01	2.30	0.03	**1.96**	**-2.30**	1190
NBS 19	6/11/2006	15:33:42	5.85	0.01	2.37	0.03	**1.94**	**-2.24**	1107
NBS 19	6/13/2006	15:34:37	5.86	0.01	2.34	0.02	**1.94**	**-2.27**	1100
NBS 19	6/13/2006	16:17:11	5.88	0.02	2.34	0.02	**1.96**	**-2.26**	1053
NBS 19	6/13/2006	12:55:55	5.92	0.01	2.43	0.02	**2.00**	**-2.18**	1046
NBS 19	6/13/2006	13:31:37	5.91	0.01	2.49	0.03	**1.99**	**-2.12**	997
NBS 19	6/16/2006	13:58:33	5.90	0.02	2.44	0.03	**1.98**	**-2.16**	943
NBS 19	6/16/2006	20:20:29	5.85	0.00	2.32	0.02	**1.93**	**-2.29**	1129
NBS 19	6/16/2006	20:58:47	5.91	0.02	2.28	0.02	**1.99**	**-2.33**	929
NBS 19	6/18/2006	11:51:20	5.86	0.02	2.42	0.02	**1.94**	**-2.18**	1153
NBS 19	6/19/2006	01:23:26	5.86	0.02	2.29	0.01	**1.95**	**-2.31**	1168
NBS 19	6/19/2006	01:59:13	5.88	0.02	2.36	0.02	**1.96**	**-2.25**	701
NBS 19	6/19/2006	11:55:22	5.89	0.01	2.43	0.03	**1.97**	**-2.18**	1087
NBS 19	6/19/2006	12:33:22	5.87	0.02	2.32	0.01	**1.95**	**-2.28**	1112
NBS 19	6/13/2006	04:35:44	5.91	0.01	2.48	0.03	**1.99**	**-2.12**	943
NBS 19	6/13/2006	05:10:32	5.90	0.02	2.48	0.03	**1.98**	**-2.12**	545
NBS 19	6/12/2006	15:17:54	5.85	0.01	2.30	0.03	**1.94**	**-2.31**	1056
NBS 19	6/12/2006	15:57:30	5.91	0.03	2.35	0.04	**1.99**	**-2.26**	1180
NBS 19	6/12/2006	12:44:48	5.92	0.02	2.37	0.02	**2.00**	**-2.23**	1178
NBS 19	6/12/2006	13:23:37	5.89	0.02	2.40	0.02	**1.98**	**-2.21**	1019
NBS 19	6/21/2006	02:45:01	5.90	0.01	2.28	0.02	**1.98**	**-2.32**	1217
NBS 19	6/21/2006	03:21:24	5.83	0.02	2.46	0.02	**1.92**	**-2.15**	772
NBS 19	6/19/2006	11:55:22	5.89	0.01	2.43	0.03	**1.97**	**-2.18**	1087
NBS 19	6/19/2006	12:33:22	5.87	0.02	2.32	0.01	**1.95**	**-2.28**	1112
NBS 19	6/19/2006	01:23:26	5.86	0.02	2.29	0.01	**1.95**	**-2.31**	1168
NBS 19	6/19/2006	01:59:13	5.88	0.02	2.36	0.02	**1.96**	**-2.25**	701
NBS 19	6/20/2006	02:04:43	5.91	0.03	2.43	0.04	**2.00**	**-2.17**	926

NBS 19	6/20/2006	02:42:51	5.91	0.02	2.44	0.03	**1.99**	**-2.16**	985
NBS 19	6/20/2006	12:09:53	5.86	0.02	2.35	0.02	**1.94**	**-2.26**	1109
NBS 19	6/30/2006		5.82	0.01	2.31	0.02	**1.90**	**-2.30**	1117
NBS 19	6/30/2006		5.89	0.01	2.29	0.03	**1.97**	**-2.31**	1180
NBS 19	7/1/2006		5.87	0.02	2.35	0.02	**1.95**	**-2.26**	1100
NBS 19	7/1/2006		5.86	0.01	2.35	0.01	**1.95**	**-2.25**	1087
NBS 19	7/2/2006		5.79	0.02	2.20	0.02	**1.88**	**-2.41**	1090
NBS 19	7/3/2006		5.89	0.01	2.35	0.01	**1.97**	**-2.25**	1190
NBS 19	7/3/2006		5.87	0.01	2.35	0.02	**1.95**	**-2.25**	1107
NBS 19	7/3/2006		5.85	0.01	2.31	0.01	**1.93**	**-2.30**	1170
NBS 19	7/3/2006		5.87	0.01	2.37	0.02	**1.96**	**-2.24**	1082
NBS 19	8/18/2006	16:42:01	5.91	0.02	2.43	0.03	**1.98**	**-2.21**	1112
NBS 19	8/18/2006	17:23:09	5.89	0.01	2.34	0.02	**1.96**	**-2.30**	1273
NBS 19	8/19/2006	23:21:21	5.89	0.01	2.40	0.02	**1.96**	**-2.24**	1109
NBS 19	8/20/2006	14:23:28	5.92	0.01	2.49	0.03	**1.98**	**-2.15**	1046
NBS 19	8/20/2006	15:03:43	5.89	0.01	2.47	0.02	**1.96**	**-2.18**	1146
NBS 19	8/20/2006	0:02:02	5.88	0.01	2.47	0.02	**1.95**	**-2.17**	1009
NBS 19	8/20/2006	6:48:54	5.84	0.01	2.53	0.03	**1.91**	**-2.11**	760
NBS 19	8/20/2006	7:29:20	5.90	0.02	2.49	0.02	**1.97**	**-2.15**	911
NBS 19	8/21/2006	15:15:27	5.91	0.01	2.59	0.02	**1.98**	**-2.05**	826
NBS 19	8/21/2006	15:55:15	5.91	0.02	2.56	0.04	**1.98**	**-2.09**	938
NBS 19	8/22/2006	0:28:43	5.89	0.02	2.50	0.03	**1.96**	**-2.14**	836
NBS 19	8/30/2006	12:49:35	5.86	0.03	2.43	0.02	**1.93**	**-2.21**	1273
NBS 19	8/30/2006	13:34:01	5.89	0.01	2.32	0.03	**1.96**	**-2.32**	1278
NBS 19	8/31/2006	16:13:24	5.89	0.01	2.52	0.02	**1.95**	**-2.13**	811
NBS 19	8/31/2006	16:55:00	5.90	0.02	2.43	0.02	**1.97**	**-2.22**	1180
NBS 19	8/31/2006	3:27:08	5.87	0.01	2.32	0.02	**1.94**	**-2.33**	987
NBS 19	8/31/2006	4:14:53	5.90	0.03	2.43	0.04	**1.97**	**-2.21**	1222
NBS 19	9/1/2006	7:47:48	5.85	0.02	2.29	0.03	**1.92**	**-2.35**	1251
NBS 19	9/1/2006	8:29:32	5.87	0.02	2.41	0.05	**1.93**	**-2.24**	911
NBS 19	9/2/2006	13:45:37	5.89	0.01	2.51	0.02	**1.96**	**-2.14**	1134
NBS 19	9/2/2006	16:17:53	5.90	0.02	2.52	0.03	**1.97**	**-2.12**	1134
NBS 19	9/2/2006	16:57:00	5.91	0.02	2.49	0.01	**1.98**	**-2.16**	1019
NBS 19	8/31/2006	16:13:24	5.89	0.01	2.52	0.02	**1.95**	**-2.13**	811
NBS 19	8/31/2006	16:55:00	5.90	0.02	2.43	0.02	**1.97**	**-2.22**	1180
NBS 19	9/1/2006	7:47:48	5.85	0.02	2.29	0.03	**1.92**	**-2.35**	1251
NBS 19	9/1/2006	8:29:32	5.87	0.02	2.41	0.05	**1.93**	**-2.24**	911
NBS 19	9/2/2006	13:45:37	5.89	0.01	2.51	0.02	**1.96**	**-2.14**	1134
NBS 19	9/2/2006	16:17:53	5.90	0.02	2.52	0.03	**1.97**	**-2.12**	1134
NBS 19	9/2/2006	16:57:00	5.91	0.02	2.49	0.01	**1.98**	**-2.16**	1019
NBS 19	10/24/2006	16:34:27	5.94	0.02	2.45	0.03	**2.00**	**-2.20**	1258
NBS 19	10/24/2006	17:17:07	5.88	0.02	2.34	0.04	**1.95**	**-2.31**	1226
NBS 19	10/23/2006	14:30:49	5.86	0.01	2.55	0.02	**1.93**	**-2.10**	577
NBS 19	10/23/2006	15:14:34	5.90	0.01	2.48	0.04	**1.97**	**-2.16**	1114
NBS 19	10/24/2006	8:27:00	5.92	0.02	2.49	0.02	**1.99**	**-2.15**	1078
NBS 19	10/24/2006	9:11:02	5.93	0.02	2.56	0.02	**2.00**	**-2.09**	1063
NBS 19	10/21/2006	13:01:02	5.93	0.02	2.50	0.02	**2.00**	**-2.14**	1175
NBS 19	10/21/2006	14:44:51	5.93	0.03	2.50	0.02	**1.99**	**-2.14**	1158

NBS 19	10/21/2006	15:29:01	5.90	0.02	2.48	0.02	**1.96**	**-2.16**	1131
NBS 19	10/22/2006	20:53:06	5.91	0.01	2.34	0.02	**1.98**	**-2.30**	1417
NBS 19	10/22/2006	21:39:13	5.96	0.02	2.44	0.04	**2.03**	**-2.21**	1351
NBS 19	10/23/2006	14:30:49	5.86	0.01	2.55	0.02	**1.93**	**-2.10**	577
NBS 19	10/23/2006	15:14:34	5.90	0.01	2.48	0.04	**1.97**	**-2.16**	1114
NBS 19	1/9/2007	9:48:33	5.86	0.02	2.51	0.02	**1.93**	**-2.13**	882
NBS 19	1/9/2007	10:27:16	5.86	0.01	2.33	0.02	**1.93**	**-2.32**	1219
NBS 19	1/9/2007	15:59:52	5.90	0.06	2.43	0.11	**1.97**	**-2.21**	360
NBS 19	1/9/2007	16:39:06	5.86	0.02	2.47	0.02	**1.93**	**-2.17**	1078
NBS 19	1/17/2007	9:14:59	5.87	0.01	2.45	0.02	**1.94**	**-2.19**	1041
NBS 19	1/18/2007	13:07:24	5.85	0.02	2.43	0.02	**1.92**	**-2.22**	1012
NBS 19	1/18/2007	13:46:43	5.89	0.01	2.50	0.03	**1.95**	**-2.15**	1016
NBS 19	1/16/2007	13:08:53	5.86	0.02	2.52	0.02	**1.93**	**-2.13**	616
NBS 19	1/16/2007	13:52:33	5.88	0.01	2.37	0.02	**1.95**	**-2.28**	1261
						Mean	**1.95***	**-2.22***	
						Stdev	**0.03**	**0.08**	

***expected values +1.95/-2.2±0.1‰**

The error associated with the analysis of different populations of foraminifera or bone specimens from a single sample interval was also assessed. For the Arctic fish bones analyzed in **Chapter 4**, a bone powder was made using extra bones obtained primarily from sample 302-2A-55X-CC. The isotopic variability of this single powder following treatment was found to be ±0.4‰ for $\delta^{18}O$ and ±0.2‰ for $\delta^{13}C$ (1σ, N=11), which, because the powder was a mixture of bones from several sample intervals, provides a good estimation of the maximum error for the Arctic fish bone analyses (**Table J.3**). For the fish bone samples analyzed from the Shatsky Rise and subantactic Pacific in **Chapter 5**, material was too scarce for multiple analyses of a single bone powder. Thus, the variability associated with the treatment and analysis of fish debris was instead estimated using a powder of Pliocene fish bone from the Snake River Plain, Idaho. The error associated with the analysis of the Snake River powder was found to be ±0.2‰ for $\delta^{18}O$ and ±0.3‰ for $\delta^{13}C$ (1σ) (**Table J.4**).

Because planktonic foraminifera tend to demonstrate larger isotopic variability than benthic foraminifera, multiple measurements were also made on grouped and individual specimens of *G. bulloides* from MV0502-4JC in order to estimate the error associated with the analysis of foraminifera from the subantarctic Pacific region (**Chapters 2 and 3**). These measurements are shown in **Table J.5**, and in general the variability displayed by *G. bulloides* was found to decrease downcore.

Table J.3: Isotopic Variability of an ACEX Bone Powder

Sample	$\delta^{13}C$ (KIS)	±	$\delta^{18}O$ (KIS)	±	$\delta^{13}C$ (VPDB)	$\delta^{18}O$ (VPDB)	Max P
ACEX fish debris	-8.94	0.02	0.61	0.03	**-12.77**	**-3.96**	295
ACEX fish debris	-8.89	0.02	0.35	0.02	**-12.71**	**-4.22**	722
ACEX fish debris	-8.77	0.01	0.15	0.01	**-12.60**	**-4.42**	673
ACEX fish debris	-9.29	0.01	1.19	0.02	**-13.11**	**-3.38**	642
ACEX fish debris	-9.30	0.03	1.04	0.03	**-13.13**	**-3.53**	665
ACEX fish debris	-9.18	0.01	0.99	0.01	**-13.01**	**-3.58**	692
ACEX fish debris	-9.21	0.02	1.39	0.02	**-13.03**	**-3.18**	707
ACEX fish debris	-9.23	0.02	1.27	0.02	**-13.05**	**-3.30**	560
ACEX fish debris	-9.18	0.01	1.10	0.03	**-13.00**	**-3.47**	699
ACEX fish debris	-9.07	0.03	0.95	0.03	**-12.90**	**-3.62**	660
ACEX fish debris	-9.01	0.02	0.80	0.02	**-12.83**	**-3.77**	711
				Mean	**-12.92**	**-3.68**	
				Stdev	**0.17**	**0.39**	

Table J.4: Isotopic Variability of Snake River Plain Bone Powder

Sample	$\delta^{13}C$ (KIS)	±	$\delta^{18}O$ (KIS)	±	$\delta^{13}C$ (VPDB)	$\delta^{18}O$ (VPDB)	Max P
Snake River debris	3.76	0.02	-4.69	0.05	**-0.04**	**-9.42**	1251
Snake River debris	3.92	0.03	-4.90	0.05	**0.12**	**-9.63**	1263
Snake River debris	3.86	0.03	-4.93	0.05	**0.06**	**-9.66**	1251
Snake River debris	4.48	0.04	-5.06	0.08	**0.73**	**-9.84**	1202
Snake River debris	4.30	0.04	-5.16	0.08	**0.54**	**-9.93**	1251
Snake River debris	4.33	0.03	-5.25	0.06	**0.58**	**-10.03**	1268
Snake River debris	4.28	0.02	-5.05	0.08	**0.53**	**-9.82**	1229
Snake River debris	4.36	0.05	-5.02	0.11	**0.60**	**-9.79**	1207
Snake River debris	4.30	0.04	-5.24	0.10	**0.55**	**-10.01**	1248
				Mean	**0.41**	**-9.79**	
				Stdev	**0.28**	**0.20**	

Table J.5: Isotopic Variability of *G. bulloides* Specimens from MV0502-4JC

Sample Interval	# Individuals	$\delta^{13}C$ (KIS)	±	$\delta^{18}O$ (KIS)	±	$\delta^{13}C$ (VPDB)	$\delta^{18}O$ (VPDB)	Max P
1-3cm	4	4.64	0.03	8.30	0.01	**0.84**	**3.94**	1190
1-3cm	4	4.41	0.02	7.32	0.01	**0.61**	**2.95**	1231
1-3cm	4	4.16	0.02	7.65	0.02	**0.36**	**3.29**	1168
					mean	**0.60**	**3.39**	
					stdev	**0.24**	**0.50**	
1-3cm	8	4.74	0.02	7.60	0.02	**0.93**	**3.23**	1314
1-3cm	8	4.65	0.01	7.58	0.01	**0.84**	**3.21**	1317
1-3 cm	8	4.23	0.03	7.92	0.03	**0.43**	**3.56**	1356
					mean	**0.74**	**3.33**	
					stdev	**0.27**	**0.20**	
1-3cm	12	4.57	0.01	7.66	0.02	**0.76**	**3.29**	1358
1-3cm	13	4.41	0.02	7.62	0.03	**0.61**	**3.26**	1356
1-3cm	14	4.49	0.01	7.99	0.02	**0.69**	**3.63**	1358
					mean	**0.69**	**3.39**	
					stdev	**0.08**	**0.20**	
1-3 cm	1	4.25	0.02	8.06	0.04	**0.45**	**3.69**	992
1-3 cm	1	4.74	0.02	8.60	0.06	**0.93**	**4.24**	855
1-3 cm	1	5.31	0.01	8.59	0.02	**1.51**	**4.22**	665
1-3 cm	1	4.85	0.02	8.36	0.05	**1.05**	**4.00**	877
1-3 cm	1	4.75	0.01	6.48	0.02	**0.95**	**2.11**	938
1-3 cm	1	3.78	0.02	7.10	0.03	**-0.02**	**2.73**	865
1-3 cm	1	4.63	0.01	8.40	0.02	**0.83**	**4.04**	929
1-3 cm	1	5.21	0.02	7.85	0.02	**1.41**	**3.49**	872
					mean	**0.89**	**3.56**	
					stdev	**0.49**	**0.77**	
1-3 cm	1	4.25	0.02	8.06	0.04	**0.45**	**3.69**	992
1-3 cm	1	4.74	0.02	8.60	0.06	**0.93**	**4.24**	855
1-3 cm	1	5.31	0.01	8.59	0.02	**1.51**	**4.22**	665
1-3 cm	1	4.85	0.02	8.36	0.05	**1.05**	**4.00**	877
1-3 cm	1	4.75	0.01	6.48	0.02	**0.95**	**2.11**	938
1-3 cm	1	3.78	0.02	7.10	0.03	**-0.02**	**2.73**	865
1-3 cm	1	4.63	0.01	8.40	0.02	**0.83**	**4.04**	929
1-3 cm	1	5.21	0.02	7.85	0.02	**1.41**	**3.49**	872
					mean	**0.89**	**3.56**	
					stdev	**0.49**	**0.77**	
101-103 cm	4	4.41	0.01	6.56	0.02	**0.61**	**2.19**	1246
101-103 cm	4	5.00	0.01	7.76	0.01	**1.19**	**3.40**	1229
101-103 cm	4	4.49	0.01	7.28	0.03	**0.68**	**2.92**	1244
					mean	**0.83**	**2.83**	
					stdev	**0.32**	**0.61**	
101-103 cm	8	4.66	0.02	7.19	0.03	**0.86**	**2.82**	1314
101-103 cm	8	4.52	0.01	7.17	0.02	**0.72**	**2.81**	1314
101-103 cm	8	4.54	0.01	6.92	0.01	**0.73**	**2.55**	1314
101-103 cm	8	4.46	0.01	7.02	0.02	**0.66**	**2.65**	1339
					mean	**0.74**	**2.71**	

					stdev	**0.08**	**0.13**	
201-203 cm	4	3.74	0.01	7.85	0.02	**-0.06**	**3.49**	1200
201-203 cm	4	4.05	0.01	8.16	0.02	**0.25**	**3.80**	1261
201-203 cm	4	3.92	0.01	7.89	0.03	**0.12**	**3.52**	1244
					mean	**0.10**	**3.60**	
					stdev	**0.15**	**0.17**	
201-203 cm	8	4.14	0.01	7.96	0.03	**0.34**	**3.60**	1336
201-203 cm	8	4.19	0.02	8.01	0.03	**0.39**	**3.65**	1314
201-203 cm	8	4.19	0.02	8.06	0.04	**0.39**	**3.69**	1322
					mean	**0.37**	**3.65**	
					stdev	**0.03**	**0.05**	
201-203 cm	12	4.15	0.01	8.10	0.02	**0.35**	**3.73**	1351
201-203 cm	12	4.38	0.02	8.00	0.01	**0.57**	**3.64**	1375
201-203 cm	12	4.13	0.01	8.21	0.02	**0.33**	**3.85**	1349
					mean	**0.42**	**3.74**	
					stdev	**0.14**	**0.11**	